



Kent Academic Repository

Martyna, Agnieszka (2016) *Structure and function of the M2 amphipathic helix in Influenza virus membrane scission*. Doctor of Philosophy (PhD) thesis, University of Kent,.

Downloaded from

<https://kar.kent.ac.uk/56663/> The University of Kent's Academic Repository KAR

The version of record is available from

This document version

UNSPECIFIED

DOI for this version

Licence for this version

UNSPECIFIED

Additional information

Versions of research works

Versions of Record

If this version is the version of record, it is the same as the published version available on the publisher's web site. Cite as the published version.

Author Accepted Manuscripts

If this document is identified as the Author Accepted Manuscript it is the version after peer review but before type setting, copy editing or publisher branding. Cite as Surname, Initial. (Year) 'Title of article'. To be published in *Title of Journal*, Volume and issue numbers [peer-reviewed accepted version]. Available at: DOI or URL (Accessed: date).

Enquiries

If you have questions about this document contact ResearchSupport@kent.ac.uk. Please include the URL of the record in KAR. If you believe that your, or a third party's rights have been compromised through this document please see our [Take Down policy](https://www.kent.ac.uk/guides/kar-the-kent-academic-repository#policies) (available from <https://www.kent.ac.uk/guides/kar-the-kent-academic-repository#policies>).

**Structure and function of the M2
amphipathic helix in Influenza
virus membrane scission**

Agnieszka Martyna

**A thesis submitted to the University of Kent at Canterbury
for the degree of PhD in Microbiology in the Faculty of
Sciences**

Department of Biosciences

2016

Declaration

No part of the thesis has been submitted in the support of an application for any degree or other qualification of the University of Kent, or any other University or Institution of learning.

Agnieszka Martyna

29th April 2016

Acknowledgments

First I would like to thank my supervisor, Dr Jeremy Rossman for giving me the opportunity to do this study, his advice, support and optimism in difficult moments throughout the course.

I would also like to thank all past and present members of the Rossman group for their help and friendship. I would especially like to thank Matt Badham for his help with imaging and constant IT support and Dr Basma Bahsoun for helping with many technical issues in the lab.

Massive thanks to Dr Mark Howard for his help with running NMR experiments and data analysis as well as Dr Michelle Rowe for teaching me how to assign TOCSY and NOESY NMR spectra and run secondary structure calculation.

I would also like to thank Dr Kevin Howland for help with CD spectroscopy and Ian Brown for support during long hours of confocal imaging.

From Stockholm University I would like to thank our collaborators Dr Jordi Gómez-Llobregat and Dr Martin Lindén for performing molecular dynamics simulations. I would like to also thank our collaborator Dr Saipraveen Srinivasan from University of Texas for help and advice with SUPER template experiments.

Finally I would like to thank my family and friends for their support throughout the years. I am especially grateful to my fiancée, Charlie Hobbs for his patience and support in the most difficult moments as well as proof reading of my thesis. I would also like to thank my parents for their support on all levels of my education and my parents in law to be for support during write up period. I would also like to thank my best friend Natalia for constant motivation.

Abstract

Influenza A is an enveloped, negative sense RNA virus which causes annual epidemics and major pandemics. Assembly and budding of new viral particles is a complex and multistep process, of which many aspects remain unclear despite many years of research. The Influenza virus M2 protein is a homotetrameric transmembrane protein, containing three domains: ecto domain, transmembrane domain and cytoplasmic tail (CT). In the final stage of budding it has been shown that M2 mediates membrane scission through an amphipathic helix (AH), which is formed by the first 17 amino acids of the protein's CT, however the exact mechanism by which membrane scission is triggered was not known.

Using a collection of biochemical and biophysical techniques we have investigated the structure of the M2 AH and assessed its function in viral assembly and budding. We have shown that the M2 AH is formed upon lipid binding and remains unstructured in solution. It preferentially binds to membranes with high positive membrane curvature, which is detected by sensing the associated lipid packing defects. There are many cationic residues in the polar face of the M2 AH which could interact with anionic lipid headgroups, however charged interactions do not significantly affect the M2 AH interactions with the membranes. When inserted into the membrane the M2 AH increases lipid ordering. The M2 AH also induces positive membrane curvature and mediates membrane scission, which is the last step of Influenza virus budding, allowing for release of newly formed virions into the environment.

Membrane scission is a crucial step not only in viral budding but also in many biological processes, such as endocytosis. Many proteins have been associated with cellular membrane scission; however, the underlying molecular details are still not known. We have shown that AHs in some cellular peptides, such as Arf 1, Endophilin A3 and Epsin 1, which mediate membrane scission in biological processes, appear to work in a similar manner to the M2 AH. They represent a new protein motif that is capable of sensing curvature, inducing curvature and altering membrane fluidity, thereby mediating membrane scission and therefore belong to a novel group of AHs.

TABLE OF CONTENTS:

ABBREVIATIONS.....	6
1. INTRODUCTION.....	10
1.1 SIGNIFICANCE OF INFLUENZA VIRUS.....	11
1.2 VIRION MORPHOLOGY AND STRUCTURE.....	12
1.2.1 The Matrix protein 2 (M2)	13
1.3 VIRION ASSEMBLY.....	16
1.3.1 Lipid rafts as site of assembly	16
1.3.2 Assembly of the viral envelope proteins	16
1.3.3 Recruitment of the viral core	18
1.4 BUDDING AND MEMBRANE SCISSION.....	21
1.4.1 Assembly and budding	22
1.4.2 Membrane scission.....	24
1.4.3 Model of influenza budding	25
1.5 AIMS OF THE PROJECT	27
2. MATERIALS AND METHODS.....	28
2.1 MATERIALS.....	29
2.1.1 Peptides	29
2.1.2 Lipids.....	32
2.1.3 Cells, plasmids, viruses and antibodies	35
2.1.4 Oligonucleotides	36
2.2 METHODS	37
2.2.1 Liposomes.....	37
2.2.1.1 Small Unilamellar Vesicles (SUVs)	37
2.2.1.2 Large Unilamellar Vesicles (LUVs).....	37

2.2.1.3 Giant Unilamellar Vesicles (GUVs)	38
2.2.1.4 Dynamic Light Scattering (DLS)	38
2.2.2 Nuclear Magnetic Resonance (NMR) Spectroscopy	38
2.2.3 Peptide binding assay	39
2.2.4 Circular Dichroism (CD) Spectroscopy	40
2.2.5 Immunofluorescence microscopy	40
2.2.6 Molecular Dynamics Simulations	41
2.2.6.1 Simulation parameters	41
2.2.6.2 Lipid bilayer equilibration	42
2.2.6.3 Membrane buckling and peptide addition.....	42
2.2.6.4 Membrane alignment and peptide tracking.....	42
2.2.7 Laurdan assay for membrane order.....	44
2.2.8 Differential Scanning Calorimetry (DSC).....	44
2.2.9 Transmission Electron Microscopy (TEM).....	45
2.2.10 GUV budding system	45
2.2.11 GUV microinjection system	46
2.2.12 Supported bilayers with excess membrane reservoir (SUPER) templates system.....	46
2.2.13 Immunoblotting.....	47
2.2.14 Repeated virus passaging	48
2.2.14.1 Virus growth.....	48
2.2.14.2 Plaque assay	48
2.2.14.3 RNA extraction and reverse transcription.....	49
2.2.14.4 Sequencing	49
3. RESULTS	50
3.1 STRUCTURE OF THE M2 AMPHIPATHIC HELIX	51
3.1.1 Introduction	51

3.1.2 M2 AH formation upon membrane binding	52
3.1.3 M2 AH membrane interactions.....	61
3.1.4 Summary.....	67
3.2 M2 AMPHIPATHIC HELIX INTERACTIONS WITH THE MEMBRANE	68
3.2.1 Introduction	68
3.2.2 Binding to lipid membranes	68
3.2.3 Alpha helix stabilisation upon binding.....	71
3.2.3.1 Detection of secondary structure	71
3.2.3.2 Structural changes in different environments.....	75
3.2.3.3 A/England/09 and AH mutants	79
3.2.4 Summary.....	83
3.3 EFFECTS OF THE LIPID ENVIRONMENT ON M2 AMPHIPATHIC HELIX – MEMBRANE BINDING	86
3.3.1 Introduction	86
3.3.2 Charge interactions	87
3.3.2.1 Different anionic lipids	87
3.3.2.2 Absence of anionic lipids.....	91
3.3.2.3 Ionic strength.....	94
3.3.3 Effects of cholesterol.....	95
3.3.4 Effects of PIP ₂	97
3.3.5 Effects of lipid domain line tension	100
3.3.6 Effects of membrane curvature.....	103
3.3.6.1 Standard membranes.....	103
3.3.6.2 Absence of anionic lipids	108
3.3.7 Sensing of lipid defects in the membrane	111
3.3.8 Summary.....	114

3.4 EFFECTS OF THE M2 AMPHIPATHIC HELIX ON THE MEMBRANE	119
3.4.1 Introduction	119
3.4.2 Ordering of lipids in the membrane	120
3.4.2.1 M2 AH	120
3.4.2.2 A/England/09 and AH mutants	123
3.4.2.3 Different membrane compositions	124
3.4.3 Alteration of membrane phase-transition temperatures	128
3.4.4 Induction of positive membrane curvature	129
3.4.5 Summary	130
3.5 M2 AMPHIPATHIC HELIX MEDIATED BUDDING <i>IN VITRO</i>	133
3.5.1 Introduction	133
3.5.2 GUV budding	133
3.5.3 GUV microinjections	137
3.5.4 SUPER templates and membrane scission	141
3.5.5 Summary	143
3.6 M2 AMPHIPATHIC HELIX MEDIATED BUDDING <i>IN VIVO</i>	145
3.6.1 Introduction	145
3.6.2 Virus-like particles (VLP) release	145
3.6.3 Restoration of viral growth	147
3.6.4 Summary	153
3.7 FUNCTIONALLY HOMOLOGOUS SCISSION HELICES IN CELLULAR PROTEINS	154
3.7.1 Introduction	154
3.7.2 Arf1, CHMP4b, EndophilinA3 and Epsin1	155

3.7.2.1 Structural changes in different environments.....	155
3.7.2.2 Anionic lipids and positive membrane curvature effect on cellular AH formation.....	158
3.7.2.3 Effect of line tension on cellular AH formation.....	163
3.7.2.4 Ordering of the lipids in the membrane	165
3.7.2.5 Induction of positive membrane curvature	166
3.7.3 Summary.....	167
4. DISCUSSION	170
4.1 STRUCTURE OF THE M2 AH.....	171
4.2 MECHANISM OF ACTION.....	173
4.2.1 Membrane binding	173
4.2.2 Membrane activity	174
4.2.3 Membrane scission.....	179
4.3 M2 AH AS A PART OF A BIGGER PROTEIN FAMILY	182
4.4 CONCLUSIONS AND FUTURE WORK	184
5. REFERENCES.....	187
6. APPENDIX.....	198
6.1 Restriction map of pCAGGS plasmid encoding M2 protein from A/Udorn/72 strain.....	198
6.2 Ramachandran plots	199
6.3 DLS data.....	201
A. Standard vesicles.....	201
B. Vesicles without anionic lipids	203
6.4 Laurdan assay titration	209
6.5 Protein sequences comparison	210

ABBREVIATIONS

1D - one-dimensional

2D - two-dimensional

A - alanine

AH - amphipathic helix

ALPS - amphipathic lipid packing sensor

ATP - adenosine triphosphate

BAR - Bin-Amphiphysin-Rsv

BSA - bovine serum albumin

CD - circular dichroism

Ch - cholesterol

CRAC - cholesterol recognition amino acid consensus

CT - cytoplasmic tail

DeisPC - 1,2-dieicosenoyl-sn-glycero-3-phosphocholine

DEPC - 1,2-dierucoyl-sn-glycero-3-phosphocholine

DLS - dynamic light scattering

DMEM - Dulbecco's modified eagle medium

DMPC - 1,2-dimyristoleoyl-sn-glycero-3-phosphocholine

DNA - deoxyribonucleic acid

DOPC - 1,2-dioleoyl-sn-glycero-3-phosphocholine

DOPE - 1,2-dioleoyl-sn-glycero-3-phosphoethanolamine

DPPC - 1,2-dipalmitoleoyl-sn-glycero-3-phosphocholine

DSC - differential scanning calorimetry

DSPC - 1,2-distearoyl-sn-glycero-3-phosphocholine

DSPE - 1,2-distearoyl-sn-glycero-3-phosphoethanolamine

EDTA - ethylenediaminetetraacetic acid

ER - endoplasmic reticulum

ESCRT - endosomal sorting complex required for transport

FBS - fetal bovine serum

FITC - fluorescein isothiocyanate

GP - generalised polarisation

GTP - guanosine triphosphate

GUV - giant unilamellar vesicles

HA - hemagglutinin

HEK 293T - human embryonic kidney 293T

HEPES - 4-(2-Hydroxyethyl) piperazine-1-ethanesulfonic acid

HIV - human immunodeficiency virus

ILV - intraluminal vesicles

K - lysine

LUV - large unilamellar vesicles

M1 - matrix protein 1

M2 - matrix protein 2

MD - molecular dynamic

MDCK - Madin-Darby canine kidney

MLV - multilamellar vesicles

MOI - multiplicity of infection

MVB - multi-vesicular bodies

NA - neuraminidase

NAT - N-acetyl trypsin

NEP/NS2 - nuclear export protein/ non-structural protein 2

NGC - negative Gaussian curvature

NMR - nuclear magnetic resonance

NOE - nuclear Overhauser effect

NOESY - nuclear Overhauser effect spectroscopy

NP - nucleoprotein

NS1 - non-structural protein 1

ORF - open reading frame

PA - 1-palmitoyl-2-oleoyl-sn-glycero-3-phosphate

PB1 - polymerase basic 1

PB2 - polymerase basic 2

PBS - phosphate buffered saline

PC - 1-palmitoyl-2-oleoyl-sn-glycero-3-phosphocholine

PE - 1-palmitoyl-2-oleoyl-sn-glycero-3-phosphoethanolamine

PFU - plaque forming units

PG - 1-palmitoyl-2-oleoyl-sn-glycero-3-phospho-1-rac-glycerol

PGC - positive Gaussian curvature

PIP2 - phosphatidylinositol 4,5-bisphosphate

ppm - parts per million

PS - 1-palmitoyl-2-oleoyl-sn-glycero-3-phospho-L-serine

PVDF - polyvinylidene difluoride

rmsd - root mean squared deviation

RNA - ribonucleic acid

RNP - ribonucleoprotein

rpm - revolutions per minute

RT-PCR - reverse transcriptase polymerase chain reaction

SM - sphingomyelin

STD NMR - saturation-transfer difference nuclear magnetic resonance

SUV - small unilamellar vesicles

TBE - tris-base, boric acid and EDTA

TEM - transmission electron microscopy

TFA - trifluoroacetic acid

TFE - 2,2,2-trifluoroethanol

TMD - transmembrane domain

TOCSY - total correlation spectroscopy

TX-100 - Triton X-100

UTR - untranslated region

VLP - virus-like particle

VMD - visual molecular dynamics

vRNA - viral ribonucleic acid

vRNP - viral ribonucleoprotein

1. INTRODUCTION

1.1 SIGNIFICANCE OF INFLUENZA VIRUS

Influenza virus causes annual epidemics and occasional major pandemics. It is a major cause of morbidity and mortality worldwide. There are three influenza virus subtypes: A, B and C; but only A and B are pathogenic for humans and influenza A is most predominant worldwide. Statistical data shows that in the USA the estimated annual influenza related deaths was over 50,000 in the period from 1990 to 1999, with mortality mostly associated with influenza A virus in those older than 65 (Thompson et al. 2003). Influenza virus continuously changes its antigenic properties by accumulation of mutations in viral antigens in a process called “antigenic drift”, which leads to annual epidemics. Occasionally influenza virus causes global pandemics, due to introduction into the human population of a new virus subtype. Pandemic strains, which rapidly spread around the world, arise mainly by reassortment of the segmented genome of human and avian influenza virus co-infecting one cell, in process called “antigenic shift” (Strauss and Strauss 2008). In the 20th century three main influenza pandemics arose. The most dreadful influenza pandemic was the “Spanish” flu outbreak at the end of the First World War: in one year influenza virus caused the death of approximately 50 million people around the world, which was greater than the total number of war victims (Johnson and Mueller 2002). The following two pandemics, “Asian” flu in 1957 and “Hong Kong” flu in 1968, were much milder than “Spanish” flu, but even so caused approximately over 1 million and 500,000 to 1 million deaths worldwide, respectively (Kilbourne 2006). The first pandemic in the 21st century arose in 2009 and was called “Swine” flu due to origin of the virus. The “Swine” flu outbreak was relatively mild however, in the USA alone over 22 million people were infected (Rossman and Lamb 2010). Each influenza outbreak has an impact on society, not only in terms of mortality and morbidity but also in financial and economic terms.

1.2 VIRION MORPHOLOGY AND STRUCTURE

Influenza A virus is an enveloped virus with negative-sense, single-stranded RNA genome and belongs to the *Orthomyxoviridae* family. It contains eight RNA segments, which encode for at least 17 proteins, including 10 structural and non-structural proteins and their truncated versions. The viral envelope is a host derived lipid membrane, which anchors three transmembrane-domain containing proteins: hemagglutinin (HA), neuraminidase (NA) and matrix protein 2 (M2) (Fig. 1.2-1). These proteins form characteristic spikes on the surface of the virus particles as seen by electron microscopy (Fujiyoshi et al. 1994). HA is the most abundant envelope protein, with about 500 copies per virion and has a receptor binding and fusion activity. NA is less numerous, has enzymatic activity and is involved in viral release. M2 is the least abundant protein in viral envelope, with only about 20-60 copies per virion, and is involved in virus entry, assembly and budding (Wilschut et al. 2006).

On the inside of the viral envelope there is a layer of matrix protein 1 (M1), which is the most abundant structural protein of the influenza virus. M1 interacts with surface glycoproteins (Enami and Enami 1996, Ali et al. 2000) and the ribonucleoprotein complexes (RNPs) (Watanabe et al. 1996), and plays a role in nuclear export, assembly and budding. The viral core contains RNPs which consist of the viral RNA (vRNA) segment, three polymerase proteins: polymerase basic 1 (PB1), polymerase basic 2 (PB2) and polymerase acid and the nucleoprotein (NP) (Palese and Shaw 2007). A number of strains produce an additional protein, PB1-F2. This protein has a pro-apoptotic activity and is transcribed from a second open reading frame (ORF) in the segment encoding the PB1 protein (Wilschut et al. 2006). Non-structural protein 1 (NS1) is multi-functional and plays a role in evasion of the host immune system. A nuclear export protein (NEP/NS2) is involved in nuclear export of viral RNPs. Previously it was considered as a non-structural protein, however, it was later found in the virus particle in low quantities (Richardson and Akkina 1991).

Influenza viruses are pleomorphic, some isolates form spherical virions, which have a diameter of approximately 100 nm, and others form filamentous particles, which also are approximately 100 nm in diameter, but up to 20 µm in length. Most of the strains used in laboratories form spherical virions, in contrast to the clinical isolates, which

mainly form filamentous virions (Chu et al. 1949). There is not much known about how filaments are produced, transmitted between the cells, or how they enter the host cell; however the ability to form filamentous virions is a genetic attribute of each strain (Kilbourne and Murphy 1960).

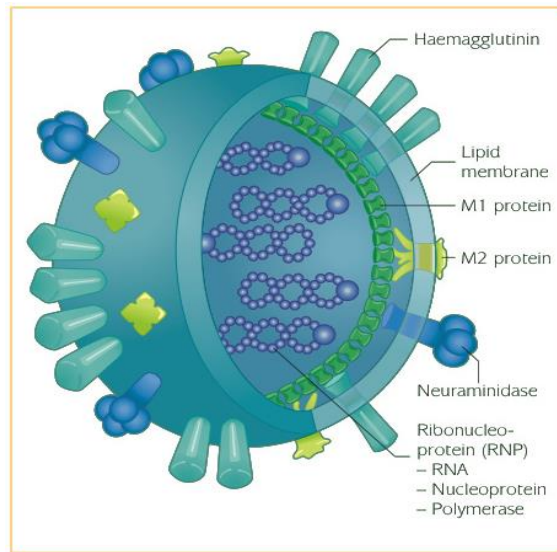


Figure 1.2 - 1 Model of influenza virus (Wilschut et al. 2006).

1.2.1 The Matrix protein 2 (M2)

The M2 protein is encoded by a spliced mRNA from segment 7 of the influenza genome. It is a 97 amino acid long protein that in the native form is a homotetramer. As mentioned before, only a few copies of the M2 protein are present in the virion, however, the protein is abundantly expressed in the plasma membrane of infected cells (Lamb et al. 1985). The M2 protein contains three domains, as shown in Figure 1.2-2: the ecto domain at the N-terminus (residues 1-24), the transmembrane domain (TMD) (residues 25-43) and the cytoplasmic tail (CT) at the C-terminus (residues 44-97) (Lamb et al. 1985, Zebedee et al. 1985, Pinto et al. 1992).

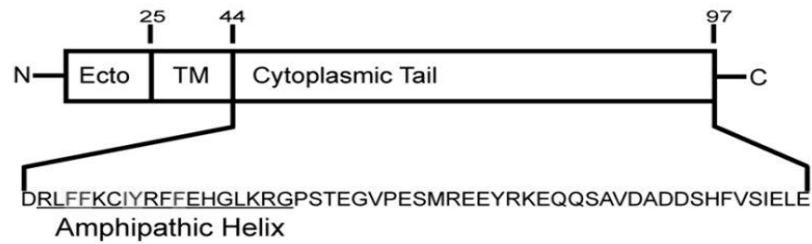


Figure 1. 2 - 2 Structural motifs of the M2 protein and sequence of the cytoplasmic tail with indicated amphipathic helix. Adapted from Rossman et al. 2010b.

TMD has an ion channel activity which is highly selective for H⁺ ions (Zebedee et al. 1985, Pinto et al. 1997) and plays a role in virus uncoating allowing for proton influx from acidified endosome inside viral particle which results in disassociation of RNPs from the M1 protein. Structure of the full length protein has not been solved up to date however, structure of the TMD with fragments of the ecto domain and CT has been intensively studied showing formation of the amphipathic helix (AH) on the beginning of the CT (between residues 51-59) that is nearly perpendicular to the TMD helices which are forming a pore and act as an ion channel (Schnell and Chou 2008). The M2 AH has been shown to play an important role in virus assembly and budding (Zebedee et al. 1985, Rossman et al. 2010b) and in formation of filamentous virions (Rossman et al. 2010a). It has been proposed that the M2 AH stabilises forming virions during assembly process and mediates budding by membrane scission (Rossman and Lamb 2011, Martyna and Rossman 2014). The M2 AH has a hydrophobic and polar face which contains a few highly conserved cationic residues (lysine and arginine) as shown in Figure 1.2-3 A and B.

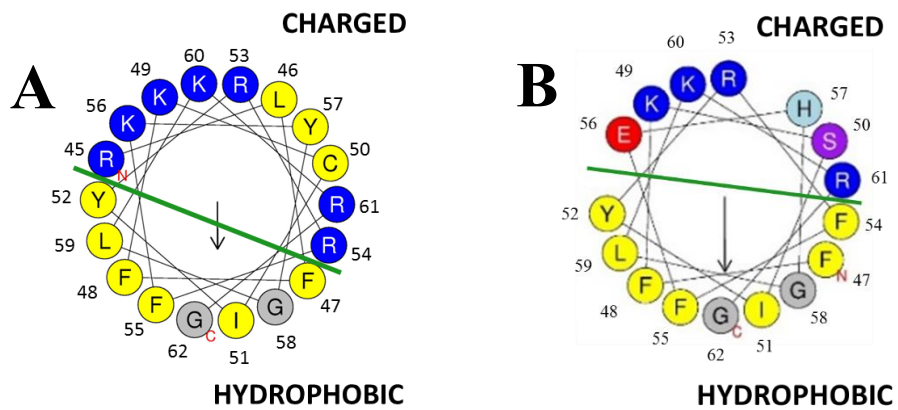


Figure 1. 2 - 3 A and B: Helical wheel plot of the 18 and 16 amino acid long influenza M2 AH based on A/England/09 and A/Udorn/72 strain respectively generated by HeliQuest (Gautier et al. 2008) found at <http://heliquet.ipmc.cnrs.fr/>. Positively charged polar residues are shown in blue, negatively charged polar residues are in red, polar uncharged residues are in purple, glycine is shown in grey, and hydrophobic residues are in yellow. Two faces of the helix are separated by green line.

1.3 VIRION ASSEMBLY

1.3.1 Lipid rafts as site of assembly

Influenza virus assembles and buds from lipid raft domains in the apical plasma membrane of polarized epithelial cells (Takeda et al. 2003, Leser and Lamb 2005, Chen et al. 2007). Lipid rafts are microdomains in the plasma membrane, which are enriched in sphingolipids and cholesterol (Brown 2001). The two viral glycoproteins, HA and NA, are associated with lipid rafts (Takeda et al. 2003, Leser and Lamb 2005, Chen et al. 2007). In contrast, the third viral envelope protein, M2, is excluded from lipid rafts, which may explain its low number in virus particles (Takeda et al. 2003, Leser and Lamb 2005, Chen et al. 2007). The site of viral assembly and budding is thought to be determined by the accumulation of individual viral envelope proteins at a specific site on the membrane. All of the influenza envelope proteins have been shown to accumulate in the apical plasma membrane when they are individually expressed (Roth et al. 1983, Jones et al. 1985, Hughey et al. 1992). However, a single amino acid change in HA cytoplasmic domain caused the protein to be sorted to the basolateral membrane (Brewer and Roth 1991). Later studies showed that basolateral sorting in HA-mutated viruses did not significantly affect the apical budding of the virus. Most of the viral particles containing mutated HA were still budding from the apical plasma membrane (Mora et al. 2002, Barman et al. 2003). This shows that determination of the site of viral assembly and budding depends on multiple factors.

1.3.2 Assembly of the viral envelope proteins

The transport and sorting of viral envelope proteins to lipid rafts in the apical plasma membrane is one of the best known parts of the influenza virus assembly and budding process. These proteins are synthesised by ribosomes bound to the endoplasmic reticulum (ER) and then enter the host cell's secretory pathway. In ER, proteins are folded, HA into trimers and NA and M2 into tetramers, and HA and NA undergo glycosylation. Later they are transported to the Golgi apparatus and in the *cis*-Golgi network cysteine residues on HA and M2 are palmitoylated (Chen et al. 2005). Subsequently, the viral envelope proteins are transported through the *trans*-Golgi network and to the plasma membrane via their apical sorting signals. The signals for

HA and NA have been well characterised and studied in detail (Scheiffele et al. 1997, Barman and Nayak 2000, Zhang et al. 2000, Takeda et al. 2003, Chen et al. 2005). In contrast, the sorting signal for M2 has not been characterised yet.

Both, HA and NA contain two apical sorting signals, one in the ectodomain and second in the TMD. Additionally, the TMD of both glycoproteins contain signals for lipid raft association of the proteins. Analysis of the TMD of NA revealed that an apical sorting signal in this protein was present in multiple regions of the TMD and that a 19 amino acid sequence of the TMD of NA was enough to direct protein to the apical plasma membrane (Barman and Nayak 2000). The same studies had shown that the C-terminal of the NA TMD was involved in lipid raft association. Both signals, for apical transport and lipid raft association, are present in the TMD of NA and overlap each other, however, they are not identical (Barman and Nayak 2000). Other studies have shown that deletion of the CT of NA resulted in reduced lipid raft association of the protein (Zhang et al. 2000). Lipid raft association of HA is mediated by the TMD and CT, which contain three, highly conserved cysteine residues (Scheiffele et al. 1997, Takeda et al. 2003, Chen et al. 2005). Studies showed that mutations in these domains cause loss of lipid raft association of the protein and, consequently, a reduction in viral replication and assembly (Chen et al. 2005). Another study also showed that the CT of HA plays an important role in lipid raft association. Similarly as in case of NA, deletion of the CT of HA decreased lipid raft association but did not affect the apical transport of the protein (Zhang et al. 2000).

Assembly and budding of influenza virus is a complicated process, which depends on multiple factors. Previous studies, using temperature sensitive mutants, have shown that HA is not required for virus assembly and budding from infected cells (Pattnaik et al. 1986). Subsequently, studies of NA-deficient influenza viruses showed that the mutant virus assembles normally but forms large aggregates on cell surface due to lack of enzymatic activity of NA. Additionally, when this mutated virus was administered to mice, low virus titres were recovered and cytotoxic T-cells were generated, indicating that cellular infection had occurred. This suggested that NA is not required for virus entry, replication and assembly but it is essential for virion release (Liu et al. 1995).

In contrast, research using virus-like particle (VLP) system, in which membrane budding is assessed following transfection and expression of individual viral proteins, has shown that, in presence of sialidase activity, HA can be released from cells without need for expression of any other viral protein (Chen et al. 2007). Correspondingly, expression of NA (Lai et al. 2010) and M2 (Chen et al. 2007) alone also caused release of VLPs, which suggest that viral envelope proteins play a role in virus assembly and budding. Moreover, co-expression of all three viral envelope proteins increased VLP release (Chen et al. 2007). Each viral envelope protein can cause budding in a VLP system, but all appear to be required for efficient virus budding. The reasons for the difference between *in vitro* budding system and virus infected cells are not known however, it is probable that in infected cells, presence of additional viral proteins may alter localization and protein interactions comparing to VLP system and have an effect on budding (Martyna and Rossman 2014). Other studies have shown that another viral protein, M2, is essential for virus assembly and budding. Recombinant viruses with deleted M2 protein (Cheung et al. 2005) or mutations in the cytoplasmic tail (McCown and Pekosz 2005, Iwatsuki-Horimoto et al. 2006, McCown and Pekosz 2006) were generated. These mutations caused a decrease in infectious virus titres, a reduction in the amount of packed vRNA and a decrease in virus budding. Additionally, mutation of the cytoplasmic tail of M2 caused a change in viral morphology (Iwatsuki-Horimoto et al. 2006). These data suggest that all three viral envelope proteins play an important role in virus assembly and budding.

1.3.3 Recruitment of the viral core

Whereas, assembly of the viral envelope proteins is a well known process, the knowledge about recruitment of the remaining viral components is relatively low. M1 is the most abundant protein among all viral particle components. It acts as a “bridge” between viral envelope proteins and viral core; therefore it interacts with most of the viral proteins. Previous studies have shown that M1 is a major driving force in influenza budding and it is essential for VLP formation and when expressed alone it assembles into virus-like budding particles (Gomez-Puertas et al. 2000). However, recent studies suggest that M1 by itself fails to form VLPs and interactions of M1 with viral envelope proteins might be essential to direct M1 to plasma membrane and

incorporate into virions (Wang et al. 2010). M1 interacts also with the NEP protein (Ward 1995) and viral RNPs (vRNPs) (Watanabe et al. 1996), however, it does not interact with NP when expressed in the absence of viral infection (Zhao et al. 1998). Details about interactions in M1/RNP complexes are not fully understood. A model has been proposed in which M1 interacts with vRNA to form a M1/RNP complex. It is supported by the fact that vRNP is a helical complex and as a result, part of the vRNA is exposed outside and is accessible for M1 binding.

Additionally, M1 does not interact with NP protein alone (Zhao et al. 1998) and interaction between M1 and vRNPs inhibits transcription (Watanabe et al. 1996). However, other studies have shown that the C-terminal fragment of M1 can bind to the vRNPs but cannot bind to the vRNA and the N-terminal fragment can bind to the vRNA but cannot bind to the vRNPs (Baudin et al. 2001). Moreover, only whole M1 protein, containing C- and N- terminal fragments can inhibit transcription (Baudin et al. 2001). M1 also interacts with itself, which is very important in many aspects of virus budding (Ruigrok et al. 2001). On the other side, the M1 protein interacts with viral envelope proteins. However, initial experiments on direct interaction resulted in contradictory reports. It has been shown that the specific interaction between M1 and glycoproteins does not influence association of M1 with the membrane (Kretzschmar et al. 1996, Zhang and Lamb 1996). In the same time, one report has been published, which showed that membrane association of the M1 protein is stimulated by the CTs of HA and NA (Enami and Enami 1996). In recent studies, a marker for lipid raft association, the insolubility of membrane proteins to Triton X-100 (TX-100)-extraction, was used (Ali et al. 2000). Both glycolipids were associated with lipid rafts and resistant to TX-100-extraction. M1, when expressed alone, was soluble and not associated with lipid rafts, but when co-expressed with HA and NA, M1 became resistant to TX-100, which suggests an interaction between M1 and glycoproteins and an association with lipid rafts. This interaction was specific for influenza virus glycoproteins because when M1 was co expressed with heterologous proteins it was soluble in TX-100 (Ali et al. 2000).

New RNP complexes are assembled in the nucleus and transported to the cytoplasm by M1 and NEP/NS2 proteins. Later M1 and RNPs need to be transported to the assembly site, and the mechanism used is not clear. One of the hypotheses suggests that M1 facilitates vRNP nuclear export and transport to the assembly site

(Bourmakina and Garcia-Sastre 2005). A study of genetically engineered influenza virus, which expressed reduced levels of M1 protein, showed that virus morphology and composition were not affected; however, virus assembly and maturation were delayed in time. This result supported the first hypothesis and suggested that a minimum amount of M1 protein is required for initiation of virus assembly (Bourmakina and Garcia-Sastre 2005). Other studies have shown that M1 interacts with the CT and TMD of HA and NA and that both glycoproteins support the lipid raft association of M1 (Ali et al. 2000, Zhang et al. 2000). Additionally, confocal microscopy revealed that in virus-infected cells M1 partially co-localised with HA. In presence of an exocytic transport inhibitor, HA was present in perinuclear Golgi region and excluded from lipid rafts. Interestingly most of the M1 protein was also associated with perinuclear region, supporting co-localisation of M1 and HA (Ali et al. 2000). Those results suggest that the M1 protein might associate with the viral glycoproteins during exocytic transport, directing M1 to the assembly site, taking RNPs with it. However, another model proposes that M1/RNP complexes use the cytoskeleton to get to lipid rafts and sites of viral budding (Avalos et al. 1997). It has been shown that NP, M1 and M1/RNP complexes interact with cytoskeletal components, mostly actin microfilaments, which might direct them to the viral assembly site (Avalos et al. 1997). An alternative model suggests that RNPs are transported to the assembly site individually, independently of the M1 and viral envelope proteins. This hypothesis is supported by evidence that NP is located in the apical plasma membrane (Mora et al. 2002) and that it is associated with lipid rafts in a cholesterol-dependent manner (Carrasco et al. 2004).

The exact details about interactions between viral proteins, their transport to the assembly site and order of the assembly remain unknown; however, they are important for the influenza assembly and budding process.

1.4 BUDDING AND MEMBRANE SCISSION

Budding is a complex and multi-stage process that is the final step in the virus life cycle. The first stage of this process involves bending of the plasma membrane and forming an outward curvature, initiating formation of the bud. The next step involves assembly and enveloping of the viral core, with the final stage involving constriction of the membrane at the base of the bud leading to membrane scission and release of a virus particle. Membrane budding is significant not only for viruses, but also plays an important role in biological processes. One of the best known cellular processes involving membrane budding is clathrin-mediated endocytosis, in which particles from the plasma membrane or outside the cell are transported to the endosomes in clathrin coated vesicles. Numerous cellular proteins are involved in clathrin-mediated endocytosis including dynamin, epsin and endophilin (McMahon and Boucrot 2011). In the first step, formation of the pit is initiated by binding of the cellular proteins to regions of the plasma membrane that are enriched in phosphatidylinositol 4,5-bisphosphate (PIP₂) (McMahon and Boucrot 2011). While the pit formation is progressing, the particle to be transported is incorporated into it and the coat is assembled with several accessory proteins and clathrin. In the last stage dynamin, together with accessory proteins, is recruited to the neck of the pit and induces constriction of the neck and membrane scission in a guanosine triphosphate (GTP) dependent process (Hinshaw and Schmid 1995, McMahon and Boucrot 2011, Faelber et al. 2012).

Another well studied cellular process involving membrane budding is formation of multi-vesicular bodies (MVBs), which are used to transport damaged proteins from the early endosome to the lysosome where they are destroyed. Damaged proteins are ubiquitinated and transported to the endosome membrane, where they bud inside forming intraluminal vesicles (ILV). MVBs then fuse with lysosomes and ILVs and its content is destroyed (Wollert et al. 2009b). Numerous cellular proteins in the endosomal sorting complex required for transport (ESCRT) machinery regulate sorting of ubiquitinated proteins and membrane budding which leads to formation of ILVs. ESCRT driven membrane scission is a well-known process and molecular details are well described in literature (Carlton and Martin-Serrano 2009, Wollert et al. 2009a, Wollert et al. 2009b). Some viruses, such as human immunodeficiency virus

(HIV), Ebola virus, paramyxovirus PIV-5 and murine leukaemia virus use ESCRT machinery to mediate membrane scission and budding. These viruses encode late domains within their structural proteins which are sequence motifs that are responsible for binding with proteins in ESCRT pathway enabling the virus to use ESCRT machinery for membrane scission and production of new virions (Carlton and Martin-Serrano 2009). Influenza virus has been shown to mediate membrane scission and budding independent from ESCRT machinery with an unknown mechanism (Rossman et al. 2010b).

1.4.1 Assembly and budding

Details about initiation of bud formation are not fully understood, however in a VLP system both HA (Chen et al. 2007) and NA (Lai et al. 2010) can induce budding from cells when expressed alone, as mentioned before (see chapter 1.3.2). These results suggest that HA and NA might be able to induce positive Gaussian curvature (PGC) of the membrane and initiate the budding process. Nevertheless HA and NA are not able to complete *in vivo* budding in virus-infected cells, which may be prevented by assembly of other viral proteins, interactions of M1 with the CT of glycoproteins and recruitment of the vRNPs (reviewed in (Rossman and Lamb 2011)).

Assembly of the virion is the next step in budding process. Newly synthesised vRNP complexes and M1 are transported to the assembly site, followed by recruitment of M2 (Rossman and Lamb 2011). During virus budding, M1 interacts with the CT of both viral glycoproteins and is recruited to the plasma membrane therefore M1 may also be able to alter membrane curvature providing that HA and NA already initiated budding event. M1 interacts with the inside layer of the lipid bilayer (Ruigrok et al. 2001), which could cause bending of the plasma membrane generating PGC and progressing viral bud formation (Rossman and Lamb 2011). It is probable that HA, NA and M1 cooperate to alter membrane curvature and progress virion assembly and budding.

M1 is the most abundant protein in the virion and has additional functions during the virus budding process. Interactions between M1 proteins lead to development of the M1 network, forming interior structure of the virion and may result in exclusion of

the host proteins from the budding site (Ruigrok et al. 2001). It has been shown that size and shape of the viral particles depends on M1. Filamentous virion formation was genetically linked with the M1 protein (Bourmakina and Garcia-Sastre 2003, Elleman and Barclay 2004). Recent work has shown that not only M1, but also M2, and interactions between both proteins, determines production of filamentous virions (Zebedee and Lamb 1988, Zebedee and Lamb 1989, Iwatsuki-Horimoto et al. 2006, McCown and Pekosz 2006, Rossman et al. 2010a). It has been shown that mutation in the M2 amphipathic helix or truncation of M2 to 70 amino acids caused a loss of viral filaments (McCown and Pekosz 2006, Rossman et al. 2010a). It is possible that the region between 70-77 amino acids in the CT of M2 is responsible for binding to M1 and for vRNP integration into virions (McCown and Pekosz 2005, McCown and Pekosz 2006).

In the later stages of virion assembly the M2 protein is incorporated into the budding site. When expressed alone the M2 protein is not associated with lipid rafts however, when expressed with other viral proteins it co-localises with lipid rafts (Rossman et al. 2010a). It is possible that M2 interacts with M1 or HA and results in direction of the M2 protein to the lipid rafts and incorporation into virions (McCown and Pekosz 2006). An additional study has shown that the amphipathic helix of M2 is able to alter membrane curvature in a cholesterol dependent manner (Rossman et al. 2010b). In low cholesterol levels, less than 17 mol %, M2 induces negative Gaussian curvature (NGC) and in high cholesterol levels it has an opposite effect as the M2 AH may not insert as deeply into the membrane (Rossman et al. 2010b, Schmidt et al. 2013). Viral budding site is enriched in cholesterol therefore incorporation of the M2 protein into the site at this stage may prevent strong elicitation of NGC, stabilizing budding site and preventing premature membrane scission.

1.4.2 Membrane scission

The final step in virus budding is membrane scission at the neck of the budding virion. A model of influenza virus budding and release suggests that the M2 protein might be responsible for membrane scission (Rossman et al. 2010b). During budding, M2 localises to the boundary between lipid raft and bulk plasma. Lipid raft domains are used to form new virions and progression of that process lead to non-raft localisation of M2 in the neck of budding virion. In this low cholesterol environment, the M2 protein's amphipathic helix may be inserted deeper into the membrane and cause alterations in its curvature. Induction of NGC in the neck of budding virion may constrict the membrane to a level that will allow spontaneous membrane scission to occur, leading to formation of a new influenza virus particle (Rossman et al. 2010b). These studies also showed that mutation in the amphipathic helix of M2 blocks membrane scission and release of the virus. Mutant virions were not able to complete budding and displayed a "beads on a string" morphology, with many virions in process of budding but unable to be released due to impaired scission (Rossman et al. 2010b). Recent studies, using solid-state nuclear magnetic resonance (NMR) spectroscopy confirmed that M2 amphipathic helix alters membrane curvature (Wang et al. 2012). It was also shown that the M2 AH binds to lipid domains with high curvatures and that this binding can cause lipid head group disruptions (Wang et al. 2012). Additionally, research using small angle X-ray scattering has shown that M2 is able to generate NGC in lipid membranes (Schmidt et al. 2013). Consistent with previous results, reduction in the hydrophobicity of the AH by amino acid substitution resulted in an inhibition M2's ability to alter membrane curvature (Schmidt et al. 2013). Although the M2 AH was necessary and sufficient to generate NGC, the presence of the M2 TMD enhanced the M2 AH-induction of NGC, suggesting that the TMD may affect AH activity, facilitating membrane curvature changes (Schmidt et al. 2013). It has been shown, that mutation of the CT of the M2 protein causes massive reduction in infectious virus titer and decrease in budding efficiency but it doesn't cause complete inhibition of virus release (McCown and Pekosz 2005, McCown and Pekosz 2006). This suggests that other cellular factors, may be involved in the budding process or may function as redundant scission factors (Martyna and Rossman 2014). It has been shown that influenza virus requires a number of host factors, such as adenosine triphosphate (ATP), G protein and casein kinase 2 for effective budding (Hui and

Nayak 2001, Hui and Nayak 2002). Another study showed that cellular GTP-binding protein, Rab11 together with Rab11-family interacting protein 3 supports formation of filamentous particles. Additionally, the Rab11 protein might be involved in final budding steps of spherical particles (Bruce et al. 2010). Further studies are required to determine the molecular mechanism of membrane scission and exact role of the M2 AH and cellular factors in it.

1.4.3 Model of influenza budding

An overall influenza assembly and budding model suggest that several virus proteins mediate the process, rather than a single one. HA and NA are transported to the lipid rafts, where they concentrate (Fig. 1.4-1 A). This molecular crowding may cause alteration of membrane curvature and initiation of the budding event. M1 may then be recruited to the site by interacting with the cytoplasmic tails of HA and NA (Fig. 1.4-1 A). Membrane bound M1 can polymerise and form the inner structure of the virion (Fig. 1.4-1 B), excluding host proteins from the budding site. Additionally, M1 may alter membrane curvature to progress the budding event; however, recruitment of vRNPs and M2 by M1 may block completion of budding process (Fig. 1.4-1 A and B). Recruitment of M2 to the budding site, which is a cholesterol rich environment, can cause stabilisation of the site and allow for proper assembly of the virion. In the later stages of budding M2 can be localised to the neck of the budding virion, in the boundary between lipid rafts and the bulk plasma membrane phase, which is a low cholesterol environment. Insertion of the amphipathic helix in to the membrane may cause NGC and in this localisation may cause membrane scission (Fig. 1.4-1 C). Despite many years of research, many aspects of Influenza A virus assembly and budding are not known. The order of viral protein assembly, interactions between them and their role in proper assembly of the virion as well as their influence on initiation and progression of viral budding are not fully understood. It has been proposed that membrane curvature may be altered in two ways: by disrupting the line tension between the two lipid phases or disruptions in the packing of the lipid membrane (Rossman et al. 2010b). However, the exact molecular mechanism of the M2 amphipathic helix mediated membrane scission, the interaction with the membrane and the role of the cytoplasmic tail in this process is not clear.

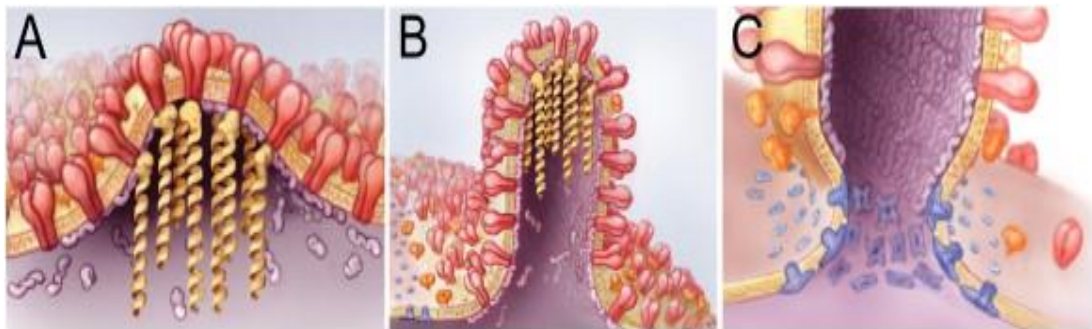


Figure 1.4 - 1 Model of influenza virus budding. A) The initiation of virus budding caused by clustering of HA (red) and NA (orange) in lipid raft domains. M1 (purple) binds to the cytoplasmic tails of HA and NA and serves as a docking site for the vRNPs (yellow). B) Elongation of the budding virion caused by polymerization of the M1 protein. M2 (blue) is recruited to the periphery of the budding virus through interactions with M1. C) Membrane scission caused by the insertion of the M2 amphipathic helix at the lipid phase boundary, altering membrane curvature at the neck of the budding virus and leading to membrane scission. Adapted from Rossman and Lamb 2011.

1.5 AIMS OF THE PROJECT

The main aim of this research project was to investigate molecular mechanisms of membrane scission, which is the last stage of influenza virus assembly and budding, mediated by the M2 protein, starting by determining the structure of the M2 AH in different environments and its interactions with membranes. The studies were to investigate how different properties of the membrane affect functions of the M2 AH and the changes to the lipid membranes introduced by the M2 AH. Budding mediated by the M2 AH both *in vitro* and *in vivo* was then investigated. This will allow for better understanding of influenza virus assembly and budding.

2. MATERIALS AND METHODS

2.1 MATERIALS

2.1.1 Peptides

Peptides were synthesized by GenScript (NJ, USA) or Biomatik (DE, USA) at 95% purity, with trifluoroacetic acid (TFA) removed. Peptide sequences, introduced mutations and modifications such as N-terminal acylation and C-terminal amidation where indicated are listed in Table 2.1-1. All peptides were dissolved in MiliQ water to form a 1 mM stock concentration and stored at -20°C. Fluorescent M2 AH peptide, based on the A/Udorn/72 strain, incorporates fluorescein isothiocyanate (FITC) conjugated to residue K60.

Peptide	Length	Sequence	Source	Mutations	Purpose of the mutation	Reference
M2 AH (47-62 of A/Udorm/72)	16	Ac-FFKSIYRFFEHLKRG-Am	Biomatik	C50S	To avoid oxidation of the cysteine	This project
M2 AH (46-62 of A/Udorm/72)	17	Ac-LFFKCIYRFFEHLKRG-Am	GenScript			This project
M2 AH FITC (47-62 of A/Udorm/72)	20	Ac-FFKSIYRFFEHLKRGGGG-Lys(FITC)	Biomatik	C50S	To avoid oxidation of the cysteine	This project
M2 AH (47-62 of A/England/09)	16	Ac-FFKSIYRFRFKYGLKRG-Am	Biomatik	C50S	To avoid oxidation of the cysteine	This project
M2 AH (45-62 of A/England/09)	18	Ac-RLFFKCIYRFRFKYGLKRG-Am	GenScript			This project
M2 AH F47A F48A (45-62 of A/England/09)	18	Ac-RLAAKCIYRFRFKYGLKRG-Am	GenScript	F47A F48A	Weakening of the hydrophobic face of the helix	This project
M2 AH CRAC (45-62 of A/England/09)	18	Ac-RLFFKCIAAARFKYGLKRG-Am	GenScript	Y52A R53A	Disruption of the cholesterol recognition amino acid consensus (CRAC) domain	This project
M2 AH 5 PM (45-62 of A/England/09)	18	Ac-RLAAKCAARRAKYGLKRG-Am	GenScript	F47A F48A I51A Y52A F55A	Disruption of the helix, growth impairment	(Rossman et al. 2010a)

M2 AHL46K C50K Y57K (45-62 of A/England/09)	18	Ac-RKFFKKIYRRFKKGLKRG-Am	GenScript	L46K C50K Y57K	Enhancement of the polar face of the helix	This project
M2 AH K49A K56A K60A (45-62 of A/England/09)	18	Ac-RLFFACIYRRFAYGLARG-Am	GenScript	K49A K56A K60A	Weakening of the polar face of the helix	This project
M2 AH R54A R61A (45-62 of A/England/09)	18	Ac-RLFFKCIYRAFKYGLKAG-Am	GenScript	R54A R61A	Weakening on the helix interface	This project
M2 AH +A (45-62 of A/England/09)	19	Ac-ARLFFKCIYRRFKYGLKRG-Am	GenScript	+A	Disruption of the helix phase	This project
M2 AH +AA (45-62 of A/England/09)	20	Ac-AARLFFKCIYRRFKYGLKRG-Am	GenScript	+AA	Disruption of the helix phase	This project
Arf1	18	MGNIFANLFGKLFKEM-Am	GenScript			This project
CHMP4b	13	MSVFGKLFAGGGG-Am	GenScript			This project
Endophilin A3	21	MSVAGLKKQFHKASQL FSEKI-Am	GenScript			This project
Epsin1	17	MSTSSLRRQMKNIHNY-Am	GenScript			This project

Table 2. 1 – 1 Characteristics of peptides used during this study.

2.1.2 Lipids

Lipids used in this studies were purchased from Avanti Polar Lipids (AL, USA) or Sigma-Aldrich (MO, USA). All lipids were dissolved in chloroform and stored at -20°C under an overlay of argon gas to prevent oxidation. Full details are shown in Table 2.1-2.

Short name	Full name	Structure	Source (catalogue number)
POPC PC	1-palmitoyl-2-oleoyl-sn-glycero-3-phosphocholine		Avanti (850457C), Sigma-Aldrich (P3017)
POPG PG	1-palmitoyl-2-oleoyl-sn-glycero-3-phospho-1-rac-glycerol		Avanti (840457C)
POPA PA	1-palmitoyl-2-oleoyl-sn-glycero-3-phosphate		Avanti (840857C)
POPS PS	1-palmitoyl-2-oleoyl-sn-glycero-3-phospho-L-serine		Avanti (840034C)
POPE PE	1-palmitoyl-2-oleoyl-sn-glycero-3-phosphoethanolamine		Avanti (850757C)
PIP2 PI(4,5)P2	L-α-phosphatidylinositol-4,5-bisphosphate		Avanti (840046X)
TopFluor PIP2	1-oleoyl-2-[6-(4-(dipyrrrometheneboron difluoride)butanoyl)amino]hexanoyl-sn-glycero-3-phosphoinositol-4,5-bisphosphate		Avanti (810184P)
DEPC	1,2-dierucoyl-sn-glycero-3-phosphocholine		Avanti (850398C)
DeisPC	1,2-dieicosenoyl-sn-glycero-3-phosphocholine		Avanti (850396C)
DOPC	1,2-dioleoyl-sn-glycero-3-phosphocholine		Avanti (850375C)
DPPC	1,2-dipalmitoleoyl-sn-glycero-3-phosphocholine		Avanti (850358C)
DMPC	1,2-dimyristoleoyl-sn-glycero-3-phosphocholine		Avanti (850346C)

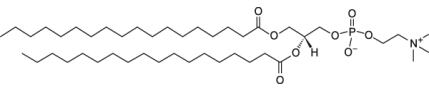
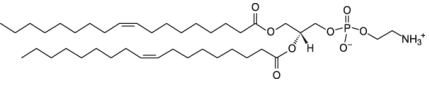
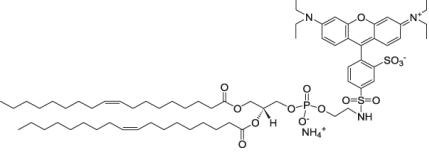
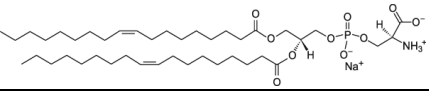
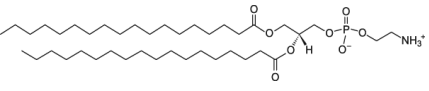
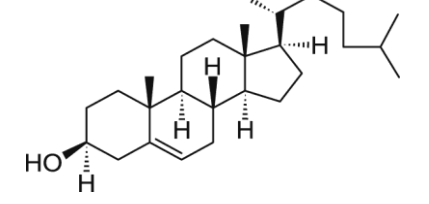
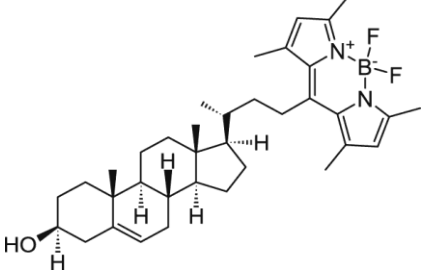
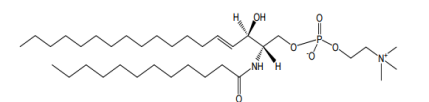
DSPC	1,2-distearoyl- <i>sn</i> -glycero-3-phosphocholine		Avanti (850365C)
DOPE	1,2-dioleoyl- <i>sn</i> -glycero-3-phosphoethanolamine		Avanti (810150C)
RhoPE	1,2-dioleoyl- <i>sn</i> -glycero-3-phosphoethanolamine-N-(lissamine rhodamine B sulfonyl)		Avanti (810150C)
DOPS	1,2-dioleoyl- <i>sn</i> -glycero-3-phospho-L-serine		Avanti (840035C)
DSPE	1,2-distearoyl- <i>sn</i> -glycero-3-phosphoethanolamine		Sigma- Aldrich (P3531)
Ch	Cholesterol		Avanti (700000P) Sigma- Aldrich (C8503)
TopFluor	23-(dipyrrrometheneboron difluoride)-24-norcholesterol		Avanti (810255P)
SM	Sphingomyelin		Avanti (860061C)

Table 2. 1 - 2 Characteristics of lipids used in this study. Structures adapted from <http://www.avantilipids.com/>.

2.1.3 Cells, plasmids, viruses and antibodies

Madin-Darby canine kidney (MDCK) cells and human embryonic kidney 293T (HEK 293T) cells used in this study were as described previously (Chen et al. 2008). Cells were grown in T-75 cm² flasks with vented caps (Sarstedt, Germany) at 37°C in 5% CO₂ in Dulbecco's Modified Eagle Medium (DMEM) (Gibco) with 10% fetal bovine serum (FBS) (Gibco) and 1% Penicillin-Streptomycin (Sigma-Aldrich). Subculturing of cells was performed by removing the growth medium from the confluent flask of cells and washing with 5 ml of phosphate buffered saline (PBS). The buffer was subsequently removed and replaced with 3 ml of TrypLE Express (Gibco), followed by incubation for 10-20 min at 37°C in 5% CO₂ until all cells had detached from the flask. 7 ml of DMEM was then added to the flask and the sample was then transferred to a sterile 15 ml falcon tube (Sarstedt, Germany) and centrifuged for 10 min at 1000 revolutions per minute (rpm) in a Heraeus Megafuge 40R (Thermo Scientific) to pellet the cells. After centrifugation, the supernatant was removed and the cells were resuspended in 10 ml of DMEM and seeded in new flask at the desired concentration.

Two pCAGGS plasmids (map shown in appendix 6.1) encoding either wild type M2 protein from Influenza A/Udorn/72 strain or M2 5PM protein which has 5 point mutations in AH were used (as described in chapter 2.1.1) (Rossman et al. 2010a).

The Influenza A/Udorn/72-ΔM2 recombinant virus (Jackson and Lamb 2008, Rossman et al. 2010a) and anti M2 monoclonal antibody, 14C2 (Zebedee and Lamb, 1988) used in this study were as previously described.

2.1.4 Oligonucleotides

Oligonucleotides were synthesised by Eurofins Genomics (Ebersberg, Germany) with features shown in Table 2.1-3. All oligonucleotides were designed to bind to the M gene segment of the Influenza A/Udorn/72 strain, either to the untranslated region (UTR) or to the middle part of the gene.

Oligonucleotide	Sequence (5'-3')	Tm [°C]	Molecular Weight	Orientation	Binding place
M_UTR_F	CAAAAGCAGGTA GATATTGAAAG	55.3	7153	Forward	UTR in the front of the M gene
M_UTR_R	TTAGTAGAAACAA GGTAGTTTT	50.9	6812	Reverse	UTR in the end of the M gene
M_F2	CTCATATACAACA GGATGGG	55.3	6150	Forward	Middle position (413-432) in the M gene

Table 2. 1 - 3 Characteristics of oligonucleotides used in this study.

2.2 METHODS

2.2.1 Liposomes

2.2.1.1 Small Unilamellar Vesicles (SUVs)

SUVs were made by sonication of Multilamellar Vesicles (MLVs). To form MLVs, a lipid solution containing 12.5 μ moles of lipids (Avanti and Sigma-Aldrich) was made using indicated lipid compositions at the required molar ratio. The solution was dried under a stream of argon gas followed by drying in a desiccator in a vacuum for 1 h to remove residual chloroform. Lipid films were then dissolved in 500 μ l of potassium buffer (10 mM K_2HPO_4 , 50 mM K_2SO_4 , 5m M MOPS, pH 7.4) and hydrated for 30 min at a temperature above the phase transition temperature for each particular lipid mix (37°C for standard mixes, 65°C for phase separated vesicles and 80°C for mixes containing DSPE) with vortex mixing every 5 min. MLVs were then sonicated by water bath (Fisherbrand, FB15046) or by probe sonication (Soniprep 150, MSE) to form SUVs. For water bath sonication samples were sonicated at 10 min intervals, until solution changed from milky to nearly clear, usually up to 30 min. For probe sonication samples were placed on ice and were sonicated at an amplitude of 10-12 microns for 10-15 cycles consisting of 1 min sonication followed by 30 s cooling break each. SUVs were stored at 4°C for up to 24 h.

2.2.1.2 Large Unilamellar Vesicles (LUVs)

LUVs were made by extrusion of the MLVs, which were made as described above. MLVs were freeze-thawed 15 times using dry ice, in an ethanol bath, and water bath set to the hydration temperature for the lipid mix. LUVs were extruded (Avanti Mini-Extruder, Avanti Polar Lipids) 26 times with different size filter membranes (Nuclepore Track-Etched Membranes, Whatman) at hydration temperature. LUVs were stored at 4°C for up to a week. Standard LUVs used throughout this study were composed of phosphatidylcholine (PC), phosphatidylglycerol (PG) and cholesterol (Ch) at 4:1:0.05 molar ratio, were hydrated at 37°C and extruded through 100 nm filter membrane.

2.2.1.3 Giant Unilamellar Vesicles (GUVs)

GUVs were made by electroformation, as previously described in the literature (Veatch 2007, Manley and Gordon 2008). A 1 mg/ml lipid solution (Avanti and Sigma-Aldrich) was made using indicated lipid compositions at the required molar ratio and spread onto the conductive side of two indium tin oxide coated slides (15-25 Ω /sq surface resistivity, Sigma-Aldrich) at 1 μ l/cm² (6.4 μ l at 6.4 cm²). Lipids were then dried in a desiccator in a vacuum for 1 h. Lipid coated slides were sandwiched together using FastWell 9 mm spacer (Grace Bio-Labs reagent barriers, Sigma-Aldrich) and 70 μ l of hydration buffer (0.1 M sucrose, 1 mM HEPES, pH 7.2). Chamber was then connected to the function generator (Gw Instek SFG-1013 DDS function generator) using copper tape and lipids were electroformed by applying 10 Hz sine wave at 1 V for 4 h. After electroformation GUVs were recovered from the chamber using wide-bore pipette tip and used within 4 h.

2.2.1.4 Dynamic Light Scattering (DLS)

Vesicle size was measured using Zetasizer (nano series, Malvern Instruments Worldwide). 4 μ l of vesicles were mixed with 32 μ l of water, measurements were done in micro cuvettes (ZEN0040, Malvern Instruments Worldwide) at 25°C.

2.2.2 Nuclear Magnetic Resonance (NMR) Spectroscopy

NMR spectroscopy experiments were performed as previously described (Lawrence et al. 2014) in collaboration with Dr Mark Howard and Dr Michelle Rowe from University of Kent. Peptide structural studies were conducted using samples that had total volume of 330 μ l and contained 500 μ M of the 16 amino acid long M2 AH peptide based on the A/Udorn/72 strain and, where indicated, 10 μ M of standard LUVs in water with 10% of deuterium oxide. Samples were placed in 3 mm glass tubes (Shigemi) and data was collected using a 14.1 T (600 MHz ¹H) Bruker Avance III NMR spectrometer with QCI-F cryoprobe at 25°C. Total correlation spectroscopy (TOCSY) and Nuclear Overhauser effect spectroscopy (NOESY) data sets were obtained in a two-dimensional (2D) NMR experiment and were assigned using CCPN

Analysis (Vranken et al. 2005). Structural ensembles were calculated using CNS (Brunger et al. 1998). ^1H chemical shifts and through-space structural assignments were acquired from TOCSY and NOESY data sets. Dihedral angles were estimated using DANGLE (Cheung et al. 2010), which is a built-in module in CCPN Analysis. Hydrogen bonds were estimated using the software MOLMOL (Koradi et al. 1996) by analysing the calculated structure and distance between oxygen and nitrogen-bound hydrogen atoms and were added for the pairs of atoms that were less than 3 Å apart. The final ensemble was energy minimised in a water environment using YASARA software (available from <http://www.yasara.org>). The precision and quality of the calculated structures was checked by series of statistical analyses, including Ramachandran analysis, using PROCHECK (Laskowski et al. 1993) software.

Saturation-transfer difference (STD) NMR studies were performed using 500 μM of the 16 amino acid long M2 AH peptide based on the A/Udorn/72 strain and, where indicated, 10 μM of standard LUVs in water with 10% of deuterium oxide. The experiment was performed with 3-9-19 WATERGATE and Gaussian STD excitation pulses of 20 ms duration and a γB_1 of 140 Hz that were applied for 2 s at -3 ppm and -30 ppm for saturation and control respectively. ^1H T_1 relaxation time constants were obtained using an inversion-recovery sequence, including 3-9-19 WATERGATE. To obtain T_1 inversion-recovery 180° - τ - 90° delays in 0.1 s steps between 0.2 and 0.1 s were used. Quantitative STD NMR amplification factors were obtained from ^1H T_1 values using previously described GEM-CRL method. Intensities for STD and T_1 relaxation experiments were obtained using Spectrus Processor (ACD Laboratories).

2.2.3 Peptide binding assay

Various concentrations of peptide and lipids were tested to determine which one gives the best signal, as described in chapter 3.2.2, and the procedure described below is based on the best conditions determined in the optimization process. 100 μM of M2 AH FITC labelled peptide was mixed with 2.5 mM of indicated lipids and water to a final volume of 50 μl . Controls were made with 100 μM of M2 AH FITC labelled peptide and water. Samples were incubated for 1 h at room temperature in the dark. After incubation samples were filter washed twice: 450 μl of water was added before the samples were moved to 100 K centrifugal filters (Amicon Ultra, Merck Millipore)

and centrifuged at 14000 rpm in a bench top centrifuge (Eppendorf, rotor FA-45-18-11) until 100 μ l of the sample was remaining in the filter. 50 μ l of the samples or blank (water and vesicles buffer) were transferred to a 96-well plate (black walls and clear bottom) and the fluorescence was checked on a fluorescence plate reader (FLUOstar Omega, BMG LABTECH) with the excitation filter at 492 nm and emission filter at 520 nm. All data was blank corrected before processing.

2.2.4 Circular Dichroism (CD) Spectroscopy

Various concentrations of peptide and lipids were tested to determine the optimal peptide:lipid ratio, as described in chapter 3.2.3.1, and procedure described below is based on the best conditions determined in the optimization process. 250 μ M of indicated peptide and 5 mM of lipids, where indicated, were mixed with water to final volume of 300 μ l. Blank readings were taken using water or vesicles in water, for peptide in solution and peptide with lipids respectively. Where indicated 30% of 2,2,2-trifluoroethanol (TFE) was added to the samples and blanks, keeping total volume the same. All measurements were performed in quadruplicates on a JASCO spectropolarimeter (JAS.CO; J-715) using a 1 mm path length glass cuvette (Starna Scientific) at 25⁰C. Respective blank measurements were subtracted from all samples and percentage of the helix was estimated using K2D3 online bioinformatics tool (Louis-Jeune et al. 2012) found on <http://k2d3.ogic.ca/>.

2.2.5 Immunofluorescence microscopy

HEK 293T cells were grown on glass cover slips and transfected with 2.5 μ g of M2-pCAGGS plasmid using TransIT-293 transfection reagent (Mirus). After 47 h post transfection 1 μ M of fluorescently labelled PIP2 was added to the cells and incubated for 1 h at 37⁰C in 5% CO₂. After 48 h post transfection cells were washed with PBS, fixed in 10% formalin:PBS for 10 min and treated with blocking solution (DMEM with 10% FBS) for 20 min. Cells were then stained for M2 using monoclonal 14C2 antibody at a 1:400 dilution for 1 h, as primary antibody without permeabilisation, followed by four washes with PBS. Alexa 680, donkey anti-mouse antibody was used as a secondary antibody for 1 h at a 1:200 dilution followed by four washes with PBS.

Coverslips with cells were then mounted on the slides using 12 μ l of Prolong Gold (Invitrogen) and left in the dark for 12 h to set. Slides were imaged on a Leica confocal microscope (SP2) using a 63x oil objective with a 488 nm argon laser and a 633 nm helium-neon laser at 25% power, with a 496-525 emission filter for fluorescently labelled PIP2 and a 685-730 emission filter for M2 protein.

2.2.6 Molecular Dynamics Simulations

Molecular Dynamic Simulations were used to study the interaction between the M2 AH peptide and a buckled membrane. Coarse-grained simulations and the analysis protocol for simulating curvature sensing by single peptides was performed as previously described (Gómez-Llobregat et al. 2016) by collaborators, Dr Jordi Gómez-Llobregat and Dr Martin Lindén at Stockholm University using the Swedish National Infrastructure for Computing at the National Supercomputer Centre.

2.2.6.1 Simulation parameters

Coarse-grained simulations were performed using GROMACS 4.6.1 (Pronk et al. 2013) and the MARTINI force-field (version 2.P) with polarizable water (Kawaoka and Neumann 2012, Kikuchi et al. 2012, Neumann et al. 2012), and a relative dielectric constant of 2.5 (Kawaoka and Neumann 2012). Standard parameters were used for lipids POPC and POPG (Nidom et al. 2012, Victor et al. 2012) and for peptides (Murakami et al. 2012). The M2AH peptide structure was obtained from PDB 2L0J (Sharma et al. 2010), and was coarse-grained with the martinize script provided by the MARTINI developers. Constant temperature was maintained with the velocity rescaling thermostat (Kawai et al. 2012) with a 1.0 ps time constant, and pressure was controlled with the Berendsen barostat (Shi et al. 2012) using a time constant of 12 ps and a compressibility of $3 \times 10^{-4} \text{ bar}^{-1}$. Peptide (when present), lipids and solvent were coupled separately to the temperature bath. Coulomb interactions were modelled with the particle mesh Ewald method (Noda et al. 2012) setting the real-space cut to 1.4 nm and the Fourier grid spacing to 0.12 nm. Lennard-Jones interactions were shifted to zero between 0.9 and 1.2 nm. A time step of 25 fs was used in all simulations.

2.2.6.2 Lipid bilayer equilibration

First two coarse-grained symmetric lipid bilayers twice as large than wide ($L_x = 2L_y$) were built, consisting of 1024 lipids, one with a 4:1 molar ratio of POPC:POPG and another with POPC-only. The systems were solvated with $\approx 21,250$ coarse-grained water beads and neutralised with sodium and chloride ion beads. The bilayer systems were then equilibrated for 25 ns in an NPT ensemble at 300 K and 1 bar, with pressure coupling applied semi-isotropically.

2.2.6.3 Membrane buckling and peptide addition

After equilibration, both systems were laterally compressed in the x direction by a factor $\gamma = (L - L_x)/L = 0.2$, where L is the linear size of the flat system in the x direction, and L_x the size of the simulation box in the x direction. This was done by scaling all x-coordinates, and the system size L_x , by a factor $1 - \gamma = 0.8$ at the end of the equilibration run, yielding $L_x = 21.03$ and 20.93 nm for the mixed and pure membrane patches, respectively. After rescaling, the compressibilities were set to 0 in the x and y directions to keep the system size constant in those directions for subsequent simulations. Pressure coupling was then applied anisotropically in the z direction only. An energy minimisation and a short equilibration run (25 ns) was then performed to let the bilayer buckle. Next the M2 AH peptide was added to each system. The peptide was initially placed 3 nm above the membrane surface, but quickly attached to the membrane-water interface. After the binding event, the system was equilibrated for another 5 μ s before starting a production run of 35 μ s, where the data was collected every 5 ns.

2.2.6.4 Membrane alignment and peptide tracking

The buckled membrane profile diffuses during the simulation, but curvature sensing by the M2AH peptide is reflected in its distribution relative to the buckled shape, and the buckled configurations must therefore be aligned in order to extract useful information. Previous protocol (Gómez-Llobregat et al. 2016) was used to fit the xz profile of the membrane by the ground state of the Helfrich model with periodic boundary conditions, which is one of the Euler buckling profiles of an elastic beam

(Shinya et al. 2012, Hu et al. 2013). This shape depends only on the dimensionless buckling parameter γ , where $\gamma = 0$ is the flat state. Thus, if one period of the buckling profile for $L_X = 1$ is given by a parameter curve $x = s + \xi(s, \gamma)$, $z = \zeta(s, \gamma)$, $0 < s < 1$, the general case $L_X \neq 1$ can be obtained by shifting and scaling. For fast evaluation, $\xi(s, \gamma)$ and $\zeta(s, \gamma)$ were expanded in truncated Fourier series in s , and created look-up tables for Fourier coefficients versus γ . The arc-length coordinate s was scaled to have period one independent of the overall system size, and defined such that the curve $z(x)$ has a maximum at $s = 0.5$, minima at $s = 0, 1$, and inflection points at $s = 0.5 \pm 0.25$. The buckled shapes were aligned by fitting the bilayer in each frame to the buckling profile and aligning the inflection points. Specifically, the buckling profile was fit to the innermost tail beads of all lipids in each frame using least-squares in the x and z directions, i.e., minimising

$$\sum (x_0 + L_x(s + \xi(s_i, \gamma)) - x_i)^2 + (z_0 + L_x\zeta(s_i, \gamma) - z_i)^2$$

with respect to γ , the translations x_0 , z_0 , and the projected arc-length coordinates s_i of each bead (x_i , z_i are bead positions). The arclength position s of the peptide was computed by projecting the peptide centre of mass onto the buckled profile fitted to the membrane midplane in every frame (Fig. 3.3-19 B). The in-plane orientation γ was computed by fitting a line through the backbone particles of the alpha-helical part of the peptide and projecting this line to the tangent plane defined by the tangent vector t and the y unit vector, taking γ to be the angle between the projected line and the tangent vector, in the tangent plane. Variations in the buckling parameter ($\text{std}[\gamma] \approx 0.005$) reflect small shape and area fluctuations, that was neglected by using the average buckling parameter values for curvature analysis, $[\gamma] = 0.216$ and $[\gamma] = 0.225$ for the POPC:POPG and pure POPC systems, respectively. The local curvature, shown in Figure 3.3-19 D, is then given by $C(s) = (1 - [\gamma]) / L_x \, d\Psi / ds$, where Ψ is the tangent angle in Figure 3.3-19 B (also computed using average compression factors). Molecular graphics were generated using Visual Molecular Dynamics (VMD) (Langel et al. 2008).

2.2.7 Laurdan assay for membrane order

Various peptide concentrations, lipids:dye ratios and total volumes of the samples were tested to determine the best conditions for this type of assay, as described in chapter 3.4.2.1, and the final protocol is outlined below. 2.5 mM of indicated lipids were mixed with Laurdan dye (life technologies) at 1:100 dye:lipid ratio and 200 μ M of indicated peptide, the volume was made up to 50 μ l with water. Control samples were made in the same way, without adding peptide. Samples were then transferred to a 96-well plate (white walls and bottom) and the fluorescence was checked on a fluorescence spectrophotometer (Cary Eclipse, VARIAN) with the excitation filter set at 355 nm and emission filters at 440 and 490 nm. Generalised polarisation (GP) value was calculated using equation: $GP = (I_{440} - I_{490}) / (I_{440} + I_{490})$ (Parasassi et al. 1990, Sanchez et al. 2007).

2.2.8 Differential Scanning Calorimetry (DSC)

MLVs were made as described before (chapter 2.2.1.1) using 13 mmoles of DSPC lipid and 1 mM HEPES buffer (pH 7.2) to reconstitute lipid films containing, where indicated, 650 μ M of the M2 AH peptide, giving a 10 mg/ml lipid solution and a peptide : lipid ratio of 1:20. MLVs were formed following 30 min of hydration at 60^oC with regular vortexing. Samples were then analyzed on a Phox 200PC DSC (Netzsch, Germany) using sealed aluminum crucibles under nitrogen gas. All runs were corrected to a baseline run using empty crucibles. Samples were scanned from 35^oC – 75^oC at a rate of 10 K/min with 2 min isothermal holds at the end of each run. All samples were scanned four times, with the first scan discarded. Subsequent scans were compared to ensure consistency in the identified lipid T_m. After each sample run, crucibles were weighed to ensure no weight loss, and thus no sample loss, had occurred. Netzsch Proteus Analysis software was used to graph the first differential of the data and to identify T_m peaks through the automatic peak calling function near the 55^oC T_m of DSPC.

2.2.9 Transmission Electron Microscopy (TEM)

5 mM of standard LUVs were incubated with increasing concentrations of the M2 AH peptide for 1 h at room temperature and stained with uranyl acetate before imaging. Samples were imaged on a JEOL 1230 (Tokyo, Japan) electron microscope using a Gatan digital camera (CA, USA). Post image processing was limited to cropping and equal adjustment of image levels.

2.2.10 GUV budding system

GUVs composed of PC, PG and fluorescently labelled cholesterol (TopFluor, Avanti) at 4:1:0.05 molar ratio were formed as described in chapter 2.2.1.3. 5 μ l of GUVs were diluted 1:100 in resuspension buffer (0.1 M glucose, 1 mM HEPES, pH 7.2) and placed in the well of the Nunc Lab-Tek II chamber slides (Thermo Fisher Scientific, Rochester, NY) that had been blocked with 1% Bovine serum albumin (BSA) for 1 h before use followed by three washes with PBS. 0.5 mg/ml of Lucifer Yellow (Sigma) and, where indicated, 10 mM of indicated M2 AH peptide was added to the GUVs resuspension. The content of each well was gently mixed by pipette tip and incubated for 45 min in the dark prior to imaging on a Leica confocal microscope (SP2) using a 63x oil objective with a 488 nm argon laser at 25% power, a 496-525 nm emission filter for TopFluor and a 530-580 nm emission filter for both TopFluor and Lucifer Yellow. Quantification of the budding effect was performed by determining the percentage of GUVs that were containing at least one Lucifer Yellow positive intralamellar vesicle (ILV) and the percentage of GUVs that leaked and were filled with Lucifer Yellow. For each sample total number of at least 200 vesicles 10 μ m and above in diameter were counted.

2.2.11 GUV microinjection system

GUVs composed of PC, PG and fluorescently labelled cholesterol (TopFluor, Avanti) at 4:1:0.05 molar ratio were formed as described in chapter 2.2.1.3 using adjusted hydration buffer (0.2 M sucrose, 1 mM HEPES, 0.2 mM EDTA, pH 7.4). 5 μ l of GUVs were diluted 1:100 in resuspension buffer (0.1 M KCL, 1 mM HEPES, 0.2 mM EDTA, pH 7.4) and placed in the FluoroDish with glass bottom (World Precision Instruments) that had been blocked with 1% BSA for 5 min before use, followed by three washes with PBS. A solution of 1 mM 16 amino acid long M2 AH peptide based on the Udorn strain was loaded into the ICSI-Plus non-spiked injection needle (Research Instruments) that had been blocked with 1% BSA for 1.5 h before use followed by three washes with PBS using MicroFil syringe needle for filling micropipettes (World Precision Instruments). The peptide was injected next to the GUVs using the Tritech Research Microinjector System (Narishige Group, Intracel) and an automated pipette holder (Sensapex) whilst imaging on a Lumascope 620 (Etaluma) using 40x Olympus objective with blue LED light a 473-491 excitation filter and a 502-561 emission filter (channel 2).

2.2.12 Supported bilayers with excess membrane reservoir

(SUPER) templates system

SUPER templates experiments were done in collaboration with Dr Saipraveen Srinivasan from University of Texas. Samples were prepared as previously described (Neumann and Schmid 2013), using SUVs composed of DOPC, DOPS, PIP₂ and RhPE at 79:15:5:1 molar ratio prepared as described in chapter 2.2.1.2 using MilliQ water instead of hydration buffer. 200 μ M SUVs were mixed with 2.5 μ m silicon microspheres (Corpuscular) in potassium buffer (150 mM KCl buffer, 20 mM HEPES, pH 7.5) to total volume of 100 μ l. After 30 min incubation at room temperature templates were washed by addition of 1 ml of potassium buffer followed by centrifugation at 260 g for 2 min in bench top centrifuge (Eppendorf) and discarding 1ml from the supernatant. Washes were repeated 4 times in total and after the final wash only 850 μ l has been removed instead of 1 ml. 150 μ l of template solution was

then treated with 0.5 μ M Amphiphysin I, where indicated, and incubated for 30 min in the presence or absence of 25 μ M M2 AH or the 5 point mutant M2 AH peptide. Samples were then centrifuged at 260 g for 2 min in bench top centrifuge. The supernatant was removed and observed for released vesicles via fluorescence measurements in a plate reader set to look at Rhodamine fluorescence following treatment with 0.1% Triton-X and compared to the total lipid present in the remaining templates, determined by dissolving the SUPER templates in 0.1% Triton-X before measurement.

2.2.13 Immunoblotting

HEK 293T cells were grown in 6 well plates and transfected, where indicated, with 2.5 μ g of M2-pCAGGS plasmid, M25PM-pCAGGS plasmid and an empty pCAGGS plasmid using TransIT-293 transfection reagent (Mirus). At 48 h post transfection the media were harvested by pouring into a 15 ml Falcon tube and centrifuging at 3000 rpm for 10 min in bench top centrifuge (Eppendorf). Both cell lysates and supernatant from the centrifuged samples were prepared according to the protocol contained in Bolt Bis-Tris Plus Mini Gel Electrophoresis system (Life Technologies) with an optional reducing agent present and modified with an increased temperature to 90°C instead of 70°C at the sample preparation step. The precast polyacrylamide gel compatible with this system was loaded with up to 20 μ l of each sample per well and with one well containing 10 μ l of SeeBlue Plus2 Pre-Stained Protein Standard (Novex, Life Technologies). The gel was run at 165 V for 35 min using an EC570-90 Power Supply (ThermoEC). Proteins were then transferred from the gel to a polyvinylidene difluoride (PVDF) membrane using an iBlot Dry Blotting System (Life Technologies) with an iBlot Gel Transfer Device (Life Technologies) set to programme 3. Immunoblotting of the membrane was done with 14C2 as the primary antibody and an anti-mouse secondary antibody using a Western Breeze chromogenic immunodetection kit (Invitrogen, catalogue number: WB7103).

2.2.14 Repeated virus passaging

2.2.14.1 Virus growth

MDCK cells were grown in T-75 cm² flasks and infected with Influenza A/Udorn/72-ΔM2 recombinant virus by removing the growth media and adding 3 ml of DMEM containing virus at 0.01 multiplicity of infection (MOI). Cells were incubated for 2 h at 37°C, 5% CO₂ and shaking every 15 min to prevent from drying. After incubation the media was replaced with 15 ml of DMEM with 1% N-acetyl trypsin (NAT) and cells were incubated until cytopathic effects, such as changed morphology and dead cells in the media, were observed. The virus was then harvested by pouring the media into a 15 ml sterile tube and centrifuging for 20 min at 1000 rpm in a Heraeus Megafuge 40R (Thermo Scientific). The virus contained in the supernatant was then transferred into a new sterile 15 ml tube and stored at -20°C for further analysis and subsequent passages.

2.2.14.2 Plaque assay

Virus titer was checked after each passage by plaque assays. MDCK cells were grown in 6 well plates until 100% confluency. Series of dilutions of harvested virus, 10⁻² to 10⁻⁷, were prepared in DMEM with 1% BSA. The media was aspirated from the cells followed by a wash with 2 ml PBS and addition of 400 μl of diluted virus into each well. Cells were incubated for 2 h at 37°C, 5% CO₂ and shaking every 15 min to prevent from drying. After incubation, the media was removed from the wells and 2 ml of replacement media (50% volume of 2% agarose at 50°C and 50% volume of 2X DMEM, 2X Penicillin-Streptomycin and 2 μg/ml of NAT at 37°C) was added. Plates were left for 5 min at room temperature to allow agarose overlay to set up and then inverted and incubated at 37°C, 5% CO₂ for about 3 days, until plaques appeared. Plaque assay was performed in duplicates and virus titer (in plaque forming units (PFU) per ml) was calculated using equation:

$$\text{viral titer} = \text{number of plaques} / \text{dilution} \times \text{volume of virus added to the well (ml)}$$

2.2.14.3 RNA extraction and reverse transcription

Viral RNA was extracted from samples using QIAamp Viral RNA Mini Kit (Qiagen) and maximum volume of the sample. Concentration of viral RNA after extraction was measured by NanoDrop 2000 (Thermo Scientific). Reverse Transcriptase Polymerase Chain Reaction (RT-PCR) were performed using One-Step RT-PCR Kit (Qiagen) in ³Prime PCR machine (Techne) with 0.6 µM of each primer: M_UTR_F and M_UTR_R (described in chapter 2.1.4) and 2 µg of template RNA. Cycling conditions were set up according to the protocol with 40 cycles in 3-step PCR, each cycle consisting of 3 steps: denaturation, 1 min at 94°C; annealing, 1 min at 47°C and extension, 1 min at 72°C. After RT-PCR all samples were run on agarose gel to select correct synthesis product prior to purification. A 1.2% agarose (Melford, UK) gel was made in 1xTBE buffer (Tris-Base, Boric acid and 0.5M, pH 8 EDTA) with 1,5 µl of ethidium bromide (Sigma) in an electrophoresis unit (Fisher Scientific) and left for 20 min at room temperature to set. The gel was then covered with 1xTBE buffer and 10 µl of a 1 kb HyperLadder (Bioline), was loaded into the wells along with RT-PCR samples mixed with 5 µl of gel loading buffer (0.25% bromophenol blue and 40% sucrose in water). The gel was run at 100 V for 1 h using an EC570-90 Power Supply (ThermoEC) and was viewed in a BenchTop UV transilluminator (UVP). Bands of the correct size were cut out from the gel with a sterile blade and DNA was extracted using a Gel Extraction Kit (Thermo Scientific). DNA concentration in each sample was measured on NanoDrop.

2.2.14.4 Sequencing

Aliquots of DNA at 1 ng/µl per 100 base pairs of the PCR product (10 ng/µl total) and three primers: M_UTR_F, M_UTR_R and M_F2 at 3.2 pmol/µl were prepared in sterile Eppendorf tubes. The tubes were sent for sequencing to Source BioScience (Nottingham, UK).

3. RESULTS

3.1 STRUCTURE OF THE M2 AMPHIPATHIC HELIX

3.1.1 Introduction

The M2 protein from the Influenza A virus is 97 amino acids long, which in its native form is a homotetramer and contains three domains: the ecto domain (residues 1-24), the transmembrane domain (residues 25-43) and the cytoplasmic tail (residues 44-97) (Lamb et al. 1985, Zebedee et al. 1985, Pinto et al. 1992), as shown in Figure 1.2-2. To date the full high resolution structure of the M2 protein has not been solved, however, the structure of the TMD, which functions as an ion channel, has been intensively studied. The structure of the TMD between residues 22-46 has been solved by X ray crystallography (Stouffer et al. 2008) and the N-terminal of the cytoplasmic tail, up to residue 60, has been solved together with the TMD and few residues from the ecto domain (from residue 18) by NMR (Schnell and Chou 2008), which suggests formation of an amphipathic helix on the beginning of CT, between residues 51-59. It has been shown that this AH plays an important role in virus assembly and budding, especially in membrane scission. Therefore the structure of the 16 amino acid long M2 AH, which corresponds to residues 47-62 of the full length M2 protein, based on A/Udorn/72 strain, has been solved in solution and in presence of standard LUVs using NMR. To determine which part of the helix is responsible for interactions with membranes Saturation-transfer difference (STD) NMR experiments have been performed. STD NMR is a technique that allows for detection of a small molecule binding to a larger receptor and detection of the molecular regions of the ligand that are responsible for recognition and binding to the receptor.

3.1.2 M2 AH formation upon membrane binding

The structure of the M2 AH in solution and in the presence of standard LUVs (composed of POPC, POPG and Ch at 4:1:0.05 molar ratio, 100 nm) was resolved using ^1H 2D NMR, mainly nuclear Overhauser effect (NOE) through-space contacts. The peptide used in this study was a 16 amino acid long M2 AH based on the A/Udorn/72 strain and corresponds to residues 47-62 on the full length M2 protein. ^1H chemical shift assignments in parts per million (ppm) for the peptide in solution and in presence of LUVs were obtained from 2D NMR TOCSY and NOESY experiments and are shown in Table 3.1-1 and Table 3.1-2 respectively.

Residue	H^{N}	H^{a}	H^{b}	H^{c}	H^{d}	H^{e}
1 Phe	-	4.41	2.86			
2 Phe	8.03	4.49	2.91 3.05			
3 Lys	7.98	4.17	1.73	1.29	1.61	
4 Ser	8.09	4.34	3.76			
5 Ile	7.92	4.08	1.74		0.73	
6 Tyr	8.04	4.45	2.80 2.91			
7 Arg	7.91	4.11	1.50	1.30	3.02	7.04
8 Phe	7.88	4.44	2.88 2.95			
9 Phe	7.94	4.51	2.89 2.99		7.12	
10 Glu	8.14	4.12	1.82 1.90	2.17		
11 His	8.41	4.59	3.11 3.24			
12 Gly	8.32	3.88				
13 Leu	8.01	4.28	1.53		1.53	
14 Lys	8.3	4.25	1.68 1.74	1.35	1.60	2.91
15 Arg	8.37	4.27	1.69 1.79	1.56	3.12	7.11
16 Gly	8.39	3.86				

Table 3. 1 - 1 Chemical shifts (ppm) of the M2 AH peptide in solution.

Residue	H ^N	H ^α	H ^β	H ^γ	H ^δ	H ^ε
1 Phe	-	4.41	2.86		7.09	7.16
2 Phe	8.04	4.49	2.90 3.04		7.16	7.27
3 Lys	7.98	4.17	1.73	1.29	1.61	2.92
4 Ser	8.09	4.34	3.77			
5 Ile	7.92	4.08	1.74	1.15 1.00	0.73	
6 Tyr	8.04	4.45	2.90 2.79		6.99	7.08
7 Arg	7.91	4.11	1.5	1.30	3.02	7.04
8 Phe	7.88	4.44	2.88 2.96		7.12	7.26
9 Phe	7.95	4.5	2.89 2.99		7.13	7.26
10 Glu	8.14	4.12	1.81 1.89	2.16		
11 His	8.41	4.6	3.11 3.26		7.23	
12 Gly	8.33	3.88				
13 Leu	8.01	4.28	1.53		0.83	
14 Lys	8.29	4.24	1.74 1.69	1.35	1.61	2.91
15 Arg	8.37	4.27	1.69 1.79	1.55	3.12	7.12
16 Gly	8.39	3.86				

Table 3. 1 - 2 Chemical shifts (ppm) of the M2 AH peptide in presence of standard LUVs.

¹H NMR spectra for the M2 AH in solution and in presence of LUVs were also obtained from TOCSY and NOESY experiments with fingerprint regions of each spectra shown in Figures 3.1-1 to 3.1-4 respectively. Peaks in each spectra were assigned and the structure of the peptide in each environment was resolved mainly using NOE through-space contacts. TOCSY spectra for the M2 AH peptide in solution and in the presence of LUVs appear similar (Fig. 3.1-1 and 3.1-3 respectively) however, the NOESY spectra show more peaks in presence of LUVs than for a peptide in solution (Fig. 3.1-2 and 3.1-4 respectively) suggesting a higher amount of internal interactions in presence of LUVs and hence more structured peptide.

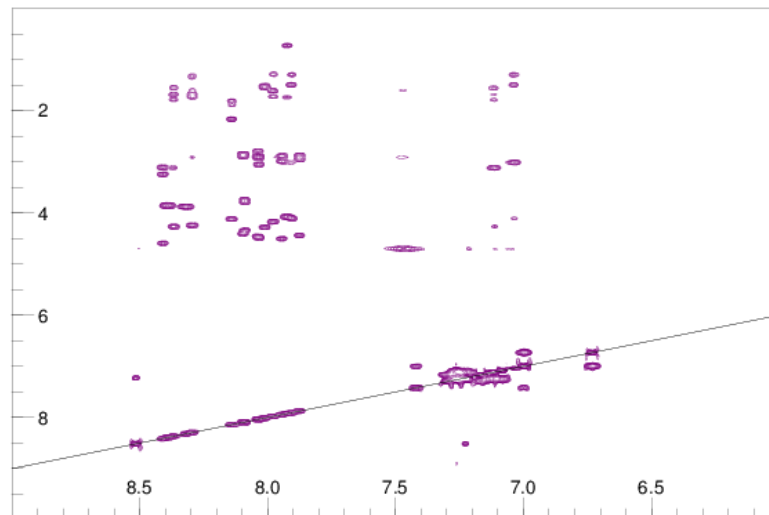


Figure 3. 1 - 1 TOCSY NMR spectra of the fingerprint region for M2 AH peptide in solution.

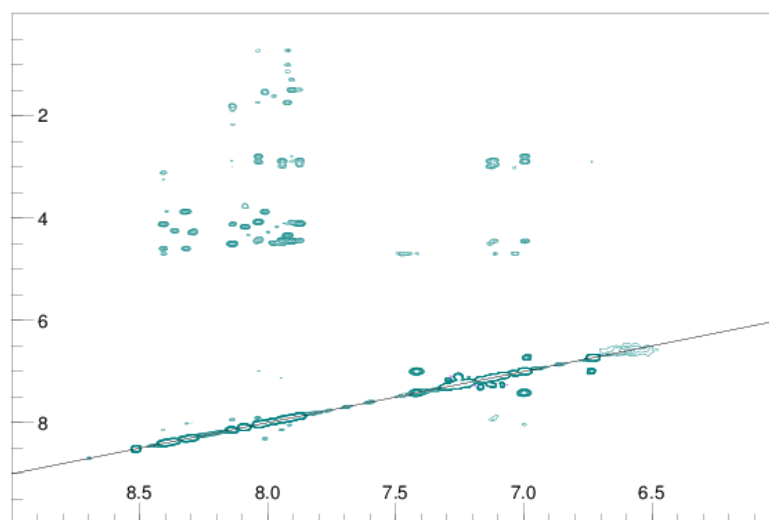


Figure 3. 1 - 2 NOESY NMR spectra of the fingerprint region for M2 AH peptide in solution.

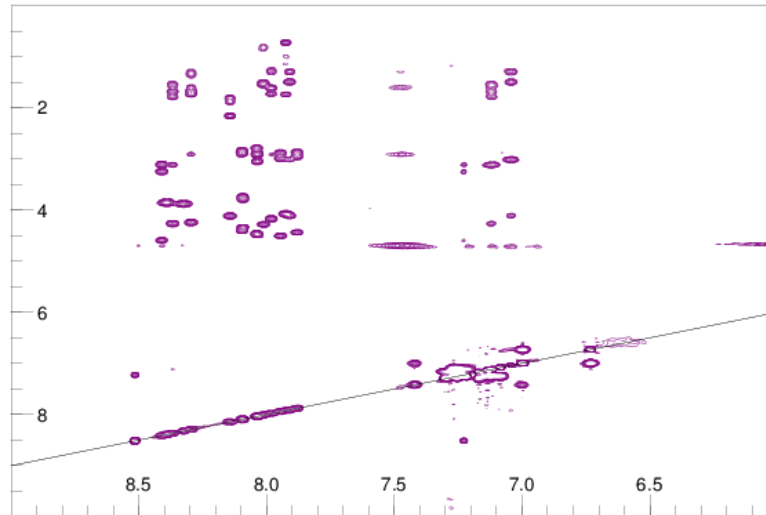


Figure 3. 1 - 3 TOCSY NMR spectra of the fingerprint region for M2 AH peptide in presence of standard LUVs.

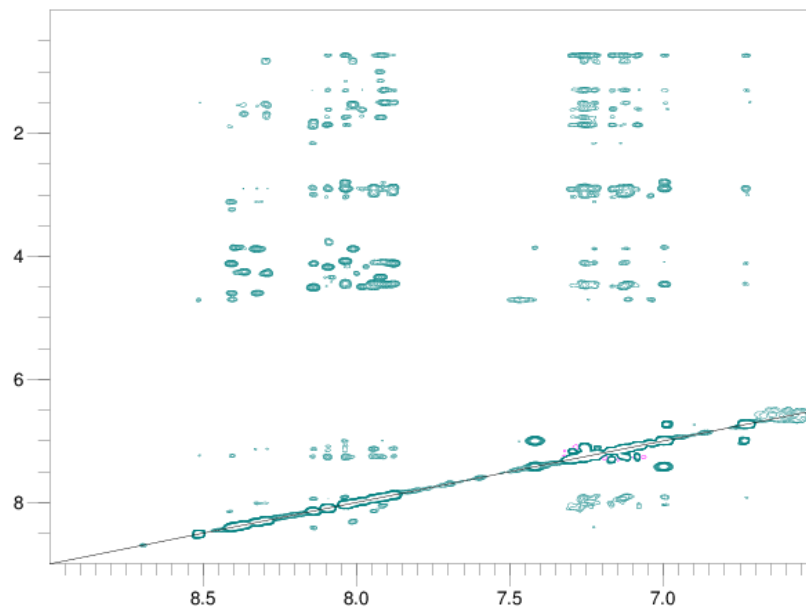


Figure 3. 1 - 4 NOESY NMR spectra of the fingerprint region for M2 AH peptide in presence of standard LUVs.

The observed NOE contacts and statistics of the calculated structures for peptide in solution and in the presence of LUVs are shown in Table 3.1-3. When the M2 AH peptide was in solution, the number of observed NOE contacts - both inter and intra-residue - was drastically reduced compared to the same peptide in the presence of LUVs which suggests that peptide is unstructured in solution and becomes structured upon binding with membranes. Due to the lack of interactions for the peptide in solution no dihedral restraints were used to calculate this structure. The structure statistics for the peptide in both environments show that NOE and dihedral angle violations (where present) are on a very low level which suggests that each structure was optimal. Ramachandran analysis for 20 structure ensembles shows nearly 90% of each structure to be in most favoured region and additionally allowed region which is expected from a good quality model. Additionally Ramachandran plot for the peptide in the presence of LUVs show concentration of data points in the region corresponding to an α -helix conformation (see appendix 6.2). Root mean squared deviation (rmsd) values for 20 structure ensembles calculated over residues 4-16 of each model were around two times higher for peptide in solution than for the peptide in presence of LUVs which suggest that there is more variability in the model for peptide in the solution and it might be a result of reduced number of observed NOE contacts and lack of structure present.

	In solution	In presence of LUVs
NMR distance and dihedral constrains		
Distance constraints		
Total NOE	38	218
Intra-residue	3	55
Inter-residue	35	163
Sequential ($ i - j = 1$)	35	91
Medium-range ($ i - j < 4$)	35	160
Long-range ($ i - j > 4$)	0	3
Dihedral restraints	0	18
Lennard-Jones Energy (kJ mol ⁻¹)	-231± 23	-300 ± 20
Structure statistics		
Violations		
NOE violations >0.2 Å	0	0 ± 0.00375
Dihedral angle violations >2.0 Å	-	0 ± 0.18234
Ramachandran (%)		
Most favoured region	52.7	67.3
Additionally allowed region	33.1	25.8
Generously allowed region	9.6	3.1
Disallowed region	4.6	3.8
Average pairwise r.m.s. deviation (Å)*		
Heavy	5.140	2.610
Backbone	3.171	1.570

* Pairwise r.m.s. deviation was calculated over residues 4-16

Table 3. 1 - 3 NMR and structure statistics for 20 structure ensembles of the M2 AH peptide in solution and in presence of standard LUVs.

Models of the M2 AH peptide in solution and in the presence of LUVs were composed of 20 structure ensembles fitted over the backbone atoms in residues 4-16 and the structure closest to the mean of the ensemble was used to make a cartoon representation of each structure. Calculated structures show random coil confirmation for the M2 AH peptide in solution (Fig. 3.1-5 A and B) and formation of an α -helix between residues 4-16 (residues 50-62 of a full length M2 protein) of the peptide in the presence of LUVs (Fig. 3.1-5 C and D). This confirms that the M2 AH is formed upon binding with the membrane.

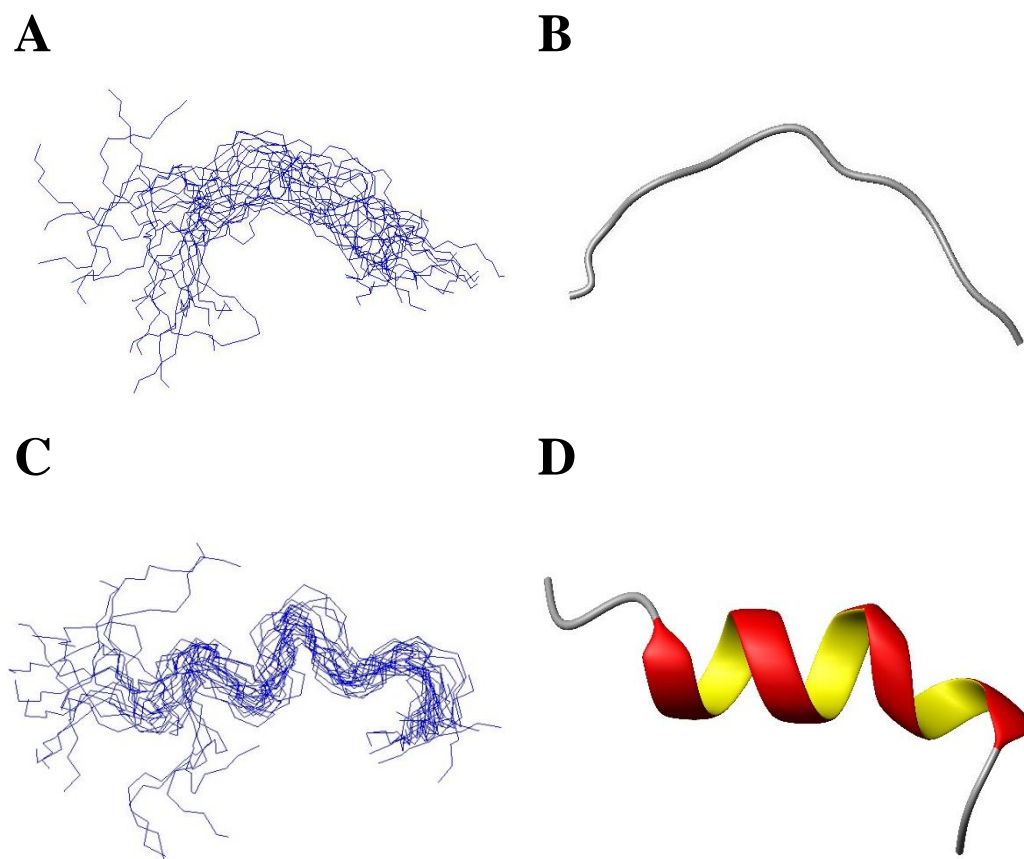


Figure 3.1-5 Structures of the M2 AH peptide in solution (A and B) and in presence of standard LUVs (C and D). 20 structure ensembles fitted over backbone atoms in residues 4-16 are shown in A and C. Cartoon representations of the structure closest to the mean of the ensemble are shown in B and D.

NOE contacts, hydrogen bond donors, dihedral restraints and secondary structure showing limitations of helix formation according to Ramachandran analysis of 20 structure ensembles for the M2 AH peptide in solution and in the presence of LUVs are shown in Figure 3.1-6 and 3.1-7 respectively. As expected, there are not many NOE contacts when peptide is in a solution however, there are many H_{α} - H_N , H_N - H_N and H_{β} - H_N $i-i+1$ NOEs observed when LUVs are present. Additionally, when the M2 AH peptide is in the presence of LUVs, some H_{α} - H_N $i-i+3$ NOEs have been observed which are characteristic for an α -helix formation. However, secondary structure for the M2 AH peptide in the presence of LUVs doesn't show formation of a continuous α -helix between residues 4-16 which is caused by limitations in Ramachandran analysis.

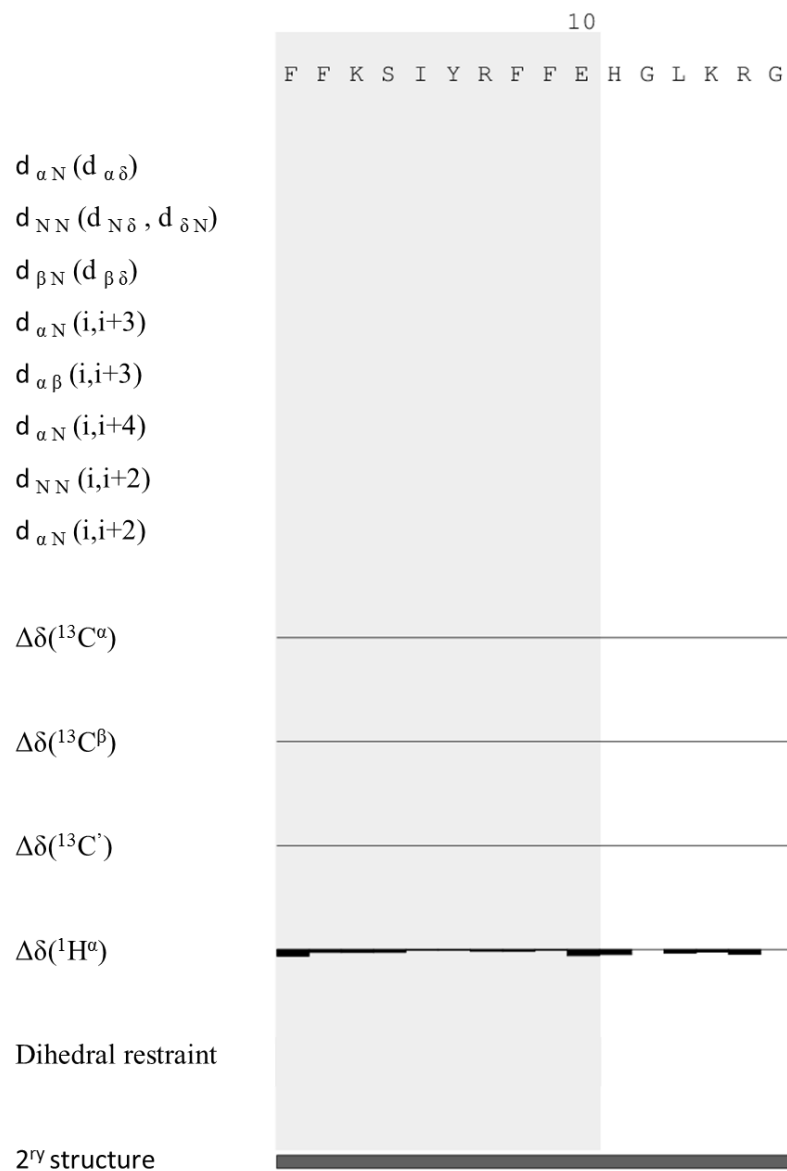


Figure 3. 1 - 6 NOE contacts, chemical shift difference, hydrogen bond donors and dihedral restrains for M2 AH peptide in solution. The secondary structure indicates the limits of helix formation according to Ramachandran analysis of the final 20 structure ensemble.

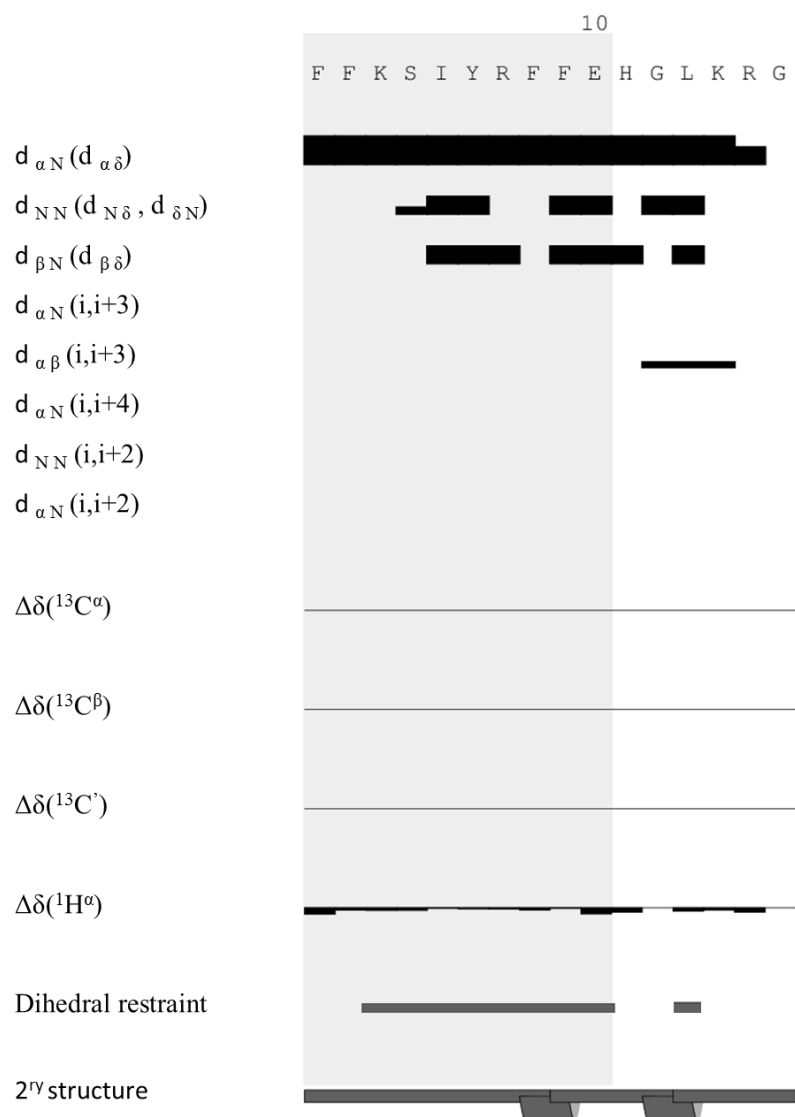


Figure 3.1 - 7 NOE contacts, chemical shift difference, hydrogen bond donors and dihedral restrains for M2 AH peptide in presence of standard LUVs. The secondary structure indicates the limits of helix formation according to Ramachandran analysis of the final 20 structure ensemble.

3.1.3 M2 AH membrane interactions

One-dimensional (1D) STD NMR was performed by Dr Mark Howard from University of Kent and was used to determine the interaction between the M2 AH and the lipid membrane. STD control and difference spectra for the M2 AH in solution and with LUVs present are shown in Figure 3.1-8 and 3.1-9 respectively. When the peptide is in solution there are no interactions present and therefore no peaks are visible in the difference spectrum (Fig. 3.1-8). However, when the peptide is in the presence of LUVs, there are interactions between the peptide and the lipids in the membrane and therefore there are peaks visible in the STD difference spectrum, with some of the peaks identified as some of the amino acids present in the AH, based on the chemical shift characteristic for the particular amino acids (Fig. 3.1-9).

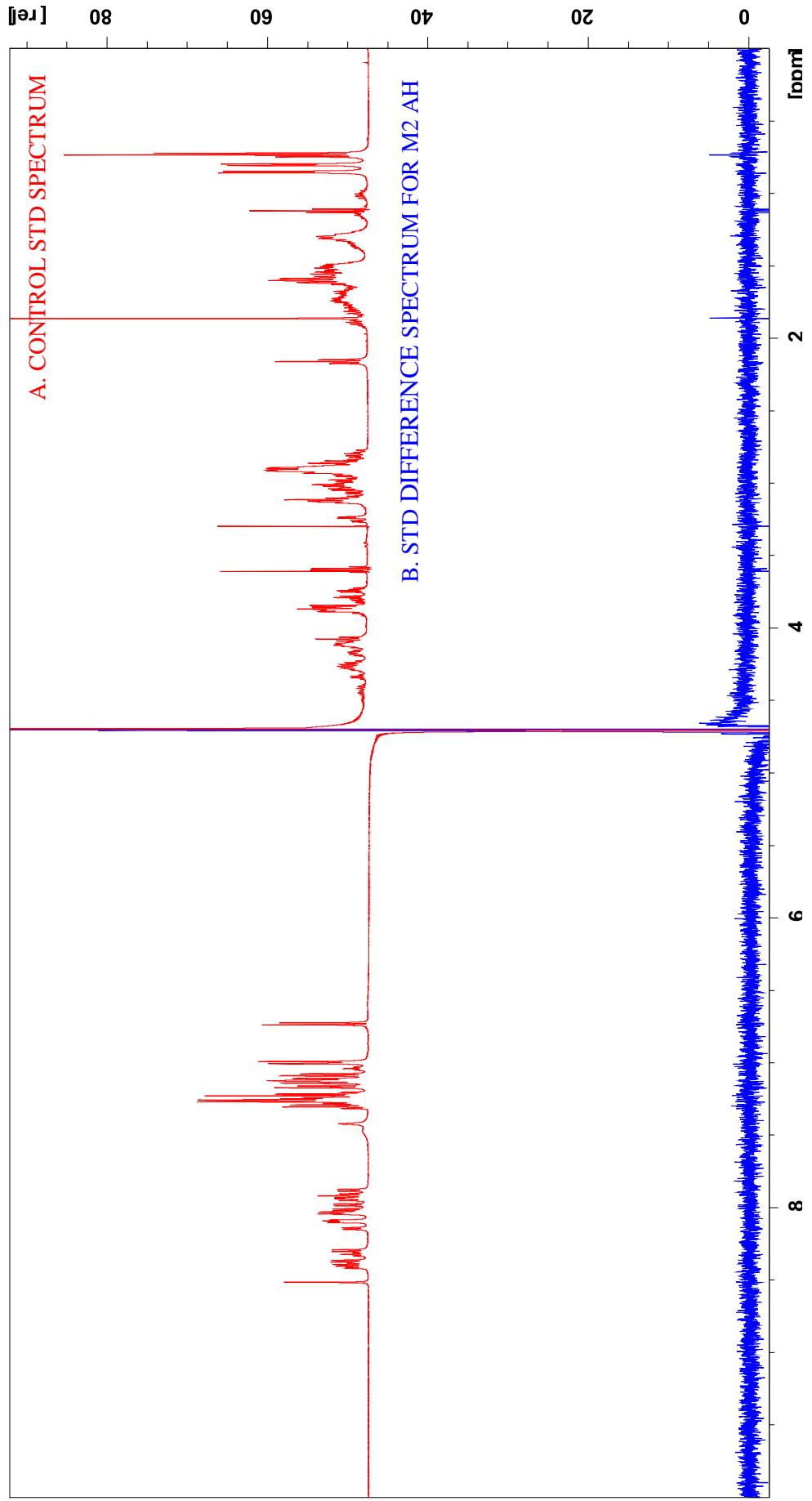


Figure 3.1 - 8 ^1H STD NMR for M2 AH peptide in solution showing control spectrum (A) and STD difference spectrum (B).

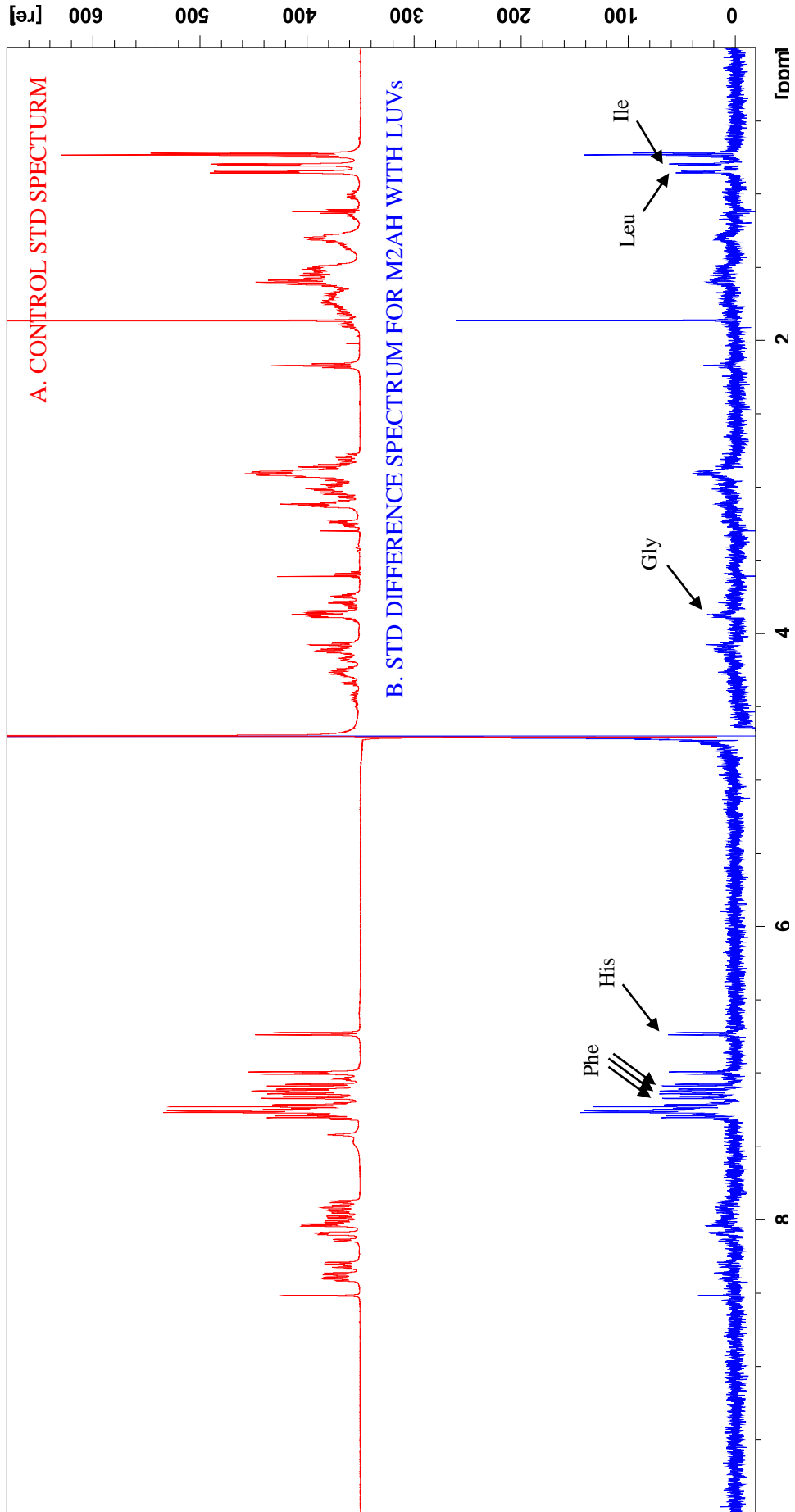


Figure 3.1 - 9 1D ¹H STD NMR for M2 AH peptide in presence of LUVs showing control spectrum (A) and STD difference spectrum for the M2 AH peptide in presence of standard LUVs with peaks corresponding to different amino acids indicated by black arrows (B).

Quantitative STD values were calculated by modifying STD values according to the T_1 relaxation rate, both of which were obtained through correlation of signal intensity to the nuclei of specific residues from the peptide (data not shown). These values were then converted to a percentage of the maximum transfer value, which was observed for phenylalanine at residue 9, as shown in Table 3.1-4.

Residue	Assignment	Integral [abs]	% of max
8Phe	H ϵ 1/2	1239392	34.6
9Phe	H ϵ 1/2	3587120	100.0
11His	H δ 1/2	1764799	49.2
2Phe	H δ 1/2	1054350	29.4
8/9 Phe	H δ 1/2	2082138	58.0
6Tyr	H ϵ 1/2	979446	27.3
6Tyr	H δ 1/2	865698	24.1
12Gly	H α 2/3	733069	20.4
Phe	H α	1581385	44.1
13Leu	H δ 1	864895	24.1
13Leu	H δ 2	837269	23.3
5Ile	H δ	1879250	52.4

Table 3.1 - 4 Quantitative STD values and percentage of the maximum transfer value for selected residues from the M2 AH peptide.

The percentage of the maximum STD transfer values from Table 3.1-4 were mapped on the calculated structure closest to the mean of the ensemble for the M2 AH peptide in the presence of LUVs, highlighting residues across the face of the helix responsible for interaction with the membrane based on their significance (Fig. 3.1-10). The most important residues involved in interactions with the membranes are phenylalanine at residues 9 and 8 and isoleucine at residue 5 (residues 55, 54 and 51 in the full length M2 protein respectively) with phenylalanine at residue 2, histidine at residue 11 and glycine at residue 12 (residues 48, 57 and 58 in the full length M2 protein respectively) also being involved in the interaction but to a lesser degree. All of these residues, except the histidine, are in the hydrophobic face of the helix suggesting that the M2 AH interacts with lipids using hydrophobic interactions, which confirms previous suggestions (Rossman et al. 2010b).

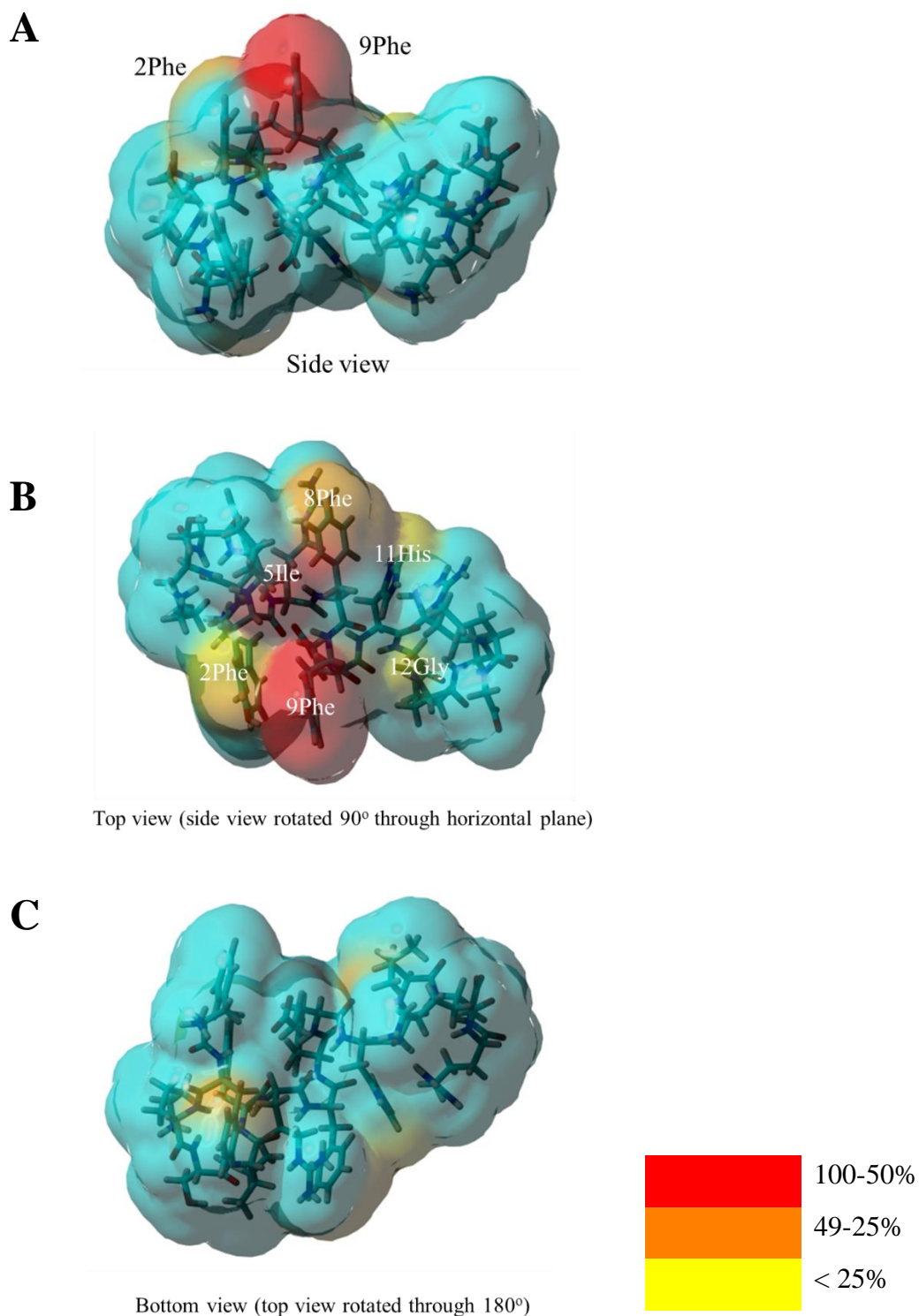


Figure 3. 1 - 10 Calculated structure closest to the mean of the ensemble for the M2 AH peptide in presence of LUVs with residues across the face of the helix responsible for interaction with the membrane coloured based on a percentage of the maximum STD transfer. All images were generated in YASARA program, side view (A), top view- side view rotated 90° through horizontal plane (B) and bottom view- top view rotated through 180° (C).

3.1.4 Summary

In conclusion, NMR spectroscopy has been used to investigate the structure of the M2 AH. Calculated models based on the ^1H 2D NMR experiment show that peptide in solution is in random coil conformation however, when liposomes are present the peptide becomes helical, with an α -helix being formed between residues 4 and 16 (residues 50-62 in a full length M2 protein) (Fig. 3.1-5). To further investigate the interactions between the M2 AH and the lipid membrane, a 1D STD NMR experiment was performed. Results show that the phenylalanines at residues 9 and 8 and isoleucine at residue 5 are mostly responsible for the interactions with the membrane, with phenylalanine at residue 2, histidine at residue 11 and glycine at residue 12 being involved to a lesser degree (Fig. 3.1-10). This shows that residues 48, 51, 54, 55, 57 and 58 are important for the peptide to be able to bind to lipids and with the majority of them being in the hydrophobic face of the helix, it suggests that the helix interacts with membranes through hydrophobic interactions.

3.2 M2 AMPHIPATHIC HELIX INTERACTIONS WITH THE MEMBRANE

3.2.1 Introduction

NMR experiments have shown that the M2 AH is formed upon binding with membranes (see chapter 3.1.2) and that the hydrophobic face of the helix is responsible for interaction with lipids (see chapter 3.1.3). To investigate how efficiently the M2 AH can bind to lipid membranes a binding assay has been developed. Further investigation of the formation of the M2 AH in different environments, how well this is conserved between influenza virus strains and how different mutations affect this process, has been done using circular dichroism spectroscopy to determine the secondary structures of these peptides.

3.2.2 Binding to lipid membranes

The NMR has shown that the M2 AH is formed upon binding with lipid membranes (see chapter 3.1.2) therefore, an assay to quantify binding ability of the M2 AH with liposomes has been created. In this assay, fluorescently labelled M2 AH peptide was incubated with liposomes- SUVs, LUVs or GUVs. Unbound peptide was removed by filter washes and the fluorescence of each sample was checked by a plate reader. To determine the optimal concentration of the peptide, samples with a constant concentration of standard LUVs (2.5 mM) and a varied concentration of peptide (0-100 μ M) were tested, with it being determined that 100 μ M of peptide gave the best signal (Fig. 3.2-1).

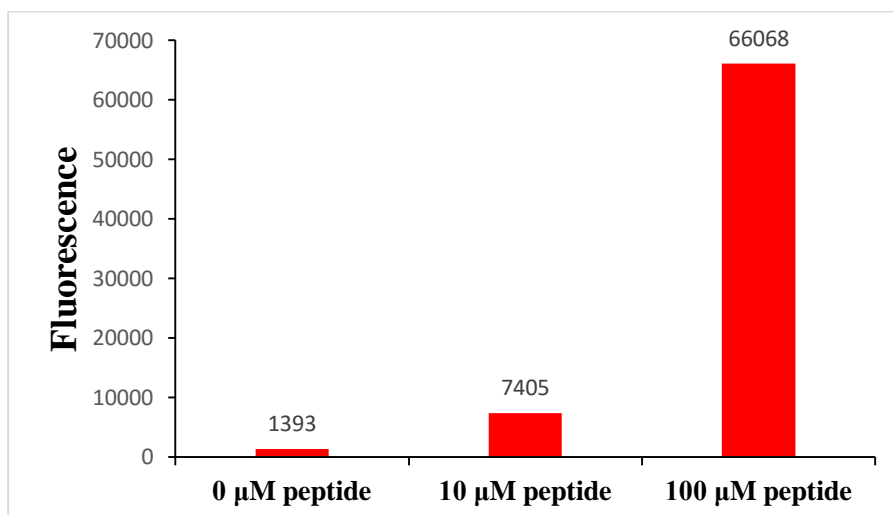


Figure 3. 2 – 1 Fluorescence readings for samples with 2.5 mM of standard LUVs incubated with increasing concentration of fluorescently labelled M2 AH peptide.

100 μM of peptide was then used with varied amount of lipids, to further optimise assay conditions. Results showed that 2.5 mM of lipids gives the best signal out of the concentrations tested, with higher concentrations being out of detection range (Fig. 3.2-2). Therefore 100 μM of peptide and 2.5 mM of lipids were chosen as optimal concentrations for this type of assay and used during all further experiments.

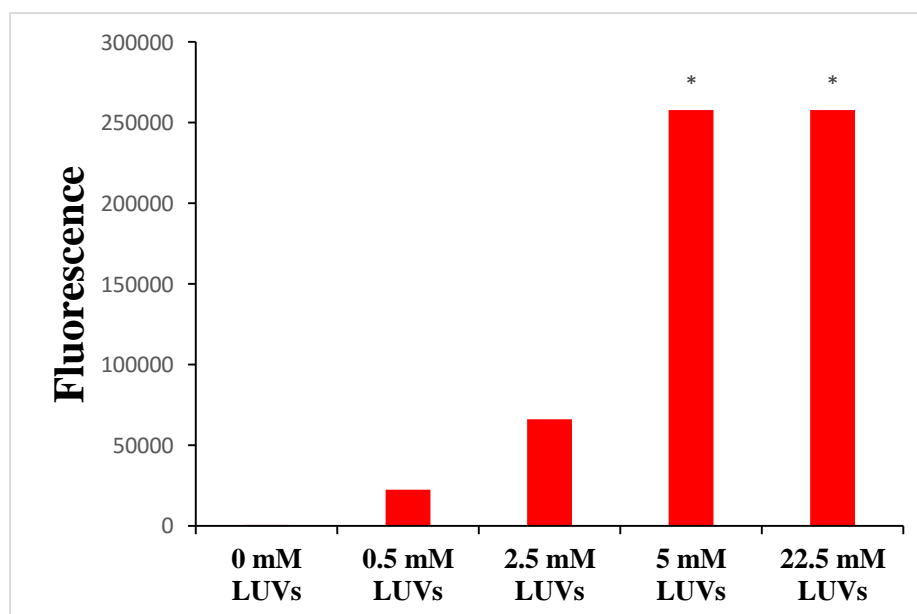


Figure 3. 2 - 2 Fluorescence readings for samples with 100 μM of fluorescently labelled M2 AH peptide with increasing concentration of standard LUVs.

Each experiment, peptide with liposomes or a control sample (containing peptide without liposomes), was measured in triplicate. Average Fold Binding was calculated from Fold Binding values, calculated by dividing fluorescent readings of a peptide with liposomes sample by an average value for the control samples. Control samples would contain residual peptide that has not been removed by the washes and from any background fluorescence that has been detected by the plate reader. The fluorescence signal from M2 AH peptide bound to standard LUVs was over 5 fold greater than the background, with standard error of 1.3, which shows that M2 AH peptide has bound to liposomes (Table 3.2-1).

	Fluorescence			Average values	Standard deviation
	Sample 1	Sample 2	Sample 3		
Control (100 μ M FITC peptide)	7653	8658	9291	8534	826
100 μ M FITC peptide with 2.5 mM standard LUVs	35463	41444	58325		
Fold Binding (peptide with LUVs value divided by average control value)	4.155	4.856	6.834	5.282	1.389

Table 3. 2 - 1 Fluorescence readings for samples with 100 μ M fluorescently labelled M2 AH peptide incubated with 2.5 mM standard LUVs and control samples without LUVs present. Fold Binding values were obtained by dividing fluorescence readings for samples with peptide and LUVs by average control value.

3.2.3 Alpha helix stabilisation upon binding

3.2.3.1 Detection of secondary structure

To confirm NMR observations, the secondary structure of the M2 AH peptide in a lipid environment was determined by circular dichroism (CD) spectroscopy. CD is the difference in absorption of left-handed circularly polarised light and right-handed circularly polarised light over a range of wavelengths (Greenfield 2006). Structured molecules give characteristic spectra, for example, an α -helix gives troughs at around 222 nm and 208 nm whereas β -sheets give a trough at around 218 nm (Fig. 3.2-3). Based on the spectra, the percentage of each structure in the molecule was estimated using K2D3, an online bioinformatics tool (Louis-Jeune et al. 2012) found at <http://k2d3.ogic.ca/>.

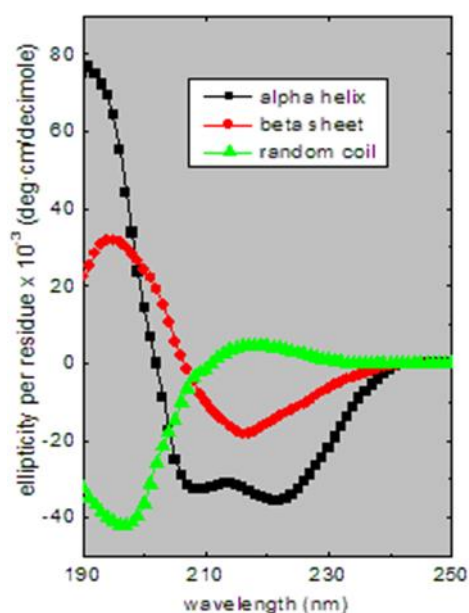


Figure 3.2-3 Characteristic CD spectra for different protein secondary structures. Adapted from http://www.ap-lab.com/circular_dichroism.htm.

Initial experiments have been performed using a range of different peptide and lipid concentrations to determine the optimal peptide:lipid ratio that would give the best signal. Throughout these experiments, a 16 amino acid long M2 AH peptide based on the A/Udorn/72 strain and standard LUVs have been used. When 100 μ M of the M2 AH peptide was used the CD spectra showed two troughs at around 223 and 208 nm which suggests formation of an α -helix (Fig. 3.2-4 A). Increasing the lipid concentration, from 200 μ M to 5 mM, resulted in increase of the troughs depth and led to an increase in the estimated helix percentage from 1.31 to 33.64 (Fig. 3.2-4 B).

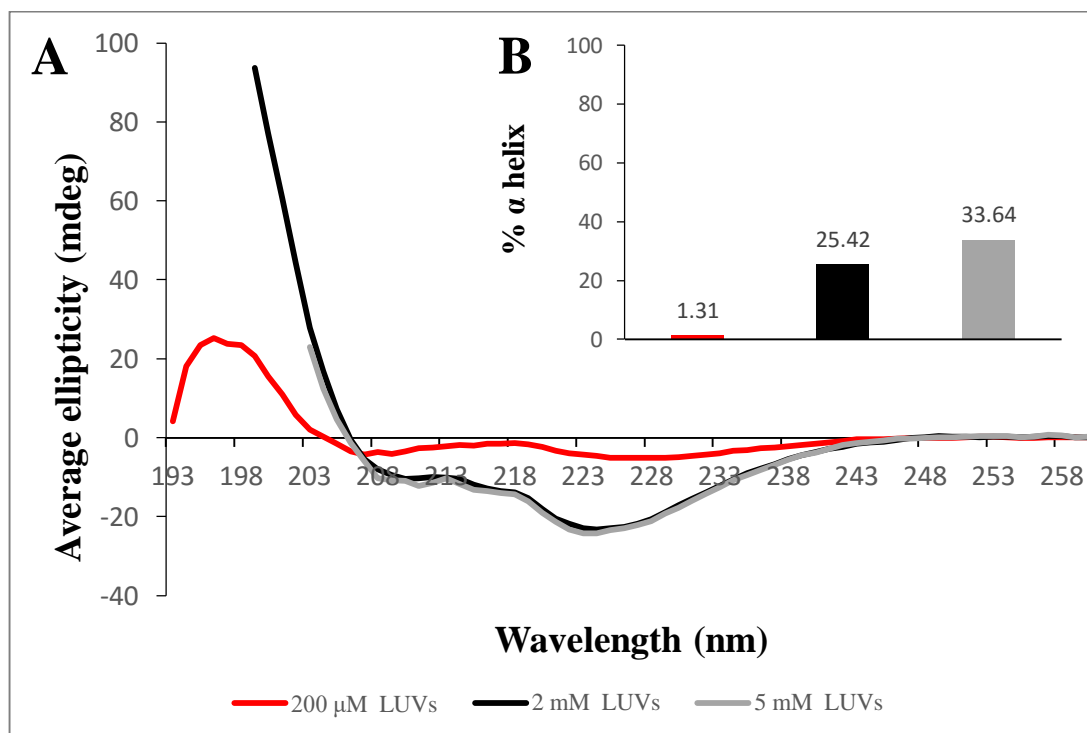


Figure 3. 2 - 4 CD spectra for 100 μ M M2 AH peptide with increasing concentration of standard LUVs (A) and estimated percentage of an α helix present in each sample calculated based on the spectra using K2D3 bioinformatics tool on <http://k2d3.orgic.ca/> website (B).

When 250 μM of the M2 AH peptide was used with the same range of lipid concentrations, the CD spectra only resembled an α -helix in the presence of the two highest lipid concentrations (2 and 5 mM). In the lowest concentration of lipid (200 μM), the spectra showed a peak at around 218 nm, suggesting a random coil formation (Fig. 3.2-5 A). Increasing the peptide concentration caused an increase in the troughs depth (Fig. 3.2-5 A) when compared with the 100 μM dataset (Fig. 3.2-4 A), and an increase in the estimated helix percentage values, which now ranged from 4.65 up to 94.19% (Fig. 3.2-5 B),

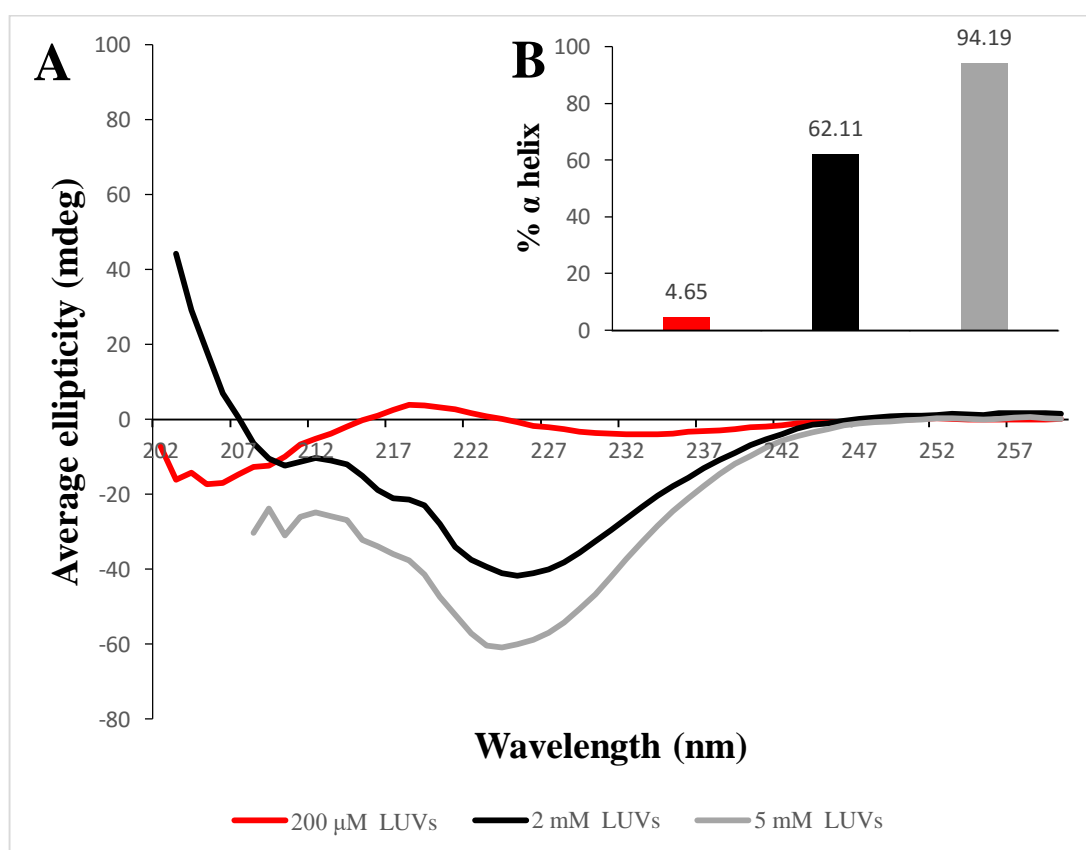


Figure 3.2-5 CD spectra for 250 μM M2 AH peptide with increasing concentration of standard LUVs (A) and estimated percentage of an α helix present in each sample calculated based on the spectra using K2D3 bioinformatics tool on <http://k2d3.orgic.ca/> website (B).

When the peptide concentration was increased to 500 μM , the CD spectra showed similar trends as seen with 250 μM : In low lipid concentrations (up to 200 μM) the spectra resembled a random coil conformation and with high lipid concentrations (2 mM and above) the spectra resembled an α -helix conformation (Fig. 3.2-6 A). The estimated helix percentage also showed a similar trend, with stable and high levels of helix (above 94%) for all high lipid concentrations (Fig. 3.2-6 B).

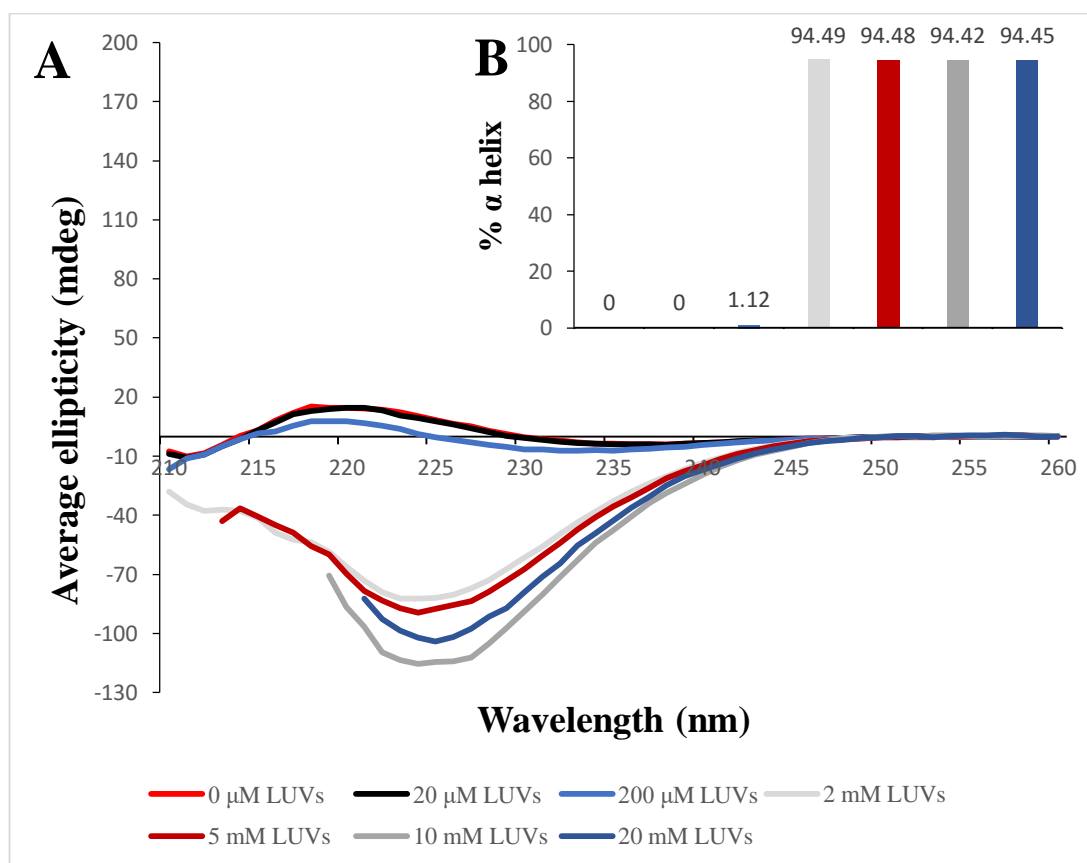


Figure 3.2 - 6 CD spectra for 500 μM M2 AH peptide with increasing concentration of standard LUVs (A) and estimated percentage of an α helix present in each sample calculated based on the spectra using K2D3 bioinformatics tool on <http://k2d3.orgic.ca/> website (B).

These results confirm that the M2 AH is formed upon addition of lipids and its formation is lipid and peptide concentration dependant. The estimated helix percentage increased when the lipid concentration increased, with the total value being dependent on the peptide concentration (Fig. 3.2-4 B and Fig. 3.2-5 B). However, when a certain threshold was reached, 5 mM and 2 mM of lipids with 250 μ M and 500 μ M of peptide respectively, helix percentage was staying at similar, high level (Fig. 3.2-5 B and Fig. 3.2-6 B). It was concluded that 5 mM of lipids and 250 μ M of peptide would be the optimal concentrations for this type of assay and therefore were used during all experiments (unless otherwise stated).

3.2.3.2 Structural changes in different environments

NMR experiments have shown that an amphipathic helix is formed between residues 4 and 16 of the M2 AH peptide in a lipid environment and the peptide remains unstructured in solution (see chapter 3.1.2). To confirm these observations, a M2 AH peptide structure (16 amino acid long based on A/Udorn/72 strain) has been determined in a detergent-free solution, in presence of 30% 2,2,2-trifluoroethanol (TFE, an agent that drives formation of secondary structures (Povey et al. 2007)), and in presence of standard LUVs. Results showed that the peptide in solution is a random coil but when liposomes are present the peptide becomes nearly 90% helical. A similar effect was observed with the addition of 30% TFE in the absence of liposomes (Fig. 3.2-7 A and B). In the presence of TFE, the M2 AH shows classical AH formation, whereas in presence of liposomes the signal is slightly distorted but retains the key minimum at 222 nm for the structure to be predicted using bioinformatics program. This confirms that the M2 AH peptide is becoming stabilised and a helix is being formed upon binding with liposomes.

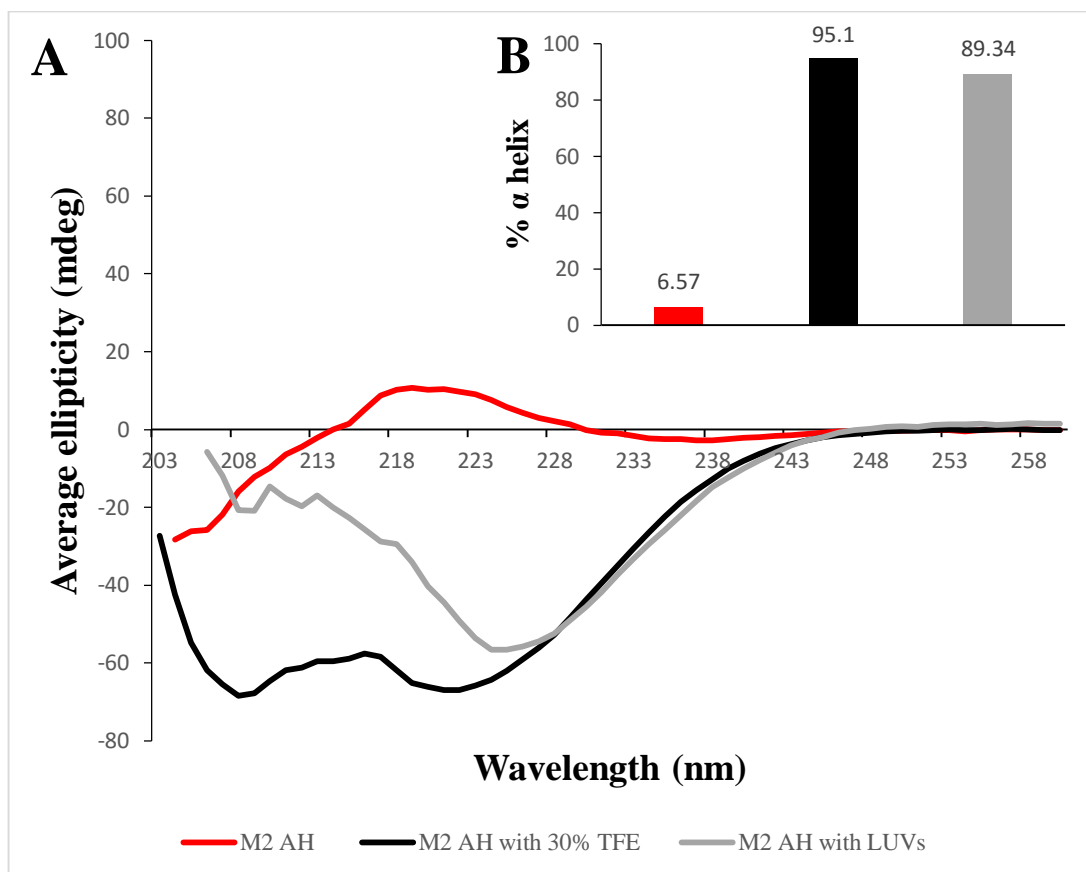


Figure 3.2 - 7 CD spectra for 500 μ M 16 amino acid long M2 AH peptide based on A/Udorn/72 strain in solution, with 30% TFE and with 12.5 mM standard LUVs present (A) and estimated percentage of an α helix present in each sample calculated based on the spectra using K2D3 bioinformatics tool on <http://k2d3.orgic.ca/> website (B).

The M2 protein is highly conserved among influenza virus strains, with only three amino acids different in the M2 AH between the most widely used laboratory strain, A/Udorn/72 and the recent pandemic influenza strain, A/England/09 (Fig. 3.2-8). Two of those amino acids, at positions 54 and 57, are residues that have been identified by STD NMR to be responsible for binding with lipid membranes (Fig. 3.1-10).

A. A/Udorn/72 strain M2 AH:

R L F F K C I Y R F F E H G L K R G
 45 46 47 48 49 50 51 52 53 54 55 56 57 58 59 60 61 62

B. A/England/09 strain M2 AH:

R L F F K C I Y R R F K Y G L K R G
 45 46 47 48 49 50 51 52 53 54 55 56 57 58 59 60 61 62

Figure 3.2 - 8 Comparison of the M2 AH sequence between A/Udorn/72 (A) and A/England/09 strain (B). Differences are highlighted in red and numbers indicated position of each residue in regards to full length protein.

The CD spectra for the peptide based on A/England/09 strain has shown two troughs when in presence of standard LUVs, with about 89% of the helix present, or a peak when peptide was in solution, resembling random coil confirmation and only about 5% of the helix present (Fig. 3.2-9 A and B). Similar results have been observed for the M2 AH peptide based on the A/Udorn/72 strain (Fig. 3.2-7 A and B) which suggests that formation of the M2 AH upon binding with membranes is conserved among different influenza virus strains, despite some differences in the region that has been shown to be responsible for binding.

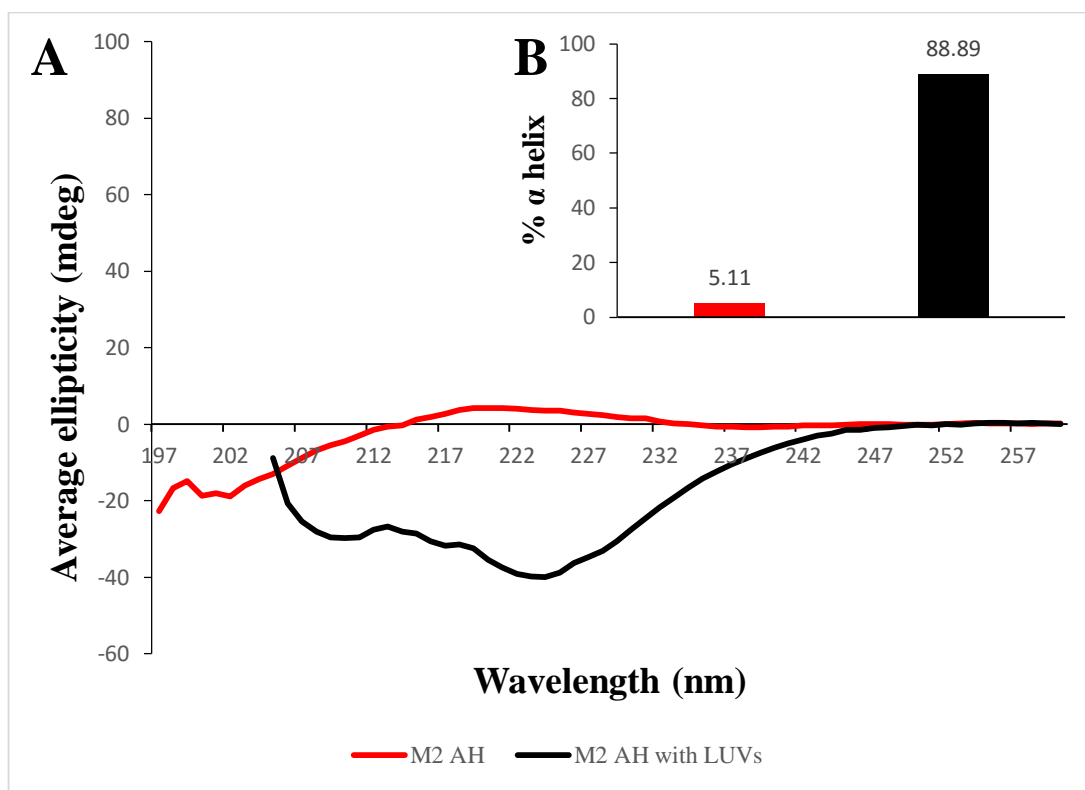


Figure 3.2 - 9 CD spectra for 250 μ M 16 amino acid long M2 AH peptide based on A/England/09 strain in solution and with 5 mM standard LUVs present (A) and estimated percentage of an α helix present in each sample calculated based on the spectra using K2D3 bioinformatics tool on <http://k2d3.ogic.ca/> website (B).

To investigate structure and function of the M2 AH two different length peptides, 16 and 17 amino acids based on laboratory A/Udorn/72 strain, were initially used, however, further analysis showed that the 16 amino acid long peptide is more soluble, with both peptides behaving in similar ways when bound to liposomes or in solution (Fig. 3.2-7 A and Fig. 3.2-10 A) and both give a similar helix percentage by CD (Fig. 3.2-7 B and Fig. 3.2-10 B). Therefore 16 amino acid long M2 AH peptide, based on A/Udorn/72 strain, was used in majority of experiments unless otherwise stated.

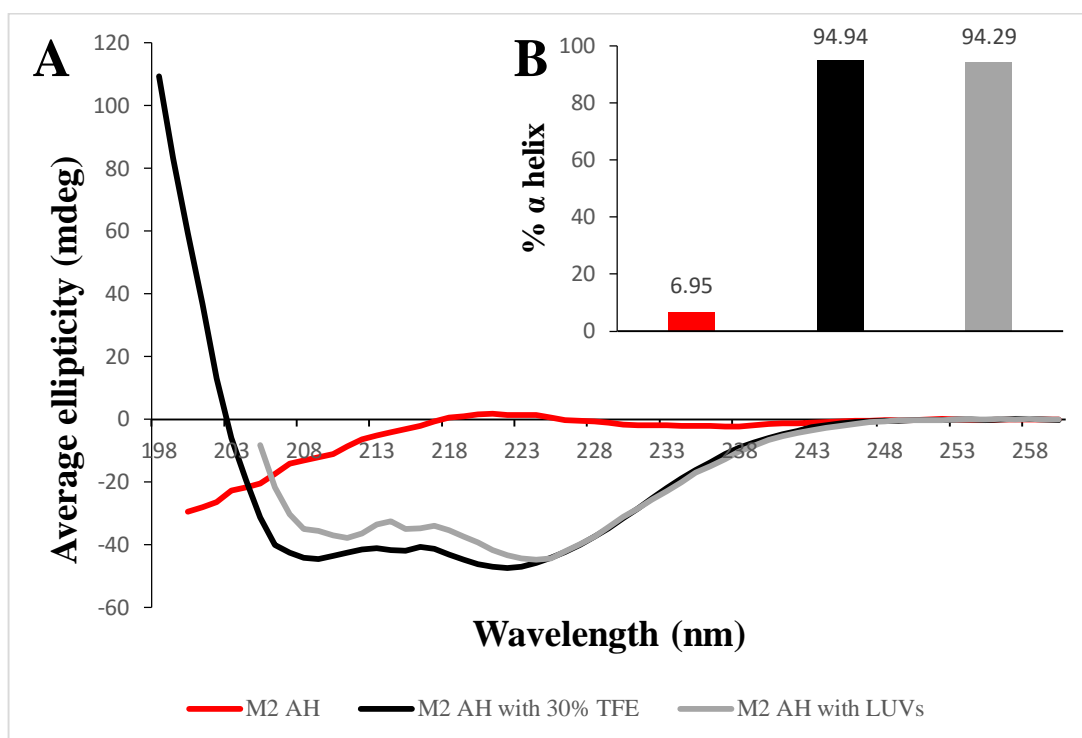


Figure 3.2 - 10 CD spectra for 250 μ M 17 amino acid long M2 AH peptide based on A/Udm/72 strain in solution, with 30% TFE and with 5 mM standard LUVs present (A) and estimated percentage of an α helix present in each sample calculated based on the spectra using K2D3 bioinformatics tool on <http://k2d3.org.ca/> website (B).

3.2.3.3 A/England/09 and AH mutants

A peptide based on the pandemic A/England/09 strain and covering first 18 amino acids of the M2 CT (residues 45-62 of the full M2 protein) was made to test differences between strains and different mutations have been introduced to the peptide to investigate how they affect peptide structure and function. Both hydrophobic and polar faces of the helix have been mutated in order to make them stronger or weaker by replacing residues with lysine (K), which is a charged amino acid or alanine (A), which is a non-polar amino acid respectively. 5 point mutations, F47A F48A I51A Y52A F55A have been introduced to the hydrophobic face of the helix to inhibit its functions, these mutations have been shown previously to impair viral growth (Rossman et al. 2010a, Rossman et al. 2010b). The hydrophobic face of the helix was also weakened

by replacing two hydrophobic residues with alanine, F47A and F48A which are part of the 5 point mutant. The M2 AH contains a cholesterol recognition amino acid consensus (CRAC) domain (Schroeder et al. 2005, Schroeder 2010) which was also disrupted by substitution of the amino acids in the domain with alanine (Y52A R53A). The polar face of the helix was enhanced by substituting three hydrophobic residues that are present in there, L46 C50 Y57, with lysine which will make the polar face completely charged. This face was also weakened by replacing three lysine residues, K49 K56 K60 with alanine, which will reduce the overall charge of the polar face. A R54A R61A double mutation was introduced into the M2 AH peptide to weaken the helix at its interface. Additionally the M2 AH was disrupted by addition of either one or two extra alanine residues on the N-terminus to alter the phase of helical rotation.

The majority of the peptides in solution behaved similarly as a wild type M2 AH, with CD spectra resembling a random coil (Fig. 3.2-11 A) and the helix percentage being below 10% (Fig. 3.2-11 B). However, three mutations – F47A F48A, CRAC mutation and addition of one alanine in the N-terminus showed slightly increased helix percentage, up to 20% (Fig. 3.2-11 B), which suggests that these mutations allowed the peptide to start changing its conformation, but formation of the helix was not successful. Interestingly addition of two alanine residues in the N-terminus resulted in formation of a helix in solution, with over 95% of the estimated helix percentage present (Fig. 3.2-11 A and B).

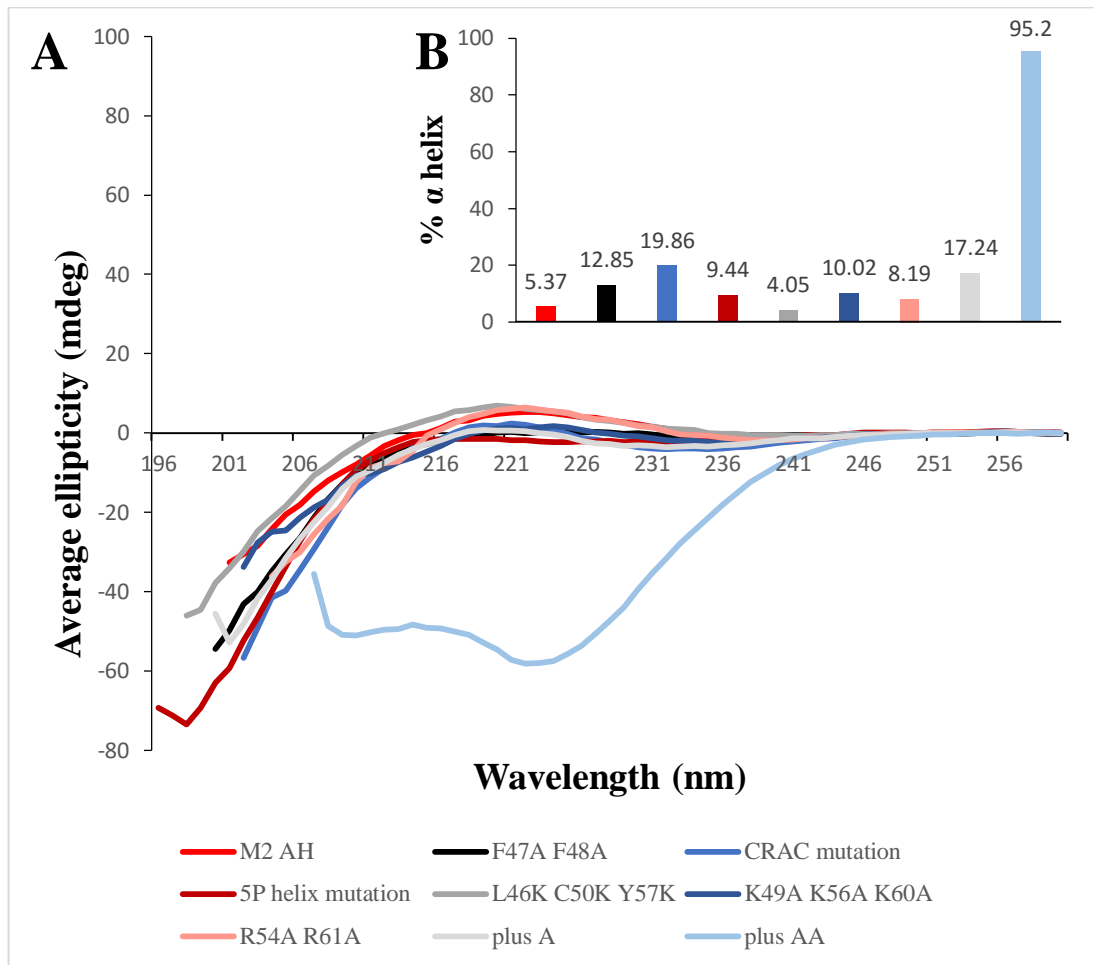
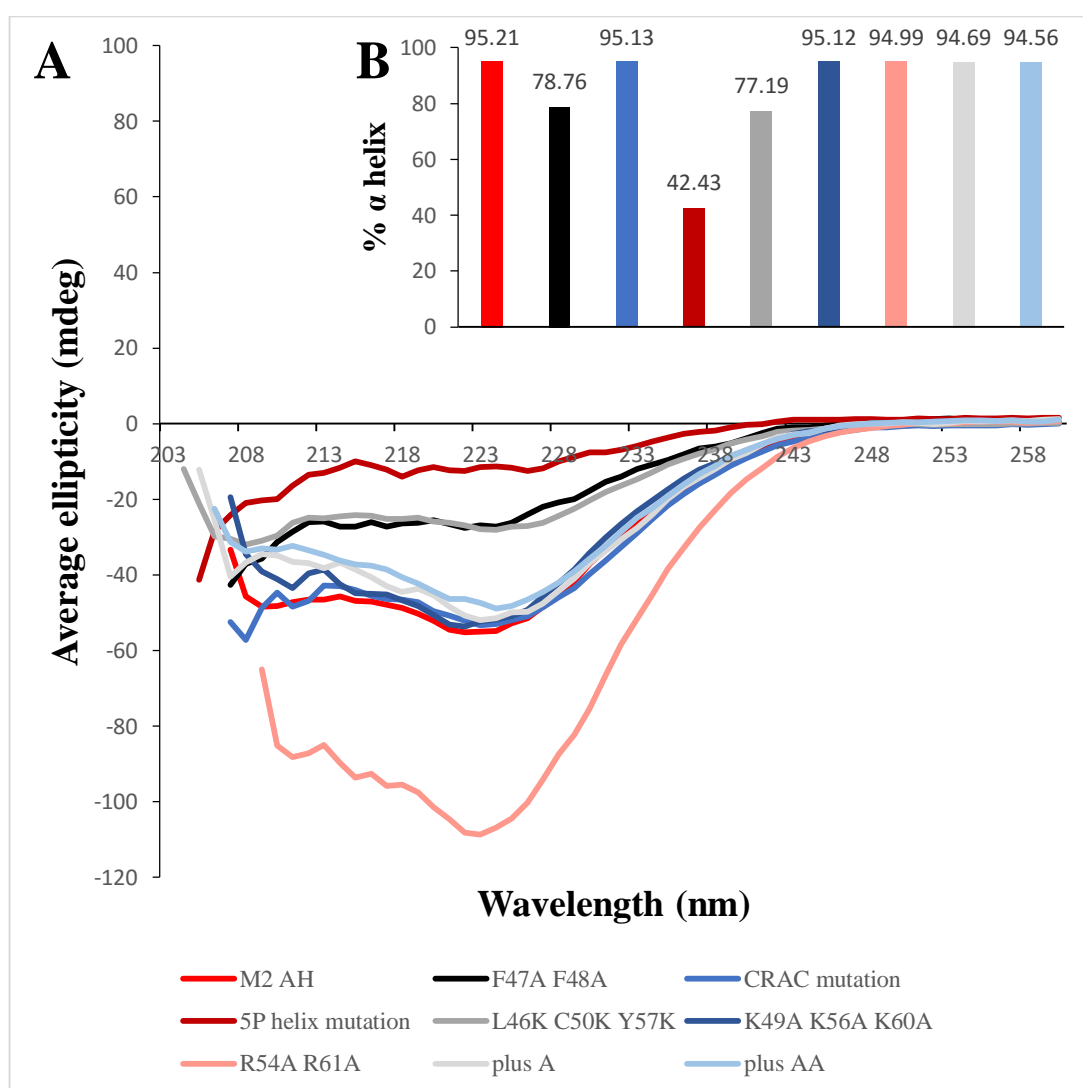


Figure 3.2-11 CD spectra for 250 μ M 18 amino acid long M2 AH peptide based on A/England/09 strain and its mutants (as described in chapter 2.1.1) in solution (A) and estimated percentage of an α helix present in each sample calculated based on the spectra using K2D3 bioinformatics tool on <http://k2d3.orgic.ca/> website (B).

In the presence of standard LUVs, most of the peptides show two deep troughs that resemble spectra for an α -helix and over 94% of the helix present (Fig. 3.2-12 A and B), with very deep troughs (about two fold increase in depth) for the R54A R61A double mutant. This suggests that those mutations do not affect the peptide's ability to form an α -helix in a lipid environment. As expected, introduction of a 5 point mutation in the hydrophobic face of the helix resulted in huge reduction of the troughs depth and, as a result, in the helix percentage (Fig. 3.2-12 A and B), which confirms that the growth impairment mutant is not able to form a helix. The F47A F48A mutation, which is also a part of the 5 point mutant, caused a slight reduction in the troughs

depth, with the helix percentage dropping from over 94% to around 78% (Fig. 3.2-12 A and B). Interestingly, a similar result has been observed with the L46K C50K Y57K mutant, which had mutations in the polar face of the helix designed to complete the polar face with charged residues. This suggests that it is not only the hydrophobic face, but also the polar face of the helix which may be important for its formation, especially the few hydrophobic residues that are present in the polar face.



3.2.4 Summary

NMR experiments have shown that the M2 AH is formed upon binding with liposomes and when the peptide is in solution it is unstructured (see chapter 3.1.2). To quantify the binding ability of the M2 AH, an assay has been created in which fluorescently labelled peptide is incubated with liposomes, unbound peptide is removed by filter washes and fluorescence is measured on a fluorescence plate reader. Initial experiments have shown that the optimal concentrations for this type of assay are 100 μM of peptide and 2.5 mM of lipids (Fig. 3.2-1 and 3.2-2). The M2 AH bound to standard LUVs give 5 fold greater signal than the controls, which shows the peptide bound well to the liposomes (Table 3.2.2).

To further investigate the structure of the M2 AH and the effect of different environments on it, CD spectroscopy has been used. Initial experiments have been performed with a range of different lipid and peptide concentrations showing that an α -helix is being formed in presence of liposomes and that it is lipid and peptide concentration dependent. At lower lipid and peptide concentrations, 250 μM and 100 μM respectively, the estimated helix percentage was low but it was rising with an increase in concentrations until a certain threshold was reached, 5 mM and 2 mM of lipids with 250 μM and 500 μM of peptide respectively, after which high level of estimated helix percentage, above 90%, was maintained (see chapter 3.2.3.1). Therefore 5 mM lipid concentration and 250 μM peptide concentration were chosen as optimal concentrations for this type of assay.

Further CD experiments confirmed that the M2 AH peptide is unstructured in solution and an α -helix is being formed in presence of liposomes or TFE (Fig. 3.2-7). Similar results have also been observed with 17 amino acid long M2 AH peptide based on the A/Udorn/72 strain and with the M2 AH peptide based on recent pandemic strain, A/England/09 (Fig. 3.2-10 and Fig. 3.2-9 respectively). Interestingly these two influenza virus strains differ in the M2 AH sequence by only three amino acids at positions 54, 56 and 57 (Fig. Fig. 3.2-8) with regard to full length M2 protein. Residues at two of these positions, 54 and 57 have been shown to be responsible for binding

with the lipid membranes by STD NMR (Fig. 3.1-10) and therefore are important for formation of the helix. This shows that formation of the M2 AH upon binding with liposomes is conserved among influenza virus strains and that these changes in sequence between those two strains do not inhibit helix formation or binding with membranes, even if they are present in a region that has been shown to be responsible for binding with membranes. This suggests that either the changes are not significant enough to fully disrupt helix formation, they affect the strength of interaction (which was not possible to determine in these assays), or other residues in the helix become involved to compensate for the changes.

A series of different mutations were introduced to different parts of the M2 AH, as described in chapter 2.1.1, and were then tested by CD spectroscopy to investigate how they affect formation of the helix. The majority of mutations did not affect peptide's behaviour in solution, showing very low levels of estimated helix percentage (below 10%) (Fig. 3.2-11) however, three of the mutations: F47A F48A, CRAC mutation and addition of one alanine in the N-terminus showed slightly increased the helix percentage which suggests that they allowed the peptide to start changing its conformation, but formation of the helix could not be completed. Interestingly one mutation, addition of two alanine residues in the N-terminus of the peptide allowed for formation of an α -helix in solution (Fig. 3.2-11).

In the presence of LUVs, the majority of mutations did not affect the peptide's behaviour, showing formation of the helix (Fig. 3.2-12). As expected, the introduction of the 5 point mutation into the peptide, which causes growth impairment in the virus (Rossman et al. 2010a, Rossman et al. 2010b), caused a huge reduction in the estimated helix percentage (Fig. 3.2-12). Two mutations caused slight reduction in estimated helix percentage: F47A F48A, which is also a part of a 5 point mutant, and L46K C50K Y57K, which is a mutation that enhances and completes the polar face of the helix (Fig. 3.2-12). The latter of these suggests that it is not only the hydrophobic face, but also polar face of the helix that may be important for helix formation, especially the hydrophobic residues that are present there.

These results correspond well to the STD NMR data (see chapter 3.1.3) which shows that residues in hydrophobic face of the helix at positions 48, 51, 54, 55, 58 and the hydrophobic residue in the polar face at residue 57 are responsible for binding with lipid membranes. Therefore if an amino acid in one of these positions has been replaced with a non-polar alanine residue (as in case of F47A F48A) or the polar lysine residue (as with the L46K C50K Y57K mutants) helix formation was slightly reduced. When three of the amino acids were replaced with alanine, as in case of 5 point mutant (F47A F48A I51A Y52A F55A) helix formation was significantly reduced.

3.3 EFFECTS OF THE LIPID ENVIRONMENT ON M2 AMPHIPATHIC HELIX – MEMBRANE BINDING

3.3.1 Introduction

It has been shown that the M2 AH is formed upon binding with liposomes with the hydrophobic face of the helix mainly being responsible for binding (see chapters 3.1.2; 3.1.3; 3.2.2 and 3.2.3). However, these interactions were investigated in presence of a standard lipid membrane. Different compositions of the membrane may influence the formation and binding of the M2 AH. The M2 AH is composed of polar and hydrophobic faces. The polar face of the helix contains charged amino acids, of which many are cationic, and therefore these residues may interact with anionic lipids present in the membrane.

Some lipids, such as cholesterol in higher concentrations and sphingomyelin have been shown to inhibit the M2 AH (Rossman et al. 2010b), but the mechanism of action behind this inhibition is unknown. PIP2 has been shown to play a role in the transport of viral proteins and assembly of HIV (Carlson and Hurley 2012) and HIV budding occurs at defined lipid raft domains similar to Influenza A virus, which suggests that it may also play a role in influenza virus assembly. However, lipid composition of the membrane is not the only factor that can affect the M2 AH formation and binding, the presence of different domains or defects and curvature of the membrane may also affect the M2 AH formation and binding.

The influenza virus buds off from lipid raft domains, which are liquid ordered phases located on the liquid disordered phase plasma membrane, with the M2 protein localised just outside of the lipid rafts (Takeda et al. 2003, Leser and Lamb 2005, Chen et al. 2007). Therefore line tension, which is an interfacial energy at the edge between liquid ordered and disordered phase may have an effect on the M2 AH. In the final stages of viral budding the M2 protein is localised to the neck of newly formed virion (Rossman et al. 2010b), which is a region of high positive membrane curvature thus M2 AH may preferentially bind to membranes with high positive membrane curvature. Defects present in the membrane, which are spacing in one leaflet of the membrane caused by membrane curvature may also affect the M2 AH allowing for deeper

insertion of the AH into the membrane. To investigate how different lipids and different membrane properties affect the M2 AH formation and binding with membranes, different size liposomes have been made composed of variety of lipids and the M2 AH structure and function have been tested mainly by CD and the binding assay.

3.3.2 Charge interactions

3.3.2.1 Different anionic lipids

M2 AH has a lot of cationic residues on the polar face (Fig. 1.2-3) and so the different types of charged lipids may have an effect on the protein. To investigate this, the M2 AH peptide has been tested in the presence of standard LUVs in which PG has been replaced with different types of anionic lipids. Both phosphatidylserine (PS) and phosphatidic acid (PA) are anionic lipids and phosphatidylethanolamine (PE) is zwitterionic and has a cone shape (Li et al. 2015). In presence of PG, PS and PA spectra resembled spectra characteristic for an α -helix with high helix percentage, at around 90% (Fig. 3.3-1 A and B). That suggests that type of anionic lipid present in the membrane does not influence formation of the M2 AH. However, when PG was replaced by PE, the troughs depth and helix percentage significantly dropped (to about 60%) suggesting that PE disrupts the membrane because of its shape and this inhibited M2 AH formation (Fig. 3.3-1 A and B).

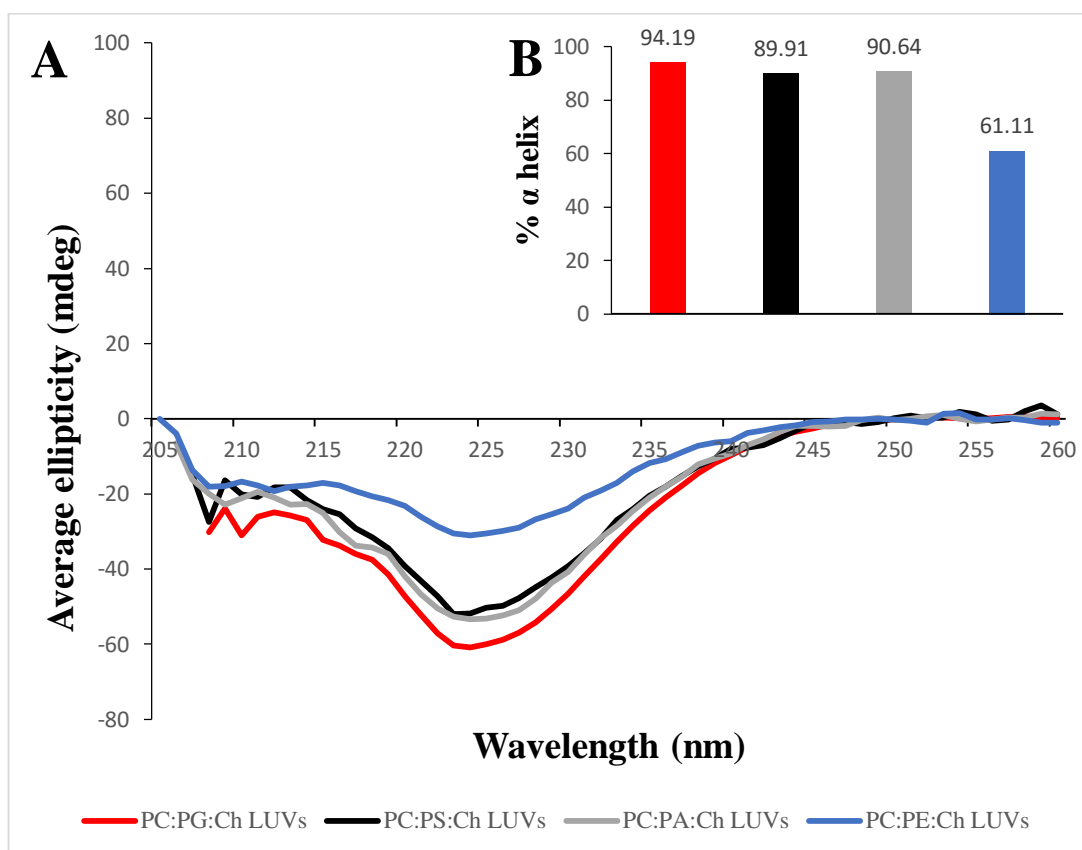


Figure 3.3-1 CD spectra for 250 μ M M2 AH peptide with 5 mM of standard LUVs (PC:PG:Ch at 4:1:0.05 molar ratio) and LUVs containing different types of anionic lipids (PS and PA) or zwitterionic lipid (PE) instead of PG, at the same molar ratio (A) and estimated percentage of an α helix present in each sample calculated based on the spectra using K2D3 bioinformatics tool on <http://k2d3.ogic.ca/> website (B).

The binding assay confirmed good binding of the M2 AH peptide to the membranes composed of PC, PG and Ch (Fig. 3.3-2). Surprisingly when PG was replaced by PS or PA average fold binding doubled (Fig. 3.3-2), which might suggest that although the type of anionic lipid does not influence formation of the M2 AH, as shown by CD (Fig. 3.3-1 A and B), it may enhance its ability to bind to the membranes. When PG was replaced by PE, average fold binding has been significantly reduced (Fig. 3.3-2), which confirms CD observations.

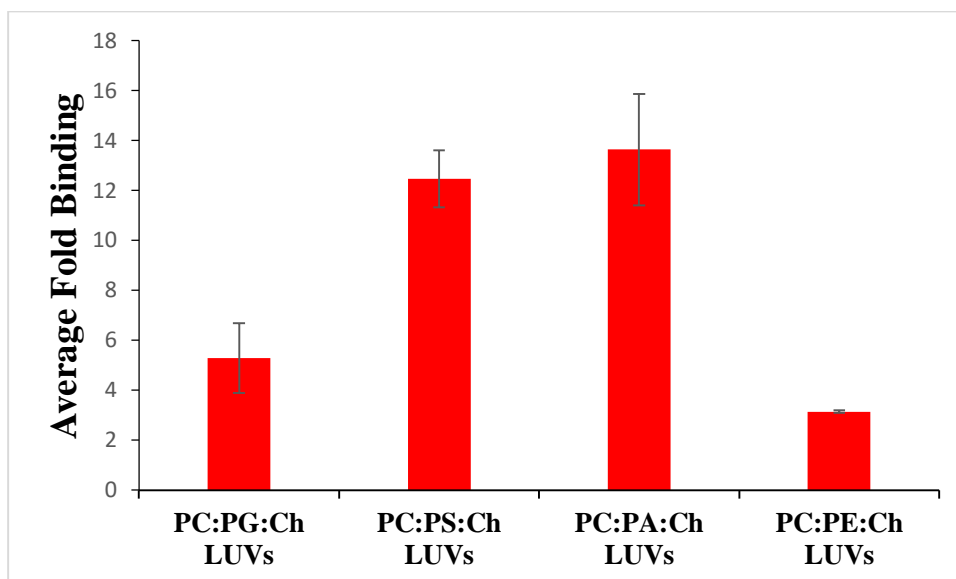


Figure 3.3 - 2 Average Fold Binding values for samples with 100 μ M of fluorescently labelled M2 AH peptide incubated with 2.5 mM of standard LUVs (PC:PG:Ch) and LUVs containing different types of anionic lipids (PS and PA) or zwitterionic lipid (PE) instead of PG.

To further investigate the role of anionic lipids in the M2 AH formation and binding with lipid membranes, a range of different PS concentrations have been tested. When used as a replacement for another anionic lipid (PG) so far, PS was at 1 molar ratio in LUVs which corresponds to 20 molar %. In this concentration range PS was used at few lower concentrations - 1,5,10 molar % and one higher - 40 molar %. All concentrations tested showed similar CD spectra, which suggest formation of an α -helix, but trough depth has been slightly reduced for 1% and 10% of PS present (Fig. 3.3-3 A). The helix percentage for 1% and 10% PS membranes was also reduced, by approximately 10% and 20% respectively (Fig. 3.3-3 B) however, higher percentage of PS in the membrane, 20% (Fig. 3.3-1 B) and 40% (Fig. 3.3-3 B) show very high helix percentage, above 87%. These results suggest that, although in low PS concentrations (between 1-10%) formation of the M2 AH is varied and may be reduced, higher PS concentrations in the membrane (above 20%) support M2 AH formation.

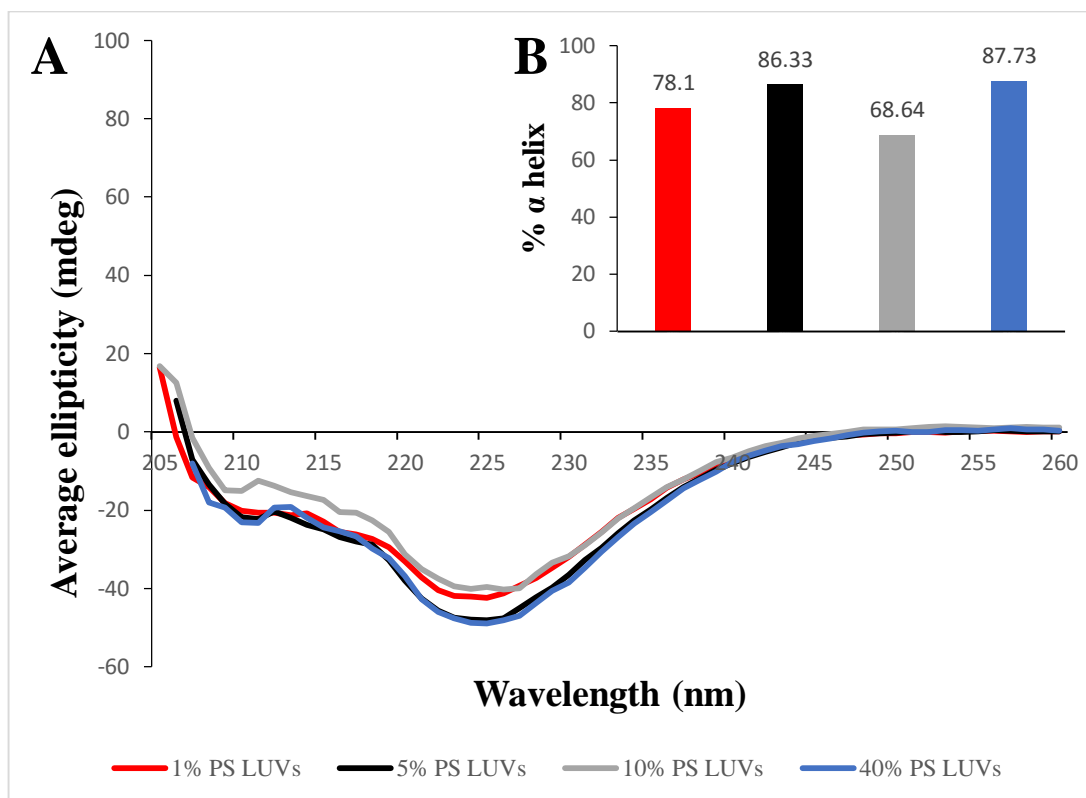


Figure 3.3 - 3 CD spectra for 250 μ M M2 AH peptide with 5 mM of 100 nm LUVs composed of PC:PS:Ch with increasing concentration of PS present (A) and estimated percentage of an α helix present in each sample calculated based on the spectra using K2D3 bioinformatics tool on <http://k2d3.ogic.ca/> website (B).

Binding assays with a range of different PS concentrations in the membrane showed reduced binding in case of 1% PS, and increased binding activity for higher PS concentrations (Fig. 3.3-4), when compared with standard LUVs (Table 3.2-1). Despite high variability in the measurements, which leads to high standard error values (especially in case of 10% PS membranes), average fold binding is significantly increased with PS concentration above 5% (Fig. 3.3-4), which suggest that higher concentrations of PS support M2 AH binding with membranes.

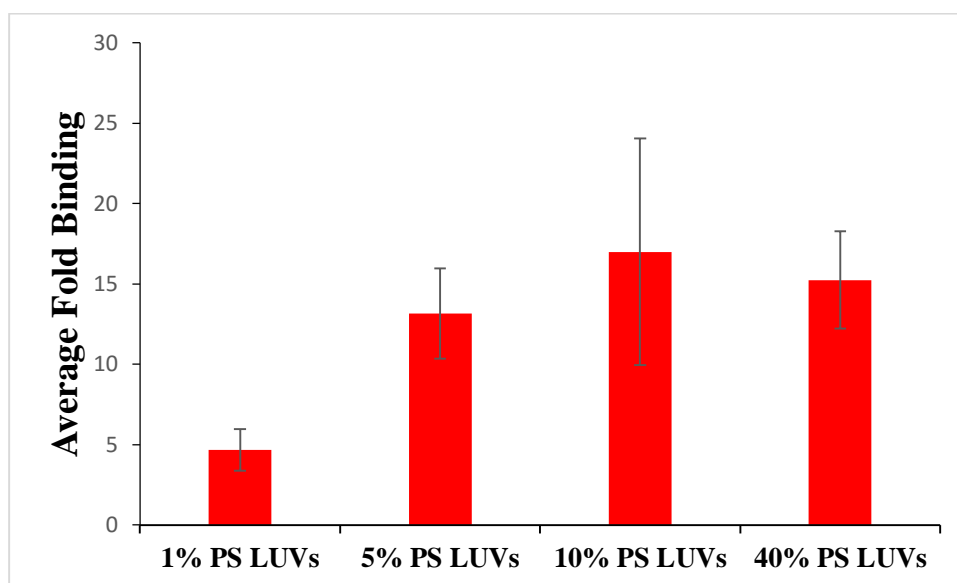


Figure 3.3 - 4 Average Fold Binding values for samples with 100 μ M of fluorescently labelled M2 AH peptide incubated with 2.5 mM of 100 nm LUVs composed of PC:PS:Ch with an increasing concentration of PS present.

3.3.2.2 Absence of anionic lipids

To investigate if there are interactions between the cationic face of the helix and anionic lipids in the membrane, which influences formation of the M2 AH and its ability to bind to lipid membranes, LUVs with and without anionic lipids have been used. In the presence of standard LUVs, the M2 AH peptide gave a spectra resembling an α -helix formation, with a deep trough at around 222 nm and helix percentage above 94% (Fig. 3.3-5 A and B). When PG was removed and only PC and Ch were present in the membrane, the trough depth in the CD spectra was significantly reduced and helix percentage dropped to approximately 77% (Fig. 3.3-5 A and B). These results suggest that anionic lipids support formation of the M2 AH but are not essential as helix formation is not completely inhibited in their absence.

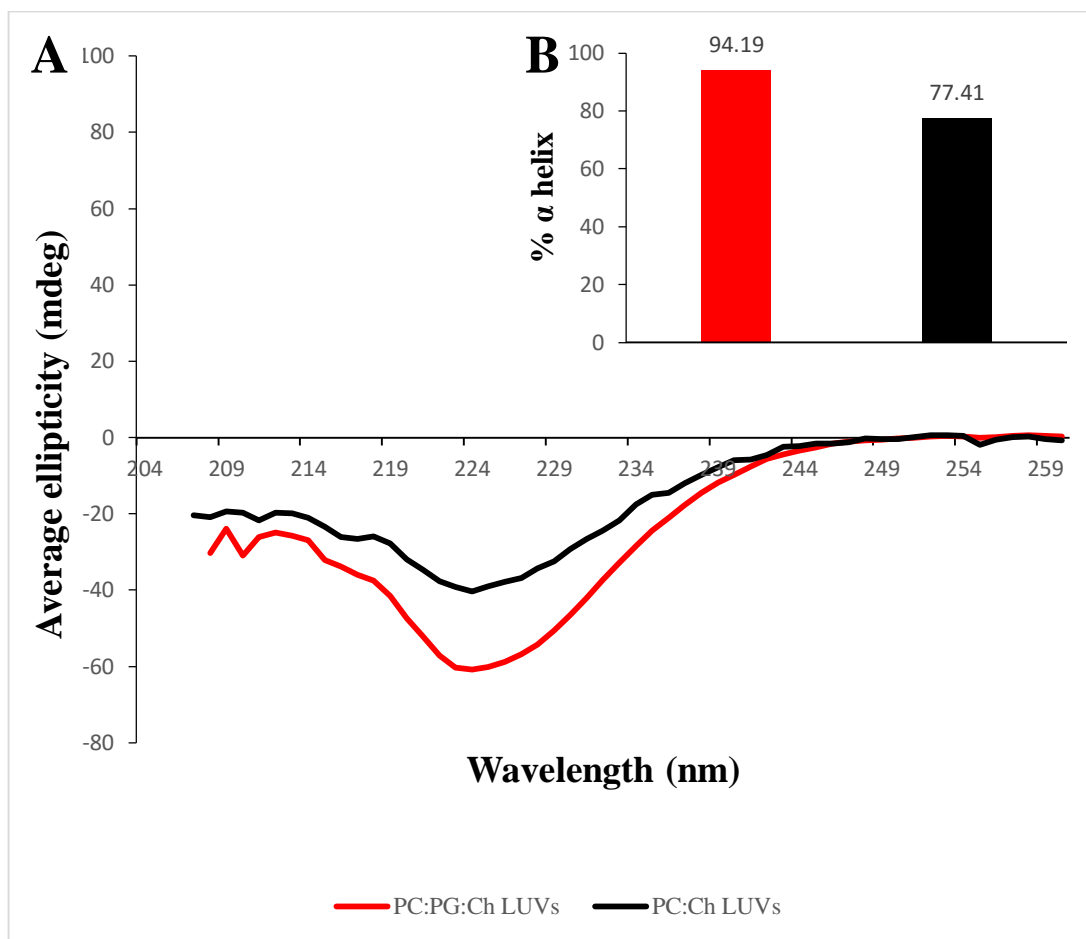


Figure 3.3 - 5 CD spectra for 250 μ M M2 AH peptide with 5 mM of standard LUVs and LUVs without anionic lipid (PG) present (A) and estimated percentage of an α helix present in each sample calculated based on the spectra using K2D3 bioinformatics tool on <http://k2d3.orgic.ca/> website (B).

Surprisingly, analysis of peptide binding showed an increased binding activity to the membranes without anionic lipids present (Fig. 3.3-6). This suggests that, although anionic lipids may support formation of the helix, they are not supporting the peptide's ability to bind to membranes. Similar experiments have been performed using LUVs made in 1 mM HEPES buffer instead of potassium buffer, showing a similar trend, with an increase in overall binding activity in both cases, which suggests that HEPES buffer may increase peptide binding to the membranes, but does not influence interactions between them (Fig. 3.3-7).

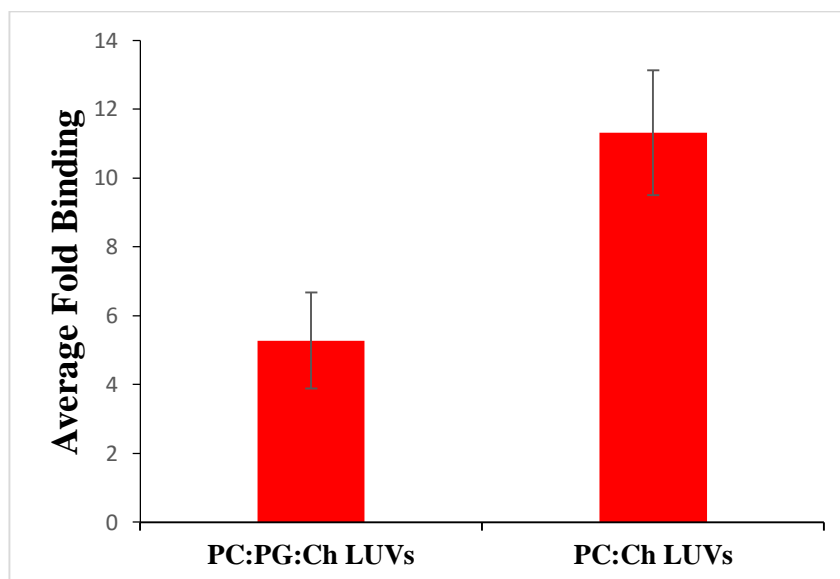


Figure 3.3 - 6 Average Fold Binding values for samples with 100 μ M of fluorescently labelled M2 AH peptide incubated with 2.5 mM of standard LUVs and LUVs without anionic lipid (PG) present.

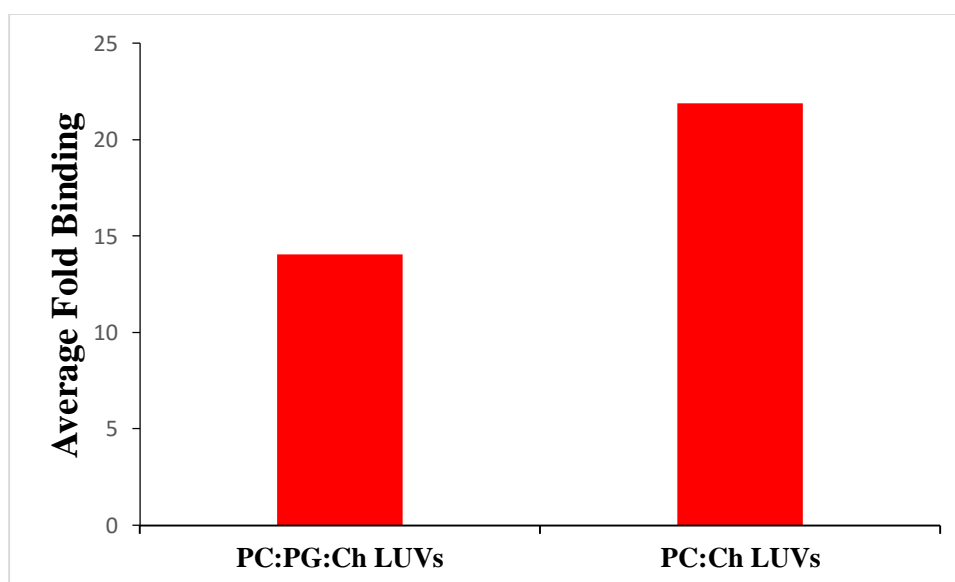


Figure 3.3 - 7 Average Fold Binding values for samples with 100 μ M of fluorescently labelled M2 AH peptide incubated with 2.5 mM of LUVs and LUVs without anionic lipid (PG) present made in 1 mM HEPES buffer.

3.3.2.3 Ionic strength

To further investigate if charge interactions affects the M2 AH interaction with membranes, binding assays were performed using standard LUVs made in 1mM HEPES with an increasing ionic strength in the buffer which was accomplished with the addition of increasing concentrations of sodium chloride instead of water, which was used before. With low ionic strength (32 mM) in the buffer the average fold binding drops slightly, followed by a slight increase with an increase in the ionic strength in the buffer (32-482 mM), after which average fold binding value is dropping again for the highest ionic strength concentration to a level observed with 0 mM concentration (Fig. 3.3-8). This suggests that, although there are slight changes in the peptide's ability to bind to the membrane with a changing buffer ionic strength, there are no drastic changes associated with a particular concentration. All samples showed at least a two fold increase in peptide binding compared to when potassium buffer was used to make LUVs (Fig. 3.3-6), but this is a characteristic specific for this type of LUVs (Fig. 3.3-7), not an effect caused by increasing ionic strength in the buffer. Ionic strength of the buffer does not influence the interaction between the M2 AH and the lipid membrane due to charged interactions. This is because increase in ionic strength of the buffer will saturate the AH charge interactions and prevent charge interactions with the membrane, so if charge interactions are involved in binding loss of signal would be observed, which is not the case.

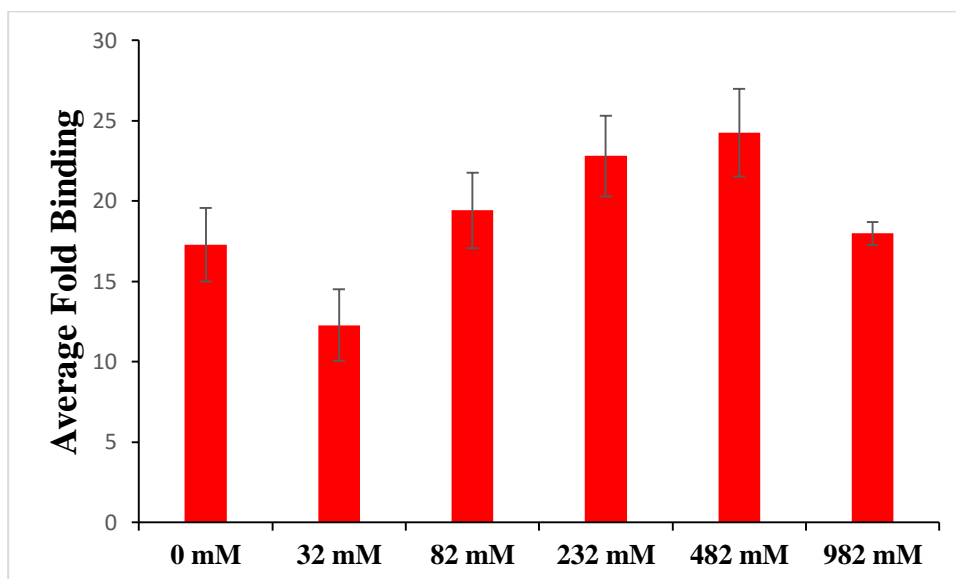


Figure 3.3 - 8 Average Fold Binding values for samples with 100 μ M of fluorescently labelled M2 AH peptide incubated with 2.5 mM of LUVs made in 1 mM HEPES with an increasing ionic strength in the buffer.

3.3.3 Effects of cholesterol

Cholesterol and sphingomyelin have been shown to inhibit the budding activity caused by the M2 protein. High levels of cholesterol, 20 molar % and above, inhibit the M2 AH mediated budding but when cholesterol is at a physiologically relevant level, about 17 molar % or below, the M2 AH induces budding in LUVs (Rossman et al. 2010b). To investigate the role of cholesterol in the M2 AH formation and binding with the membrane, a range of LUVs with different concentrations of cholesterol have been used. Standard LUVs are normally formed with PC, PG and Ch mix at 4:1:0.05 molar ratio, which corresponds to 1 molar % for cholesterol. In this range 5, 10, 20, 30 and 40 molar % of cholesterol have been used reducing molar % of PC respectively and keeping molar % of PG at a constant level to form LUVs. Surprisingly, all samples showed similar CD spectra, which resembles spectra characteristic for an α -helix, with only slight reduction in trough depth in the highest cholesterol concentration (Fig. 3.3-9 A). Helix percentages were on a high and stable level, around 90% for all samples, for all concentrations with exception of the highest cholesterol concentration (40%), when helix percentage dropped by 5% (Fig. 3.3-9 B), suggesting that the level of cholesterol present in the membrane does not influence formation of the M2 AH.

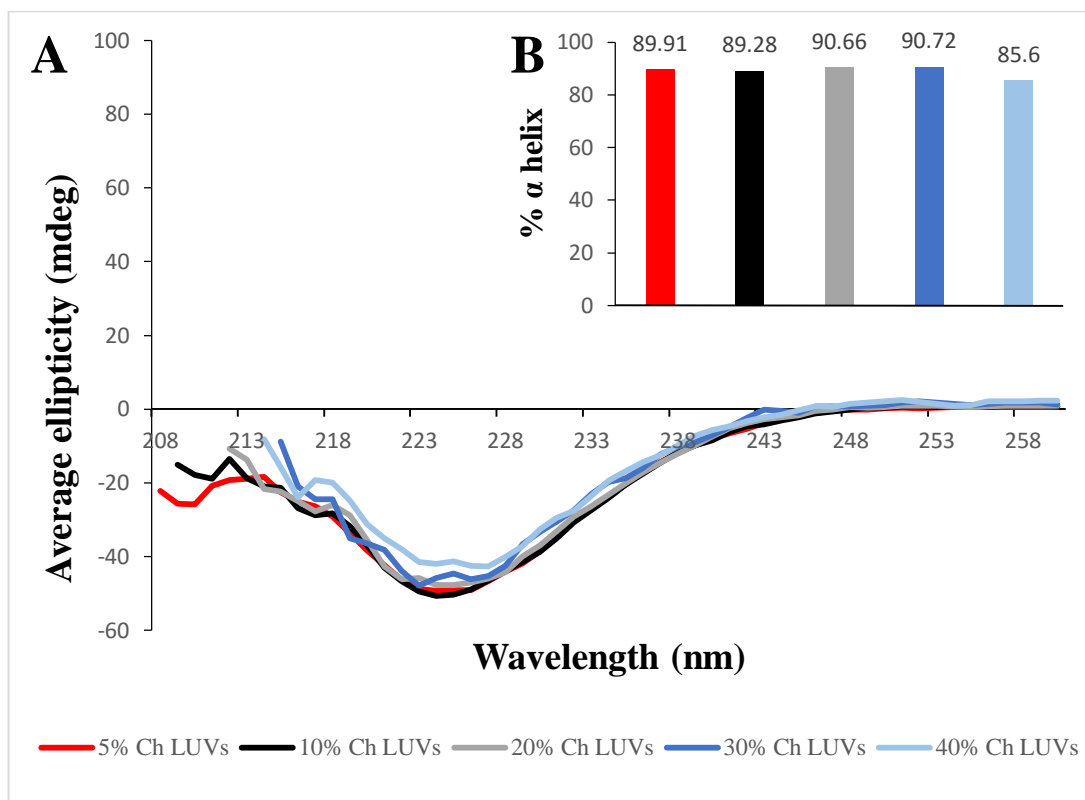


Figure 3.3-9 CD spectra for 250 μ M M2 AH peptide with 5 mM of standard LUVs with increasing concentration of cholesterol present (A) and estimated percentage of an α helix present in each sample calculated based on the spectra using K2D3 bioinformatics tool on <http://k2d3.ogic.ca/> website (B).

Binding assays showed a similar level of binding with 5 molar % of cholesterol present in the membrane as with the standard LUVs, which are composed of 1 molar % of cholesterol (Fig. 3.3-10). Increasing the cholesterol concentration, up to 10 molar % caused an increase in binding activity, however, further increase in cholesterol concentration, above 20 molar %, caused constant decrease in binding activity (Fig. 3.3-10). In the presence of the highest cholesterol concentration, 40 molar %, the average fold binding dropped below the level observed for 5 molar % (Fig. 3.3-10). This suggests that although the low cholesterol concentrations, 5 and 10 molar %, may support the M2 AH peptide binding to membranes, higher cholesterol concentrations, above 20 molar % reduce binding.

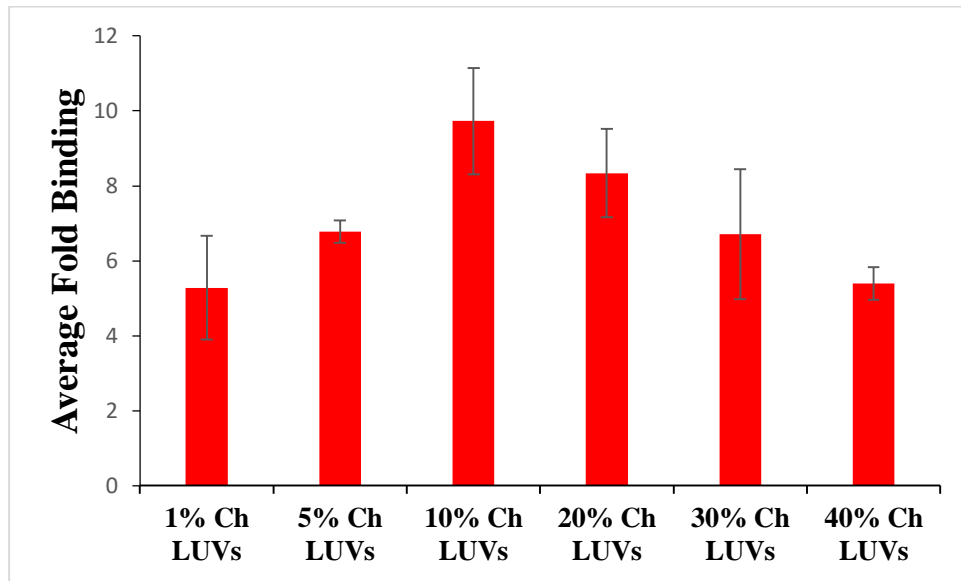


Figure 3.3 - 10 Average Fold Binding values for samples with 100 μM of fluorescently labelled M2 AH peptide incubated with 2.5 mM of standard LUVs with increasing concentration of cholesterol present.

3.3.4 Effects of PIP2

The lipid composition of the membrane can affect the budding of viruses from the cells. PIP2 is one of the lipids that is present in the plasma membrane and has been shown to play a role in clustering of the Gag protein that initiates assembly of the HIV virus (Carlson and Hurley 2012). Immunofluorescence microscopy was used to investigate if PIP2 affects the M2 AH and budding. HEK 293T cells were grown that had been transfected with a plasmid encoding for the M2 protein, which was detected by the 14C2 antibody and stained for with a fluorescently labelled secondary antibody. Fluorescently labelled PIP2 was also incubated with the cells and removed before fixation and mounting on the slides. As shown in Figure 3.3-11, M2 and PIP2 rarely co-localise but are frequently proximal to each other, with PIP2 localised just cytoplasmically from the plasma membrane localised M2. This suggests that PIP2 may play a role in M2 mediated budding due to close localisation but the mechanism for this or interactions between PIP2 and M2 are not known.

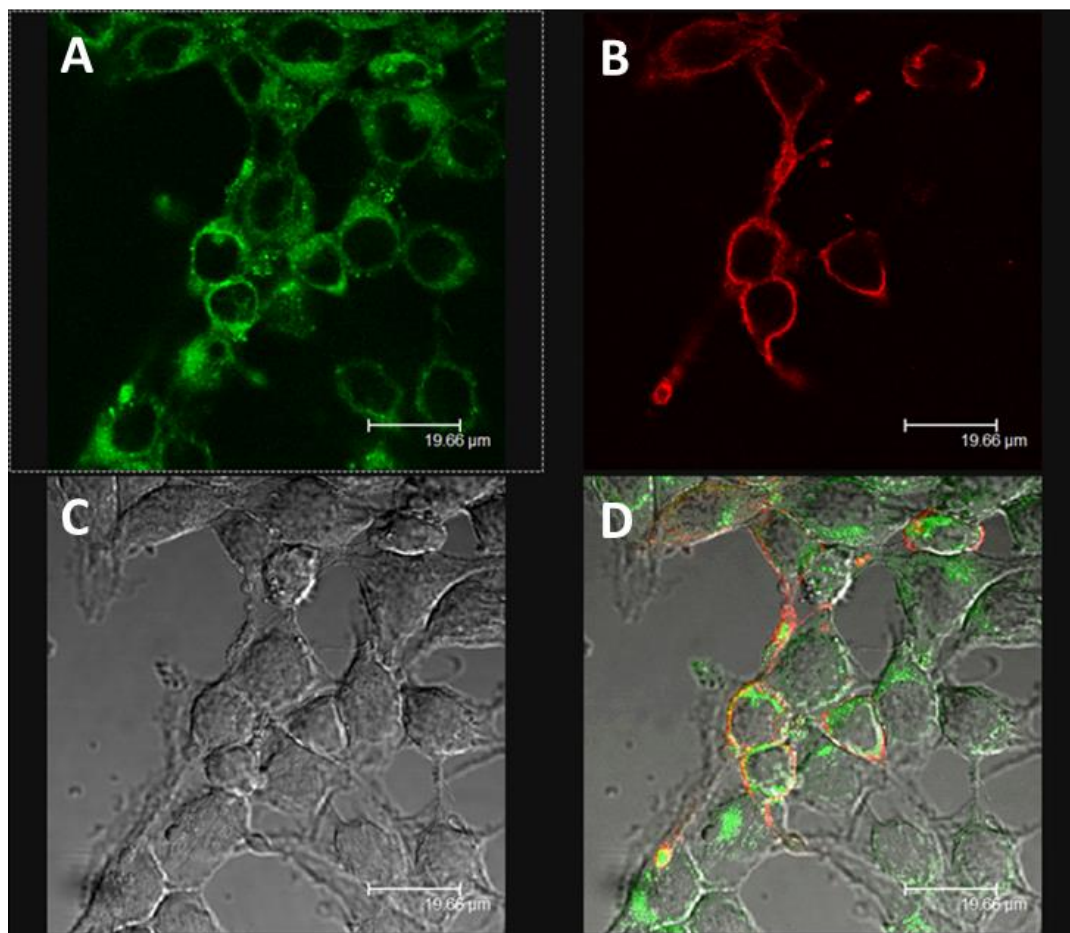


Figure 3.3 - 11 Confocal images of HEK 293T cells transfected with 2.5 μ g of plasmid expressing M2 protein, stained with fluorescently labelled PIP2 and fixed after 47 h and 48 h post transfection respectively, followed by immunostaining with 14C2 antibody. A- PIP2, B- M2, C- HEK 293T cells, D- merged.

PIP2 has therefore been incorporated into the LUVs at 3 different concentrations, 0.55, 1 and 5 molar %, to test whether its presence can influence the M2 AH formation or its ability to bind to the membranes. CD has shown very similar spectra for all three PIP2 concentrations, with very high helix percentage, between 91-94% (Fig. 3.3-12 A and B). The binding assay also showed similar levels of binding for all three PIP2 concentrations used (Fig. 3.3-13), with average fold binding only slightly higher than values obtained with standard LUVs (Table 3.2-1). These results suggest that PIP2 may support formation of the M2 AH and it is binding with the membranes but it is not essential as the peptide structure and functions are not affected when PIP2 is lacking (Fig. 3.2-7 and Table 3.2-1).

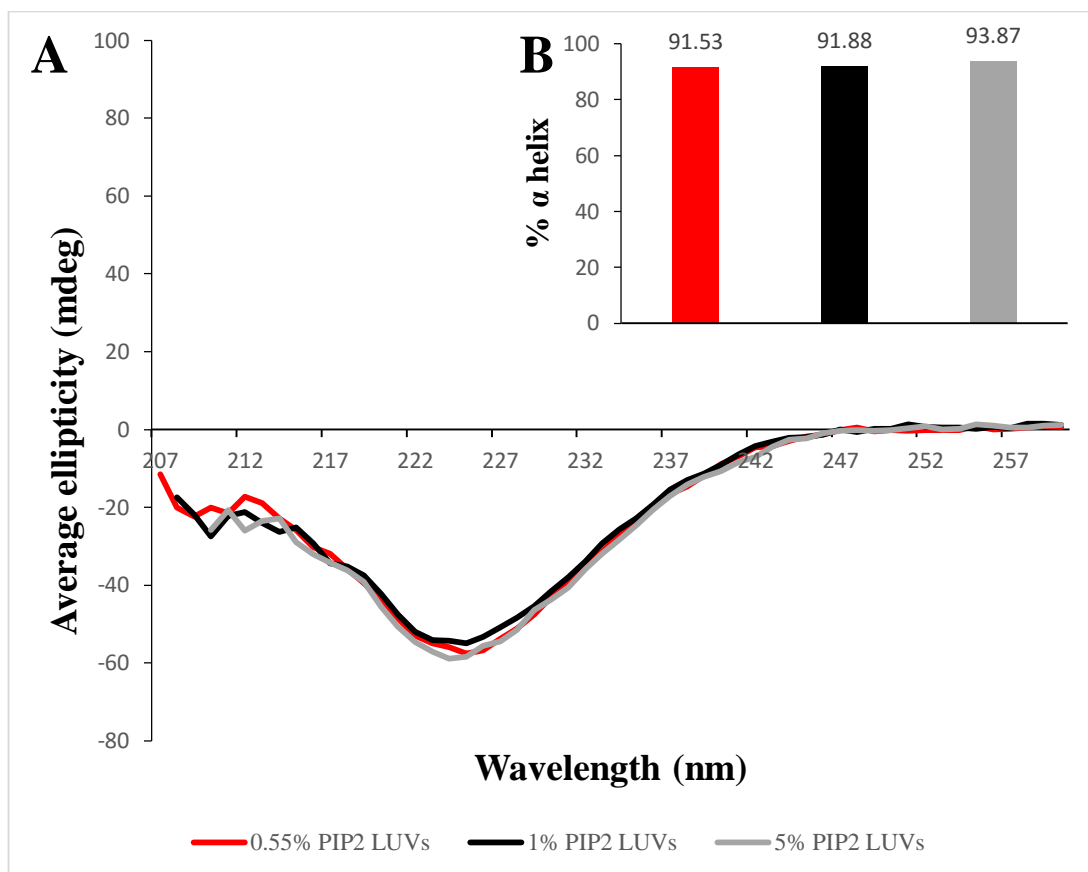


Figure 3.3 - 12 CD spectra for 250 μ M M2 AH peptide with 5 mM of standard LUVs with increasing concentration of PIP2 incorporated into the membrane (A) and estimated percentage of an α helix present in each sample calculated based on the spectra using K2D3 bioinformatics tool on <http://k2d3.org.ca/> website (B).

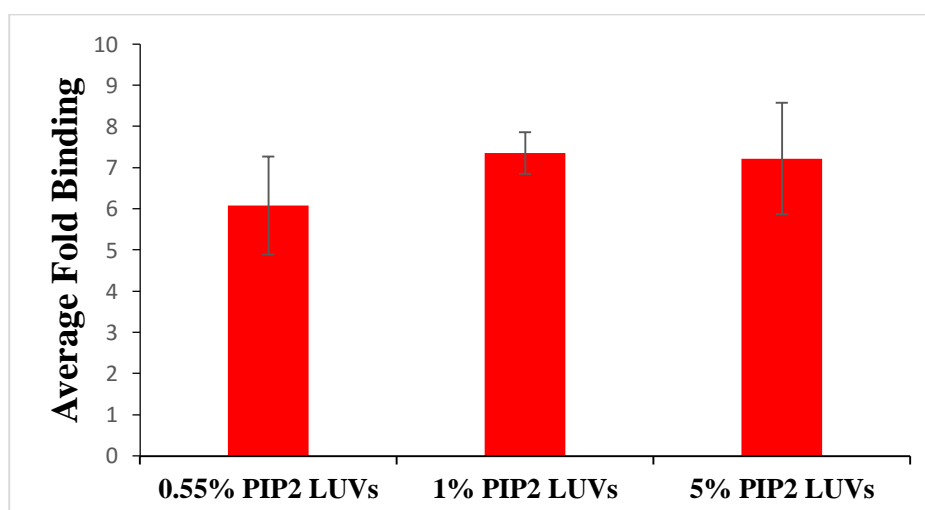


Figure 3.3 - 13 Average Fold Binding values for samples with 100 μ M of fluorescently labelled M2 AH peptide incubated with 2.5 mM of standard LUVs with increasing concentration of PIP2 incorporated into the membrane.

3.3.5 Effects of lipid domain line tension

Influenza virus buds off from lipid raft domains, but the M2 protein is localised just outside of the lipid rafts, on the boundary between liquid ordered and disordered phases (Takeda et al. 2003, Leser and Lamb 2005, Chen et al. 2007), therefore changes in the line tension between domains may have an effect on the M2 AH binding, interaction and insertion into the membranes. To test how line tension in the membrane affects M2 AH, a range of phase separated LUVs in which part of the vesicle is in a lipid ordered phase and part in a lipid disorder phase, with increasing line tension in the boundary on the phases interface have been used. A series of different PC types, with a decreasing length of the acyl chain, have been used to modify thickness of the lipid disordered phase, which leads to increasing height mismatch between the two phases, and hence an increase in the line tension between domains, as shown previously (Garcia-Saez et al. 2007). LUVs have been formed in the temperature above the phase transition temperature respective for each lipid mix and composed of 40 molar % of sphingomyelin, 20 molar % of cholesterol and 40 molar % of different PC types, shown in Table 3.3-1, where dierucoyl-phosphocholine (DEPC) has the longest acyl chain and hence the smallest line tension and dimyristoleoyl-phosphocholine (DMPC) has the shortest acyl chain and the highest line tension in the series.

PC type (in increasing line tension order)	Full name	Chemical formula	Acyl chain length
DEPC	dierucoyl-phosphocholine	$C_{52}H_{100}NO_8P$	22
DeisPC	dieicosenoyl-phosphocholine	$C_{48}H_{92}NO_8P$	20
DOPC	dioleoyl-phosphocholine	$C_{44}H_{84}NO_8P$	18
DPPC	dipalmitoleoyl-phosphocholine	$C_{40}H_{76}NO_8P$	16
DMPC	dimyristoleoyl-phosphocholine	$C_{36}H_{68}NO_8P$	14

Table 3.3 - 1 Characteristics of different PC types with decreasing length of acyl chain that have been used to form series of LUVs with increasing line tension.

CD spectra show a single trough for all samples, which corresponds to the first α -helix trough (Fig. 3.3-14 A). The second characteristic α -helix trough is not visible due to an early voltage cut off, after which data is not available. The trough depth has been significantly reduced for first four PC types in the series (DEPC, DeisPC, DOPC and DPPC) and small reduction has been observed for DMPC, which has the shortest acyl chain (Fig. 3.3-14 A). The helix percentage appears to be significantly reduced when the PC with long acyl chains was used, with only 3.3% for DEPC and 29.49% for DeisPC (Fig. 3.3-14 B). However, as the acyl chain got shorter, the percentage increased, with DMPC reaching 64.89% (Fig. 3.3-14 B). These results show that the shorter the acyl chain in the PC lipid, and hence the higher the line tension in the domains, the more helix is being formed.

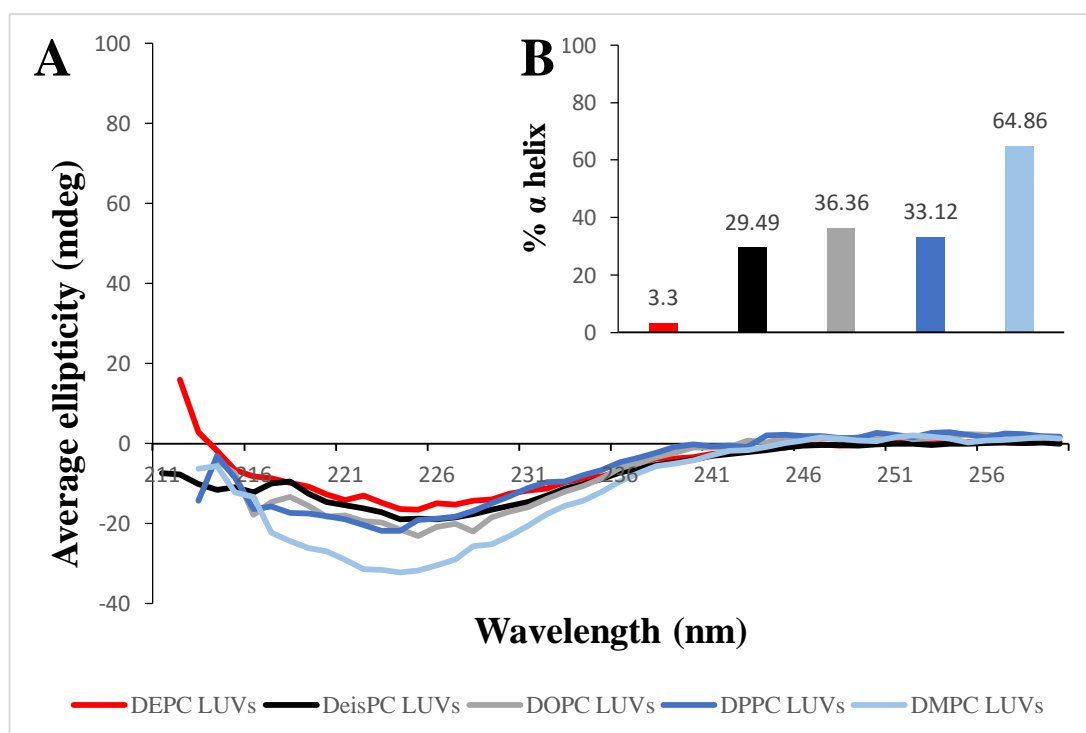


Figure 3.3 - 14 CD spectra for 250 μ M M2 AH peptide with 5 mM of 100 nm LUVs composed of sphingomyelin, cholesterol and series of different PC types (at 2:1:2 ratio) with decreasing length of acyl chain which results in increase of the line tension, where DEPC has the longest acyl chain and DMPC the shortest (A). Estimated percentage of an α helix present in each sample calculated based on the spectra using K2D3 bioinformatics tool on <http://k2d3.orgic.ca/> website (B).

CD showed significant reduction in trough depth and helix percentage for all samples, with the highest values for DMPC LUVs not reaching levels observed with standard LUVs (Fig. 3.2-7). Binding assays also showed a reduction in binding activity compared with standard LUVs (Table 3.2-1), which might be caused by the composition of phase separated LUVs- high levels of sphingomyelin and cholesterol and no anionic lipids, such as PG present. For most of the samples, average fold binding was reduced but on similar stable level, between 2 and 3 (Fig. 3.3-15). Surprisingly the highest binding activity was detected in presence of DeisPC, where average fold binding come to a level observed with standard LUVs (Fig. 3.3-15). These results suggest that although line tension in the domains influence formation of the M2 AH it does not influence its ability to bind to the membrane, as in majority of samples average fold binding is on similar level. The increase in binding in presence of DeisPC may suggest that this lipid supports M2 AH binding with membranes but mechanism behind that is not known.

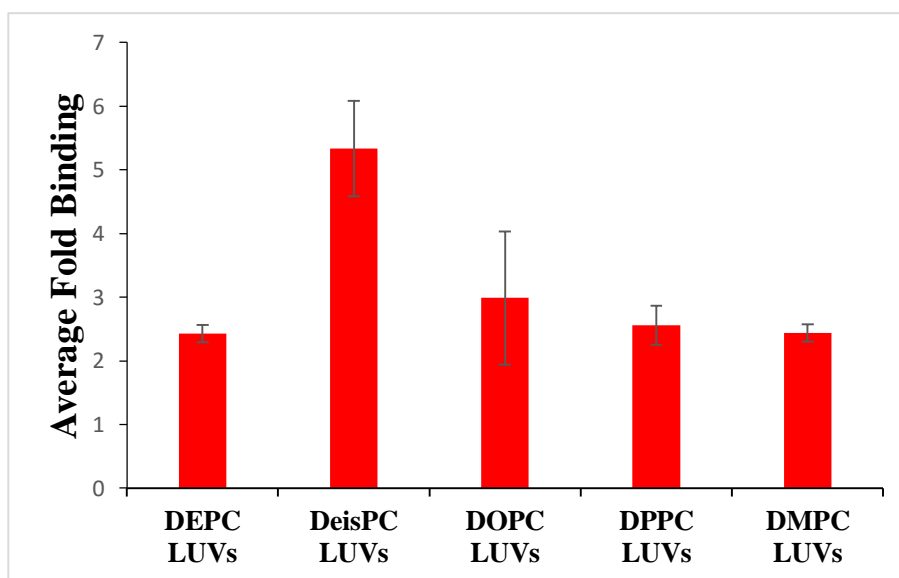


Figure 3. 3 - 15 Average Fold Binding values for samples with 100 μ M of fluorescently labelled M2 AH peptide incubated with 2.5 mM of 100 nm LUVs composed of sphingomyelin, cholesterol and series of different PC types (at 2:1:2 ratio) with decreasing length of acyl chain which results in increase of the line tension, where DEPC has the longest acyl chain and DMPC the shortest.

3.3.6 Effects of membrane curvature

3.3.6.1 Standard membranes

During virus budding, the M2 protein localises to the neck of the budding virion (Rossman et al. 2010b), which in its narrowest point is a region of high positive membrane curvature. To test how positive curvature of the membrane influences the structure and function of the peptide, a series of different size liposomes were made either by sonication (SUVs), by the extrusion through different filter sizes (LUVs), or by electroformation (GUVs). Vesicle sizes were checked using Dynamic Light Scattering (DLS). For 100 nm LUVs, the size distribution showed a single peak (Fig. 3.3-16) and based on that data, the average vesicle size was 102.6 nm (Table 3.3-2). The whole range of different size vesicles size distribution data is shown in appendix 6.3 A and average vesicle sizes are summarised in Table 3.3-2. These averages show that LUV sizes vary from the filter pore size however, they were within the advertised limits, and gave a range of different size liposomes between 58.88 nm and 350.4 nm in diameter.

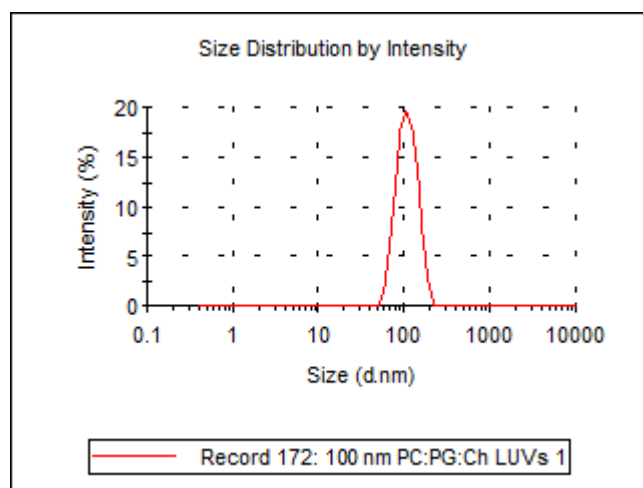


Figure 3.3 - 16 Graph showing size distribution by intensity for 100 nm LUVs composed of PC:PG:Ch measured by DLS.

designed size (extrusion membrane size)	actual size (average size measured on DLS)
SUVs	58.88 d.nm
30 nm LUVs	89.19 d.nm
50 nm LUVs	77.7 d.nm
100 nm LUVs	102.6 d.nm
200 nm LUVs	150.4 d.nm
1000 nm LUVs	350.4 d.nm

Table 3.3 - 2 Designed and actual average size of the PC:PG:Ch vesicles in the size range measured on DLS.

The CD spectra showed troughs of varied depth for range of SUVs and LUVs, however, when GUVs were present the spectra changed, with all three concentrations tested showing a small peak, (Fig. 3.3-17 A), similar to what was observed for a peptide in solution (Fig. 3.2-7). The helix percentage was at a very high level, around 90% for all range of small vesicles, which have more positive membrane curvature (with an exception of 89 nm LUVs, where helix percentage dropped to around 60%) which dropped significantly, to around 5%, when large vesicles has been present, which correspondingly have less positive membrane curvature (Fig. 3.3-17 B). Those results suggest that M2 AH is formed in wide range of positively curved membranes but helix formation can be inhibited with less curved membranes, as seen with GUVs.

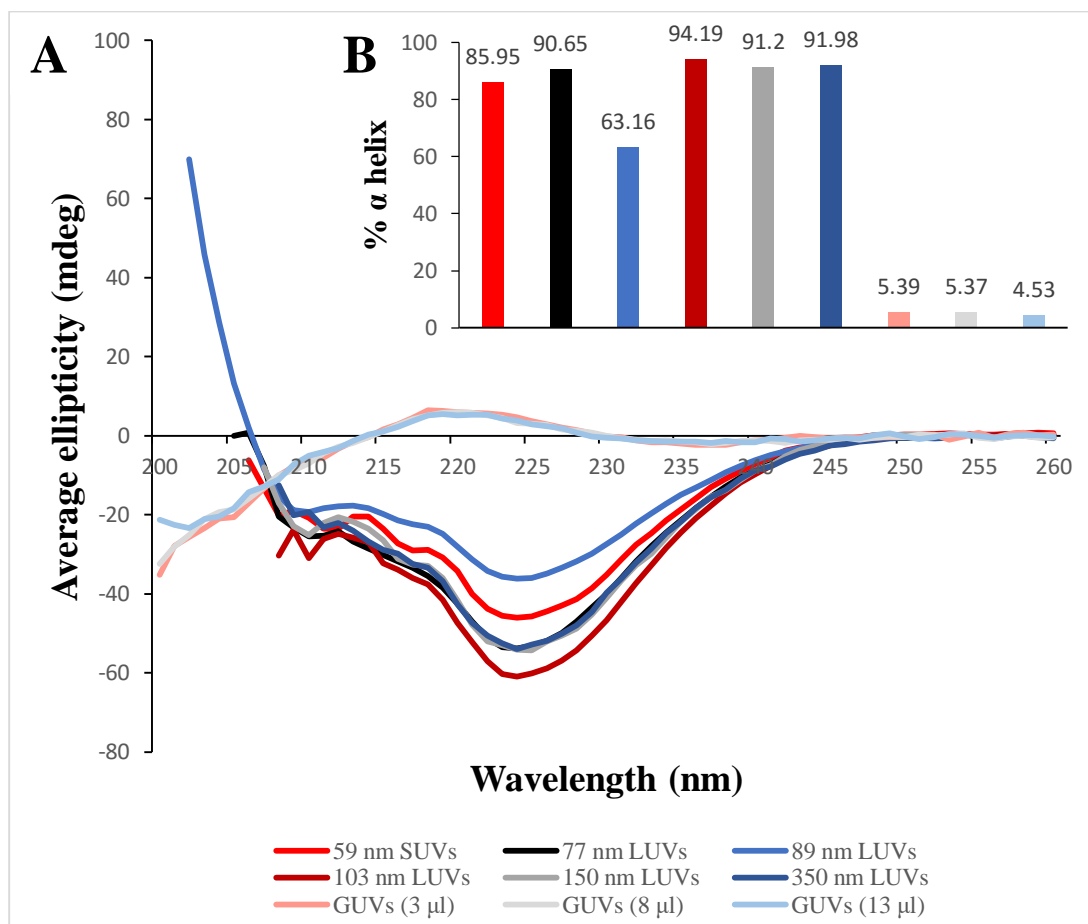


Figure 3.3 - 17 CD spectra for 250 μ M M2 AH peptide with 5 mM of different size SUV, LUVs and increasing concentration of GUVs composed of PC:PG:Ch (A). Estimated percentage of an α helix present in each sample calculated based on the spectra using K2D3 bioinformatics tool on <http://k2d3.ogic.ca/> website (B).

Binding assays showed similar levels of binding for vesicles sized 103 nm in diameter and above and increasing binding activity with decrease of the vesicle size below 103 nm, with the highest value observed for the smallest 59 nm SUVs (Fig. 3.3-18). These results confirm that the M2 AH can work in a wide range of positively curved membranes but preferentially binds to membranes with high positive membrane curvature, such as SUVs.

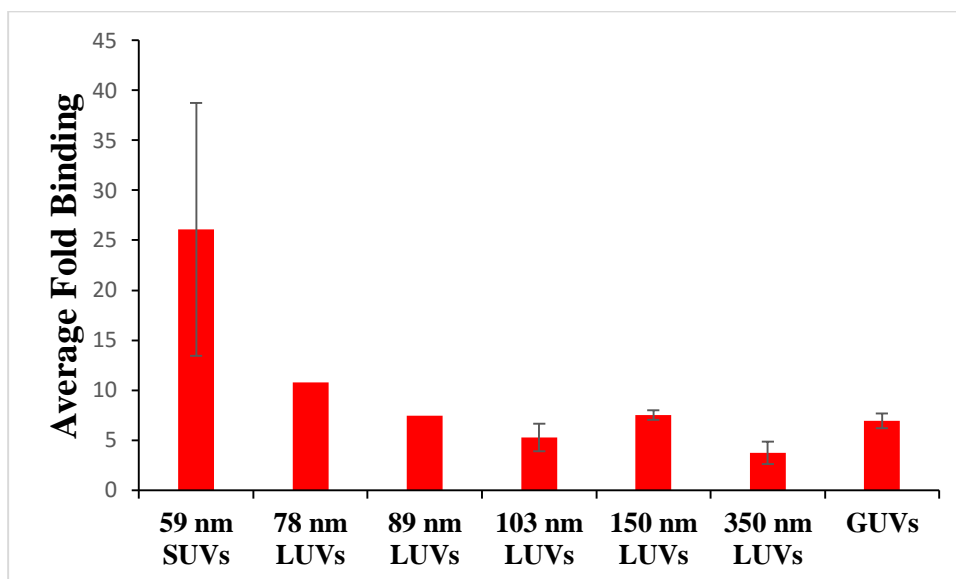


Figure 3.3 - 18 Average Fold Binding values for samples with 100 μ M of fluorescently labelled M2 AH peptide incubated with 2.5 mM of different size SUV, LUVs and GUVs composed of PC:PG:Ch.

To further investigate how membrane curvature influences the M2 AH and to determine specific localisation of the M2 AH in the lipid bilayer molecular dynamic (MD) simulation was performed – performed by collaborators, Dr Jordi Gómez-Llobregat and Dr Martin Lindén from the Center for Biomembrane Research at Stockholm University. MD simulation was done on a buckled lipid bilayer with regions of positive, negative and neutral curvature, composed of PC and PG lipids. The simulation showed that the M2 AH is mostly associated with high levels of positive membrane curvature (Fig. 3.3-19 A and B), with maximum binding to the membranes corresponding to a 20 nm vesicle (Fig. 3.3-19 B and C) however, it is not restricted to highly curved membranes, being able to work in wide range of positive curvature. It is not associated with negative membrane curvature, as showed in the probability distribution graph and corresponding curvature profile (Fig. 3.3-19 C and D). These results confirm our previous observations by CD and binding assays, that the M2 AH is mainly associated with highly curved membranes, such as those seen at the neck of budding virion, but can also work in wide range of positively curved membranes.

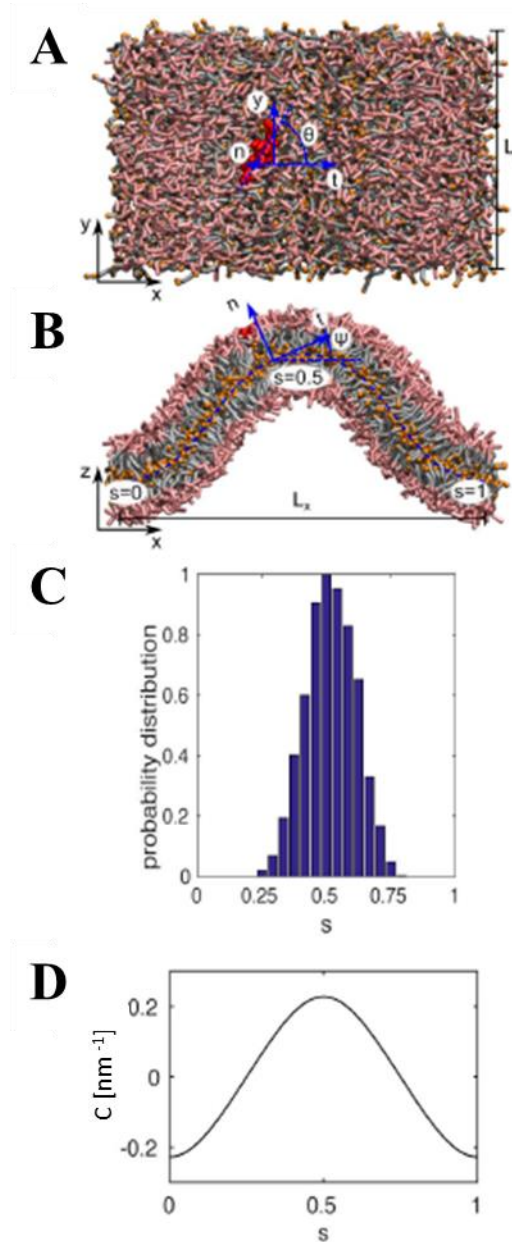


Figure 3.3 - 19 Representative top-view (A) and side-view (B) snapshots of the Molecular Dynamics simulation of the M2 AH on lipid bilayers composed of PC and PG, buckled in the L_x dimension. The system size is $L_x = 20.88$ nm and $L_y = 13.05$ nm. Lipid headgroups are shown in pink, acyl chains in grey, lipid tail ends as orange spheres and the M2 AH in red. Indicated vectors represent the orientation of the M2 AH peptide on the bilayer. θ is the angle between the centre line of the helix (arrow pointing towards the C-terminal end) and the XZ plane. The side view also shows the tangent angle ψ , the Euler buckling profile (red line) fitted to the bilayer mid-plane and S values representing the different curvatures in one repeat of the buckled bilayer, with $S=0.5$ being the most positively curved point of the membrane. Molecular graphics generated with VMD. Localisation of the M2 AH to regions of different curvature during the simulation, shown as a probability distribution (C) and reflecting the curvature profile along the arc length parameter S (D).

3.3.6.2 Absence of anionic lipids

To further investigate how positive membrane curvature influences the M2 AH structure and function, a range of different SUV and LUV sizes were made which only contained the lipid PC, to remove any effect of charge-charge interactions that might obscure any subtle curvature sensing. Vesicle sizes have been checked by DLS, showing the size distribution (see appendix 6.3 B) and average vesicle size for each sample (Table 3.3-3). Once again the average sizes of LUVs varied from the filter pore size, and were slightly higher than corresponding standard LUVs (Table 3.3-2), giving a wider range of vesicle sizes and suggesting that the lipid mix may predispose to the formation of slightly bigger LUVs which may be a result of, for example, an energetically unstable lipid mix.

designed size (extrusion membrane size)	actual size (average size measured on DLS)
sonicated SUVs	34.52 d.nm
sonicated SUVs	85.56 d.nm
50 nm LUVs	101.9 d.nm
100 nm LUVs	136.5 d.nm
200 nm LUVs	153.6 d.nm
1000 nm LUVs	3135 d.nm

Table 3. 3 - 3 Designed and actual average size of the PC:Ch vesicles in the size range measured on DLS.

CD showed a similar trend as with the standard vesicles range, with a varied trough depth for SUVs and LUVs and peaks for both GUVs concentrations suggesting a random coil confirmation (Fig. 3.3-20 A). Roughly 70% of the peptide becomes helical in the presence of vesicles ranging between 102-3135 nm and the percentage increasing with the decrease of the vesicle size to about 85% and 90% in case of 86 nm and 35 nm SUVs respectively, which have a much more curved membrane (Fig. 3.3-20 B). However, when vesicles are increasing in size (GUVs) and membrane is less curved, peptide helicity again drops to a level similar to peptide in the solution (Fig. 3.3-20 B). These results confirms that the M2 AH peptide is associated with highly curved membranes, such as SUVs or those at the neck of budding virion but can also work well in wide range of positive curvature membranes.

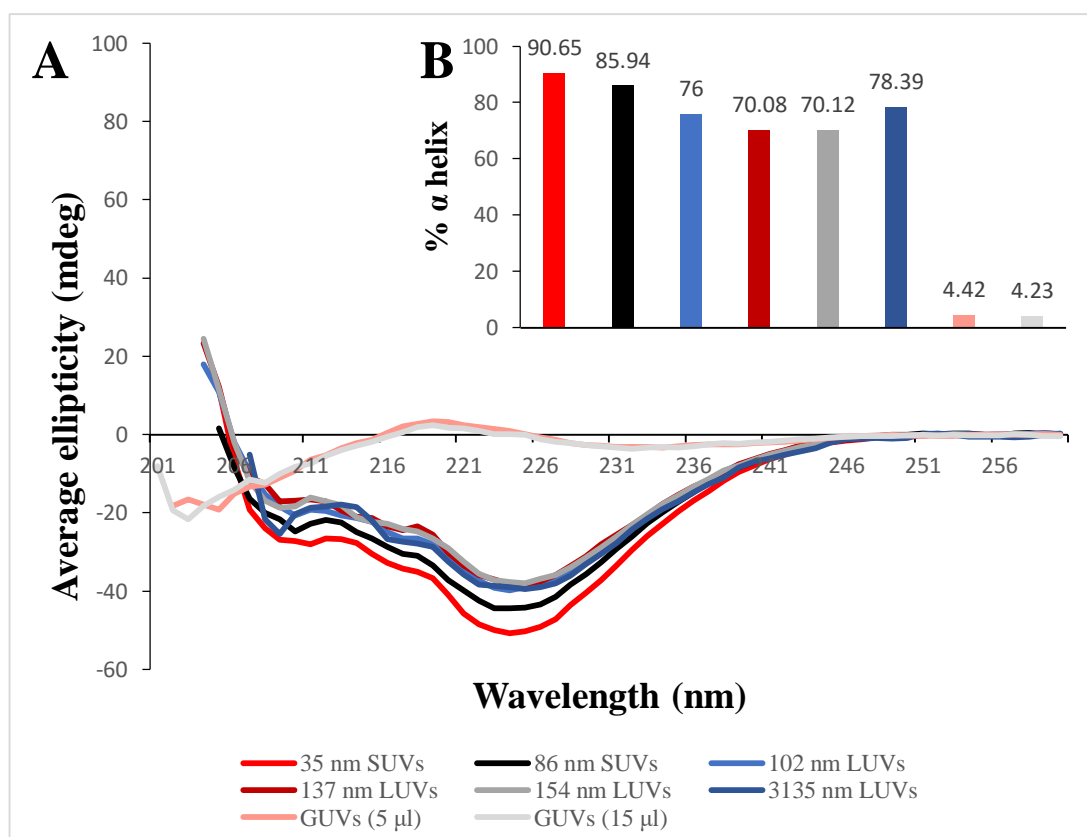


Figure 3.3 - 20 CD spectra for 250 μM M2 AH peptide with 5 mM of different size SUV, LUVs and increasing concentration of GUVs composed of PC:Ch (A). Estimated percentage of an α helix present in each sample calculated based on the spectra using K2D3 bioinformatics tool on <http://k2d3.ogic.ca/> website (B).

Binding assays have shown a huge increase in average fold binding in the presence of 35 nm SUVs and slight increase in the presence of 86 nm SUVs, with similar level of average fold binding for vesicles sized 102 nm and above (Fig. 3.3-21). These results show a similar trend as seen with standard vesicles (Fig. 3.3-18) and corresponds well to the MD simulation data, which shows maximal binding to membranes at values corresponding to a 20 nm vesicle (Fig. 3.3-19 B and C) with maximum binding to 35 nm SUVs observed in the binding assay (Fig. 3.3-21).

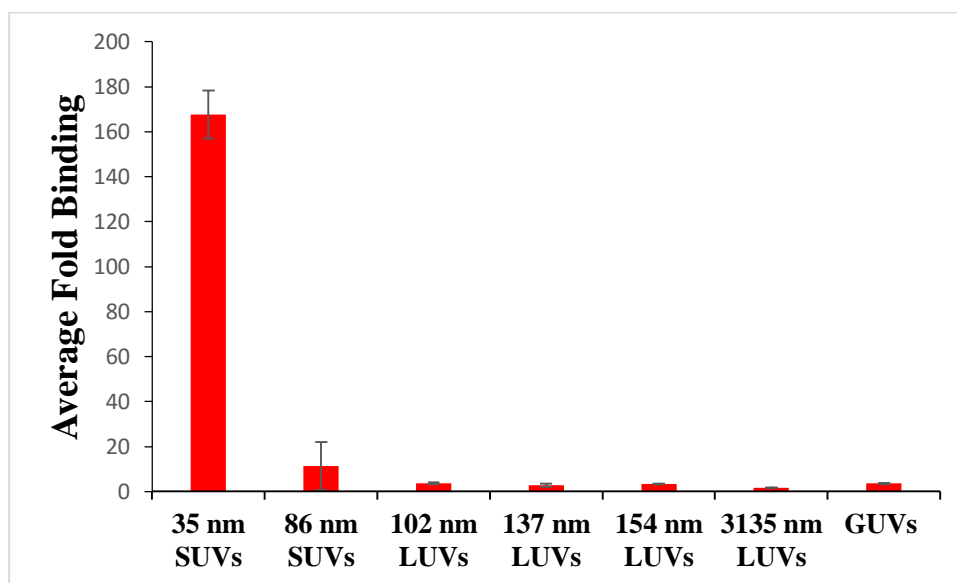


Figure 3.3 - 21 Average Fold Binding values for samples with 100 μ M of fluorescently labelled M2 AH peptide incubated with 2.5 mM of different size SUV, LUVs and GUVs composed of PC:Ch.

Overall, these results indicate that M2 AH is mainly associated with highly curved membranes, such as those present in the neck of a budding virion. However, it can also work in a wide range of positively curved membranes, such as LUVs but when membranes become less curved, such as GUVs, the M2 AH formation and binding to the membranes is significantly reduced. Presence of anionic lipids in the vesicles and possible charge-charge interactions do not influence the ability of the M2 AH to sense membrane curvature.

3.3.7 Sensing of lipid defects in the membrane

Some peptides and AHs can sense membrane curvature directly and others by sensing lipid packing defects in the membrane, which are gaps in the headgroup region of the bilayer formed in membranes with high positive membrane curvature (Drin et al. 2007, Drin and Antonny 2010). To investigate if the M2 AH senses membrane curvature by sensing lipid packing defects in the membrane two PE types has been used to form liposomes- dioleoyl-phosphoethanolamine and distearoyl- phosphoethanolamine (DOPE and DSPE respectively).

DOPE contains mono-unsaturated lipid tails and it is a cone shaped lipid which, due to its shape, affects lipid packing in the curved bilayer and causes formation of many lipid packing defects. On the other hand, DSPE contains fully saturated lipid tails and it is a cylindrical lipid which results in tighter lipid packing in the membrane and causes fewer defects in the membrane than DOPE (Nath et al. 2014). CD showed similar spectra for both DOPE and DSPE containing LUVs, with a slightly deeper trough in presence of DOPE (Fig. 3.3-22 A). The helix percentage was also increased (about 10%) in presence of DOPE, reaching nearly 80% (Fig. 3.3-22 B). This shows that when more defects are present in the membrane slightly more M2 AH is formed.

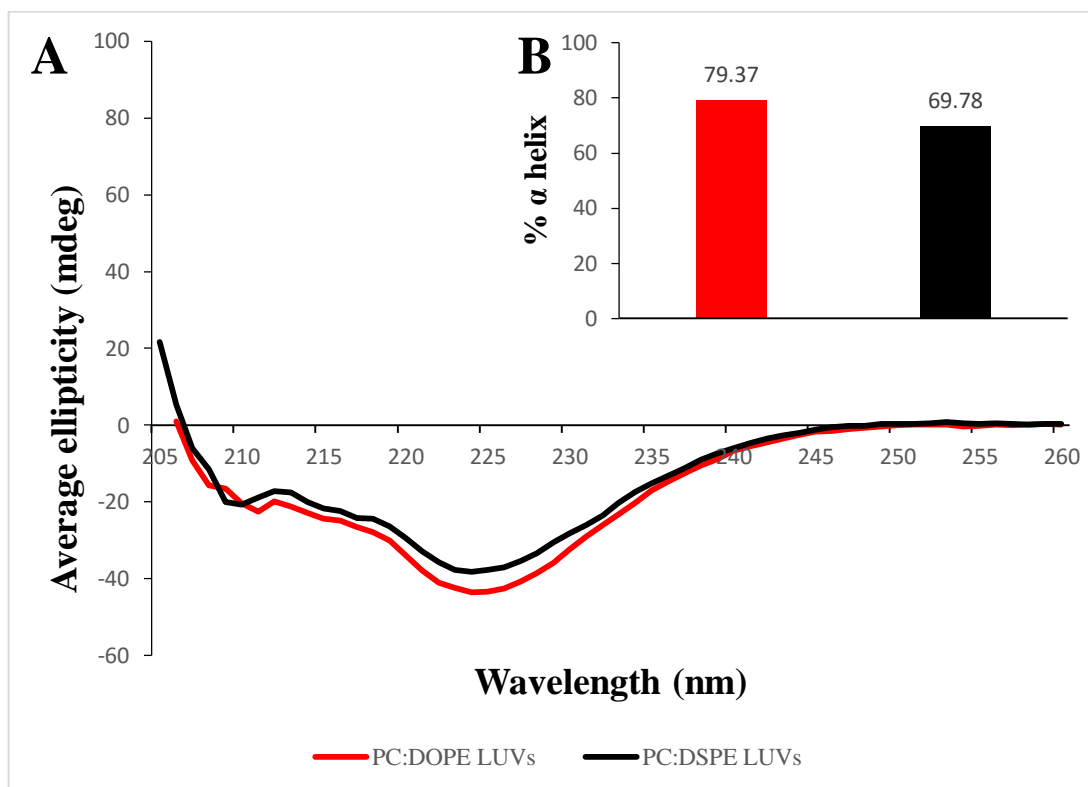


Figure 3.3 - 22 CD spectra for 250 μM M2 AH peptide with 5m M of 100 nm LUVs composed of PC and DOPE or DSPE at 4:1 ratio (A). Estimated percentage of an α helix present in each sample calculated based on the spectra using K2D3 bioinformatics tool on <http://k2d3.orgic.ca/> website (B).

Binding assays have shown a huge increase in binding activity when DOPE (causing more packing defects than DSPE) was present compared with when DSPE (causing fewer packing defects than DOPE) was present in the membrane (Fig. 3.3-23). These results shows that the M2 AH forms better and binds tighter to a membrane with packing defects present, which suggest that the M2 AH senses membrane curvature by sensing membrane packing defects in the bilayer.

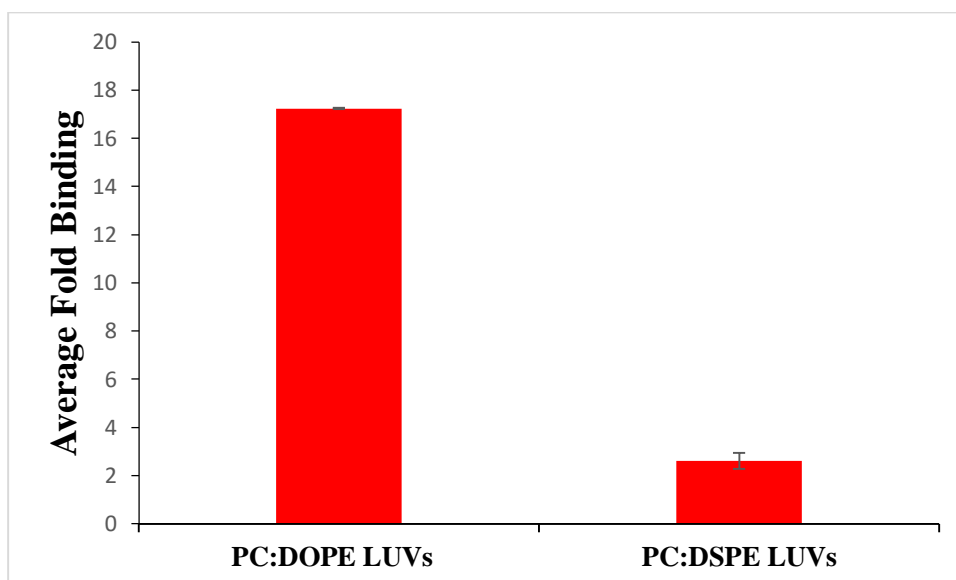


Figure 3. 3 - 23 Average Fold Binding values for samples with 100 μ M of fluorescently labelled M2 AH peptide incubated with 2.5 mM of 100 nm LUVs composed of PC and DOPE or DSPE at 4:1 ratio.

3.3.8 Summary

The M2 AH is formed upon binding with lipid membranes (see chapters 3.1.2 and 3.2.3) and the hydrophobic face of the helix is the one that interacts and binds with lipid membranes as shown by NMR and STD NMR (see chapter 3.1.3). However, membrane properties such as lipid composition, presence of defects, changes to the line tension between different domains and curvature of the membrane may affect formation and binding of the M2 AH. Cationic residues that are present in the polar face of the helix may, for example, interact with anionic lipids present in the membrane. Interaction between different types of anionic lipids and the M2 AH and effect on helix formation and binding were investigated by using LUVs in which anionic lipid, PG was replaced with different anionic lipids, PS and PA or zwitterionic PE.

CD experiments have shown that the type of anionic lipid present in the membrane does not influence the M2 AH formation but when PG was replaced with PE helix formation was reduced by about 30%, suggesting that PE disrupted the membrane, probably due to its shape, which influenced formation of the helix (Fig. 3.3-1). Interestingly binding assays showed a two fold increase in binding activity when PG was replaced with PA or PS, which suggests that although different types of anionic lipids do not influence formation of the M2 AH they might influence binding affinity of the helix (Fig. 3.3-2). Presence of PE in the membrane instead of PG caused a reduction of the average fold binding, which suggests that PE does not support formation of the M2 AH and its binding with the membranes (Fig. 3.3-2). To further investigate how anionic lipids affect the M2 AH formation and binding, LUVs with a range of different concentrations of PS have been used.

Previously different anionic lipids have been used as a replacement of PG at concentration of 20 molar %, in this range 1, 5, 10 and 40 molar % concentrations of PS have been tested. Interestingly CD showed that formation of the M2 AH was slightly reduced with 1 and 10 molar % of PS present and was on a high level, around 87% for 5 and 40 molar % of PS present (Fig. 3.3-3), which was similar to what had been observed previously with 20 molar % of anionic lipid in the membrane (Fig. 3.3-1). This suggests that formation of the M2 AH is varied when lower levels of PS are present in the membrane, below 20 molar % but high levels of PS present in the

membranes (20 and 40 molar %) supports the formation of the helix. Binding assays also showed that higher concentrations of PS in the membrane, above 5 molar %, increase the ability of the peptide to bind (Fig. 3.3-4).

Anionic lipids have been removed from the membrane to test if their presence is necessary for the M2 AH to be formed and binding with the membranes. CD has showed a reduction in estimated helix percentage by about 20% when anionic lipids were removed from the membrane (Fig. 3.3-5), which suggests that anionic lipids support helix formation but are not necessary as helix formation was not completely inhibited. Surprisingly binding assays showed an increase in fold binding when anionic lipids were removed from the membrane (Fig. 3.3-6), suggesting that although anionic lipids support helix formation they do not support helix binding with the membranes.

To further investigate binding properties of the M2 AH and influence of charge interactions on them binding assays have been performed in the presence of an increasing ionic strength in the buffer using sodium chloride. Average fold binding decreased with a low ionic strength buffer (32 mM) compared to 0 mM buffer but after that it was slightly increasing with an increase in the ionic strength but with the highest concentration it dropped to the level observed with 0 mM (Fig. 3.3-8). Additionally values for all samples were about two fold greater than in presence of water. This shows that there are slight changes in peptide binding due to changes of the ionic strength of the buffer, but there are no drastic changes observed that are associated with any particular concentration. This suggest that ionic strength of the buffer may strengthen the binding between helix and the membrane but does not influence it due to charged interactions.

Cholesterol has been shown to inhibit M2 AH mediated budding in LUVs in a dose dependent manner, with budding observed with up to 17 molar % of cholesterol present in the membrane (Rossman et al. 2010b). Therefore LUVs with a range of different molar % of cholesterol (5-40%) have been used to investigate how cholesterol levels in the membrane affect the M2 AH formation and binding. Surprisingly, CD have shown high levels of estimated helix percentage (around 90%) for all cholesterol concentrations tested, with just 5% drop when the highest concentration of cholesterol (40 molar %) was present in the membrane (Fig. 3.3-9).

On the other hand binding assays showed a similar level of binding with membranes containing low cholesterol levels (5 molar %) as with standard LUVs (containing 1 molar % of cholesterol) which slightly increased with increase when the cholesterol level was raised to 10 molar % (Fig. 3.3-10). Further increases in cholesterol levels in the membrane (20 molar % and above) caused a reduction in binding (Fig. 3.3-10), which correlates with previous findings showing inhibition of the M2 AH induced budding when higher concentrations of cholesterol are present in the membrane (Rossman et al. 2010b). These results suggest that although the cholesterol concentration in the membrane may not affect formation of the M2 AH it does affect ability of the M2 AH to bind with the membranes.

Some lipids have been shown to play an important role in assembly of other viruses, such as PIP2 which is involved in assembly of the HIV virus (Carlson and Hurley 2012). Immunofluorescence microscopy has shown that PIP2 and M2 do not co-localise in cells but often are proximal to each other (Fig. 3.3-11). Furthermore, different concentrations of PIP2 have been incorporated in to the LUVs to test how PIP2 affects formation and binding of the M2 AH. CD spectroscopy has shown high levels of estimated helix percentage, about 90% for all concentrations tested (Fig. 3.3-12) with binding assays also showing similar levels of binding across all concentrations, with average fold binding value being slightly higher than for standard LUVs (Fig. 3.3-13 and Table 3.2-1). Those results suggest that PIP2 might play a role in the M2 AH mediated budding due to their close localisation in the cells. It might also enhance formation of the M2 AH and binding of the AH with membranes but it is not necessary and the full mechanism is not known.

The lipid composition of the membrane can affect structure and function of the M2 AH, but other membrane properties such as curvature, presence of different domains or defects may also play a role. A range of phase separated LUVs in which the thickness of the lipid disordered phase has been modified, by using different PC types with decreasing acyl chain length, leading to an increase in the line tension between domains, as described before (Garcia-Saez et al. 2007), have been used to test how line tension affects the M2 AH formation and binding with lipids. CD spectroscopy

has shown that the estimated helix percentage increases with an increase in the line tension (Fig. 3.3-14), but it does not reach the levels observed with standard LUVs (Fig. 3.2-7). Surprisingly binding assays have shown a reduced yet similar level of binding for majority of the samples, with exception of LUVs composed of DeisPC (second in the series) in which binding was nearly two fold higher than for the rest (Fig. 3.3-15) and reached the levels observed with standard LUVs (Table 3.2-1). Overall, the reduction in both the estimated helix percentage and average fold binding levels may be caused by a different lipid composition of the LUVs used, with results suggesting that the line tension plays a role in the formation of the M2 AH, but it does not influence AH binding with the membranes.

In the final stages of budding, the M2 protein is localised to the neck of budding virion which is region of high positive membrane curvature (Rossman et al. 2010b). Therefore the effect of positive membrane curvature on the M2 AH structure and function was investigated using a range of SUVs, LUVs and GUVs composed of standard lipids (PC, PG and Ch) and increasing in diameter, which was confirmed by DLS (Table 3.3-2). The estimated helix percentage was on a high level, around 90%, for the majority of SUVs and LUVs (with exception of 89 nm LUVs when helix percentage dropped by about 30%), but in the presence of GUVs it dropped to about 5% (Fig. 3.3-17). Binding assays showed the highest binding levels for the smallest vesicles, with the value decreasing as the vesicles increased in size (Fig. 3.3-18). This suggests that the M2 AH can work in wide range of positively curved membranes but it preferentially binds with membranes of high positive membrane curvature and when the membrane is less curved, as seen with GUVs, formation and binding of the M2 AH is inhibited.

To further investigate how membrane curvature affect the M2 AH, MD simulations were performed on a buckled lipid bilayer. Results confirmed previous observations, showing that the M2 AH is mostly associated with positively curved membranes, with maximum binding occurring at regions corresponding to a 20 nm vesicle, with no association observed in negatively curved regions of the membrane (Fig. 3.3-19). A range of different size SUVs, LUVs and GUVs composed of PC only were also used to test how positive membrane curvature affects the M2 AH, without any anionic lipids present in the membrane and therefore no potential charge-charge interactions that could affect subtle curvature sensing. CD spectroscopy has shown the highest

estimated helix percentage in presence of the smallest vesicles, which was slightly decreasing as the vesicles became larger, before a huge drop in presence of the biggest vesicles, GUVs (Fig. 3.3-20). Binding assays showed very strong binding between the M2 AH and the smallest vesicles (35 nm SUVs), which was significantly reduced with an increase of vesicle size (Fig. 3.3-21). This confirms that the M2 AH preferentially binds with high positive curvature membranes but can also work with wide range of positively curved membranes.

Membranes with high positive curvature can be detected by peptides or AHs either by directly sensing membrane curvature or by sensing lipid packing defects associated with high curvature. LUVs composed of two different PE types, DOPE and DSPE, which due their shape form either a lot of defects or just a few defects in the membrane respectively (Nath et al. 2014), have been used to investigate if the M2 AH senses membrane curvature by sensing lipid packing defects in the membrane. CD spectroscopy showed a slight difference in helix formation between two lipid types, with about 10% more helix in presence of the membrane containing DOPE (Fig. 3.3-22). Binding assays showed very strong binding when DOPE was present in the membrane, about 6 fold greater than when DSPE was present (Fig. 3.3-23). These results suggest that the M2 AH forms and binds better to the membranes when a lot of packing defects are present, suggesting that this is how the M2 AH detects membranes with high positive curvature.

3.4 EFFECTS OF THE M2 AMPHIPATHIC HELIX ON THE MEMBRANE

3.4.1 Introduction

The M2 AH is formed upon binding with lipid membranes (see chapters 3.1.2 and 3.2.3) and therefore the lipid composition of the membrane and its properties, such as curvature or presence of defects, affects the M2 AH structure and its ability to bind with membranes (see chapter 3.3). From the other side, insertion of the peptide into the bilayer may cause changes to the membrane. M2 has lipid order binding preferences and is located at a lipid phase boundary therefore an assay has been developed to detect changes to membrane fluidity and ordering of the lipids in the membrane cause by insertion of the M2 AH. In this assay Laurdan dye and the M2 AH peptides based on two different strains and its mutations have been used to detect if the M2 AH causes changes to membrane fluidity and how different mutations affect this. Changes in membrane fluidity and lipid ordering also result in changes of the lipids transition temperature so to further investigate changes in the bilayer caused by the M2 AH lipids transition temperature were analysed by differential scanning calorimetry. The M2 AH has been shown to play a role in final stage of influenza virus budding where it is located to the neck of budding virion, which is a region of high positive membrane curvature (Rossman et al. 2010b), in this environment the M2 AH may enhance positive membrane curvature, causing membrane scission and leading to the release of the new virion to the environment. Therefore the ability of the M2 AH to induce positive membrane curvature has been tested upon binding to LUVs using transmission electron microscopy.

3.4.2 Ordering of lipids in the membrane

3.4.2.1 M2 AH

Insertion of the M2 AH into the bilayer may create lipid clusters, which could affect membrane fluidity and therefore membrane curvature. To test if the M2 AH changes the order of lipids in the membrane, an assay that detects lipid phase changes using Laurdan dye has been designed. Laurdan is a fluorescent dye that detects changes in the membrane phase through sensitivity to the polarity of the environment in the bilayer. When lipids are in an ordered phase the emission maximum is at 440 nm, which shifts to 490 nm in a disordered phase. This shift can be quantified by Generalised Polarisation (GP), which is calculated using the equation: $GP = (I_{440} - I_{490}) / (I_{440} + I_{490})$ (Parasassi et al. 1990, Sanchez et al. 2007). In this assay liposomes were incubated with Laurdan dye in the presence and absence of the M2 AH peptide for 1 hour followed by fluorescence measurements at 440 and 490 nm. GP was then calculated for each sample and the change in Laurdan GP was obtained by subtracting the GP value for the sample without M2 AH from the same sample with the M2 AH present. Initial experiments were done in the presence of standard LUVs to determine optimal lipid:dye ratio and peptide concentration. Three different lipid:dye ratios have been tested; 1:100, 1:400 and 1:1000; with 100 μ M of the M2 AH peptide, showing the biggest increase in Laurdan GP for 1:100 ratio, with slightly reduced, yet similar levels for other two ratios tested (Fig. 3.4-1). A range of different M2 AH concentrations (1-200 μ M) were then tested, showing increase of the Laurdan GP with an increasing peptide concentration, between 10-200 μ M and decrease when 1 μ M of peptide was present (Fig. 3.4-2). Those results show that the M2 AH increases ordering of the lipids in the membrane after insertion, in a dose dependent manner. Therefore 200 μ M peptide concentration and 1:100 lipid: dye ratio were chosen as optimal concentrations for this type of assay and used during all subsequent experiments, unless otherwise stated.

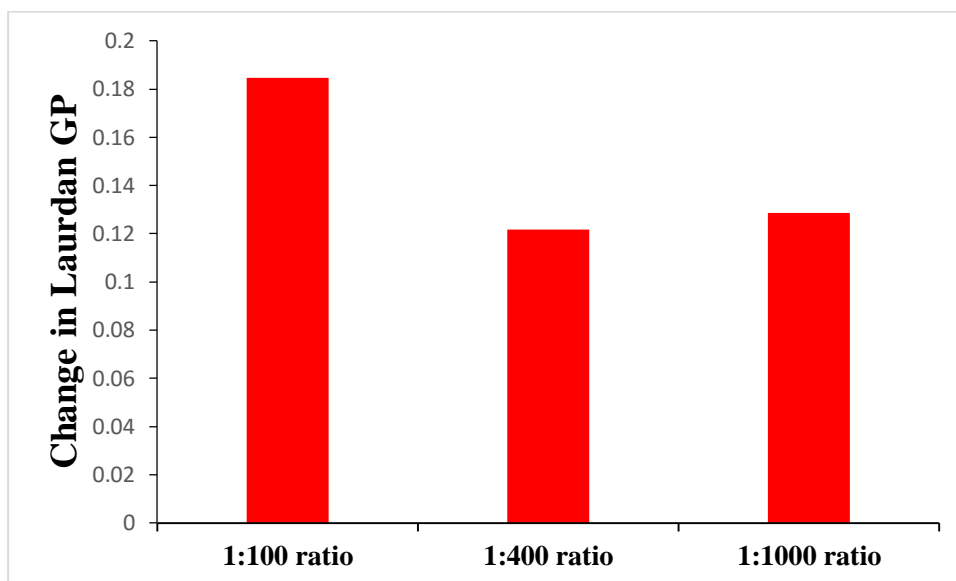


Figure 3. 4 - 1 Change in Laurdan GP value with 100 μM of the M2 AH and 2.5 mM of standard LUVs with an increasing lipid:dye ratio.

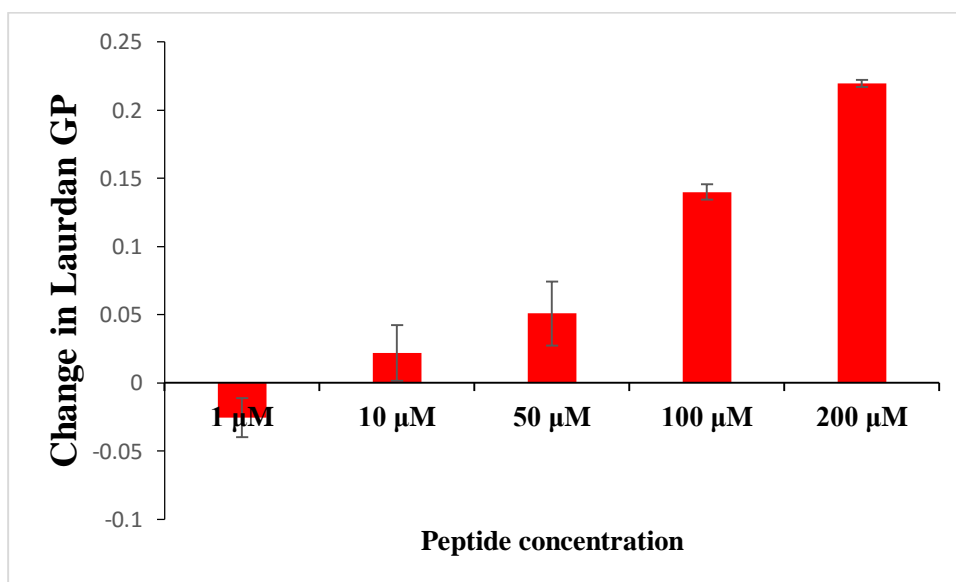


Figure 3. 4 - 2 Change in Laurdan GP value with increasing concentrations of M2 AH peptide and 2.5 mM of standard LUVs at 1:100 lipid:dye ratio.

Different total sample volumes; 50, 100 and 200 μl have also been tested, showing similar levels of increase in Laurdan GP (see appendix 6.4), which suggests that the sample volume does not influence results. To test if the M2 AH peptide itself does not increase the Laurdan GP control, experiments have been performed with Laurdan dye in presence and absence of the peptide. Results showed a small decrease in Laurdan GP when the peptide was present, independently from the volume of the sample tested (Fig. 3.4-3). That shows that the M2 AH peptide itself is not able to cause an increase in Laurdan GP and previously observed increase was due to changes in the membrane caused by the peptide (Fig. 3.4-1 and 3.4-2).

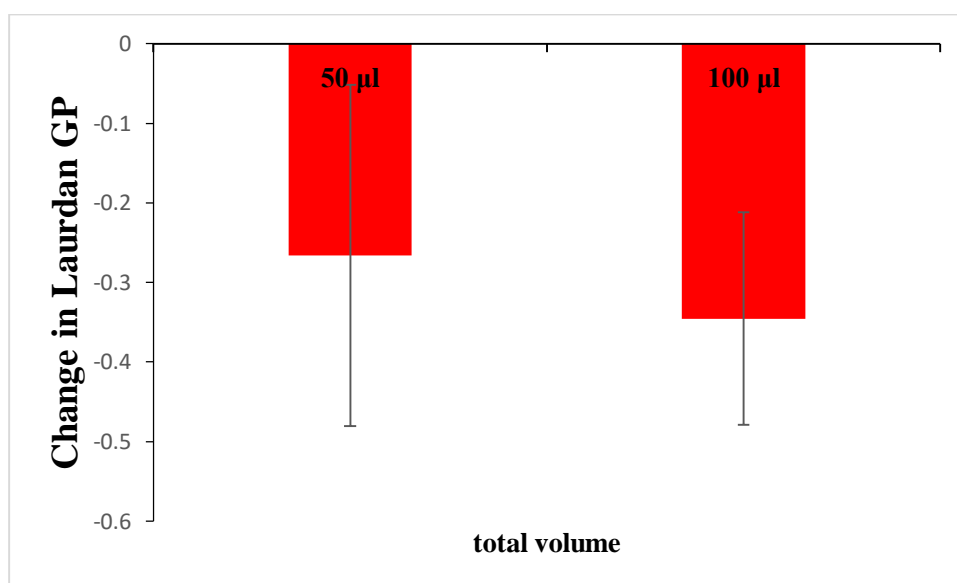


Figure 3. 4 - 3 Change in Laurdan GP value with 100 μM of M2 AH peptide and 25 μM of the Laurdan dye in solution (without LUVs) at different total volumes.

3.4.2.2 A/England/09 and AH mutants

The M2 AH is mostly conserved among different influenza virus strains, with only 3 different residues between A/Udorn/72 strain, which is mostly used laboratory strain, and the most recent pandemic A/England/09 strain, (Fig. 3.2-8). CD has shown similar results for wild type peptides based on both strains (Fig. 3.2-7 and 3.2-9), however, certain mutations, especially in the hydrophobic face of the helix, can cause a reduction in the helix's structure and function (Fig. 3.2-11 and 3.2-12). To investigate if strain differences and mutations in the helix influence its ability to increase lipid ordering in the membrane the M2 AH peptide based on A/England/09 strain and two of its mutants, R54A R61A and the 5 point mutant, that based on the CD results (Fig. 3.2-11 and 3.2-12), cause increase and decrease in helix formation respectively, compared to wild type A/England/09 have been used.

Surprisingly, wild type A/England/09 M2 AH causes only slight increase in Laurdan GP (Fig. 3.4-4) which, when compared, is only half the magnitude seen by the peptide based on the A/Udorn/72 strain (Fig. 3.4-2). On the other hand, the M2 AH peptide with the 5 point mutations in the helix is not able to increase Laurdan GP and causes small decrease (Fig. 3.4-4). Interestingly the double mutation, R54A R61A, causes more than a twofold greater increase in Laurdan GP than the wild type A/England/09 peptide (Fig. 3.4-4). These results suggest that although the M2 AH sequence is conserved among the strains and small differences in its sequence do not influence formation of the helix, as shown by CD (Fig. 3.2-7 and 3.2-9), they affect functions of the helix and its ability to increase lipid ordering in the membrane. However, mutations on the helix interface, R54A R61A, seem to compensate for the strain differences bringing the change in Laurdan GP to the levels observed with the wild type peptide based on the A/Udorn/72 strain (Fig. 3.4-2). Introducing a 5 point mutation into the helix not only affects the structure of the helix (Fig. 3.2-12) and virus growth, but also its function, which suggest that hydrophobic face of the helix plays an important role.

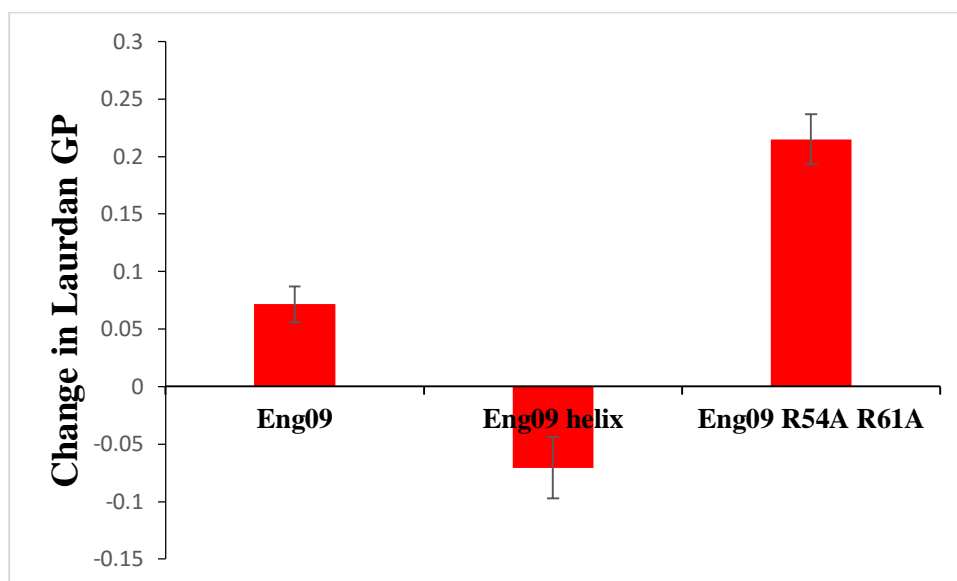


Figure 3. 4 - 4 Change in Laurdan GP value with 100 μ M of M2 AH peptide based on Eng/09 strain and its mutants and 2.5 mM of standard LUVs at 1:100 lipid:dye ratio.

3.4.2.3 Different membrane compositions

To investigate how the membrane composition affects the ability of M2 AH to order lipids, SUVs and LUVs composed of different lipids have been used. When anionic lipids have been removed and LUVs were composed of PC and Ch only, the M2 AH peptide caused an increase in Laurdan GP (Fig. 3.4-5), and it was on a similar level to when standard LUVs were used (Fig. 3.4-2). Interestingly, when SUVs were used instead of LUVs, increase in Laurdan GP was reduced (Fig. 3.4-5). Those results suggest that anionic lipids do not affect the M2 AH ability to order lipids in the membrane and that although high positive membrane curvature supports helix formation (Fig. 3.3-17 and 3.3-20) and binding to the membrane (Fig. 3.3-18 and 3.3-21) it does not allow for as efficient lipid ordering in the membrane.

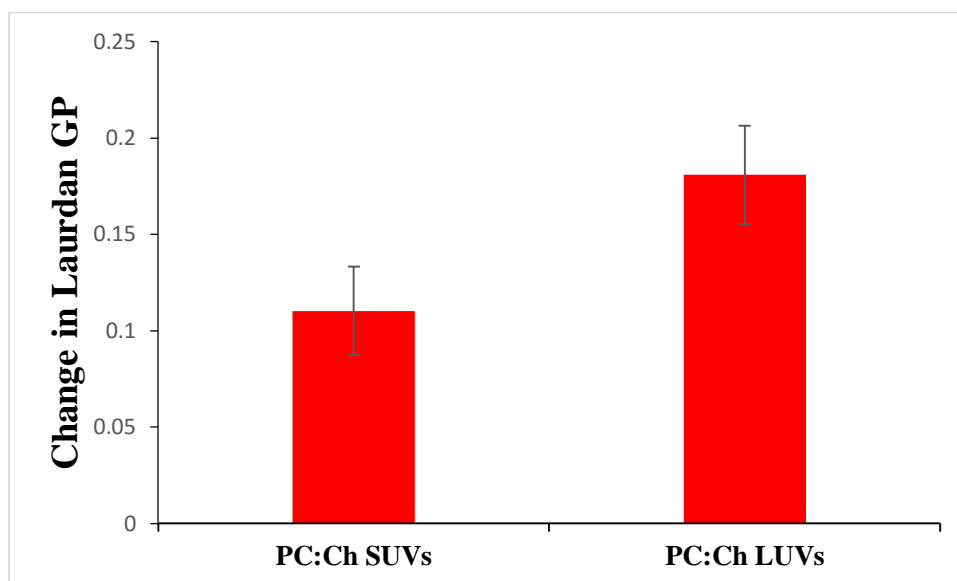


Figure 3. 4 - 5 Change in Laurdan GP value with 100 μ M of M2 AH peptide and 2.5 mM of SUVs or 100 nm LUVs composed of PC:Ch, at 1:100 lipid:dye ratio.

To test the effect of cholesterol on the M2 AH ability to order lipids in the membrane, a series of LUVs with an increasing cholesterol percentage have been used, as described in chapter 3.3.3. Unfortunately the measurements contained a high degree of variation, which has led to high standard errors especially in case of 5 and 30 molar % of cholesterol samples. Despite that, the increase in Laurdan GP appears to decrease with the rising levels of cholesterol level in the membrane, with negative values observed for the highest cholesterol concentration tested (Fig. 3.4-6). This suggests that having high levels of cholesterol present in the membranes not only affects the M2 AH binding ability (Fig. 3.3-10), but also its ability to order lipids.

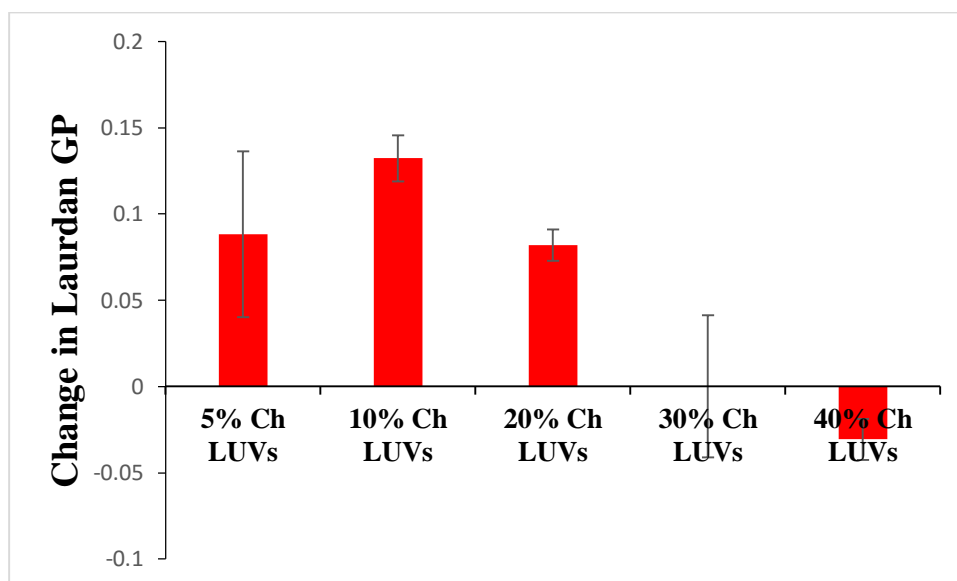


Figure 3. 4 - 6 Change in Laurdan GP value with 100 μ M of M2 AH peptide and 2.5 mM of standard LUVs with an increasing concentration of cholesterol, at 1:100 lipid:dye ratio.

A series of phase separated LUVs composed of different PC types, with decreasing length of acyl chains and hence increased line tension, as described in chapter 3.3.5, have been used to test how line tension influences the M2 AH ability to order lipids in the membrane. A small increase in Laurdan GP has been observed when DEPC LUVs were present, where the line tension in the domains was the smallest from the series (Fig. 3.4-7). This increase in Laurdan GP was then seen to be increasing as the line tension increased, with the highest increase seen in the presence of DMPC LUVs, where the line tension in the domains were the highest from the series (Fig. 3.4-7). Those results show that line tension influence the M2 AH ability to order lipids in the membrane as well as formation of the helix (Fig. 3.3-14).

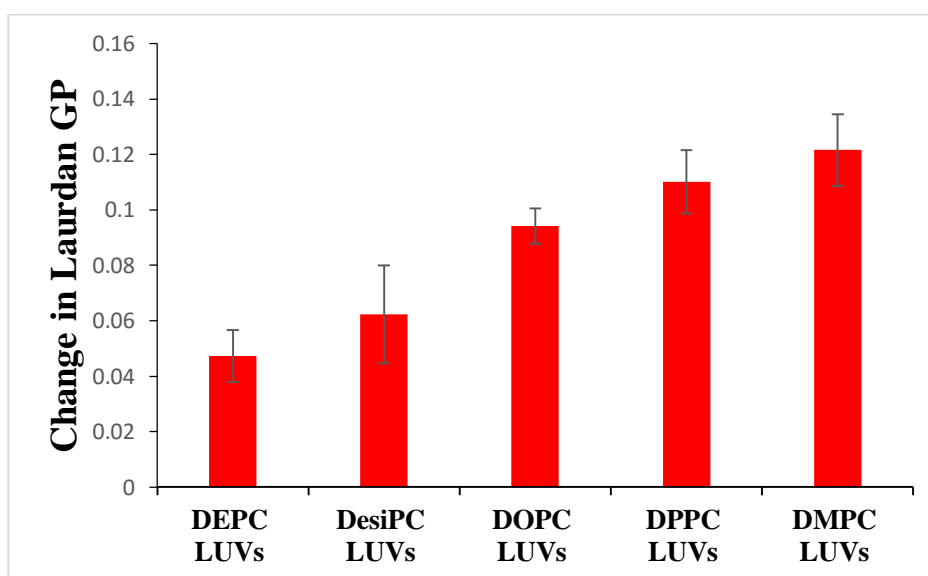


Figure 3. 4 - 7 Change in Laurdan GP value with 100 μ M of M2 AH peptide and 2.5 mM of 100 nm LUVs composed of sphingomyelin, cholesterol and series of different PC types (at 2:1:2 ratio) with decreasing length of acyl chain which results in increase of the line tension, where DEPC has the longest acyl chain and DMPC the shortest, at 1:100 lipid:dye ratio.

It has been show that the M2 AH senses membrane curvature by sensing membrane packing defects in the bilayer, see chapter 3.3.7. Therefore, LUVs with different levels of packing defects present in the membrane have been used to test if membrane packing defects influence the M2 AH ability to order lipids. In presence of both, DSPE and DOPE, the M2 AH caused an increase in Laurdan GP at similar level (Fig. 3.4-8), which suggests that lipid packing defects do not play a role in the M2 AH ordering of the lipids on the membrane.

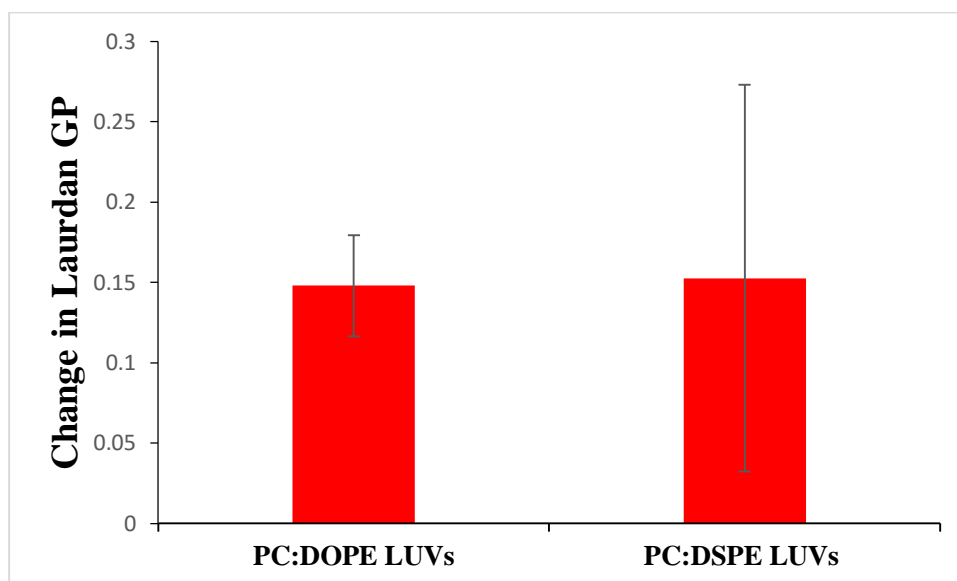


Figure 3. 4 - 8 Change in Laurdan GP value with 100 μ M of M2 AH peptide and 2.5 mM of 100 nm LUVs composed of PC and DOPE or DSPE (at 4:1 ratio), at 1:100 lipid:dye ratio.

3.4.3 Alteration of membrane phase-transition temperatures

M2 AH is associated with highly curved membranes (see chapter 3.3.6) and increases lipid ordering in the membrane, as showed above (chapter 3.4.2.1). Increase in lipid order in the membrane decreases its fluidity which in turn increases lipid transition temperature. To further investigate the M2 AH effect on the lipid order, membrane phase transition temperatures were analysed by differential scanning calorimetry (DSC). In this experiment multilamellar vesicles (MLVs), composed of DSPC were used and when the M2 AH peptide was added to the MLVs lipid transition temperature of the membrane increased (Fig. 3.4-9). This shows that M2 AH increases lipid ordering and thus decrease in membrane fluidity, which confirms our previous observations.

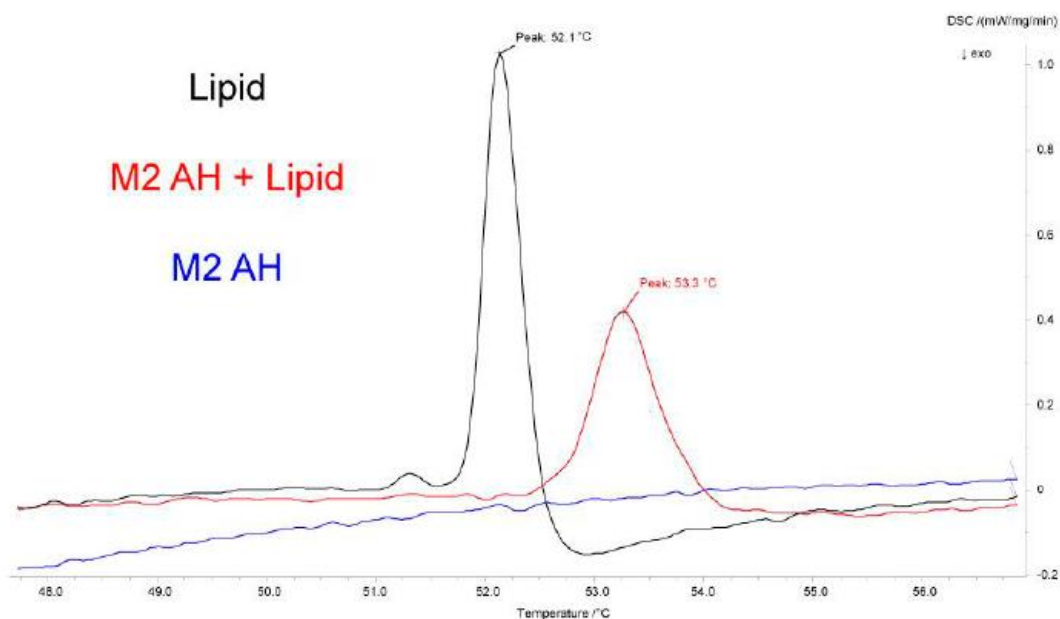


Figure 3.4 - 9 DSC curves of DSPC MLVs (black), DSPC MLVs reconstituted with M2 AH at a peptide: lipid ratio of 1:20 (red) or M2 AH alone (blue) with the main lipid phase transition temperature noted.

3.4.4 Induction of positive membrane curvature

As shown before (see chapter 3.3.6), the M2 AH associates with membranes of high positive membrane curvature. To test if M2 AH can also induce membrane curvature, standard LUVs were incubated with varied concentrations of the M2 AH peptide and changes in the liposomes morphology have been observed by TEM – work done in collaboration with Matthew D. Badham, School of Biosciences, University of Kent. TEM analysis showed that at higher concentrations (125 μM), M2 AH causes formation of tubes and blebs on the LUVs surface indicated by red arrows, which are not present at lower concentrations (12.5 μM) and in control samples (Fig. 3.4-10). Those results suggest, that M2 AH binds to positively curved membranes, inserts to the membrane and induce positive membrane curvature.

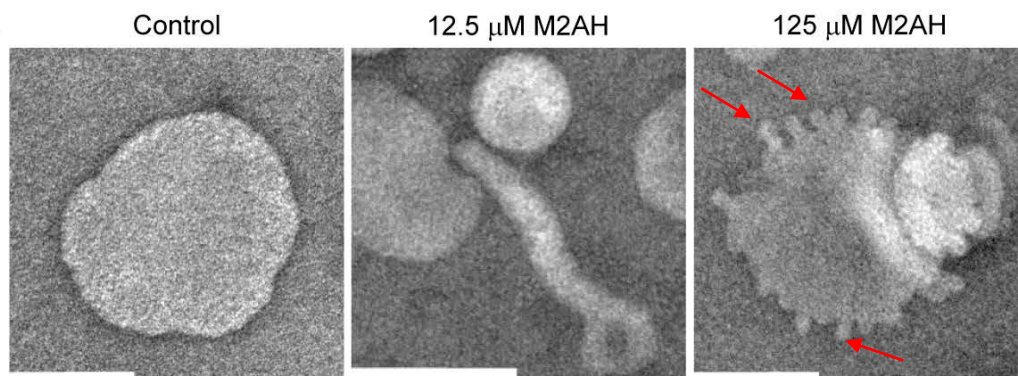


Figure 3.4 - 10 TEM images of 5 mM of standard LUVs incubated for 1 h with increasing concentrations of the M2 AH peptide and negative stained. Arrows indicate membrane blebs and scale bars indicate 100 nm.

3.4.5 Summary

Properties of the lipid membrane, such as composition, curvature or presence of the defects can affect formation and binding of the M2 AH, however, insertion of the helix into the membrane can also cause changes in the bilayer. To detect changes in the membrane fluidity caused by changes to the lipid ordering in the membrane by the M2 AH an assay has been developed in which changes to the lipid phase are detected by Laurdan dye (Parasassi et al. 1990, Sanchez et al. 2007). Initial experiments have been performed using standard LUVs with a range of different peptide concentrations and lipid: dye ratios, showing the M2 AH increases ordering of the lipids in the membrane in dose dependent manner and that optimal peptide concentration for this assay is 200 μM with 1:100 lipid: dye ratio (Fig. 3.4-1 and 3.4-2). Peptides based on the A/England/09 and two of its mutants, R54A R61A and 5 point mutant which increase or decrease helix formation based on the CD results respectively, have also been tested to check if the ability to increase lipid ordering in the membrane is conserved among influenza virus strains and how different mutations affect that.

Results showed that peptide based on A/England/09 strain can increase ordering of lipids in the membrane (Fig. 3.4-4), but not as much as peptide based on A/Udorn/72 strain (Fig. 3.4-2), which suggest that although differences between strains do not influence formation of the M2 AH (Fig. 3.2-7 and 3.2-9) they affect peptide ability to change membrane fluidity. As expected, the introduction of 5 point mutations into the helix, which affects helix formation (Fig. 3.2-12) and cause growth impairment in the virus, also inhibited the M2 AH ability to increase lipid ordering (Fig. 3.4-4). Surprisingly double mutant on the helix interface, R54A R61A caused increase in lipid ordering (Fig. 3.4-4) to the levels observed for peptide based on A/Udorn/72 strain (Fig. 3.4-2) which suggests that these mutations compensate for the differences between strains which appear to reduce the M2 AH's ability to order lipids in the membrane. Liposomes composed of different lipids have been used to investigate how the composition of the membrane affects the M2 AH ability to increase lipid ordering. When anionic lipids have been removed, and LUVs were composed of PC and Ch only, the M2 AH increased lipid ordering to a level that was similar to what has been observed for standard LUVs (Fig. 3.4-5 and 3.4-2 respectively), which suggests that anionic lipids and charge-charge interactions do not affect the M2 AH ability to change membrane fluidity. Surprisingly, when SUVs composed of PC and Ch have been used instead of LUVs, the increase in lipid ordering was significantly reduced (Fig. 3.4-5). Cholesterol has been shown previously to inhibit the M2 AH mediated budding in a dose dependent manner (Rossman et al. 2010b) and to reduce binding with membranes. Therefore a range of LUVs with increasing concentrations of cholesterol have been used to investigate the effect of cholesterol on the M2 AH ability to increase lipid ordering. There was a high degree of variability in the samples, but overall results suggest the increase in cholesterol concentration in the membrane reduces the M2 AH ability to increase lipid ordering (Fig. 3.4-6).

To investigate how line tension affects changes in the membrane fluidity induced by the M2 AH range of LUVs with increasing line tension between domains, as described in chapter 3.3.5 have been used. Results showed that an increase in the line tension increases lipid ordering of the membrane by the M2 AH (Fig. 3.4-7). Membrane curvature is sensed by the M2 AH by sensing lipid defects in the membrane. LUVs composed of DOPE and DSPE with a varied amount of lipid packing defects, as described in chapter 3.3.7 have been used to investigate if membrane defects affect

the M2 AH ability to increase lipid ordering in the membrane. Results showed similar increase in lipid ordering in presence of both types of LUVs (Fig. 3.4-8), which suggests that presence of lipid packing defects in the membrane do not affect the M2 AH ability to change membrane fluidity.

To further investigate changes to the membrane induced by the M2 AH lipids transition temperature was analysed by DSC. An increase in lipid ordering decreases fluidity of the membrane, resulting in an increase in the lipid transition temperature. Results showed that the addition of the M2 AH into the membrane increases lipid transition temperature (Fig. 3.4-9), which confirms that insertion of the M2 AH into the lipid membranes increases lipid ordering and changes membrane fluidity.

The M2 AH plays a role in membrane scission, which is the last stage of influenza virus budding. It has been shown to associate with membranes of high positive curvature and localises to the neck of budding virion (Rossman et al. 2010b) where might induce positive membrane curvature leading to scission. To test if the M2 AH induces positive membrane curvature, the peptide has been incubated with LUVs and morphological changes to the vesicles have been observed by TEM. At higher concentrations the M2 AH forms tubes and blebs on LUVs surface (Fig. 3.4-10) which shows that the peptide induces positive membrane curvature.

3.5 M2 AMPHIPATHIC HELIX MEDIATED BUDDING *IN VITRO*

3.5.1 Introduction

The M2 AH is being formed upon binding with membranes (see chapters 3.1.2 and 3.2.3), it preferentially binds with membranes with high positive membrane curvature (see chapter 3.3.6) and can induce positive membrane curvature in LUVs (see chapter 3.4.4). It has been shown that the M2 AH plays an important role in influenza virus budding, and when mutated budding is inhibited (Rossman et al. 2010b), but the full details still remain unknown. The ability of the M2 AH to induce budding was therefore investigated using a system involving GUVs. This system is very difficult to work with, and so a single-vesicle imaging system has been developed using microinjectors for further and more detailed investigation of budding mediated by the M2 AH. Additionally supported bilayers with excess membrane reservoir (SUPER) templates system has been used to study membrane scission induced by the M2 AH.

3.5.2 GUV budding

M2 AH is associated with membranes with high positive membrane curvature (see chapter 3.3.6) and can induce positive membrane curvature in LUVs (see chapter 3.4.4). To investigate if M2 AH can cause budding a model imitating biological membranes, the GUVs system, has been used. In this system, fluorescently labelled GUVs were diluted in buffer followed by addition of the M2 AH peptide and an aqueous dye (lucifer yellow, shown in red). After incubation morphological changes in the GUVs have been observed by confocal microscopy. When the peptide did not cause any effect on GUVs they appeared black inside with coloured rim and when GUVs had small internal vesicles with red inside but the main GUV having black inside it indicated budding activity. When GUVs appeared completely red inside it indicated leaking of the aqueous dye into the vesicles, which might suggest that the M2 AH peptide is able to initiate formation of a pore or breakage in the bilayer leading to leakage. A series of experiments were performed to test the M2 AH peptide based

on A/England/09 strain and all its mutants (as described in chapter 2.1.1) in the system using a mix of lipids: PC, PG and fluorescently labelled cholesterol (at 4:1:0.05 ratio) to form vesicles. Examples of confocal images of GUVs treated with different peptides are shown in Figure 3.5-1.

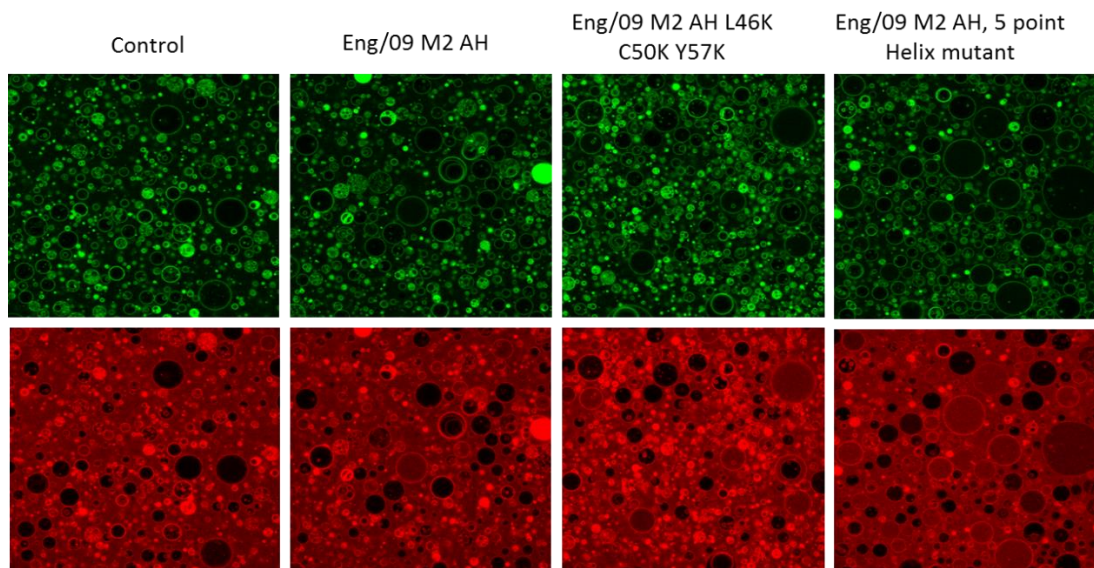


Figure 3. 5 - 1 Confocal images of GUV's composed of PC, PG and fluorescently labelled cholesterol, at 4:1:0.05 ratio, incubated with 10 μ M of Eng/09 M2 AH and its mutants with 0.5 mg/ml of an aqueous dye present in the buffer. Top panel shows detection of the signal from the GUV's and bottom panel shows signal from both, GUV's and aqueous dye.

To quantify the effect of each peptide on the GUVs morphology, the percentage of budding and leaking for different peptides was calculated for vesicles above 10 μ m in diameter, using 10 images for each sample. Some peptides, such as the 5-point mutant, R54A R61A double mutant or mutants with disrupted helix phase, caused increased leaking whereas others, such as F47A F48A (weakened hydrophobic face), L46K C50K Y57K (stronger polar face) or CRAC mutant cause a slight increase in budding activity (Fig. 3.5-2). Surprisingly, the wild type M2 AH for A/England/09 strain does not cause the expected robust budding, which may be related to its reduced AH formation or its reduced lipid ordering (Fig. 3.5-2). Control samples have shown a level of budding and leaking activity (Fig. 3.5-2) which might be caused by the diversity in GUVs population due to electroformation artefacts. This results in a small difference between controls and tested peptides, showing some of the peptides effect as statistically insignificant.

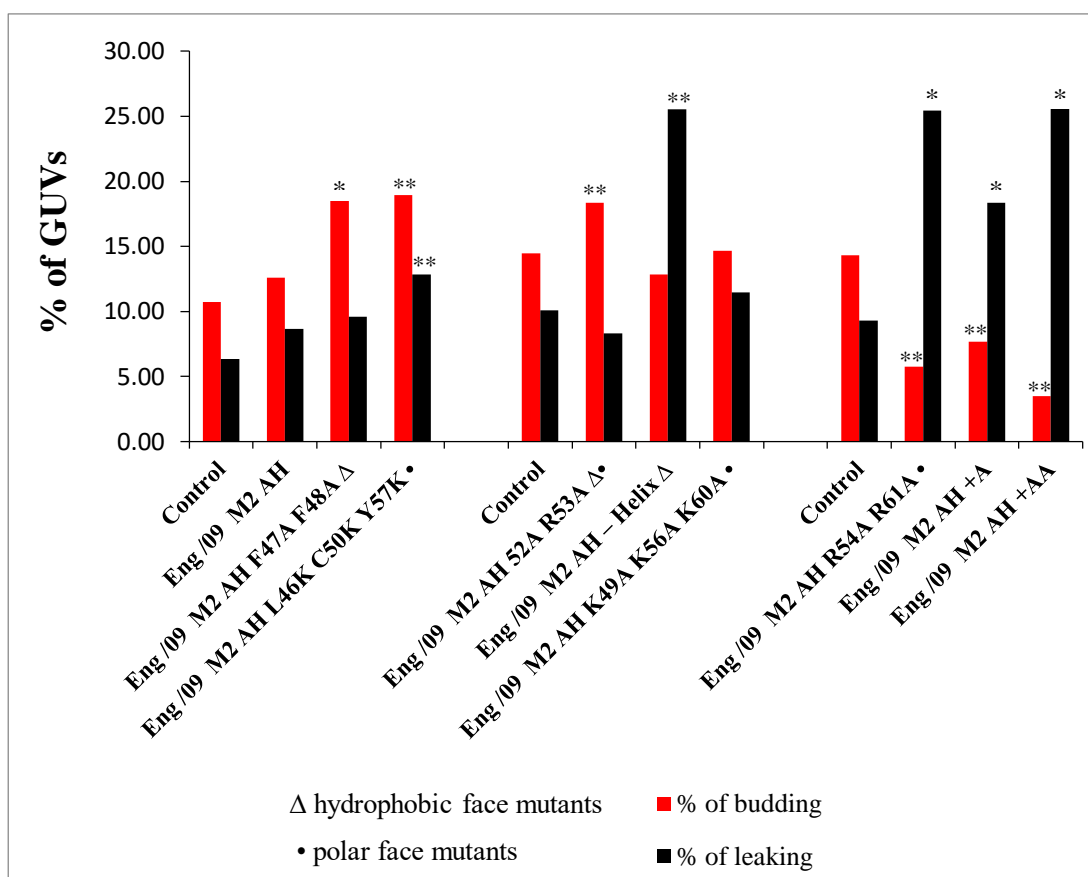


Figure 3.5 - 2 Budding activity induced by Eng/09 M2 AH and its mutants in GUV's composed of PC, PG and fluorescently labelled cholesterol, at 4:1:0.05 ratio. Data analysed by Student's t-test, P values < 0.05 indicated by * and < 0.01 by **.

Among influenza virus strains, there are slight differences in the M2 protein sequence. In the previous experiment the A/England/09 strain was used, whereas the most commonly used laboratory strain, in which budding activity of the M2 AH has been shown before is A/Udorn/72 (McCown and Pekosz 2006, Chen et al. 2008, Rossman et al. 2010a). To compare how strain differences affect budding activity a wild type M2 AH peptide based on the A/Udorn/72 strain was tested in the GUV's system. As shown in Figure 3.5-3, the Udorn M2 AH cause more robust budding effect and very small leaking effect compared to wild type A/England/09 based peptide.

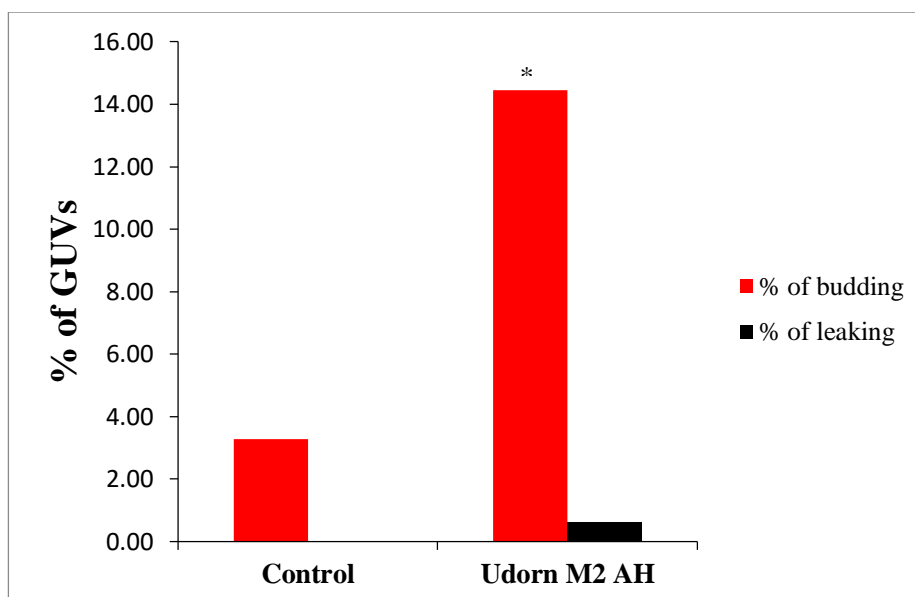
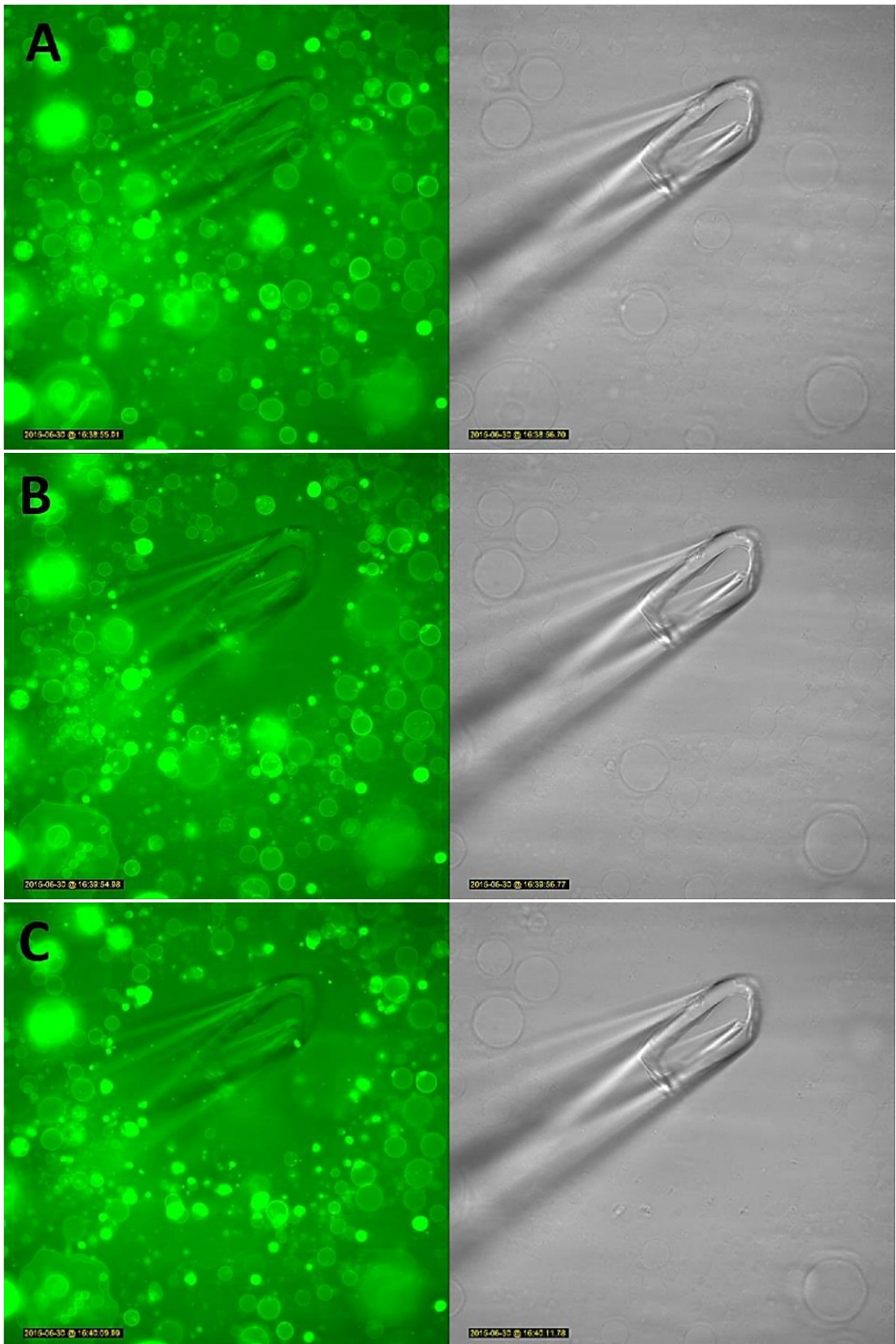


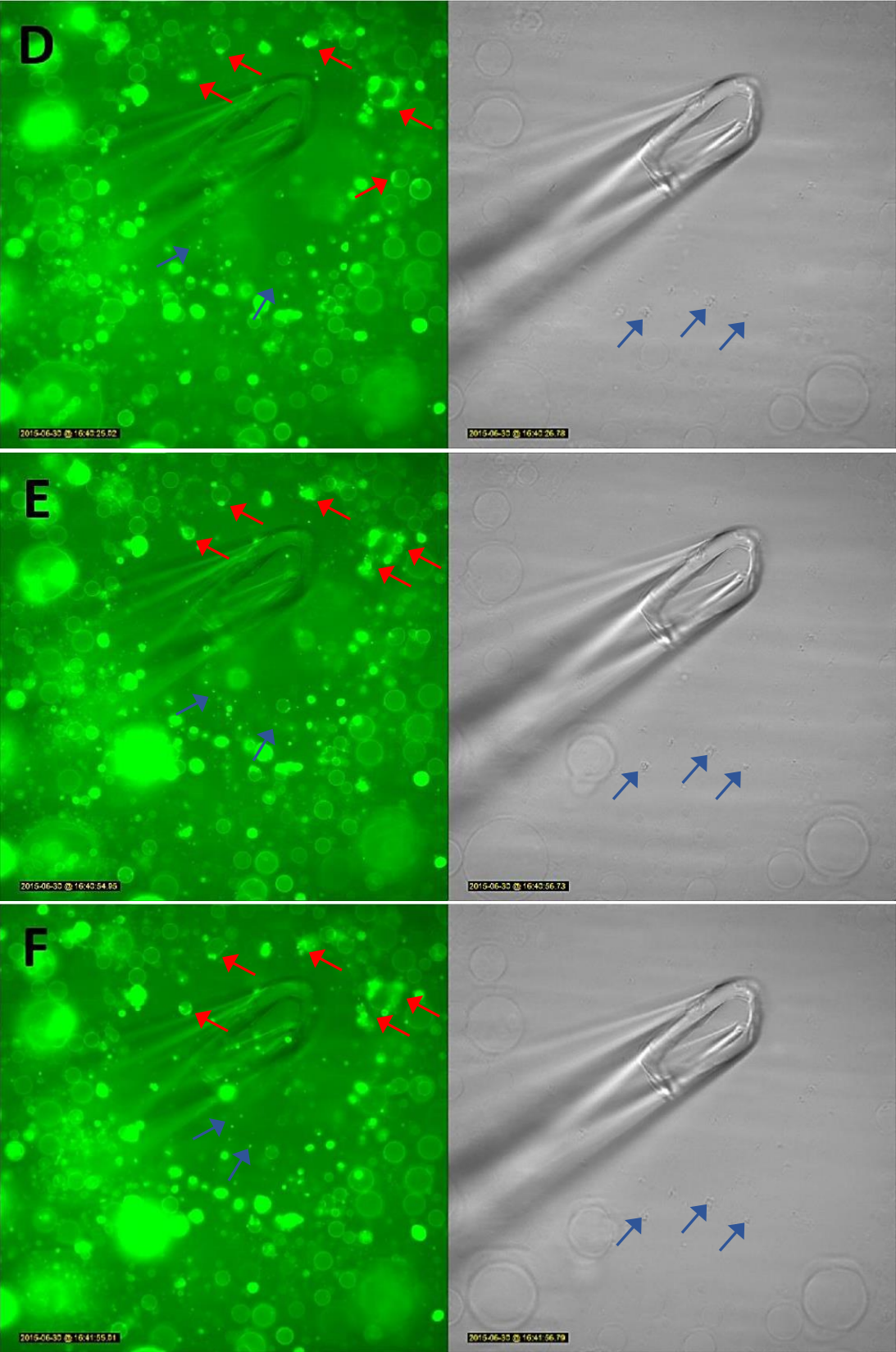
Figure 3. 5 - 3 Budding activity induced by M2 AH based on Udorn strain in GUV's composed of PC, PG and fluorescently labelled cholesterol, at 4:1:0.05 ratio. Data analysed by Student's t-test, P values < 0.01 indicated by *.

The GUVs system is highly variable and difficult to work with, with a lot of diversity and forming errors in the GUV population which amongst small vesicles shows the same morphology as budding or leaking effect caused by the peptide, which leads to high values in control samples and is not seen in larger vesicles. In samples with peptide present, a significant effect cannot be quantified with larger vesicles, possibly due to the lower positive membrane curvature preventing activity from the helix (see chapter 3.3.6). Those results suggest that, due to formation errors in small vesicles and a lack of activity in large vesicles, the M2 AH budding might not be efficient enough to be detected and quantified using this system.

3.5.3 GUV microinjections

As discussed before (see above), the GUVs system is highly variable, time consuming (especially data analysis and microscope image counting) and the M2 AH induced budding might not be efficient enough to be quantified in it. To overcome these problems, a single vesicle imaging system has been developed. In this system the unlabelled M2 AH peptide has been injected using a microinjection needle into the fluorescently labelled GUVs diluted in buffer. Changes in GUVs morphology have been observed in real time after injection on a fluorescence microscope. The M2 AH peptide, based on A/Udorn/72 strain, has been used due to the higher budding activity observed in the GUVs system compared to the A/England/09 strain based peptide (Fig. 3.5-2 and 3.5-3) with GUVs composed of PC, PG and fluorescently labelled cholesterol (at 4:1:0.05 ratio). Injection of the M2 AH peptide pushed nearby vesicles aside, forming a zone of clearance around the needle (Fig. 3.5-4 B). Small vesicles and blebs have been formed on the GUVs membranes placed around the needle (on the edge of the clearance zone) 30 seconds after injection, indicated by red arrows on Figure 3.5-4 D. A lot of very small vesicles or lipid puncta have also been formed in the buffer 30 seconds after injection, indicated by blue arrows on Figure 3.5-4 D, which could be some of the small vesicles that have budded off from GUVs membranes or been degraded GUVs by the M2 AH peptide. Both effects have been maintained during the experiment, up to 10 minutes after injection (Fig. 3.5-4 D-H). Those results suggest that the M2 AH is able to induce membrane curvature, form small vesicles on the membrane and mediate budding. The M2 AH facilitated budding is a rapid process, taking 15-30 seconds, but effects can be observed for a long time, for at least 10 minutes.





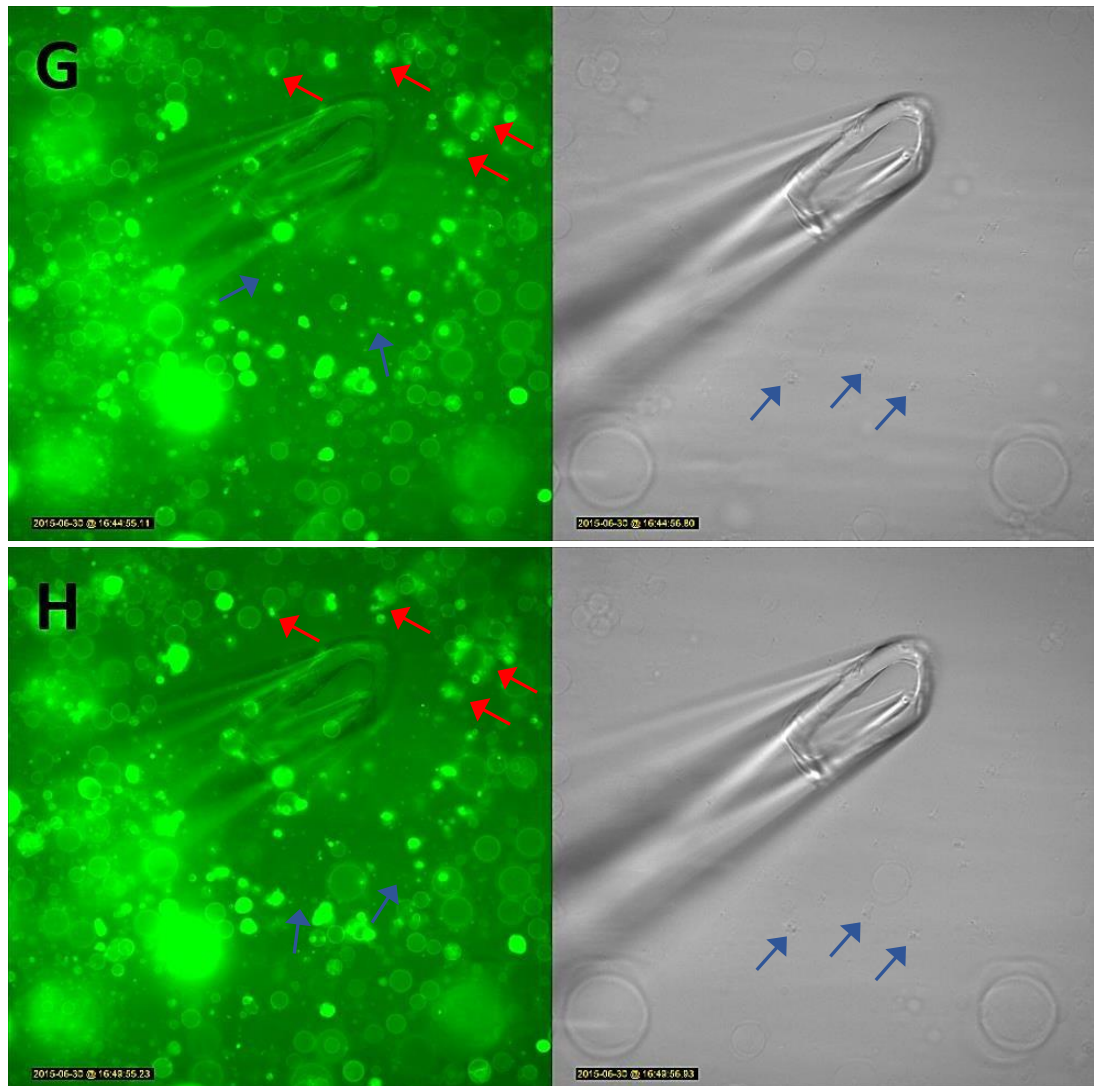


Figure 3. 5 - 4 Fluorescent microscopy images of GUVs composed of PC, PG and fluorescently labelled cholesterol at 4:1:0.05 ratio injected with M2 AH peptide. A - pre-injection, B - injection, C - 15 s post-injection , D - 30 s post-injection , E - 1 min post-injection, F - 2 min post-injection, G - 5 min post-injection and H - 10 min post-injection. Red arrows indicate small vesicles/blebs formed on the GUVs membrane after injection of the peptide and blue arrows indicate formation of small vesicles/lipid puncta in the solution.

3.5.4 SUPER templates and membrane scission

To investigate and quantify membrane scission mediated by the M2 AH supported bilayers with excess membrane reservoir (SUPER) templates system has been used. In this system SUPER templates were formed by incubating SUVs with silica beads following washes to remove residual lipids. SUPER templates were then tubulated by addition of Amphiphysin I and incubated with the M2 AH peptide after which membrane scission activity was assessed by detection of released fluorescent lipid from the templates. Addition of Amphiphysin I to the templates caused a scaffolding reaction and led to formation of membrane tubes that undergo a background level of spontaneous membrane extraction which is unrelated to scission (Fig. 3.5-5). The M2 AH caused significant lipid release from the templates whereas the 5 point mutant peptide was not able to cause release of lipids, with only background levels being observed (Fig. 3.5-5). Interestingly the M2 AH peptide did not cause lipid release in the absence of Amphiphysin I mediated scaffolding (Fig. 3.5-5). These results show that the M2 AH mediates membrane scission but it acts only on specially scaffolded or pre-constricted lipid domains and the introduction of 5 point mutations into the helix inhibits this effect.

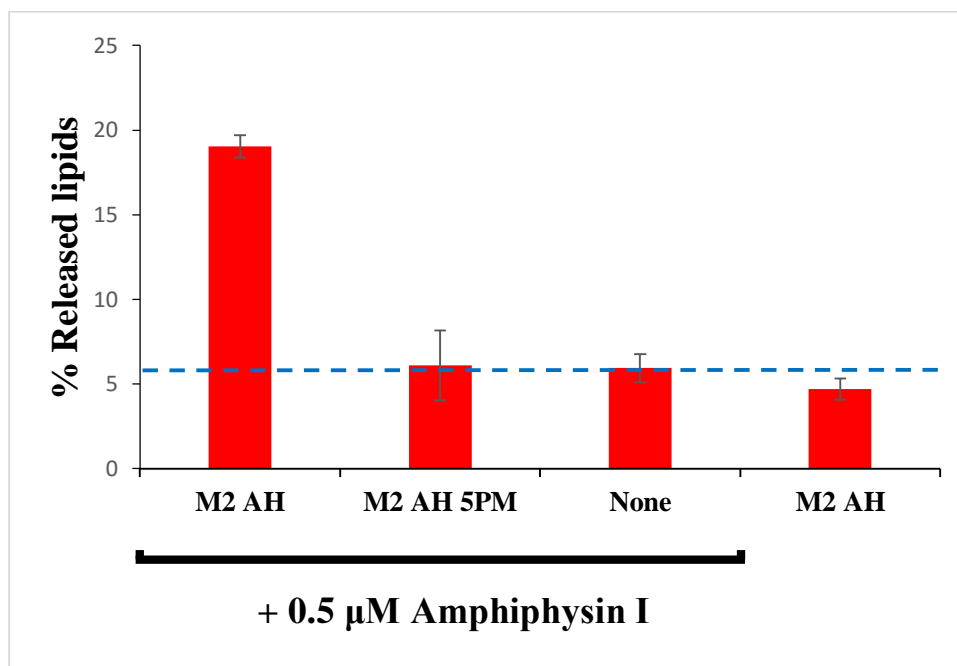


Figure 3. 5 – 5 Percentage of fluorescent lipids released from DOPC:DOPS:PIP2:RhoPE-containing SUPER templates at molar ratio of 79:15:5:1 (RhoPE released into the supernatant as % of total RhoPE fluorescence of SUPER templates, shown as mean \pm SD for three independent repeats performed in duplicate), tubulated with the addition of 0.5 μ M Amphiphysin I where indicated. Membrane scission was observed in the presence or absence of 25 μ M M2 AH and 5 point mutant peptide (M2 AH-Mut). Dashed blue line indicates the level of background lipid release.

3.5.5 Summary

The M2 AH has been previously shown to play a role in influenza virus budding (Rossman et al. 2010b) by mediating membrane scission. It is associated with membranes of high positive membrane curvature and induces positive membrane curvature in LUVs. Therefore the M2 AH ability to mediate budding has been investigated using GUVs system. In this system the M2 AH peptide has been incubated with fluorescently labelled GUVs in presence of a second fluorescent dye in the buffer followed by quantification of morphological changes observed in LUVs. Wild type M2 AH peptide, based on A/England/09 strain, has been tested in this system together with different helix mutants, as described in chapter 2.1.1 and two types of effects have been observed in GUVs populations: budding, when small internal vesicles filled with buffer dye were present in the main vesicles which did not have buffer dye present inside and leaking, when the interior of the main vesicles was filled with buffer dye. Increased budding activity has been observed with F47A F48A, L46K C50K Y57K and CRAC mutants whereas the 5-point mutant, R54A R61A double mutant and mutants with disrupted helix phase caused increased leaking (Fig. 3.5-2). Surprisingly, the wild type M2 AH based on A/England/09 strain did not show the expected robust budding (Fig. 3.5-2), which may be related to its reduced AH formation or its reduced lipid ordering. However, this could also be caused by strain differences as the majority of the previous work on the M2 AH induced budding was performed using the A/Udorn/72 strain, which differs in sequence by 3 amino acids (Fig. 3.2-8). Due to this, a wild type M2 AH peptide based on the A/Udorn/72 strain was also tested in the system, showing much more robust budding and very a small amount of leaking (Fig. 3.5-2). Unfortunately, controls also showed considerable amount of budding and leaking effect and as a result many of the samples did not show high enough values to be statistically significant (Fig. 3.5-2), which suggests that the M2 AH induced budding is not efficient enough to be detected by this system or that the other effects of the M2 AH, such as induction of membrane curvature and ordering lipids in the membrane are more relevant for the M2 AH functions than budding.

The GUVs system is highly variable, technically demanding and the M2 AH mediated budding may not be efficient enough to be detected and quantified using this system. Therefore a single imaging system has been developed, in which the M2 AH peptide is injected right next to the fluorescently labelled GUVs using a microinjector and morphological changes in vesicles are observed in a real time on fluorescent microscope. Results have shown formation of small vesicles on the GUVs membrane 30 s post-injection as well as formation of small vesicles or lipid puncta in the buffer, which could be a result of the small vesicles budding off from the membrane (Fig. 3.5-4). These effects have been observed throughout the whole experiment. This shows that the M2 AH, which can induce positive membrane curvature in LUVs (Fig. 3.4-4), also mediates budding and the process is rapid but effects are maintained for a long time.

The SUPER templates system has been used to investigate membrane scission mediated by the M2 AH. In this system SUPER templates, which are formed by incubation of LUVs with silica beads, were tubulated by addition of Amphiphysin I and incubated with the M2 AH peptide. Results showed that the M2 AH but not the 5 point mutant M2 AH cause significant release of lipids from the templates (Fig. 3.5-5). Interestingly that effect is only observed if SUPER templates are tubulated with Amphiphysin I (Fig. 3.5-5). These results show that the M2 AH mediates membrane scission but it acts only on specially scaffolded or pre-constricted lipid domains and this ability is inhibited by introducing 5 point mutations into the helix.

3.6 M2 AMPHIPATHIC HELIX MEDIATED BUDDING *IN VIVO*

3.6.1 Introduction

Using LUVs and GUVs, which imitate biological membranes, it has been shown that the M2 AH can induce positive membrane curvature and mediates budding (see chapters 3.4.4 and 3.5). However, both those systems are artificial and therefore there are no cellular factors involved which might play an important role in virus budding. Previously it has been shown that the Rab11 protein might be involved in formation of filamentous virions (Bruce et al. 2010), but knowledge about other cellular proteins involved in influenza virus budding is limited. To investigate if M2 also induces budding, *in vivo* supernatant from cells transfected with M2 protein and its 5 point mutant version have been analysed by immunoblotting. An influenza virus with 5 point mutations in the M2 AH have also been repeatedly passaged in cells and the sequence of the M segment of the genome has been analysed to identify any acquired reverse mutations that restored virus properties.

3.6.2 Virus-like particles (VLP) release

It has been shown that the M2 AH induces positive membrane curvature in LUVs (Fig. 3.4-10), forms small vesicles and mediates budding in GUVs (Fig. 3.5-5). Further investigation of the M2 AH mediated budding has been performed *in vivo*. HEK 293T cells have been transfected with plasmids expressing either a wild type M2 or a M2 with 5 point mutants in the AH (which cause growth impairment in virus), and after 48 h of incubation the presence of the M2 protein in the cells and the supernatant has been detected by immunoblotting using the M2 specific monoclonal antibody, 14C2. As expected M2 has been detected in cells transfected with the M2 expressing plasmid, with reduced levels of M2 being observed in cells transfected with the 5 point mutant M2 expressing plasmids (Fig. 3.6-1). In both cases two bands have been detected, one about 15 kDa in size which corresponds to a full length M2 protein (Iwatsuki-Horimoto et al. 2006) and second, slightly smaller, about 13 kDa in size which is a truncated version of the M2 protein that has undergone caspase cleavage processing (Zhirnov and Klenk 2009). Interestingly similar bands, but much less intensive have

been detected in the corresponding cell's supernatants, with additional faint band at around 28 kDa, which corresponds to the M2 dimer (Fig. 3.6-1) (Iwatsuki-Horimoto et al. 2006). Those results suggest that the M2 AH does not only induce positive membrane curvature in LUVs (Fig. 3.4-10), lead to the formation of small vesicles on the membrane of GUVs and initiate budding in GUVs (Fig. 3.5-5), but also mediates budding in transfected cells.

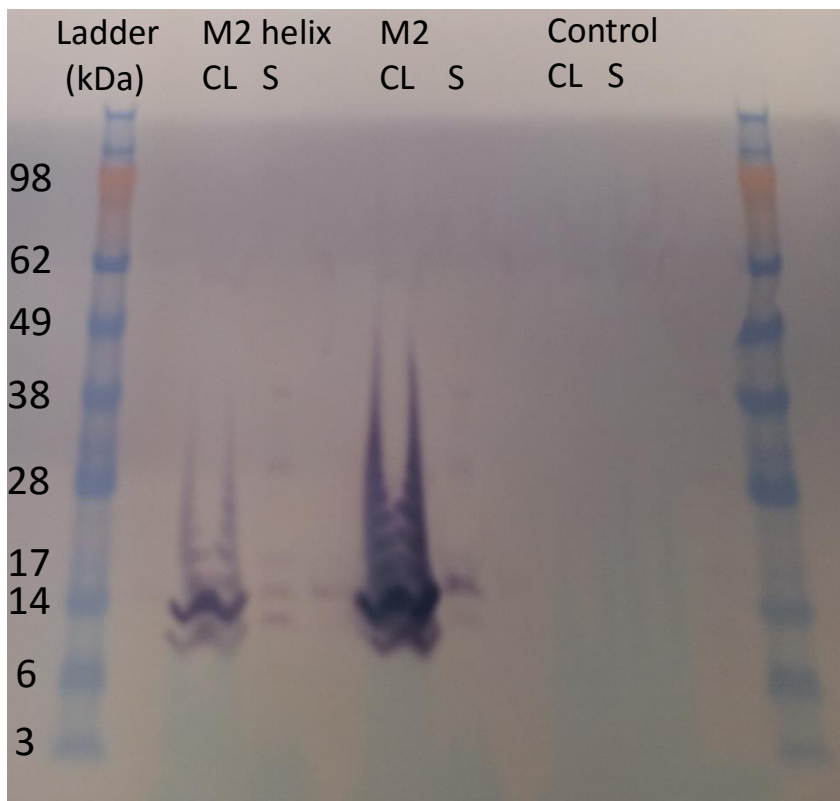


Figure 3. 6 - 1 Western blot of HEK 293T cells 48 h post-transfection with 2.5 μ g of plasmid expressing M2 and M2 5 point helix mutant (growth impairment) proteins. Cell lysates (CL) and supernatant (S) for transfected cells and control were immunoblotted with specific monoclonal antibody against M2, 14C2.

3.6.3 Restoration of viral growth

NMR showed that the M2 AH is formed in presence of liposomes (see chapter 3.1.2) and that it is mainly the hydrophobic face of the helix that is responsible for binding with membranes (see chapter 3.1.3). These results have been confirmed by CD spectroscopy (see chapters 3.2 and 3.3). To further investigate which parts of the helix are important for the M2 AH structure and the effect of the cellular environment on its function, the sequence of the viral M gene have been analysed before and after repeated passaging. Influenza A virus with 5 point mutants in the M2 protein, which previously had been shown to impair virus growth (Rossman et al. 2010a, Rossman et al. 2010b) have been repeatedly passaged in the MDCK cells in order to see if any compensating mutations emerge. Virus titer was checked after each passage by plaque assay and viral RNA have been isolated for two samples: in the early stages of passaging (passage 4), when viral titer was very low; and after 10 more passages (passage 14), when viral titer was high and on similar levels for a few consecutive passages (Table 3.6-1). The M segment of both viruses have been sequenced to detect any reversion mutations that may have arisen after repeated passaging that may have restored virus growth and functions.

Passage number	Virus titer (detected by plaque assay)
4	1×10^4
5	1.5×10^5
6	4.7×10^3
11	1.66×10^6
12	4.8×10^6
13	7.5×10^6
14	6.25×10^6

Table 3.6 - 1 Virus titers detected by plaque assays for the Influenza A virus with 5 point mutations in the M2 protein for passages 4-6 and 11-14.

Sequencing analysis of the M segment showed no change to the viral genome after 4 passages which, together with a low virus titer, suggests that the virus was not able to restore the functions that are lost due to the introduced mutations (Fig. 3.6-2). Two point mutations in the M segment at positions 910 and 925, which correspond to the region coding for the CT of the M2 protein (residue 66 and 71 of the full length protein respectively) arose after 14 passages (Fig. 3.6-3). However, those mutations were only detected in one of the two sequencing reactions covering that region of the M gene but they do affect sequence of the M2 protein's CT resulting in E66G and S71F mutations (see appendix 6.5). This suggests that virus growth and functions have been restored as the titer was very high, without any reverse mutations in the M2 AH, but with possible mutations in the further parts of the CT. This suggests that mutations in parts of the M2 CT may compensate for the decreased M2 AH functions but other viral proteins and cellular factors may also be involved. The molecular mechanism behind this is not yet known and further research is needed.

Agnieszka Martyna

	10 20 30 40 50 60				
M gene 5-Point mutati	1	AGCAAAAGCAGGTAGATATTGAAAGATGAGCCTTCTGACCGAGGTGAAACGTATGTTCT	60		
M_UTR_F	1	~~~~~	1		
M_F2	1	~~~~~	1		
M_UTR_R	1	~~~~~	1		
70 80 90 100 110 120					
M gene 5-Point mutati	61	CTCTATCGTTCCGTCAGGTCGCCCTCAAAGCCGAGATCGCGCAGAGACTTGAAGATGCTTT	120		
M_UTR_F	1	~~~~~	2		
M_F2	1	~~~~~	1		
M_UTR_R	1	~~~~~	1		
130 140 150 160 170 180					
M gene 5-Point mutati	121	TGCTGGAAGAACACAGATCTTGAGGCTCTCATGGAATGGCTAAAGACAAGACCAATCCT	180		
M_UTR_F	3	TGCTGGAAGAACACAGATCTTGAGGCTCTCATGGAATGGCTAAAGACAAGACCAATCCT	62		
M_F2	1	~~~~~	1		
M_UTR_R	1	~~~~~	1		
190 200 210 220 230 240					
M gene 5-Point mutati	181	GTCACCTCTGACTAAAGGGATTTTGGGATTTGTATTACAGCTCACCGTGCCAGTGAGCG	240		
M_UTR_F	63	GTCACCTCTGACTAAAGGGATTTTGGGATTTGTATTACAGCTCACCGTGCCAGTGAGCG	122		
M_F2	1	~~~~~	1		
M_UTR_R	1	~~~~~	1		
250 260 270 280 290 300					
M gene 5-Point mutati	241	AGGACTGCAGCGTAGACGCTTTGTCCAAAATGCCCTCAATGGGAATGGGGATCCAAATAA	300		
M_UTR_F	123	AGGACTGCAGCGTAGACGCTTTGTCCAAAATGCCCTCAATGGGAATGGGGATCCAAATAA	182		
M_F2	1	~~~~~	1		
M_UTR_R	1	~~~~~	1		
310 320 330 340 350 360					
M gene 5-Point mutati	301	CATGGACAGAGCAGTTAAACTGTATAGAAAACCTAAGAGGGAGATAACATTCCATGGGGC	360		
M_UTR_F	183	CATGGACAGAGCAGTTAAACTGTATAGAAAACCTAAGAGGGAGATAACATTCCATGGGGC	242		
M_F2	1	~~~~~	1		
M_UTR_R	1	~~~~~	1		
370 380 390 400 410 420					
M gene 5-Point mutati	361	CAAAGAAATAGCACTCAGTTATTCTGCTGGTGCACCTTGCCAGTTGCATGGGGCTCATATA	420		
M_UTR_F	243	CAAAGAAATAGCACTCAGTTATTCTGCTGGTGCACCTTGCCAGTTGCATGGGGCTCATATA	302		
M_F2	1	~~~~~	1		
M_UTR_R	1	~~~~~	22		
430 440 450 460 470 480					
M gene 5-Point mutati	421	CAACAGGATGGGGCTGTGACCACTGAAGTGGCCTTTGGCCTGGTTTGTGCAACCTGTGA	480		
M_UTR_F	303	CAACAGGATGGGGCTGTGACCACTGAAGTGGCCTTTGGCCTGGTTTGTGCAACCTGTGA	362		
M_F2	1	~~~~~	1		
M_UTR_R	23	CAACAGGATGGGGCTGTGACCACTGAAGTGGCCTTTGGCCTGGTTTGTGCAACCTGTGA	82		
490 500 510 520 530 540					
M gene 5-Point mutati	481	ACAGATTGCTGACTCCCAGCACAGGTCTCATAGGCAAATGGTGGCAACAACCAATCCAAT	540		
M_UTR_F	363	ACAGATTGCTGACTCCCAGCACAGGTCTCATAGGCAAATGGTGGCAACAACCAATCCAAT	422		
M_F2	1	~~~~~	48		
M_UTR_R	83	ACAGATTGCTGACTCCCAGCACAGGTCTCATAGGCAAATGGTGGCAACAACCAATCCAAT	142		
550 560 570 580 590 600					
M gene 5-Point mutati	541	AATAAGACATGAGAACAGAATGGTTCTGGCCAGCACTACAGCTAAGGCTATGGAGCAAAT	600		
M_UTR_F	423	AATAAGACATGAGAACAGAATGGTTCTGGCCAGCACTACAGCTAAGGCTATGGAGCAAAT	482		
M_F2	49	AATAAGACATGAGAACAGAATGGTTCTGGCCAGCACTACAGCTAAGGCTATGGAGCAAAT	108		
M_UTR_R	143	AATAAGACATGAGAACAGAATGGTTCTGGCCAGCACTACAGCTAAGGCTATGGAGCAAAT	202		

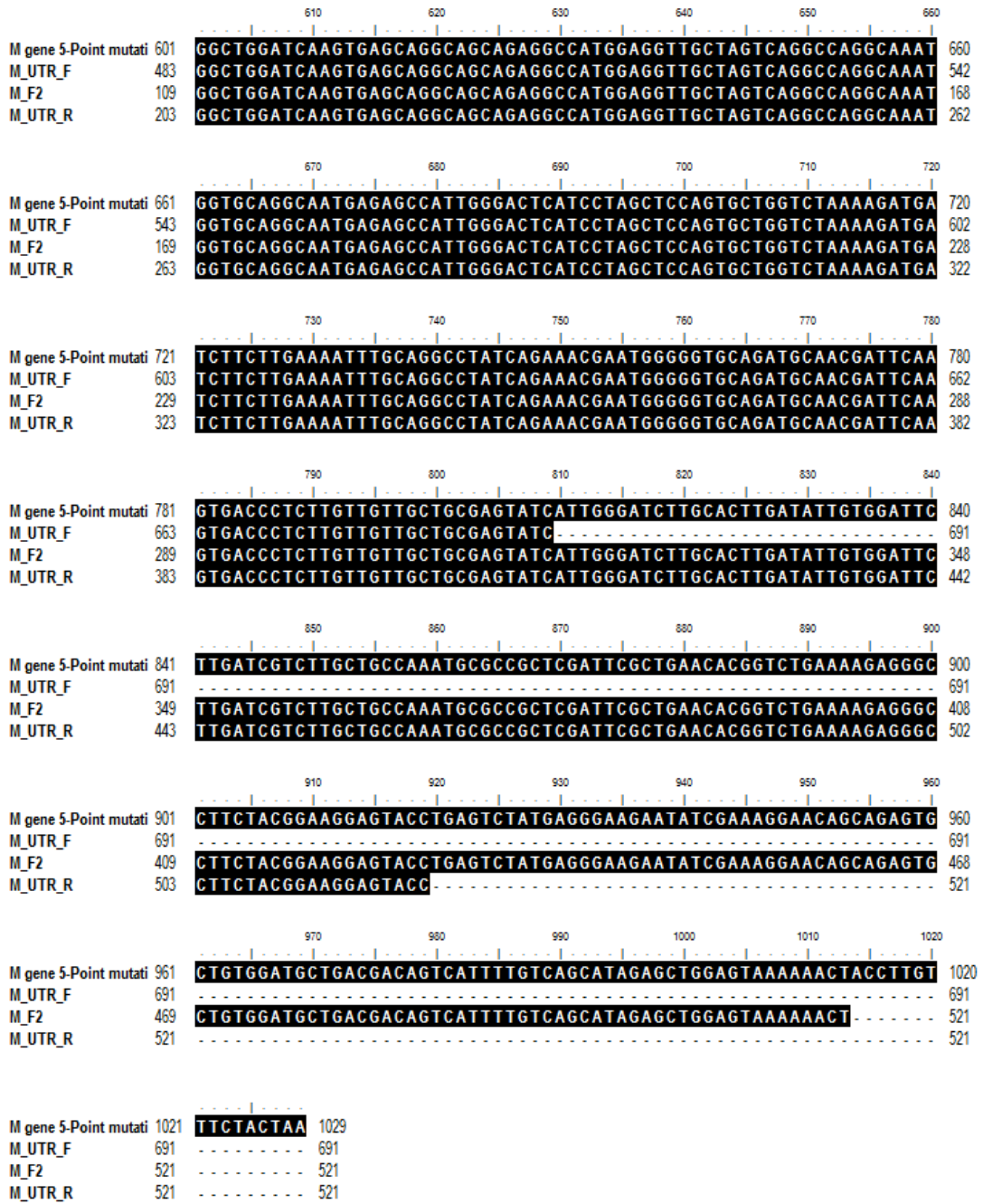


Figure 3. 6 - 2 Sequence alignment of the M gene of the influenza A/Udorn/72 virus with 5 point mutations in the M2 protein (top) aligned with the M gene of that virus after 4 passages (row 2-4) in MDCK cells sequenced with three primers: M_UTR_F, M_F2 and M_UTR_R. The same residues are highlighted in black and the different ones in white.

Agnieszka Martyna

		10	20	30	40	50	60	
M gene 5-Point Mutant	1	AGCAAAAGCAGGTAGATATTGAAAGATGAGCCTTCGACCGAGGTCGAAACGTATGTTCT					60	
M_UTR_F	1						3	
M_F2	1	~~~~~					1	
M_UTR_R	1	~~~~~					1	
		70	80	90	100	110	120	
M gene 5-Point Mutant	61	CTCTATCGTTCCGTCAGGTCCCCTCAAAGCCGAGATCGCGCAGAGACTTGAAGATGCTT					120	
M_UTR_F	4	CTCTATCGTTCCGTCAGGCCCCCTCAAAGCCGAGATCGCGCAGAGACTTGAAGATGCTT					63	
M_F2	1	~~~~~					1	
M_UTR_R	1	~~~~~					1	
		130	140	150	160	170	180	
M gene 5-Point Mutant	121	TGCTGGAAAGAACACAGATCTTGAGGCTCTCATGGAATGGCTAAAGACAAGACCAATCCT					180	
M_UTR_F	64	TGCTGGAAAGAACACAGATCTTGAGGCTCTCATGGAATGGCTAAAGACAAGACCAATCCT					123	
M_F2	1	~~~~~					1	
M_UTR_R	1	~~~~~					1	
		190	200	210	220	230	240	
M gene 5-Point Mutant	181	GTCACCTCTGACTAAAGGGATTTTGGGATTTGTATTCACGCTCACCGTGCCAGTGAGCG					240	
M_UTR_F	124	GTCACCTCTGACTAAAGGGATTTTGGGATTTGTATTCACGCTCACCGTGCCAGTGAGCG					183	
M_F2	1	~~~~~					1	
M_UTR_R	1	~~~~~					1	
		250	260	270	280	290	300	
M gene 5-Point Mutant	241	AGGACTGCAGCGTAGACGCTTTGTCCAAAATGCCCTCAATGGGAATGGGGATCCAAATAA					300	
M_UTR_F	184	AGGACTGCAGCGTAGACGCTTTGTCCAAAATGCCCTCAATGGGAATGGGGATCCAAATAA					243	
M_F2	1	~~~~~					1	
M_UTR_R	1	~~~~~					1	
		310	320	330	340	350	360	
M gene 5-Point Mutant	301	CATGGACAGAGCAGTTAAACTGTATAGAAAACCTTAAGAGGGAGATAACATTCCATGGGGC					360	
M_UTR_F	244	CATGGACAGAGCAGTTAAACTGTATAGAAAACCTTAAGAGGGAGATAACATTCCATGGGGC					303	
M_F2	1	~~~~~					1	
M_UTR_R	1	CATGGACAGAGCAGTTAAACTGTATAGAAAACCTTAAGAGGGAGATAACATTCCATGGGGC					60	
		370	380	390	400	410	420	
M gene 5-Point Mutant	361	CAAAGAAATAGCACTCAGTTATTCTGCTGGTGCAC TTGCCAGTTGCATGGGCCTCATATA					420	
M_UTR_F	304	CAAAGAAATAGCACTCAGTTATTCTGCTGGTGCAC TTGCCAGTTGCATGGGCCTCATATA					363	
M_F2	1	~~~~~					1	
M_UTR_R	61	CAAAGAAATAGCACTCAGTTATTCTGCTGGTGCAC TTGCCAGTTGCATGGGCCTCATATA					120	
		430	440	450	460	470	480	
M gene 5-Point Mutant	421	CAACAGGATGGGGCTGTGACCACTGAAGTGGCCTTTGGCCTGGTTTGTGCAACCTGTGA					480	
M_UTR_F	364	CAACAGGATGGGGCTGTGACCACTGAAGTGGCCTTTGGCCTGGTTTGTGCAACCTGTGA					423	
M_F2	1	~~~~~GC~ACCTGTGA					10	
M_UTR_R	121	CAACAGGATGGGGCTGTGACCACTGAAGTGGCCTTTGGCCTGGTTTGTGCAACCTGTGA					180	
		490	500	510	520	530	540	
M gene 5-Point Mutant	481	ACAGATTGCTGACTCCCAGCACAGGTCTCATAGGCAAATGGTGGCAACAACCAATCCACT					540	
M_UTR_F	424	ACAGATTGCTGACTCCCAGCACAGGTCTCATAGGCAAATGGTGGCAACAACCAATCCACT					483	
M_F2	11	~~~~~					70	
M_UTR_R	181	ACAGATTGCTGACTCCCAGCACAGGTCTCATAGGCAAATGGTGGCAACAACCAATCCACT					240	
		550	560	570	580	590	600	
M gene 5-Point Mutant	541	AATAAGACATGAGAACAGAATGGTTCTGGCCAGCACTACAGCTAAGGCTATGGAGCAAAT					600	
M_UTR_F	484	AATAAGACATGAGAACAGAATGGTTCTGGCCAGCACTACAGCTAAGGCTATGGAGCAAAT					543	
M_F2	71	~~~~~					130	
M_UTR_R	241	AATAAGACATGAGAACAGAATGGTTCTGGCCAGCACTACAGCTAAGGCTATGGAGCAAAT					300	

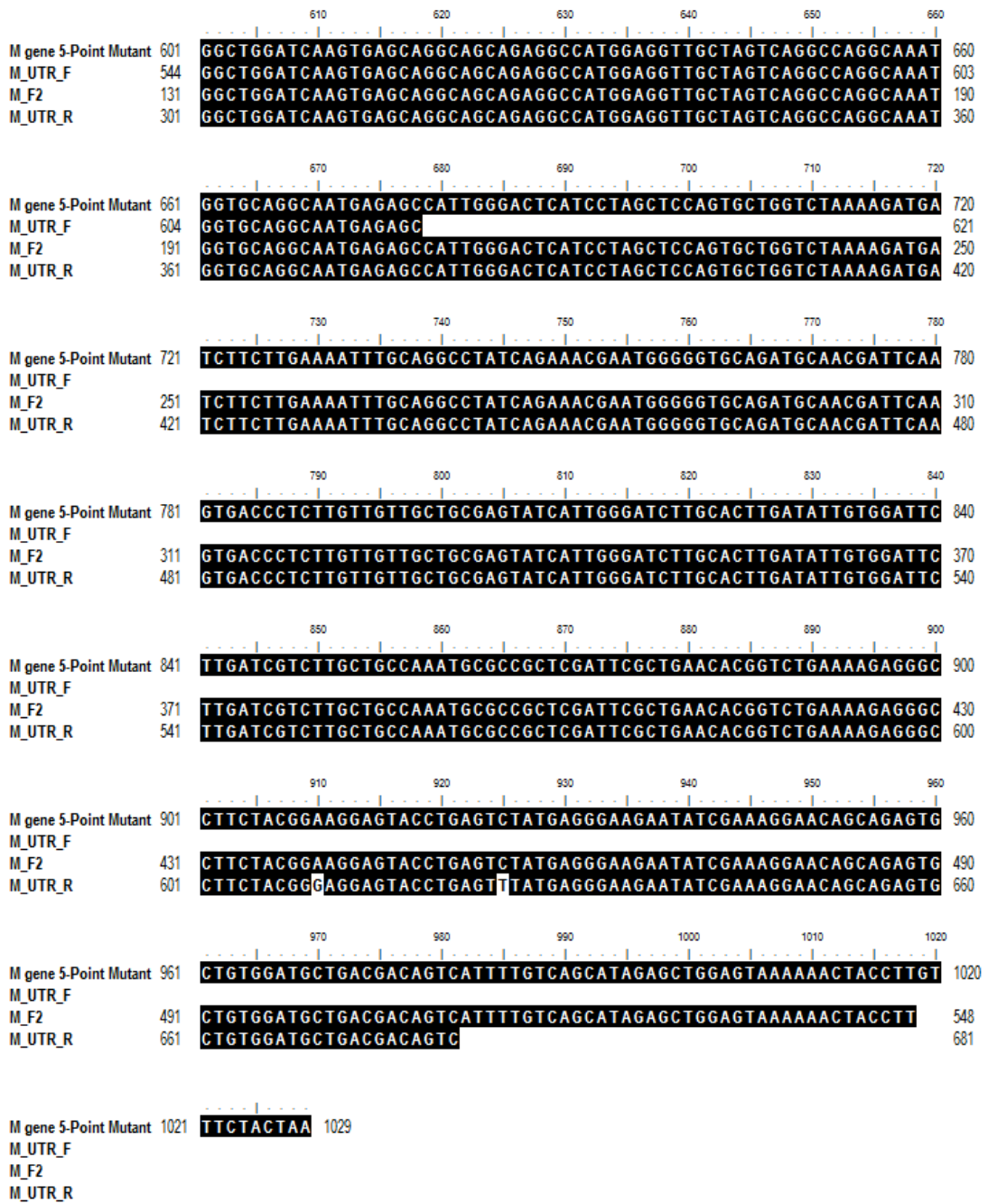


Figure 3. 6 - 3 Sequence alignment of the M gene of the influenza A/Udorn/72 virus with 5 point mutations in the M2 protein (top) aligned with the M gene of that virus after 14 passages (row 2-4) in the MDCK cells sequenced with three primers: M_UTR_F, M_F2 and M_UTR_R. The same residues are highlighted in black and the different ones in white.

3.6.4 Summary

The M2 AH has been shown to: associate with membranes with high positive curvature (see chapter 3.3.6), induce positive membrane curvature (see chapter 3.4.4) and mediate budding in artificial lipid membranes (see chapter 3.5). Further investigation of the M2 AH mediated budding was performed *in vivo* as it has been shown previously that some of cellular proteins may play a role in influenza virus budding, such as Rab11 which is involved in formation of filamentous virions (Bruce et al. 2010) and therefore the cellular environment may affect the M2 AH ability to mediate budding. Supernatant and cell lysates from cells transfected with plasmids expressing either the wild type M2 protein or the M2 protein with 5 point mutants in the AH, have been analysed by immunoblotting. The M2 protein and its truncated version have been detected in both cell lysates, with reduction of band intensity for the M2 with 5 PM (Fig. 3.6-1). Interestingly similar bands, but much less intense have been detected in the supernatant fractions (Fig. 3.6-1), suggesting that M2 mediates budding *in vivo*, and the introduction of the 5 PM into the AH significantly reduces M2 induced budding.

To further investigate the effect of the cellular environment on the M2 AH, the influenza A virus with 5 PM in the AH, which causes growth impairment in the virus as described before (Rossman et al. 2010a, Rossman et al. 2010b), has been repeatedly passaged in MDCK cells. The sequence of the M segment of the genome has been analysed at an early stage of passaging, at passage 4, when viral titer was low, and following 10 more passages, when viral titer was high for few consecutive passages, to detect any reverse mutations that arose and restored virus growth and functions. Sequencing analysis showed no changes in the M segment in the early stages (Fig. 3.6-2), but after 14 passages sequencing with one of two primers covering the region of the M segment coding for the CT of the M2 protein showed 2 point mutations (Fig. 3.6-3). These point mutations resulted in two single mutations in the sequence of the M2 CT, E66G and S71F suggesting that further parts of the CT may compensate for loss of function in the M2 AH. Interestingly previous research has shown that mutations in residue 71 of the M2 protein showed resistance to the 14C2 antibody, moreover one of the identified mutations responsible for this was S71F (Zebedee and Lamb 1989). However, cellular factors and other viral proteins may also play a role and further work is needed to investigate molecular mechanism behind that.

3.7 FUNCTIONALLY HOMOLOGOUS SCISSION HELICES IN CELLULAR PROTEINS

3.7.1 Introduction

The M2 AH has been shown to form a helix upon binding with membranes (see chapters 3.1.2 and 3.2.3), with the hydrophobic face of the helix mainly being responsible for lipid binding (see chapter 3.1.3), and it is associated with highly curved membranes (see chapter 3.3.6), such as the neck of the budding virion. In this environment, the M2 AH can induce positive membrane curvature (see chapter 3.4.4) leading to membrane scission, facilitating budding (see chapters 3.5 and 3.6). Membrane budding is a multi-step process which is important not only for viruses, but also plays a role in many biological processes, such as endocytosis or vesicle trafficking involving many different proteins and AHs. Many of those AHs either sense or generate membrane curvature in few different ways. Curvature sensing proteins or AHs may contain a Bin-Amphiphysin-Rsv (BAR) domain or Amphipathic Lipid Packing Sensor (ALPS), which sense membrane curvature either by forming a crescent shape and binding to the membrane with the preferred curvature (Peter et al. 2004) or by insertion into the membrane and sensing curvature by using hydrophobic interactions (Drin and Antony 2010). On the other hand, generation of membrane curvature can be induced by insertion of the cationic face of the AH into the membrane, as is the case with many antimicrobial peptides (Ford et al. 2002, Peter et al. 2004, Boucrot et al. 2012). Many proteins contain both BAR domains and AHs that can generate membrane curvature with its polar face, meaning they are able to sense and generate membrane curvature however, both those activities are associated with different domains. The M2 AH has been shown to have both features, as it contains many hydrophobic residues together with several cationic ones and its able to sense and induce membrane curvature therefore it might belong to a novel group of AH which binds to membranes with high positive membrane curvature, induce positive membrane curvature which in this environment leads to membrane scission. Several AHs from cellular proteins have been tested to determine if their mechanism of membrane scission is the same as the M2 AH and therefore all belong to a novel group of AHs.

3.7.2 Arf1, CHMP4b, EndophilinA3 and Epsin1

3.7.2.1 Structural changes in different environments

A range of cellular peptides containing AH that have been shown to play a role in vesicle budding and scission have been analysed, with the exact mechanism for the scission currently unknown. Peptides with AHs that were close sequence homologues with the M2 AH have not been identified however, AHs that have similar features to the M2 AH, such as hydrophobicity, hydrophobic moment and net charge have been identified in the Arf 1, Endophilin A3, Epsin 1 and CHMP4b proteins, as shown in Figure 3.7-1. Arf 1 is involved in COP-vesicle budding (Beck et al. 2011), Endophilin A3 plays a role in non-clathrin-mediated-endocytosis (Boucrot et al. 2012) whereas Epsin 1 has a role in dynamin-dependent scission which is a part of clathrin-mediated-endocytosis (Boucrot et al. 2012) and CHMP4b is involved in multi-vesicular body (MVB) budding (Fabrikant et al. 2009).

Protein	Hydrophobicity	Hydrophobic Moment	Net Charge	FreqPolar	Angle	Z-Distance
M2 (47-62)	0.431	0.493	4	0.556	12.5	15.5
Arf1 (1-18)	0.474	0.4	2	0.5	25	16.5
CHMP4b (1-13)	0.539	0.403	1	0.538	17.5	7.5
Endophilin A3 (1-21)	0.325	0.368	3	0.571	7.5	17.5
Epsin1 (1-17)	0.234	0.388	3	0.647	2.5	17.5

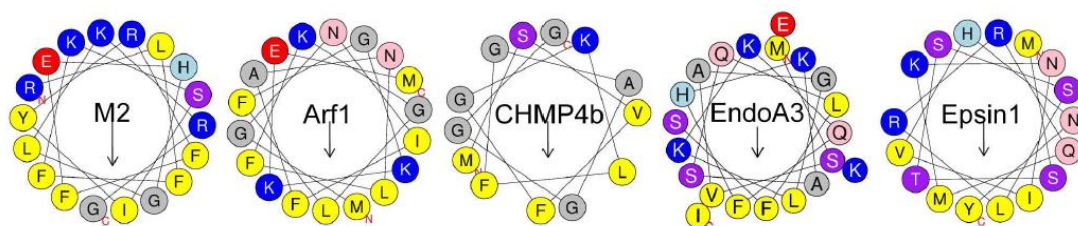


Figure 3. 7 – 1 Biophysical properties and helical wheel plots of M2 AH and the human Arf 1, CHMP4b, Endophilin A3 and Epsin 1 AHs were calculated and generated using HeliQuest (Gautier et al. 2008) found at <http://heliquest.ipmc.cnrs.fr/> and E(z)3D. Positively charged polar residues are shown in blue, negatively charged polar residues are in red, polar uncharged residues are in purple and pink, glycine and alanine are shown in grey, and hydrophobic residues are in yellow.

CD spectra showed that in solution the majority of these peptides are unstructured, with exception of Epsin 1 which shows the deepest trough, suggesting partial formation of an α -helix in solution (Fig. 3.7-2). In presence of standard LUVs Endophilin A3 and Epsin 1 peptides showed two big troughs, corresponding to formation of an α -helix, with over 95% of the helix present (Fig. 3.7-3). Arf 1 peptide also showed two troughs, but their depth was significantly reduced compared to Endophilin A3 and Epsin 1 peptides, despite that the estimated helix percentage showed nearly 95% of the helix present (Fig. 3.7-3). On the other hand CHMP4b peptide showed a similar CD spectra in solution and with LUVs, with less than 5% helix present for both (Fig. 3.7-2 and 3.7-3). Those results show that three cellular AH Endophilin A3, Epsin 1 and Arf 1 behave same as the M2 AH and form helix upon binding with liposomes.

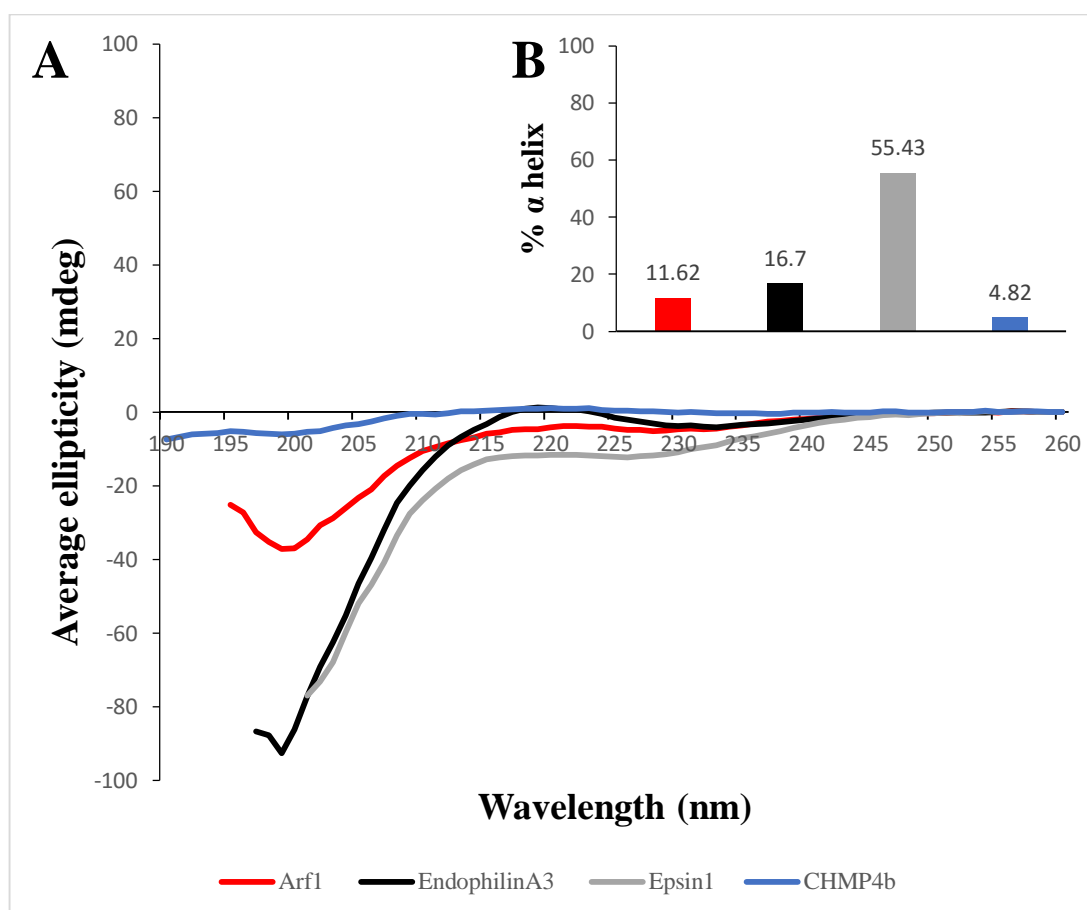


Figure 3.7 - 2 CD spectra for 250 μ M of cellular peptides: Arf 1, Endophilin A3, Epsin 1 and CHMP4b in solution (A). Estimated percentage of an α helix present in each sample calculated based on the spectra using K2D3 bioinformatics tool on <http://k2d3.ogic.ca/> website (B).

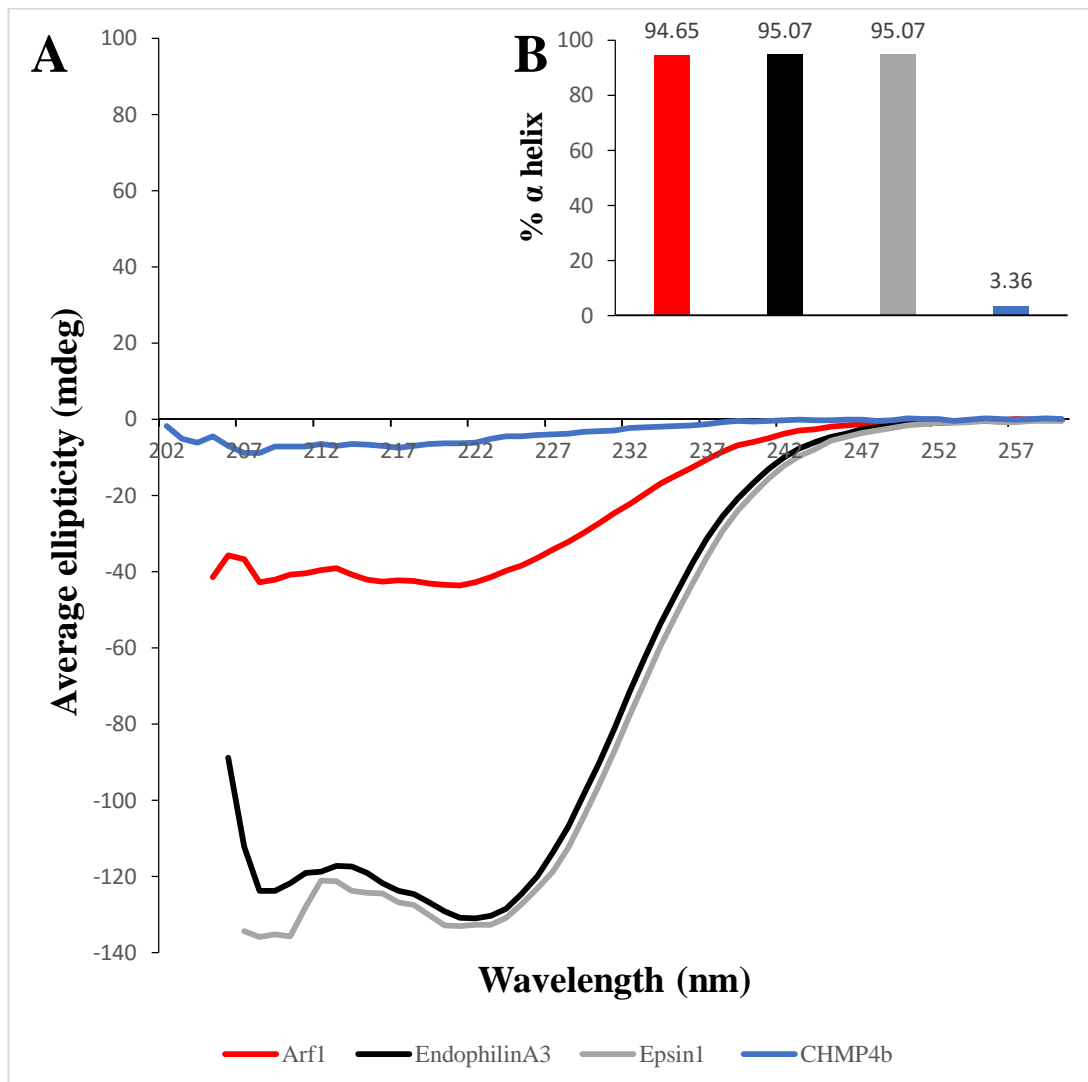


Figure 3.7 - 3 CD spectra for 250 μ M of cellular peptides: Arf 1, Endophilin A3, Epsin 1 and CHMP4b with 5 mM of standard LUVs (A). Estimated percentage of an α helix present in each sample calculated based on the spectra using K2D3 bioinformatics tool on <http://k2d3.ogic.ca/> website (B).

3.7.2.2 Anionic lipids and positive membrane curvature effect on cellular AH formation

To further investigate similarities between the cellular AHs and the M2 AH a range of SUVs, LUVs and GUVs of different sizes, composed of PC and Ch have been used to test if anionic lipids and positive membrane curvature affect helix formation. Vesicle sizes have been checked by DLS, showing size distribution (see appendix 6.3 B) and average vesicle size for each sample (Table 3.7-1). Again LUVs average sizes varied from the filter pore size, showing higher or lower average size than the filter size for 50 nm and 1000 nm LUVs respectively (Table 3.7-1). Interestingly, the average GUV size was only just above 1000 nm (Table 3.7-1) with the size distribution graph showing two distinct peaks, at around 1000 and 5000 nm (see appendix 6.3 B), which suggests huge diversity in the GUVs population leading to small average vesicle size.

designed size (extrusion membrane size)	actual size (average size measured on DLS)
SUVs	41.69 d.nm
50 nm	101.9 d.nm
100 nm	113.7 d.nm
1000 nm	540 d.nm
GUVs	1119 d.nm

Table 3.7 - 1 Designed and actual average size of the PC:Ch vesicles in the size range measured on DLS.

The Arf 1 peptide showed troughs for vesicles ranging between 42 and 540 nm and a peak when GUVs were present (Fig. 3.7-4). The highest helix percentage - 81.47% was in the presence of the smallest vesicles, increasing the vesicle size caused a decrease in percentage of helix present, with the lowest value of around 18% in presence of GUVs (Fig. 3.7-4). This shows that the smaller the vesicles, and hence the higher the positive membrane curvature, the better helix formation. The helix percentage for 100 nm LUVs was around 70% (Fig. 3.7-4) and was reduced compared to standard LUVs (Fig. 3.7-3), which suggest that anionic lipids support formation of the Arf 1 AH, but are not essential.

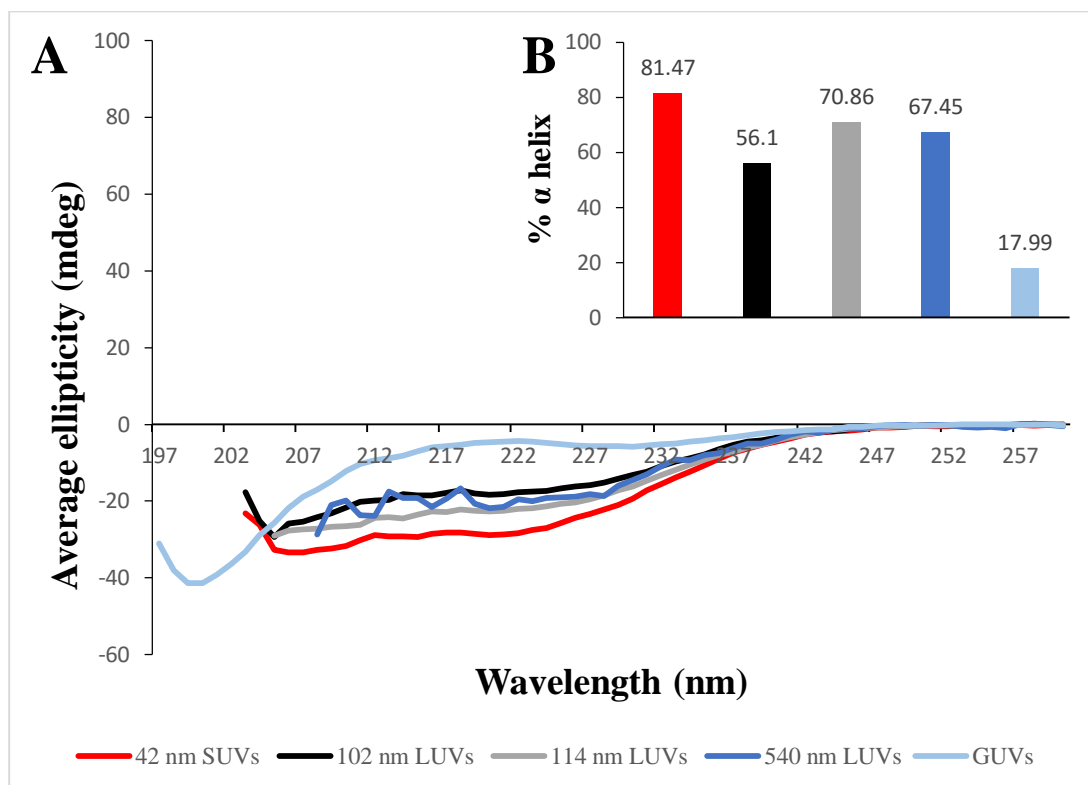


Figure 3.7-4 CD spectra for 250 μ M of Arf 1 peptide with 5 mM of different size SUV, LUVs and GUVs composed of PC:Ch (A). Estimated percentage of an α helix present in each sample calculated based on the spectra using K2D3 bioinformatics tool on <http://k2d3.orgic.ca/> website (B).

CD spectra for Endophilin A3 showed peaks for vesicles sized 102 nm and above and one big trough for the smallest vesicles (Fig. 3.7-5). The helix percentage in presence of 42 nm SUVs was the highest – 94.54% and when vesicles increased in size to 102 nm and 114 nm helix percentage dropped significantly, to about 43% and 53% respectively (Fig. 3.7-5). Further increases in vesicle size led to a further decrease in helix percentage, with only 9.37% of helix formed in presence of GUVs (Fig. 3.7-5). Those results suggest that Endophilin A3 AH is formed in highly curved membranes and even a small increase in vesicle size, and hence decrease in positive membrane curvature, influences the formation of the helix. The absence of anionic lipids in the membrane caused significant reduction in helix percentage – from over 95% to about 53% (Fig. 3.7-3 B and 3.7-5 B), which suggest that anionic lipids might play some role in structure and function of the Endophilin A3 AH.

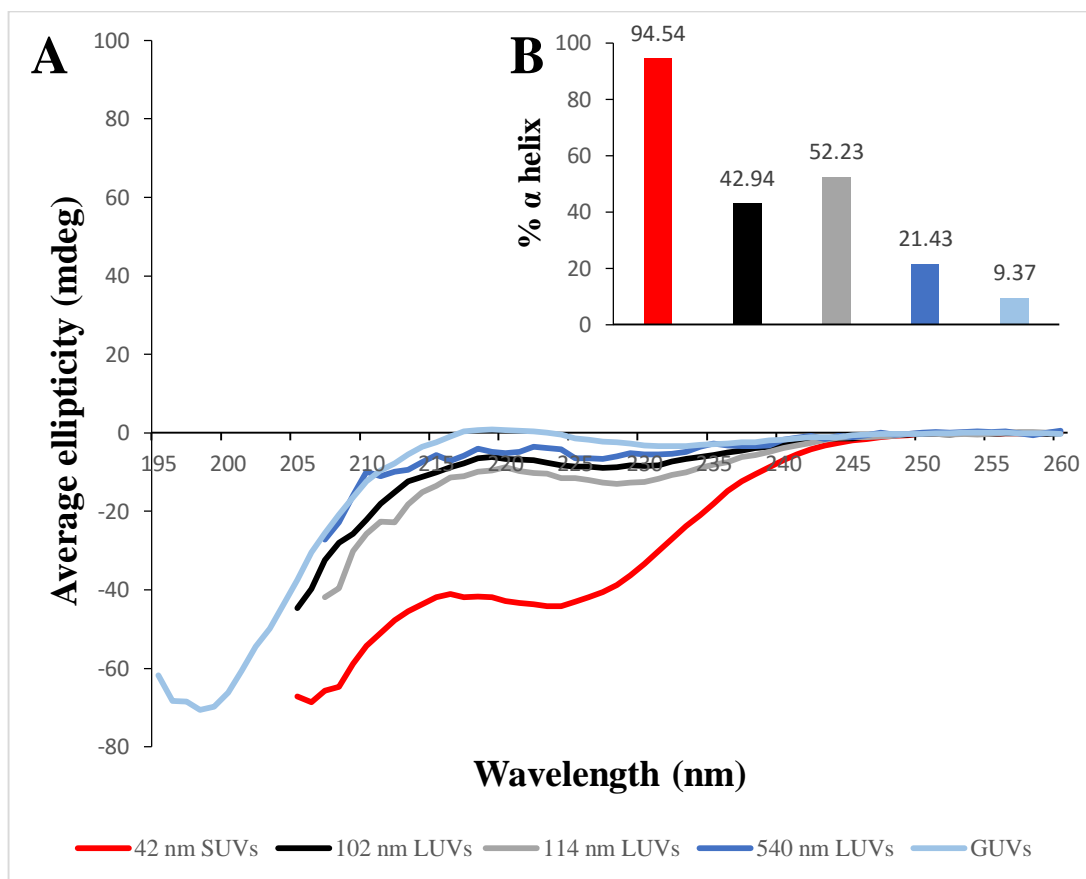


Figure 3. 7 - 5 CD spectra for 250 μ M of Endophilin A3 peptide with 5 mM of different size SUV, LUVs and GUVs composed of PC:Ch (A). Estimated percentage of an α helix present in each sample calculated based on the spectra using K2D3 bioinformatics tool on <http://k2d3.ogic.ca/> website (B).

The Epsin 1 peptide showed a deep trough in presence of 42 nm SUVs, with about 94% of the helix present, and in presence of vesicles 102 nm in size and above, CD showed smaller troughs with helix percentage ranging between 63 and 76% (Fig. 3.7-6). Increasing the vesicle size, and hence decrease in positive membrane curvature, caused only slight reduction in percentage of helix formed, which suggests that Epsin 1 AH prefers membranes with high positive curvature but can work in wide range of positively curved membranes. In the presence of 100 nm LUVs helix percentage was about 75% (Fig. 3.7-6), which corresponds to about 20% drop compared with standard 100 nm LUVs (Fig. 3.7-3). Those results suggest that similar as the M2 AH, Epsin 1 AH formation is supported by anionic lipids present in the membrane, but they are not necessary as their absence does not inhibit helix formation.

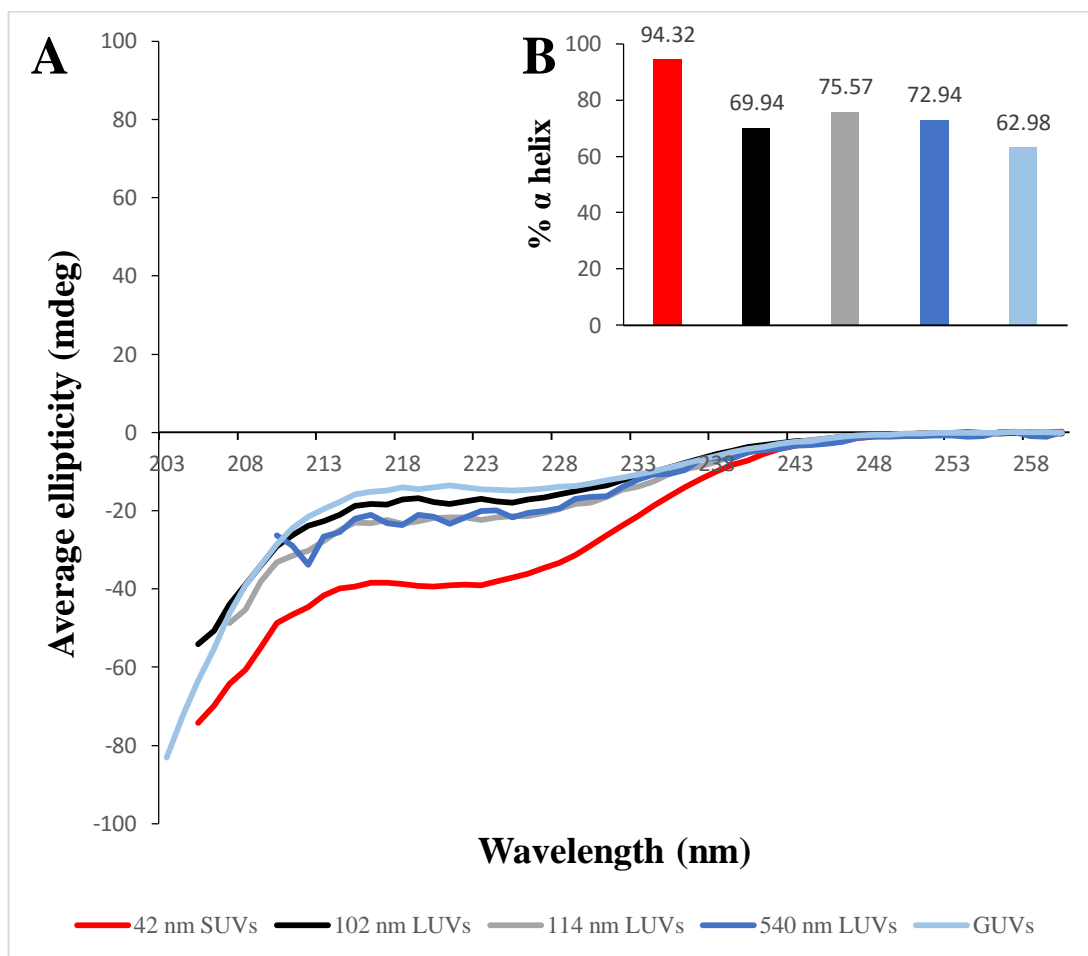


Figure 3.7 - 6 CD spectra for 250 μ M of Epsin 1 peptide with 5 mM of different size SUV, LUVs and GUVs composed of PC:Ch (A). Estimated percentage of an α helix present in each sample calculated based on the spectra using K2D3 bioinformatics tool on <http://k2d3.orgic.ca/> website (B).

The CD spectra for the CHMP4b AH were very wavy with a lot of variability, suggesting a random coil confirmation in presence of all vesicles (Fig. 3.7-7 A). Estimated helix percentages was also on a very low level, between 1.84 – 4.88% (Fig. 3.7-7 B), confirming our earlier observations (Fig. 3.7-3) and show that CHMP4b AH is not formed upon binding with membrane and positive membrane curvature and anionic lipids present in the membrane do not influence its formation.

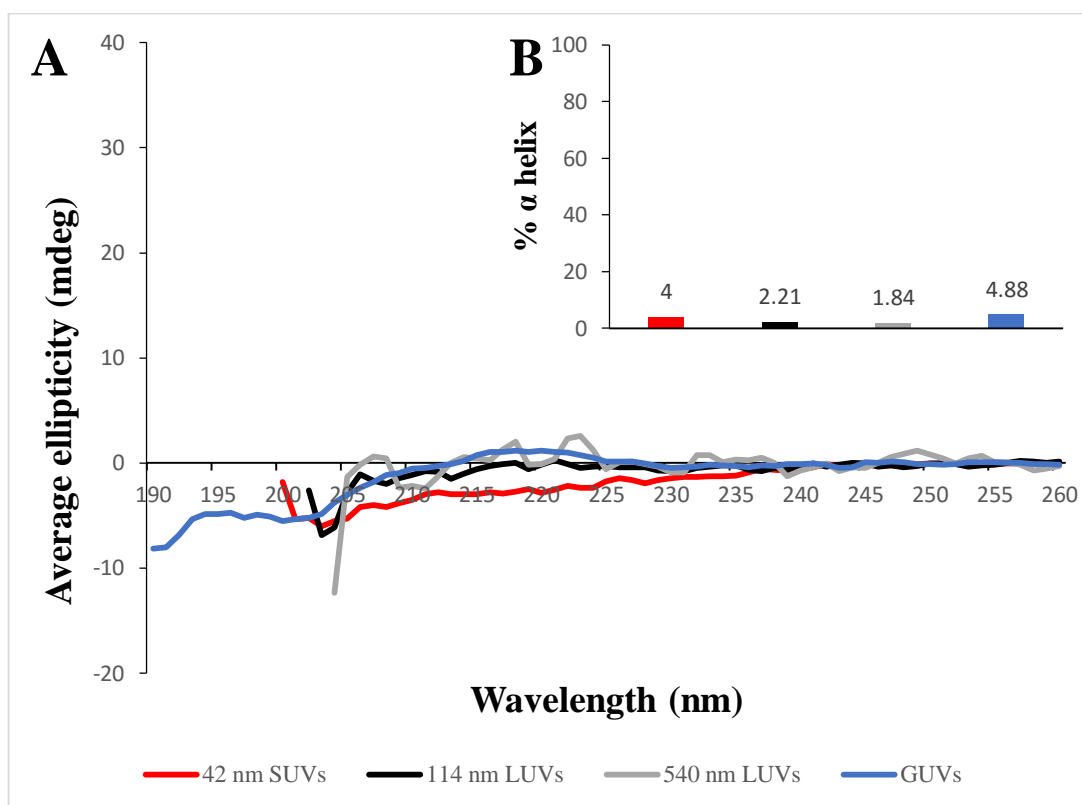


Figure 3.7 - 7 CD spectra for 250 μ M of CHMP4b peptide with 5 mM of different size SUV, LUVs and GUVs composed of PC:Ch (A). Estimated percentage of an α helix present in each sample calculated based on the spectra using K2D3 bioinformatics tool on <http://k2d3.ogic.ca/> website (B).

3.7.2.3 Effect of line tension on cellular AH formation

The M2 AH is associated with membranes with high positive membrane curvature (see chapter 3.3.6) and can sense membrane curvature by sensing lipid packing defects that are formed with high curvature and an increased line tension in the membrane (see chapter 3.3.7). To test how line tension in the membrane affects cellular AHs, peptides have been tested in the presence of two LUVs from the range of phase separated LUVs in which the line tension of the domains have been increased by using a series of different PC with decreasing length of the acyl chain (see chapter 3.3.5). DEPC and DMPC containing LUVs have been used that have the longest and the shortest acyl chain and hence the smallest and the highest line tension in the series respectively. CD spectra showed small troughs for Arf 1 and Endophilin A3 peptides and deeper troughs for the Epsin 1 peptide (Fig. 3.7-8 A).

In the presence of DMPC LUVs troughs were slightly deeper than in presence of DEPC LUVs for all peptides (Fig. 3.7-8 A). An increase in helix percentage in presence of LUVs with higher line tension have been observed for all cellular peptides tested, however, for Arf 1 and Endophilin A3 helix percentage was low in presence of both LUVs types and the increase was not as substantial as for the Epsin 1 peptide (Fig. 3.7-8 B). These results show that high line tension in the LUVs domain increases formation of Arf 1, Endophilin A3 and Epsin 1 AHs, which suggest that those cellular peptides might sense positive membrane curvature by sensing membrane packing defects and increased line tension, as has been seen with the M2 AH (see chapter 3.3.7).

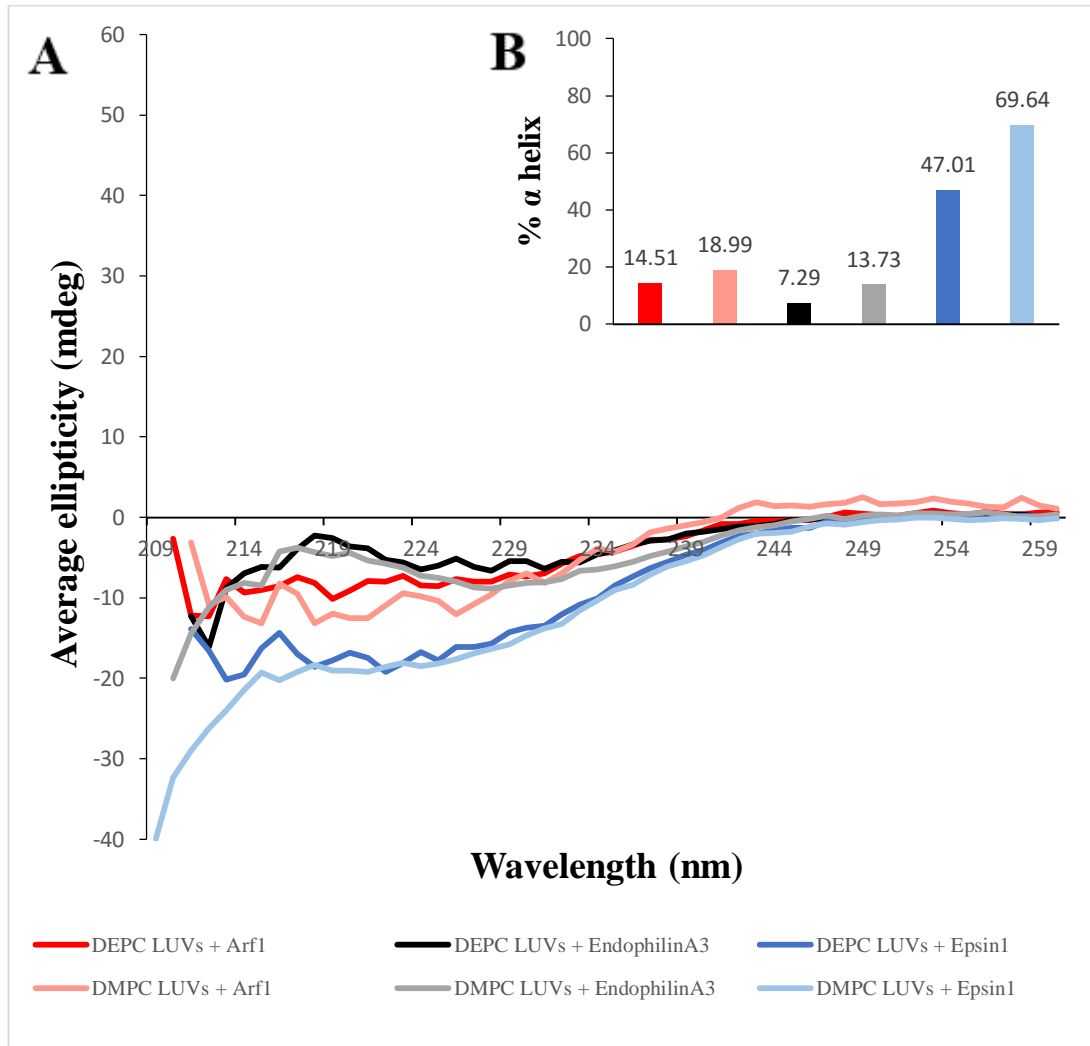


Figure 3. 7 - 8 CD spectra for 250 μ M of cellular peptides: Arf 1, Endophilin A3 and Epsin 1 with 5 mM of 100 nm LUVs composed of sphingomyelin, cholesterol and either DEPC or DMPC (at 2:1:2 ratio) which results in low and high line tension between domains in the membrane respectively (A). Estimated percentage of an α helix present in each sample calculated based on the spectra using K2D3 bioinformatics tool on <http://k2d3.orgic.ca/> website (B).

3.7.2.4 Ordering of the lipids in the membrane

The M2 AH has been shown to increase lipid ordering upon binding with the membrane (see chapter 3.4.2), therefore the cellular AHs have been tested if they also affect membrane fluidity. Laurdan assays have shown a substantial increase in Laurdan GP caused by the Endophilin A3 and Epsin 1 peptides and a slightly smaller, but still significant increase caused by Arf 1 (Fig. 3.7-9). On the other hand, CHMP4b AH did not cause significant increase in Laurdan GP (Fig. 3.7-9), which indicates that it does not change fluidity of the membrane. Those results suggest that Arf 1, Endophilin A3 and Epsin 1 AHs work in similar way as the M2 AH and increase lipid ordering upon binding with membranes which changes fluidity of the membrane and may lead to changes in membrane curvature.

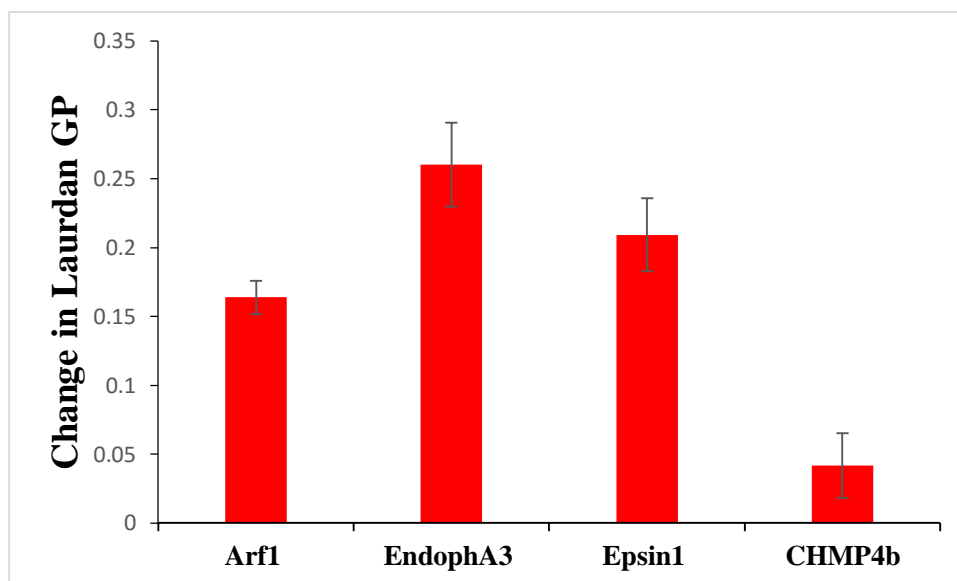


Figure 3. 7 - 9 Change in Laurdan GP value with 100 μ M of cellular peptides: Arf 1, Endophilin A3, Epsin 1 and CHMP4b and 2.5 mM of standard LUVs at 1:100 lipid:dye ratio.

3.7.2.5 Induction of positive membrane curvature

The M2 AH has been shown to induce positive membrane curvature in LUVs (see chapter 3.4.4) therefore the cellular AHs have been tested if they also induce positive membrane curvature by inducing changes to the vesicle's morphology. TEM analysis has shown that Arf 1, Endophilin A3 and Epsin 1 AHs cause formation of tubes and blebs on the LUVs surface (indicated by red arrows on Fig. 3.7-10), similar to the M2 AH (Fig. 3.4-10); however, incubation of LUVs with the CHMP4b AH does not cause changes to the vesicles morphology. Those results suggest that Arf 1, Endophilin A3 and Epsin 1 AHs, but not CHMP4b work in similar way as the M2 AH and induce positive membrane curvature.

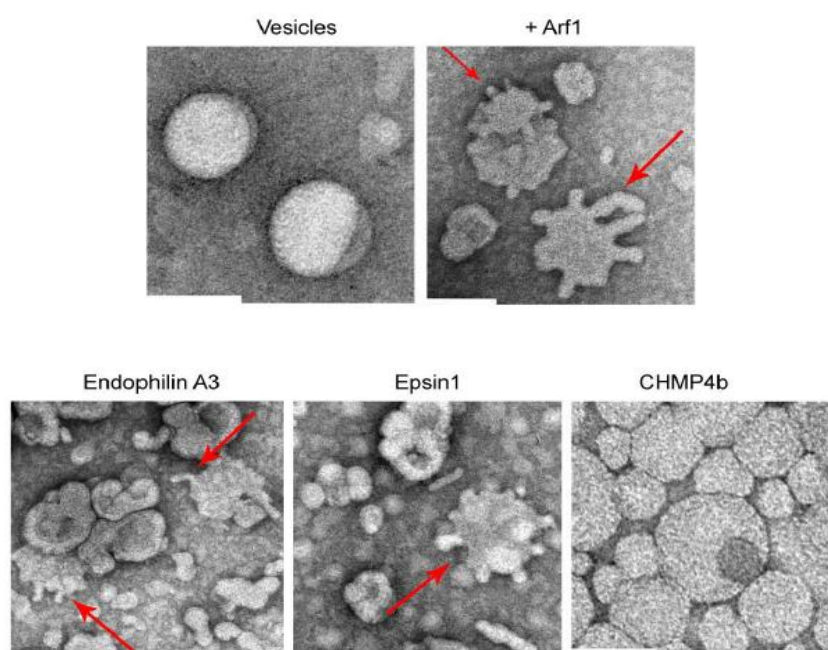


Figure 3.7 - 10 TEM images of 5 mM of standard LUVs incubated for 1 h with 125 μ M of cellular peptides: Arf 1, Endophilin A3, Epsin 1 and CHMP4b and negative stained. Arrows indicate membrane blebs and scale bars indicate 100 nm.

3.7.3 Summary

Membrane budding is an important and complex process that is crucial not only for viruses, but also plays a role in many biological processes. Many proteins and AHs have been identified to be involved in membrane budding by either sensing or generating membrane curvature (Peter et al. 2004, Drin and Antony 2010). The M2 AH contains many hydrophobic residues as well as several cationic residues and has been shown to be associated with highly curved membranes (see chapter 3.3.6), inducing positive membrane curvature (see chapter 3.4.4) and leading to scission (see chapters 3.5 and 3.6). This suggests that the M2 AH may belong to a novel group of AHs that can sense and generate membrane curvature. Four cellular proteins containing AHs; Arf 1, Endophilin A3, Epsin 1 and CHMP4b have been identified as having similar features as the M2 AH and therefore were tested to detect if their mechanism of membrane scission is the same as the M2 AH. CD spectroscopy has shown that all cellular peptides are unstructured in solution, with the exception of Epsin 1 which shows partial formation of an α -helix (Fig. 3.7-2). In presence of liposomes Arf 1, Endophilin A3 and Epsin 1 showed high levels of estimated helix percentage, around 95%, whereas CHMP4b showed similar levels of helix as in solution (Fig. 3.7-3). This indicates that Arf 1, Endophilin A3 and Epsin 1 behave similarly to the M2 AH and form an α -helix upon binding with membranes, but CHMP4b does not.

To test if anionic lipids and positive membrane curvature affect the formation of the helix of the cellular peptides, a range of SUVs, LUVs and GUVs of different sizes, composed of PC and Ch have been used. CD spectroscopy showed that two of the cellular AHs, Arf 1 and Endophilin A3, are formed in membranes with high positive membrane curvature, with a decrease in positive membrane curvature resulting in a reduction of helix formation (Fig. 3.7-4 and 3.7-5), as was also seen with the M2 AH (see chapter 3.3.6). Although those AHs prefer highly curved membranes, they can work in wide range of positively curved membranes and are inhibited only in presence of vesicles with small positive curvature of the membrane, such as GUVs (Fig. 3.7-4 and 3.7-5). Epsin 1 AH seems to work in similar way, it is associated with high positive membrane curvature and an increase in vesicle size decreases helix formation (Fig. 3.7-6) however, this effect is not as drastic as in case of other AHs, which suggests that Epsin 1 AH is not as sensitive to membrane curvature changes as the other AHs. On the other hand, CHMP4b AH is not formed upon binding with the membranes with

changes in the positive curvature of the membrane not affecting its formation (Fig. 3.7-7). Anionic lipids present in the membrane facilitate formation of the M2 AH but are not essential, as the helix percentage is only slightly reduced in presence of LUVs without anionic lipids in the membrane compared to standard LUVs with an anionic lipid present (see chapter 3.3.2). Similar trends have been observed with the Arf 1 (Fig. 3.7-4), Endophilin A3 (Fig. 3.7-5) and Epsin 1 AHs (Fig. 3.7-6), but not the CHMP4b AH (Fig. 3.7-7), which shows that anionic lipids also facilitate formation of those AHs. In case of Endophilin A3 AH reduction in helix percentage was slightly higher (just above 50% compared to about 70% for Arf 1 and Epsin 1), which indicates that anionic lipids may play a role in structure and formation of this AH (Fig. 3.7-5 B). In conclusion, three cellular peptides: Arf 1, Endophilin A3 and Epsin 1 showed similarities with the M2 AH in terms of membrane curvature preference and interactions with anionic lipids.

It has been shown that the M2 AH senses membrane curvature by sensing lipid packing defects that are formed in the membranes with high curvature (see chapter 3.3.7) and that the line tension between the membrane domains affects the helix formation (see chapter 3.3.5). Phase separated LUVs composed of two types of PC with longer or shorter acyl chain, which result in low and high line tension between domains respectively (part of the LUVs range with an increasing line tension described in chapter 3.3.5)(Garcia-Saez et al. 2007), have been used to test if the line tension affects the formation of the cellular AHs. Results showed a slight increase in helix formation with an increase in line tension between domains for Arf 1 and Endophilin A3 and a significantly higher increase in helix formation for Epsin 1, with the overall levels of helix percentage much higher for that peptide (Fig. 3.7-8). These results suggest that, as with the M2 AH, an increase in line tension between domains increases formation of Arf 1, Endophilin A3 and Epsin 1 AHs.

The M2 AH has been shown to increase lipid ordering in the membrane upon binding (see chapter 3.4.2), so cellular peptides have been tested using the Laurdan assay to see if they also increase lipid ordering upon binding. Endophilin A3 and Epsin 1 caused significant increase in Laurdan GP (Fig. 3.7-9), similar to levels observed with wild type M2 AH (Fig. 3.4-2). Arf 1 also induced increase in Laurdan GP however, to slightly lesser degree than the wild type M2 AH (Fig. 3.7-9). CHMP4b did not induce significant changes in Laurdan GP (Fig. 3.7-9). Those results imply that Arf 1,

Endophilin A3 and Epsin 1 AHs increase lipid ordering upon binding with membranes, as the M2 AH but CHMP4b does not. The M2 AH has also been shown to induce positive membrane curvature in LUVs (see chapter 3.4.4), therefore cellular peptides have been tested if they are able to induce similar effect. TEM analysis have shown that when incubated with LUVs, three cellular AHs: Arf 1, Endophilin A3 and Epsin 1 cause formation of tubes and blebs on the surface (Fig. 3.7-10). On the other hand, changes to the vesicle's morphology were not observed in case of CHMP4b AH (Fig. 3.7-10). This shows that Arf 1, Endophilin A3 and Epsin 1 AHs induce positive membrane curvature, similar as the M2 AH but CHMP4b does not

All of these results suggest that three out of the four cellular AHs tested: Arf 1, Endophilin A3 and Epsin 1 appear to work in a similar manner to the M2 AH and therefore belong to a novel group of AHs. Those AHs are being formed upon binding with membranes (with exception of Epsin 1 which is partially formed in solution) and are associated with membranes with a high level of positive curvature, but can work in wide range of positively curved membranes. Anionic lipids present in the membrane facilitate formation of those AHs but are not essential and increase in line tension in the domains increases formation of the AHs. Insertion of these AHs into the membrane increases lipid ordering in the membrane and induces positive membrane curvature.

4. DISCUSSION

4.1 STRUCTURE OF THE M2 AH

The main aim of this project was to investigate molecular mechanism of membrane scission mediated by the M2 protein, which is the last stage of virus life cycle. The first step was to determine the structure of the M2 AH, which is formed at the beginning of the M2 protein's CT section and has been shown previously to play a role in virus assembly and budding. It has been hypothesised that this helix may mediate membrane scission, allowing for release of the new virion into the environment. The high resolution structure of the full length M2 protein has not been solved up to date, however, the TMD, together with small parts of the ecto domain and CT, has been determined by both x-ray crystallography and NMR (Schnell and Chou 2008, Stouffer et al. 2008). The NMR studies showed that M2, which in its native form is a homotetramer in the presence of micelles, forms a pore with its TMD (residues 25-46) that acts as a pH-gated proton channel. After the channel a flexible loop is formed between residues 47-50 and its followed by formation of an amphipathic helix between residues 51-59 which is situated nearly perpendicular to the ion channel (Schnell and Chou 2008).

In this study the structure of the M2 AH, between residues 47-62 of the full length M2 protein, based on A/Udorn/72 strain has been solved in different environments using ^1H 2D NMR. In presence of standard LUVs (100 nm composed of PC, PG and cholesterol at 4:1:0.05 molar ratio) an α -helix was formed between residues 4 and 16 (residues 50-62 of the full length protein) (Fig. 3.1-5), which corresponds well to the previous NMR research performed in micelles (Schnell and Chou 2008). Interestingly, when the M2 AH peptide was in solution, with no LUVs present, it showed a random coil confirmation (Fig. 3.1-5). This suggests that the M2 AH is formed upon binding with lipid membranes. To further investigate binding between the M2 AH and a lipid membrane, and to determine which part of the helix is responsible for binding, a 1D STD NMR experiment was performed. The results showed that the residues Phe9, Phe8 and Ile5 (residues 55, 54 and 51 respectively) are the main residues involved in binding with membranes, with Phe2, His11 and Gly12 (residues 48, 57 and 58 respectively) being involved to a lesser degree (Fig. 3.1-10). The residues involved suggest that the M2 AH interacts with the lipid membranes through hydrophobic

interactions, as most of the residues responsible for binding are in the hydrophobic face of the helix, confirming earlier suggestions (Rossman et al. 2010b). In conclusion, it has been shown that the M2 AH is formed upon binding with membranes and it interacts with lipid membranes through hydrophobic interactions, however, future work is needed to investigate the structure of the full length CT as it is probable that other important structural motifs are present in the further parts of the protein. Determining the structure of the full length M2 protein in the presence of a lipid membrane would also be important as presence of a full length protein could influence the structure and functions of the M2 AH and it would be much more physiologically relevant.

4.2 MECHANISM OF ACTION

4.2.1 Membrane binding

The NMR experiments showed that the M2 AH is formed upon binding with membranes (Fig. 3.1-5), therefore the interactions between the M2 AH and membranes have been investigated further. Good binding between the M2 AH and the standard lipid membranes have been shown with a peptide binding assay (Table 3.2-1). Further investigation using CD spectroscopy, has shown that the M2 AH is formed and stabilised upon binding with a membrane and remains unstructured in the solution (Fig. 3.2-7), which confirms previous observations by NMR (Fig. 3.1-5).

Similar trends have been observed with a slightly longer peptide (17 amino acids) based on the same strain (Fig. 3.2-10) and a 16 amino acid peptide based on the A/England/09 strain (Fig. 3.2-9), which differs from the A/Udorn/72 based peptide by only three amino acids (F54R, E56K and H57Y in regards to full length M2 protein) (Fig. 3.2-8). Interestingly, STD NMR has shown that residues at two of those positions, 54 and 57 are responsible for binding of the M2 AH with lipid membranes (Fig. 3.1-10) and therefore are important for helix formation. Differences in the sequence between strains do not affect formation of the helix, even if the changes are in the region shown to be responsible for binding with membranes. It is possible that the changes in sequence are not significant enough to affect formation of the M2 AH.

Even though the charge and hydrophobicity are changed between those two strains, with hydrophobic, negatively charged and positively charged residues being replaced with two positively charged and hydrophobic respectively, the overall shape and length of the amino acids do not change drastically therefore function of the M2 AH is not affected. It is also possible that different residues are responsible for binding with the membranes for A/England/09 strain than for A/Udorn/72 and therefore changes in the region shown to be responsible for binding with membranes for A/Udorn/72 does not influence formation of the M2 AH based on A/England/09 strain. This shows that the formation of the M2 AH upon binding with lipids is well conserved among influenza virus strains. STD NMR experiments have shown that hydrophobic residues in the helix are responsible for interaction of the peptide with lipid membranes (Fig. 3.1-10), which was confirmed by CD spectroscopy analysis of a range of M2 AH

mutants. As expected, formation of the M2 AH in presence of LUVs was significantly reduced in the case of the 5 point mutant (F47A F48A I51A Y52A F55A) (Fig. 3.2-12). Additionally, formation of the helix was slightly reduced in two of the other mutant peptides: F47A F48A, which was designed to weaken hydrophobic face, and L46K C50K Y57K which was designed to enhance polar face by making it completely charged (Fig. 3.2-12). These results correspond well to the STD NMR data (Fig. 3.1-10), which shows that residues in the hydrophobic face of the helix at positions 48, 51, 54, 55, 58 and the hydrophobic residue in the polar face at residue 57 are responsible for binding with lipid membranes. These two mutations, which cause a slight reduction in helix formation, contained one change at a position shown to be responsible for binding with membranes (position 48 and 57 respectively).

The 5 point mutant, by comparison, contained changes in three of those positions (48, 51 and 55) which caused significant reduction in helix percentage. In opposite to the changes in M2 AH sequence between influenza virus strains, which do not affect formation of the helix (as discussed above), changes introduced in these mutations were significant in changing properties of the peptide (reducing helix formation to different degree), as in the F47A F48A mutant and the 5 point mutant bulky hydrophobic residues were replaced with alanine and in the L46K C50K Y57K mutant, the hydrophobic residue at the crucial position (57) was replaced with positively charged residue. This confirms that residues 48, 51, 54-55 and 57-58 as well as the overall hydrophobicity is crucial for the M2 AH formation and binding with lipid membranes.

4.2.2 Membrane activity

Properties of the membrane such as lipid composition, presence of defects, changes to the line tension between different domains and the curvature of the membrane affect structure and functions of the M2 AH. On the other hand insertion of the helix itself into the lipid membrane also causes changes to the membrane. First the lipid composition of the membrane was varied, testing the effect of different lipids on the M2 AH, followed by structural changes in the membrane such as curvature or presence of defects and the changes to the lipid membrane caused by the M2 AH.

The polar face of the helix contains, depending on a strain, 6 or 7 of cationic residues (A/Udorn/72 and A/England/09 respectively), which may interact with anionic lipids present in the membrane. However, presence of different anionic lipids in the membrane do not affect the M2 AH formation as shown by CD spectroscopy (Fig. 3.3-1). In contrast, the presence of the zwitterionic PE reduces helix formation (Fig. 3.3-1), which could be caused either by charge difference in the lipid headgroup or by changes to the structure of the membrane caused by the cone shape of PE. Interestingly, a two fold increase in binding activity was detected in presence of different anionic lipids (PA and PS) compared to PG containing membranes, but when PE was present binding activity was reduced nearly by half (Fig. 3.3-2). These show that different anionic lipids do not influence formation of the M2 AH but they may facilitate binding of the peptide with membranes and that PE does not support any of those functions. Additionally, higher concentrations of PS present in the membrane (40 molar %) slightly supports helix formation (Fig. 3.3-3), but significantly increases binding with the membranes (Fig. 3.3-4), suggesting that anionic lipids present in the membrane support M2 AH binding in a dose dependent manner. However, the exact concentration of anionic lipids required to support the M2 AH is not known and it is not known if the concentration differs for helix formation compared to binding with membranes. On the other hand, removal of anionic lipids from the membrane caused reduction of estimated helix percentage by about 20% (Fig. 3.3-5), which suggests that anionic lipids support the formation of the M2 AH, but are not essential for its formation as their removal from the membrane did not inhibit helix formation completely.

Surprisingly removal of anionic lipids from the membrane increased average fold binding (Fig. 3.3-6) with similar effect being observed when different types of anionic lipids were used instead of PG (Fig. 3.3-2) and higher molar % of PS were present in the membrane (Fig. 3.3-4). This suggest that concentration and type of anionic lipid present in the membrane as well as lack of any anionic lipids in the membrane may affect binding ability of the M2 AH, but more research is needed to fully understand this relationship. Binding between the M2 AH and lipid membranes may also be affected by charges in the environment, which may inhibit charged interactions between the polar face of the helix and the lipid headgroups, and therefore inhibit binding. However, ionic strength of the buffer does not influence interactions of the

M2 AH with lipid membranes as an increase in ionic strength of the buffer did not cause any drastic changes in binding activity associated with any particular concentration (Fig. 3.3-8). This confirms that interaction of the M2 AH with lipid membrane is not dependent on charge-charge interactions.

As mentioned before, some lipids affect functions of the M2 AH, such as cholesterol which has been shown to inhibit M2 AH mediated budding in LUVs in a dose dependent manner, with budding observed with up to 17 molar % of cholesterol present in the membrane (Rossman et al. 2010b). Surprisingly formation of the M2 AH is not affected by cholesterol concentration in the membrane (Fig. 3.3-9), but the ability to bind with membranes may be affected instead (Fig. 3.3-10). Initial increases in cholesterol concentration increases binding activity, but a further increase causes a reduction, which suggest that low levels of cholesterol present in the membrane (up to 10 molar %) support the M2 AH but higher concentrations (above 20 molar %) affect its ability to bind with membranes (Fig. 3.3-10) which correlates well with previous budding research (Rossman et al. 2010b).

Another lipid which may affect the M2 AH structure and function is PIP₂, as it has been shown that it plays an important role in assembly of other viruses, such as HIV (Carlson and Hurley 2012). Immunofluorescence microscopy has shown that PIP₂ and M2 do not co-localise in cells, but often are proximal to each other (Fig. 3.3-11) which suggest it may support the M2 AH and can be involved in the M2 mediated budding. However, further investigation has shown that presence of PIP₂ do not affect the M2 AH formation (Fig. 3.3-12) and binding (Fig. 3.3-13) with membranes.

The next step in investigating the effect of the lipid membrane on the M2 AH structure and function was to vary structural characteristics of the membrane by changing the line tension between domains, the membrane curvature or by introducing packing defects. During late stages of budding M2 is localised on the boundary between lipid rafts and plasma membrane which is a region of high line tension (Rossman et al. 2010b), with lipid rafts being the sites of viral assembly and budding which are

enriched in sphingolipids and cholesterol (Brown 2001). Therefore an increase in line tension between lipid ordered and lipid disordered phases may have an effect on the M2 AH. Increase in line tension between domains increases formation of the M2 AH (Fig. 3.3-14). However, changes in line tension do not affect binding ability of the peptide as the values for most of the samples are similar and the only increase is with DeisPC, which is the second lowest value lipid in the series for forming vesicles with line tension, and may be a characteristic specific for this lipid (Fig. 3.3-15).

In the last stage of viral budding M2 is localised to the neck of budding virion (Rossman et al. 2010b). This is a region of high positive membrane curvature which suggests that membrane curvature may affect the structure and function of the M2 AH. Both CD spectroscopy and binding assays have shown, using a range of different size vesicles with decrease in positive membrane curvature, that the M2 AH forms best and preferentially binds to highly curved membranes (Fig. 3.3-17 and 3.3-18). However, the AH can work in wide range of positively curved membranes and is inhibited only with the largest vesicles where positive membrane curvature is the smallest (Fig. 3.3-17 and 3.3-18). These observations have been confirmed by molecular dynamic simulations on a buckled lipid bilayers containing regions of positive, negative and neutral curvature. Results have shown that the M2 AH is mostly associated with positively curved membranes and it is not associated with negatively curved regions (Fig. 3.3-19). Maximum binding occurred at regions of the membrane corresponding to a 20 nm vesicle (Fig. 3.3-19) which corresponds well to CD and binding assay data (Fig. 3.3-17 and 3.3-18). Similar results have been observed when anionic lipids have been removed from the simulated lipid membrane (Fig. 3.3-20 and 3.3-21), further confirming that charge interactions do not affect the M2 AH formation, binding with the membranes or influence the M2 AH's curvature sensing ability. Membranes with high positive curvature can be detected by peptides or AHs either by directly sensing membrane curvature or by sensing lipid packing defects associated with high curvature. The M2 AH senses membranes with high levels of positive membrane curvature by sensing lipid packing defects associated with those membranes as helix formation increases by 10% and binding activity is 6 fold greater in presence of lipid packing defects in the membrane (Fig. 3.3-22 and 3.3-23).

As described above, the M2 AH structure and function can be affected by different properties of the membrane however, the lipid membrane can also be affected by the M2 AH activity. Insertion of the helix into the membrane increases Laurdan GP, as detected by Laurdan dye (Parasassi et al. 1990, Sanchez et al. 2007) (Fig. 3.4-2), which means it increases lipid ordering of the membrane and decrease its fluidity. Ability of the M2 AH to increase lipid ordering of the membrane is conserved among different influenza virus strains, but different strains induce it to a different degrees. The wild type peptide based on A/England/09 strain increased Laurdan GP (Fig. 3.4-4), but not as much as the peptide based on the A/Udorn/72 strain (Fig. 3.4-2). This appears to be caused by differences in the sequence, especially if these differences are in the regions of the peptide responsible for binding with membranes, as in case of A/Udorn/72 and A/England/09 strains (Fig. 3.2-8). On the other hand, introduction of a 5 point mutant into the M2 AH inhibited the ability to increase lipid ordering. Interestingly, the double mutation on the helix interface (R54A R61A) introduced to the peptide based on the A/England/09 strain increased Laurdan GP to the levels observed with the wild type peptide based on A/Udorn/72 strain, which suggest that this mutation compensates for the sequence differences between strains (Fig. 3.4-4).

The lipid composition of the membrane does not only influence the M2 AH structure and function, but may also alter the effect the helix has following insertion into the membrane. The M2 AH increases lipid ordering in presence of LUVs without anionic lipids present to a similar level as in presence of standard LUVs (Fig. 3.4-5 and 3.4-2 respectively), which shows that charged interactions do not affect the M2 AH ability to increase lipid ordering and change membrane fluidity. Low concentrations of cholesterol in the membrane (up to 10 molar %) supports the M2 AH ability to increase lipid ordering and change membrane fluidity but higher concentrations reduce this ability which is inhibited with the highest concentration tested (40 molar %) (Fig. 3.4-6). This correlates well with previous research and shows that cholesterol inhibits the M2 AH ability to induce lipid ordering in dose dependent manner. Increase in line tension between domains in lipid membrane also increases lipid ordering caused by the M2 AH (Fig. 3.4-7), but increase in levels of lipid packing defects in the membrane do not change the increase in lipid ordering (Fig. 3.4-8). This shows that although the M2 AH senses membrane curvature by sensing lipid packing defects (Fig. 3.3-22), the

amount of defects in the membrane do not affect its ability to induce lipid ordering and changing membrane fluidity. Analysis of lipid transition temperature by DSC has shown that addition of the M2 AH into the membrane increases transition temperature of the membrane (Fig. 3.4-9) which confirms earlier observations that insertion of the M2 AH into the lipid membrane increases lipid ordering and changes membrane fluidity.

4.2.3 Membrane scission

Changes to the membrane fluidity are not the only ones that the M2 AH causes to the membrane. It has been proposed that in the final stages of budding M2 AH, which is localised to the neck of budding virion, mediates membrane scission by inducing positive membrane curvature leading to release of new virion into the environment (Rossman and Lamb 2011, Martyna and Rossman 2014). Analysis of TEM results confirmed that the M2 AH induces positive membrane curvature in a lipid membrane. It is a dose dependent process, at higher concentrations the M2 AH forms tubes and blebs on the surface of vesicles which are not visible in control samples and at low concentrations of the peptide (Fig. 3.4-10).

It has been shown before that the M2 AH mediates virus budding (Rossman et al. 2010b). An attempt has been made to quantify M2 AH mediated budding and identify residues involved in this process using GUV budding system. Unfortunately, control samples showed considerable amounts of budding and leaking (Fig. 3.5-2), which has masked the effect that the M2 AH peptides have on budding and leaking, making them statistically insignificant due to the low difference in values. This suggests that budding induced by the M2 AH might not be efficient enough to be detected in this system and may be due to the size of vesicles, as the M2 AH preferentially binds with membranes of high positive membrane curvature (see chapter 3.3.6) and the effects were observed in vesicles above 10 μm in diameter.

Due to this and many other restrictions and difficulties with the GUV budding system, a microinjection system has been developed to investigate the budding mediated by the M2 AH. In this system, the M2 AH mediates budding which is a rapid process, as small vesicles on the membrane of the GUVs that were localised close to the injection

needle were identified 30 s post-injection (Fig. 3.5-4). Formation of small vesicles or lipid puncta have also been observed in the buffer and those effects can be observed for a long time (Fig. 3.5-4).

In the next step membrane scission mediated by the M2 AH has been investigated using SUPER templates system. Results showed that the M2 AH mediates membrane scission but only in specially scaffolded or pre-constricted lipid domains and this function can be inhibited by introduction of 5 point mutations into the helix (Fig. 3.5-5).

As discussed above, the M2 AH mediates budding in GUVs, which are artificial lipid membranes. However, it has been shown previously that cellular proteins, such as Rab11 (Bruce et al. 2010) may play a role in influenza virus budding and the cellular environment may affect the ability of the M2 AH to mediate budding. Analysis of virus-like particles released from transfected cells confirmed that the M2 mediates budding not only in artificial systems but also *in vivo* and that introduction of 5 point mutations in the M2 AH impairs M2 mediated budding (Fig. 3.6-1).

Further investigation of the M2 mediated budding *in vivo* and the effect of cellular environment on it, have shown that further parts of the CT may compensate for the loss of function by the M2 AH restoring viral growth and functions. Two point mutations have been detected in M segment coding for CT of the M2 protein after repeated passaging of Influenza A virus with 5 point mutants (Fig. 3.6-3). Those two point mutations introduced two single mutations in the CT of the M2 protein: E66G and S71F (see appendix 6.5). Interestingly previous research has shown that mutations at residue 71 of the M2 protein showed resistance to the 14C2 antibody, moreover one of the identified mutations responsible for this was S71F (Zebedee and Lamb 1989). However, further research is needed to investigate the molecular mechanism behind the restoration of budding, including the potential role of cellular factors.

The M2 AH has been shown to bind with lipid membranes through hydrophobic interactions (see chapter 3.1.3). It preferentially binds with membranes that contain high levels of positive curvature (see chapter 3.3.6), such as the neck of the budding

virion, which is detected by the AH sensing lipid packing defects associated with highly curved membrane (see chapter 3.3.7). Insertion of the helix into the membrane increases lipid ordering in the membrane (see chapter 3.4.2) which increases constriction of the neck of the budding virion and in this condition, induction of positive membrane curvature by the M2 AH (see chapter 3.4.4) leads to membrane scission of the pre-constricted neck and facilitates budding of a new virion (see chapters 3.5 and 3.6).

4.3 M2 AH AS A PART OF A BIGGER PROTEIN FAMILY

Membrane budding is a complex, multistage process that is important for viruses as well as many biological processes, such as endocytosis and vesicle trafficking. In all of these processes, multiple different proteins and AHs are involved, but exact details are not fully understood. Many of those AHs either sense membrane curvature using different domains, such as BAR (Peter et al. 2004) or by using hydrophobic interactions after insertion into the membrane (Drin and Antonny 2010); and generate membrane curvature by insertion of the AH into the membrane (Ford et al. 2002, Peter et al. 2004, Boucrot et al. 2012). Many proteins involved in membrane budding contain BAR domains and AHs that can generate membrane curvature but typically, sensing and curvature generation activities are associated with different domains. The M2 AH has been shown to have both features as it is able to sense and induce membrane curvature and therefore may belong to a novel group of AHs.

To see if other proteins may function similarly to M2, we examined cellular proteins and saw that four of them Arf 1, Endophilin A3, Epsin 1 and CHMP4b have similar features as the M2 AH (Fig. 3.7-1) and therefore were tested to determine if their mechanism of membrane scission is the same as the M2 AH and all belong to a novel group of AHs. Three cellular AHs, Arf 1, Endophilin A3 and Epsin 1 may work in similar way as the M2 AH as they all have been shown to form an α -helix upon binding with membranes, with exception of Epsin 1 which is also partially formed in solution (Fig. 3.7-2 and 3.7-3). They all preferentially bind with membranes with high positive curvature, but can work in wide range of positively curved membranes (Fig. 3.7-4 to 3.7-7). Anionic lipids support formation of the Arf 1, Endophilin A3 and Epsin 1 AHs but are not essential (Fig. 3.7-4 to 3.7-7). Increases in line tension between domains increases helix formation in Arf 1, Endophilin A3 and Epsin 1 AHs (Fig. 3.7-8) and insertion of these three AHs into the membrane also increases lipid ordering of the membrane (Fig. 3.7-9) changing its fluidity and induces positive membrane curvature (Fig. 3.7-10). On the other side CHMP4b AH does not work in the same way, as a helix is not formed upon binding with membranes (Fig. 3.7-3) and curvature of the membrane does not influence its formation (Fig. 3.7-7). The peptide also does not

induce changes to the lipid ordering in the membrane (Fig. 3.7-9) or induce positive membrane curvature (Fig. 3.7-10).

Overall those results show that three out of four cellular AHs tested: Arf 1, Endophilin A3 and Epsin 1 may work in a similar way as the M2 AH and therefore would all appear to belong to a novel group of AHs. However, further research is needed to investigate properties of all those AHs in more details and molecular mechanism of their action, especially that in few cases results showed a similar trend for cellular AHs as for the M2 AH but not identical.

4.4 CONCLUSIONS AND FUTURE WORK

Summarising, all of these results gives new insights into an overall model of influenza A virus budding mediated by the M2 AH underlying its molecular mechanism. The M2 AH is normally unstructured with an α -helix is being formed and stabilised upon binding with lipid membranes (see chapters 3.1.2 and 3.2), which is a well conserved function among influenza virus strains (see chapter 3.2.3.2). The M2 AH binds well with membranes composed of PC, PG and low levels of cholesterol through hydrophobic interactions (see chapter 3.1.3). Interaction of the M2 AH with lipid membranes is not dependent on charge-charge interactions, however, the presence of anionic lipids in the membrane enhances formation of the helix, but it is not essential (see chapter 3.3.2). Low levels of cholesterol present in the membrane (up to 10 molar %) support the M2 AH binding with the membranes and high levels (above 20 molar %) inhibit binding and may also affect formation of the helix (see chapter 3.3.3), corresponding well to earlier research showing that cholesterol inhibits M2 AH mediated budding in dose dependent manner (Rossman et al. 2010b). Formation of the M2 AH increases with an increase in line tension between domains in the lipid membrane (see chapter 3.3.5). The M2 AH preferentially binds with highly curved membranes but can work in a wide range of positively curved membranes and it is not associated with negatively curved membranes (see chapter 3.3.6). Curvature of the membrane is sensed by the M2 AH by sensing lipid packing defects associated with membranes with high positive curvature (see chapter 3.3.7) and is not affected by charged interactions (see chapter 3.3.6). Insertion of the M2 AH into the membrane increases lipid ordering of the membrane and decreases fluidity of the membrane (see chapter 3.4.2), which can be affected by properties of the membrane. Low levels of cholesterol and an increase in line tension between domains support increase in lipid ordering by the M2 AH but high levels of cholesterol in the membrane inhibit increase in lipid ordering (see chapter 3.4.2). Charge interactions and the presence of lipid packing defects in the membrane do not affect the ability to increase lipid ordering (see chapter 3.4.2). The M2 AH can also induce positive membrane curvature in LUVs (see chapter 3.4.4), mediate membrane scission and budding both in artificial membranes and *in vivo* (see chapters 3.5 and 3.6). Budding mediated by the M2 AH is a rapid process but the effects can be observed over a long time (see chapter 3.5.3)

and the loss of function of the M2 AH might be compensated by further parts of the M2 CT to restore viral growth (see chapter 3.6.3). Some cellular peptides, such as Arf 1, Endophilin A3 and Epsin 1, which mediate membrane scission in biological processes appear to work in a similar manner to the M2 AH and therefore belong to a novel group of AHs (see chapter 3.7).

An overall model of influenza virus budding shows that the M2 AH induces membrane scission and mediates budding. During last stages of viral budding M2 protein is localised to the neck of the budding virion, which is a region on the boundary of plasma membrane made up of lipid rafts with high positive membrane curvature. At this stage curvature sensing preferences should localise the M2 AH to the middle of the pre-constricted neck of budding virion where positive membrane curvature is the highest (Fig. 4.4-1 A). Insertion of the helix into the membrane increases lipid ordering, placing the membrane under strain and constricts the neck even further by inducing positive membrane curvature (Fig. 4.4-1 B). This causes membrane scission and leads to the release of the new virion into the environment (Fig. 4.4-1 C). However, the full details of the molecular mechanism of M2 AH mediated membrane scission are still not known. Further research into the interaction of the M2 AH with the membranes, especially an inhibitory role of high cholesterol levels is needed. Also depth of the M2 AH insertion into the membrane and the structural effect on the lipid membrane need to be investigated. Determining the high resolution structure of the full length M2 protein in the presence of a lipid membrane would also be important as presence of a full length protein could influence the structure and functions of the M2 AH and it would be much more physiologically relevant. Further characterisation of the three identified cellular AHs, which appear to work in the same way as the M2 AH, is also needed. Full understanding of the process is extremely important as it would not only broaden the knowledge about influenza virus budding but also allow for inhibition of this process which could lead to the development of new anti-microbial strategies against influenza virus infections. Additionally, studies of the M2 AH mediated membrane scission also would bring an insight into cellular membrane scission, as the M2 AH is a representative member of a novel group of AHs.

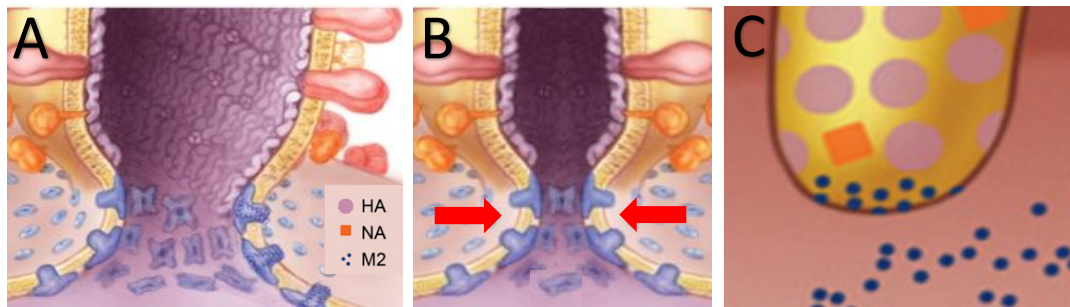


Figure 4.4 - 1 Model of influenza virus membrane scission mediated by the M2 AH. A) In the late stage of budding M2 is localised to the neck of the budding virion, which is a region of high positive membrane curvature. B) Insertion of the M2 AH into the membrane increases lipid ordering and induces positive membrane curvature, further constricting the membrane (as indicated by red arrows). C) M2 AH then induces membrane scission allowing for release of the newly formed virion into the environment. Adapted from Rossman and Lamb 2011.

5. REFERENCES

Ali, A., R. T. Avalos, E. Ponimaskin and D. P. Nayak (2000). "Influenza virus assembly: effect of influenza virus glycoproteins on the membrane association of M1 protein." J. Virol. **74**(18): 8709-8719.

Avalos, R. T., Z. Yu and D. P. Nayak (1997). "Association of influenza virus NP and M1 proteins with cellular cytoskeletal elements in influenza virus-infected cells." J. Virol. **71**: 2947-2958.

Barman, S., L. Adhikary, Y. Kawaoka and D. P. Nayak (2003). "Influenza A Virus Hemagglutinin Containing Basolateral Localization Signal Does Not Alter the Apical Budding of a Recombinant Influenza A Virus in Polarized MDCK Cells." Virology **305**(1): 138-152.

Barman, S. and D. P. Nayak (2000). "Analysis of the transmembrane domain of influenza virus neuraminidase, a type II transmembrane glycoprotein, for apical sorting and raft association." J. Virol. **74**: 6538-6545.

Baudin, F., I. Petit, W. Weissenhorn and R. W. Ruigrok (2001). "In vitro dissection of the membrane and RNP binding activities of influenza virus M1 protein." Virology **281**(1): 102-108.

Beck, R., S. Prinz, P. Diestelkotter-Bachert, S. Rohling, F. Adolf, K. Hoehner, S. Welsch, P. Ronchi, B. Brugger and J. A. Briggs (2011). "Coatomer and dimeric ADP ribosylation factor 1 promote distinct steps in membrane scission." J Cell Biol **194**: 765-777.

Boucrot, E., A. Pick, G. Camdere, N. Liska, E. Evergren, H. T. McMahon and M. M. Kozlov (2012). "Membrane fission is promoted by insertion of amphipathic helices and is restricted by crescent BAR domains." Cell **146**: 124-136.

Bourmakina, S. V. and A. Garcia-Sastre (2003). "Reverse genetics studies on the filamentous morphology of influenza A virus." J. Gen. Virol. **84**: 517-527.

Bourmakina, S. V. and A. Garcia-Sastre (2005). "The morphology and composition of influenza A virus particles are not affected by low levels of m1 and m2 proteins in infected cells." J. Virol. **79**: 7926-7932.

Brewer, C. B. and M. G. Roth (1991). "A single amino acid change in the cytoplasmic domain alters the polarized delivery of influenza virus hemagglutinin." J. Cell Biol. **114**: 413-421.

Brown, D. (2001). "Structure and function of membrane rafts." International Journal of Medical Microbiology **291**(6–7): 433-437.

Bruce, E. A., P. Digard and A. D. Stuart (2010). "The Rab11 pathway is required for influenza A virus budding and filament formation." J. Virol. **84**(12): 5848-5859.

Brunger, A. T., P. D. Adams, G. M. Clore, W. L. DeLano, P. Gros, R. W. Grosse-Kunstleve, J. S. Jiang, J. Kuszewski, M. Nilges, N. S. Pannu, R. J. Read, L. M. Rice, T. Simonson and G. L. Warren (1998). "Crystallography & NMR system: A new software suite for macromolecular structure determination." Acta Crystallogr., Sect. D: Biol. Crystallogr. **54**: 905-921.

Carlson, L. A. and J. H. Hurley (2012). "In vitro reconstitution of the ordered assembly of the endosomal sorting complex required for transport at membrane-bound HIV-1 Gag clusters." PNAS **109**: 16928-16933.

Carlton, J. G. and J. Martin-Serrano (2009). "The ESCRT machinery: new functions in viral and cellular biology." Biochem. Soc. Trans. **37**: 195-199.

Carrasco, M., M. J. Amorim and P. Digard (2004). "Lipid raft-dependent targeting of the influenza A virus nucleoprotein to the apical plasma membrane." Traffic **5**: 979-992.

Chen, B. J., G. P. Leser, D. Jackson and R. A. Lamb (2008). "The influenza virus M2 protein cytoplasmic tail interacts with the M1 protein and influences virus assembly at the site of virus budding." J. Virol. **82**: 10059-10070.

Chen, B. J., G. P. Leser, E. Morita and R. A. Lamb (2007). "Influenza virus hemagglutinin and neuraminidase, but not the matrix protein, are required for assembly and budding of plasmid-derived virus-like particles." J. Virol. **81**: 7111-7123.

Chen, B. J., M. Takeda and R. A. Lamb (2005). "Influenza virus hemagglutinin (H3 subtype) requires palmitoylation of its cytoplasmic tail for assembly: M1 proteins of two subtypes differ in their ability to support assembly." J. Virol. **79**: 13673-13684.

Cheung, M. S., M. L. Maguire, T. J. Stevens and J. W. Broadhurst (2010). "DANGLE: A Bayesian inferential method for predicting protein backbone dihedral angles and secondary structure." J. Magn. Reson. **202**: 223-233.

Cheung, T. K., Y. Guan, S. S. Ng, H. Chen, C. H. Wong, J. S. Peiris and L. L. Poon (2005). "Generation of recombinant influenza A virus without M2 ion-channel protein by introduction of a point mutation at the 5' end of the viral intron." J. Gen. Virol. **86**: 1447-1454.

Chu, C. M., I. M. Dawson and W. J. Elford (1949). "Filamentous forms associated with newly isolated influenza virus." Lancet **1**: 602.

Drin, G. and B. Antonny (2010). "Amphipathic helices and membrane curvature." FEBS Lett. **584**(9): 1840-1847.

Drin, G., J. F. Casella, R. Gautier, T. Boehmer, T. U. Schwartz and B. Antonny (2007). "A general amphipathic alpha-helical motif for sensing membrane curvature." Nat Struct Mol Biol **14**: 138-146.

Elleman, C. J. and W. S. Barclay (2004). "The M1 matrix protein controls the filamentous phenotype of influenza A virus." Virology **321**: 144-153.

Enami, M. and K. Enami (1996). "Influenza virus hemagglutinin and neuraminidase glycoproteins stimulate the membrane association of the matrix protein." J. Virol. **70**: 6653-6657.

Fabrikant, G., S. Lata, J. D. Riches, J. A. Briggs, W. Weissenhorn and M. M. Kozlov (2009). "Computational model of membrane fission catalyzed by ESCRT-III." PLoS Comput. Biol. **5**(11): e1000575.

Faelber, K., M. Held, S. Gao, Y. Posor, V. Haucke, F. Noe´ and O. Daumke (2012). "Structural Insights into Dynamin-Mediated Membrane Fission." Structure **20**: 1621-1628.

Ford, M. G., I. G. Mills, B. J. Peter, Y. Vallis, G. J. Praefcke, P. R. Evans and H. T. McMahon (2002). "Curvature of clathrin-coated pits driven by epsin." Nature **419**(6905): 361-366.

Fujiyoshi, Y., N. P. Kume, K. Sakata and S. B. Sato (1994). "Fine structure of influenza A virus observed by electron cryo-microscopy." EMBO J. **13**: 318-326.

Garcia-Saez, A. J., S. Chiantia and P. Schwille (2007). "Effect of line tension on the lateral organization of lipid membranes." J. Biol. Chem. **282**(46): 33537-33544.

Gautier, R., D. Douguet, B. Antonny and G. Drin (2008). "HELIQUEST: a web server to screen sequences with specific α -helical properties." Bioinformatics **24**(18): 2101-2102.

Gómez-Llobregat, J., F. Elías-Wolff and M. Lindén (2016). "Anisotropic Membrane Curvature Sensing by Amphipathic Peptides." Biophys J **110**: 197-204.

Gomez-Puertas, P., C. Albo, E. Perez-Pastrana, A. Vivo and A. Portela (2000). "Influenza virus matrix protein is the major driving force in virus budding." J. Virol. **74**: 11538-11547.

Greenfield, N. J. (2006). "Using Circular Dichroism spectra to estimate protein secondary structure." Nat Protoc **1** (6): 2876-2890.

Hinshaw, J. E. and S. L. Schmid (1995). "Dynamin self-assembles into rings suggesting a mechanism for coated vesicle budding." Nature **374**(6518): 190-192.

Hu, M., P. Diggins and M. Deserno (2013). "Determining the bending modulus of a lipid membrane by simulating buckling." J Chem Phys **138**(21): 214110.

Hughey, P. G., R. W. Compans, S. L. Zebedee and R. A. Lamb (1992). "Expression of the influenza A virus M₂ protein is restricted to apical surfaces of polarized epithelial cells." J. Virol. **66**: 5542-5552.

Hui, E. K. and D. P. Nayak (2001). "Role of ATP in influenza virus budding." Virology **290**: 329-341.

Hui, E. K. and D. P. Nayak (2002). "Role of G protein and protein kinase signalling in influenza virus budding in MDCK cells." J Gen Virol **83**(Pt 12): 3055-3066.

Iwatsuki-Horimoto, K., T. Horimoto, T. Noda, M. Kiso, J. Maeda, S. Watanabe, Y. Muramoto, K. Fujii and Y. Kawaoka (2006). "The cytoplasmic tail of the influenza A virus M2 protein plays a role in viral assembly." J. Virol. **80**(11): 5233-5240.

Jackson, D. and R. A. Lamb (2008). "The influenza A virus spliced messenger RNA M mRNA₃ is not required for viral replication in tissue culture." J Gen Virol **89**(Pt 12): 3097-3101.

Johnson, N. P. and J. Mueller (2002). "Updating the accounts: global mortality of the 1918-1920 "Spanish" influenza pandemic." Bull Hist Med **76**(1): 105-115.

Jones, L. V., R. W. Compans, A. R. Davis, T. J. Bos and D. P. Nayak (1985). "Surface expression of influenza virus neuraminidase, an amino-terminally anchored viral membrane glycoprotein, in polarized epithelial cells." Mol. Cell. Biol. **5**: 2181-2189.

Kawai, Y., Y. Kimura, A. Lezhava, H. Kanamori, K. Usui, T. Hanami, T. Soma, J. E. Morlighem, S. Saga, Y. Ishizu, S. Aoki, R. Endo, A. Oguchi-Katayama, Y. Kogo, Y. Mitani, T. Ishidao, C. Kawakami, H. Kurata, Y. Furuya, T. Saito, N. Okazaki, M. Chikahira, E. Hayashi, S. Tsuruoka, T. Toguchi, Y. Saito, T. Ban, S. Izumi, H. Uryu, K. Kudo, Y. Sakai-Tagawa, Y. Kawaoka, A. Hirai, Y. Hayashizaki and T. Ishikawa

(2012). "One-step detection of the 2009 pandemic influenza A(H1N1) virus by the RT-SmartAmp assay and its clinical validation." PLoS One **7**(1): e30236.

Kawaoka, Y. and G. Neumann (2012). "Influenza viruses: an introduction." Methods Mol Biol **865**: 1-9.

Kikuchi, T., K. Iwatsuki-Horimoto, E. Adachi, M. Koga, H. Nakamura, N. Hosoya, A. Kawana-Tachikawa, T. Koibuchi, T. Miura, T. Fujii, Y. Kawaoka and A. Iwamoto (2012). "Improved neutralizing antibody response in the second season after a single dose of pandemic (H1N1) 2009 influenza vaccine in HIV-1-positive adults." Vaccine.

Kilbourne, E. D. (2006). "Influenza pandemics of the 20th century." Emerg Infect Dis **12**(1): 9-14.

Kilbourne, E. D. and J. S. Murphy (1960). "Genetic studies of influenza viruses. I. Viral morphology and growth capacity as exchangeable genetic traits. Rapid in ovo adaptation of early passage asian strain isolates by combination with PR8." J. Exp. Med. **111**: 387-406.

Koradi, R., M. Billeter and K. Wüthrich (1996). "MOLMOL: A program for display and analysis of macromolecular structures." J Mol Graphics **14**: 51-55.

Kretzschmar, E., M. Bui and J. K. Rose (1996). "Membrane association of influenza virus matrix protein does not require specific hydrophobic domains or the viral glycoproteins." Virology **220**: 37-45.

Lai, J. C., W. W. Chan, F. Kien, J. M. Nicholls, J. S. Peiris and J. M. Garcia (2010). "Formation of virus-like particles from human cell lines exclusively expressing Influenza neuraminidase." J. Gen. Virol. **91**: 2322-2330.

Lamb, R. A., S. L. Zebedee and C. D. Richardson (1985). "Influenza virus M₂ protein is an integral membrane protein expressed on the infected-cell surface." Cell **40**: 627-633.

Langel, F. D., N. A. Jain, J. S. Rossman, L. M. Kingeter, A. K. Kashyap and B. C. Schaefer (2008). "Multiple protein domains mediate interaction between Bcl10 and MALT1." J. Biol. Chem. **283**(47): 32419-32431.

Laskowski, R. A., M. W. MacArthur, D. S. Moss and J. M. Thornton (1993). "PROCHECK - a program to check the stereochemical quality of protein structures." J. App. Cryst. **26**: 283-291.

Lawrence, A. D., S. Frank, S. Newnham, M. J. Lee, I. R. Brown, W. F. Xue, M. L. Rowe, D. P. Mulvihill, M. B. Prentice, M. J. Howard and M. J. Warren (2014).

"Solution Structure of a Bacterial Microcompartment Targeting Peptide and Its Application in the Construction of an Ethanol Bioreactor." ACS Synth. Biol. **3** (7): 454-465.

Leser, G. P. and R. A. Lamb (2005). "Influenza virus assembly and budding in raft-derived microdomains: a quantitative analysis of the surface distribution of HA, NA and M2 proteins." Virology **342**: 215-227.

Li, J., X. Wang, T. Zhang, C. Wang, Z. Huang, X. Luo and Y. Deng (2015). "A review on phospholipids and their main applications in drug delivery systems." Asian Journal of Pharmaceutical Sciences **10**: 81-89.

Liu, C., M. C. Eichelberger, R. W. Compans and G. M. Air (1995). "Influenza type A virus neuraminidase does not play a role in viral entry, replication, assembly, or budding." J. Virol. **69**: 1099-1106.

Louis-Jeune, C., M. A. Andrade-Navarro and C. Perez-Iratxeta (2012). "Prediction of protein secondary structure from circular dichroism using theoretically derived spectra." Proteins **80**: 374-381.

Manley, S. and V. D. Gordon (2008). Making Giant Unilamellar Vesicles via Hydration of a Lipid Film. Current Protocols in Cell Biology. **24**.

Martyna, A. and J. Rossman (2014). "Alterations of membrane curvature during influenza virus budding " Biochem. Soc. Trans. **42**: 1425-1428.

McCown, M. F. and A. Pekosz (2005). "The influenza A virus M2 cytoplasmic tail is required for infectious virus production and efficient genome packaging." J. Virol. **79**: 3595-3605.

McCown, M. F. and A. Pekosz (2006). "Distinct domains of the influenza a virus M2 protein cytoplasmic tail mediate binding to the M1 protein and facilitate infectious virus production." J. Virol. **80**(16): 8178-8189.

McMahon, H. T. and E. Boucrot (2011). "Molecular mechanism and physiological functions of clathrin-mediated endocytosis." Nature Reviews Molecular Cell Biology **12**: 517-533.

Mora, R., E. Rodriguez-Boulan, P. Palese and A. García-Sastre (2002). "Apical Budding of a Recombinant Influenza A Virus Expressing a Hemagglutinin Protein with a Basolateral Localization Signal." Journal of Virology **76**(7): 3544-3553.

Murakami, S., T. Horimoto, M. Ito, R. Takano, H. Katsura, M. Shimojima and Y. Kawaoka (2012). "Enhanced growth of influenza vaccine seed viruses in vero cells

mediated by broadening the optimal pH range for virus membrane fusion." J Virol **86**(3): 1405-1410.

Nath, S., J. Dancourt, V. Shteyn, G. Puente, W. M. Fong, S. Nag, J. Bewersdorf, A. Yamamoto, B. Antonny and T. J. Melia (2014). "Lipidation of the LC3/GABARAP family of autophagy proteins relies on a membrane-curvature-sensing domain in Atg3." Nat Cell Biol **16**: 415-424.

Neumann, G., M. Ozawa and Y. Kawaoka (2012). "Reverse genetics of influenza viruses." Methods Mol Biol **865**: 193-206.

Neumann, S. and S. L. Schmid (2013). "Dual role of BAR domain-containing proteins in regulating vesicle release catalyzed by the GTPase, dynamin-2." J Biol Chem **288**(35): 25119-25128.

Nidom, C. A., S. Yamada, R. V. Nidom, K. Rahmawati, M. Y. Alamudi, Kholik, S. Indrasari, R. S. Hayati, K. Iwatsuki Horimoto and Y. Kawaoka (2012). "Genetic characterization of H5N1 influenza viruses isolated from chickens in Indonesia in 2010." Virus Genes **44**(3): 459-465.

Noda, T., Y. Sugita, K. Aoyama, A. Hirase, E. Kawakami, A. Miyazawa, H. Sagara and Y. Kawaoka (2012). "Three-dimensional analysis of ribonucleoprotein complexes in influenza A virus." Nat Commun **3**: 639.

Palese, P. and M. L. Shaw (2007). Orthomyxoviridae: the viruses and their replication. Fields Virology B. N. Fields, D. M. Knipe and P. M. Howley. Philadelphia, Philadelphia : Wolters Kluwer Health/Lippincott Williams & Wilkins: 1647-1689.

Parasassi, T., G. De Stasio, A. d'Ubaldo and E. Gratton (1990). "Phase fluctuation in phospholipid membranes revealed by Laurdan fluorescence." Biophys J **57**: 1179-1186.

Pattnaik, A. K., D. J. Brown and D. P. Nayak (1986). "Formation of influenza virus particles lacking hemagglutinin on the viral envelope." J. Virol. **60**: 994-1001.

Peter, B. J., H. M. Kent, I. G. Millis, Y. Vallis, P. J. Butler, P. R. Evans and H. T. McMahon (2004). "BAR domains as sensors of membrane curvature: the amphiphysin BAR structure." Science **303**: 495-499.

Pinto, L. H., G. R. Dieckmann, C. S. Gandhi, C. G. Papworth, J. Braman, M. A. Shaughnessy, J. D. Lear, R. A. Lamb and W. F. DeGrado (1997). "A functionally defined model for the M₂ proton channel of influenza A virus suggests a mechanism for its ion selectivity." Proc. Natl. Acad. Sci. USA **94**: 11301-11306.

Pinto, L. H., L. J. Holsinger and R. A. Lamb (1992). "Influenza virus M₂ protein has ion channel activity." Cell **69**: 517-528.

Povey, J. F., M. Smales, S. J. Hassard and M. J. Howard (2007). "Comparison of the effects of 2,2,2-trifluoroethanol on peptide and protein structure and function." Journal of Structural Biology **157**: 329-338.

Pronk, S., S. Pall, R. Schulz, P. Larsson, P. Bjelkmar, R. Apostolov, M. R. Shirts, J. C. Smith, P. M. Kasson, D. van der Spoel, B. Hess and E. Lindahl (2013). "GROMACS 4.5: a high-throughput and highly parallel open source molecular simulation toolkit." Bioinformatics **29**(7): 845-854.

Richardson, J. C. and R. K. Akkina (1991). "NS2 protein of influenza virus is found in purified virus and phosphorylated in infected cells." Arch. Virol. **116**: 69-80.

Rossmann, J. S., X. Jing, G. P. Leser, V. Balannik, L. H. Pinto and R. A. Lamb (2010a). "Influenza virus M2 ion channel protein is necessary for filamentous virion formation." J. Virol. **84**(10): 5078-5088.

Rossmann, J. S., X. Jing, G. P. Leser and R. A. Lamb (2010b). "The influenza virus M2 protein mediates ESCRT-independent membrane scission." Cell **142**(6): 902-913.

Rossmann, J. S. and R. A. Lamb (2010). "Swine-origin influenza virus and the 2009 pandemic." Am. J. Respir. Crit. Care Med. **181**(4): 295-296.

Rossmann, J. S. and R. A. Lamb (2011). "Influenza virus assembly and budding." Virology **411**(2): 229-236.

Roth, M. G., R. W. Compans, L. Giusti, A. R. Davis, D. P. Nayak, M.-J. Gething and J. Sambrook (1983). "Influenza virus hemagglutinin expression is polarized in cells infected with recombinant SV40 viruses carrying cloned hemagglutinin DNA." Cell **33**: 435-443.

Ruigrok, R., F. Baudin, I. Petit and W. Weissenhorn (2001). "Role of influenza virus M1 protein in the viral budding process." Int. Congress Series **1219**: 397-404.

Sanchez, S. A., M. A. Tricerri, G. Gunther and E. Gratton (2007). "Laurdan Generalized Polarization: from cuvette to microscope." Modern research and educational topics in microscopy: 1007-1014.

Scheiffele, P., M. G. Roth and K. Simons (1997). "Interaction of influenza virus haemagglutinin with sphingolipid-cholesterol membrane domains via its transmembrane domain." EMBO J. **16**: 5501-5508.

Schmidt, N. W., A. Mishra, J. Wang, W. F. DeGrado and G. C. Wong (2013). "Influenza virus A M2 protein generates negative Gaussian membrane curvature necessary for budding and scission." J Am Chem Soc **135** (37).

Schnell, J. R. and J. J. Chou (2008). "Structure and mechanism of the M2 proton channel of influenza A virus." Nature **451**: 591-595.

Schroeder, C. (2010). "Cholesterol-binding viral proteins in virus entry and morphogenesis." Subcell. Biochem. **51**: 77-108.

Schroeder, C., H. Heider, E. Moncke-Buchner and T. I. Lin (2005). "The influenza virus ion channel and maturation cofactor M2 is a cholesterol-binding protein." Eur. Biophys. J. **34**: 52-66.

Sharma, M., M. Yi, H. Dong, H. Qin, E. Peterson, D. D. Busath, H. X. Zhou and T. A. Cross (2010). "Insight into the mechanism of the influenza A proton channel from a structure in a lipid bilayer." Science **330**(6003): 509-512.

Shi, J., Z. Wen, J. Guo, Y. Zhang, G. Deng, Y. Shu, D. Wang, Y. Jiang, Y. Kawaoka, Z. Bu and H. Chen (2012). "Protective efficacy of an H1N1 cold-adapted live vaccine against the 2009 pandemic H1N1, seasonal H1N1, and H5N1 influenza viruses in mice." Antiviral Res **93**(3): 346-353.

Shinya, K., Y. Gao, C. Cilloniz, Y. Suzuki, M. Fujie, G. Deng, Q. Zhu, S. Fan, A. Makino, Y. Muramoto, S. Fukuyama, D. Tamura, T. Noda, A. J. Einfeld, M. G. Katze, H. Chen and Y. Kawaoka (2012). "Integrated Clinical, Pathologic, Virologic, and Transcriptomic Analysis of H5N1 Influenza Virus-Induced Viral Pneumonia in the Rhesus Macaque." J Virol **86**(11): 6055-6066.

Stouffer, A. L., R. Acharya, D. Salom, A. S. Levine, L. Di Costanzo, C. S. Soto, V. Tereshko, V. Nanda, S. Stayrook and W. F. DeGrado (2008). "Structural basis for the function and inhibition of an influenza virus proton channel." Nature **451**: 596-599.

Strauss, J. H. and E. G. Strauss (2008). *Viruses and human disease* San Diego, Academic Press: 147- 155.

Takeda, M., G. P. Leser, C. J. Russell and R. A. Lamb (2003). "Influenza virus hemagglutinin concentrates in lipid raft microdomains for efficient viral fusion." Proc. Natl. Acad. Sci. USA **100**: 14610-14617.

Thompson, W. W., D. K. Shay, E. Weintraub, L. Brammer, N. Cox, L. J. Anderson and K. Fukuda (2003). "Mortality associated with influenza and respiratory syncytial virus in the United States." J.A.M.A. **289**: 179-186.

- Veatch, S. L. (2007). Lipid rafts. Methods in Molecular Biology. **398**: 59-72.
- Victor, S. T., S. Watanabe, H. Katsura, M. Ozawa and Y. Kawaoka (2012). "A replication-incompetent PB2-knockout influenza A virus vaccine vector." J Virol **86**(8): 4123-4128.
- Vranken, W. F., W. Boucher, T. J. Stevens, R. H. Fogh, A. Pajon, M. Llinas, E. L. Ulrich, J. L. Markley, J. Ionides and E. D. Laue (2005). "The CCPN data model for NMR spectroscopy: development of a software pipeline." Proteins **59**: 687-696.
- Wang, D., A. Harmon, J. Jin, D. H. Francis, J. Christopher-Hennings, E. Nelson, R. C. Montelaro and F. Li (2010). "The lack of an inherent membrane targeting signal is responsible for the failure of the matrix (M1) protein of influenza A virus to bud into virus-like particles." J. Virol. **84**(9): 4673-4681.
- Wang, T., S. D. Cady and M. Hong (2012). "NMR determination of protein partitioning into membrane domains with different curvatures and application of the influenza M2 peptide." Biophysical Journal **102**: 787-794.
- Ward, A. C. (1995). "Changes in the neuraminidase of neurovirulent influenza virus strains." Virus Genes **10**(3): 253-260.
- Watanabe, K., H. Handa, K. Mizumoto and K. Nagata (1996). "Mechanism for inhibition of influenza virus RNA polymerase activity by matrix protein." J. Virol. **70**: 241-247.
- Wilschut, J. C., J. E. McElhaney and A. M. Palache (2006). Influenza Rapid Reference, Mosby/Elsevier.
- Wollert, T., C. Wunder, J. Lippincott-Schwartz and J. H. Hurley (2009a). "Membrane scission by the ESCRT-III complex." Nature **458**(7235): 172-177.
- Wollert, T., D. Yang, X. Ren, H. H. Lee, Y. J. Im and J. H. Hurley (2009b). "The ESCRT machinery at a glance." J Cell Sci **122**(Pt 13): 2163-2166.
- Zebedee, S. L. and R. A. Lamb (1988). "Influenza A virus M₂ protein: monoclonal antibody restriction of virus growth and detection of M₂ in virions." J. Virol. **62**: 2762-2772.
- Zebedee, S. L. and R. A. Lamb (1989). "Growth restriction of influenza A virus by M₂ protein antibody is genetically linked to the M₁ protein." Proc. Natl. Acad. Sci. USA **86**: 1061-1065.

Zebedee, S. L., C. D. Richardson and R. A. Lamb (1985). "Characterization of the influenza virus M₂ integral membrane protein and expression at the infected-cell surface from cloned cDNA." J. Virol. **56**: 502-511.

Zhang, J. and R. A. Lamb (1996). "Characterization of the membrane association of the influenza virus matrix protein in living cells." Virology **225**: 255-266.

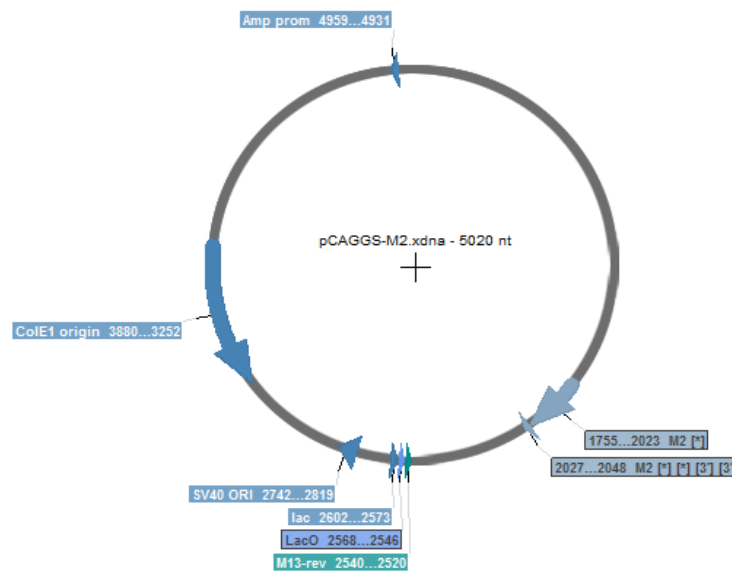
Zhang, J., A. Pekosz and R. A. Lamb (2000). "Influenza virus assembly and lipid raft microdomains: a role for the cytoplasmic tails of the spike glycoproteins." J. Virol. **74**: 4634-4644.

Zhao, H., M. Ekström and H. Garoff (1998). "The M1 and NP proteins of influenza A virus form homo- but not heterooligomeric complexes when coexpressed in BHK-21 cells." Journal of General Virology **79**(10): 2435-2446.

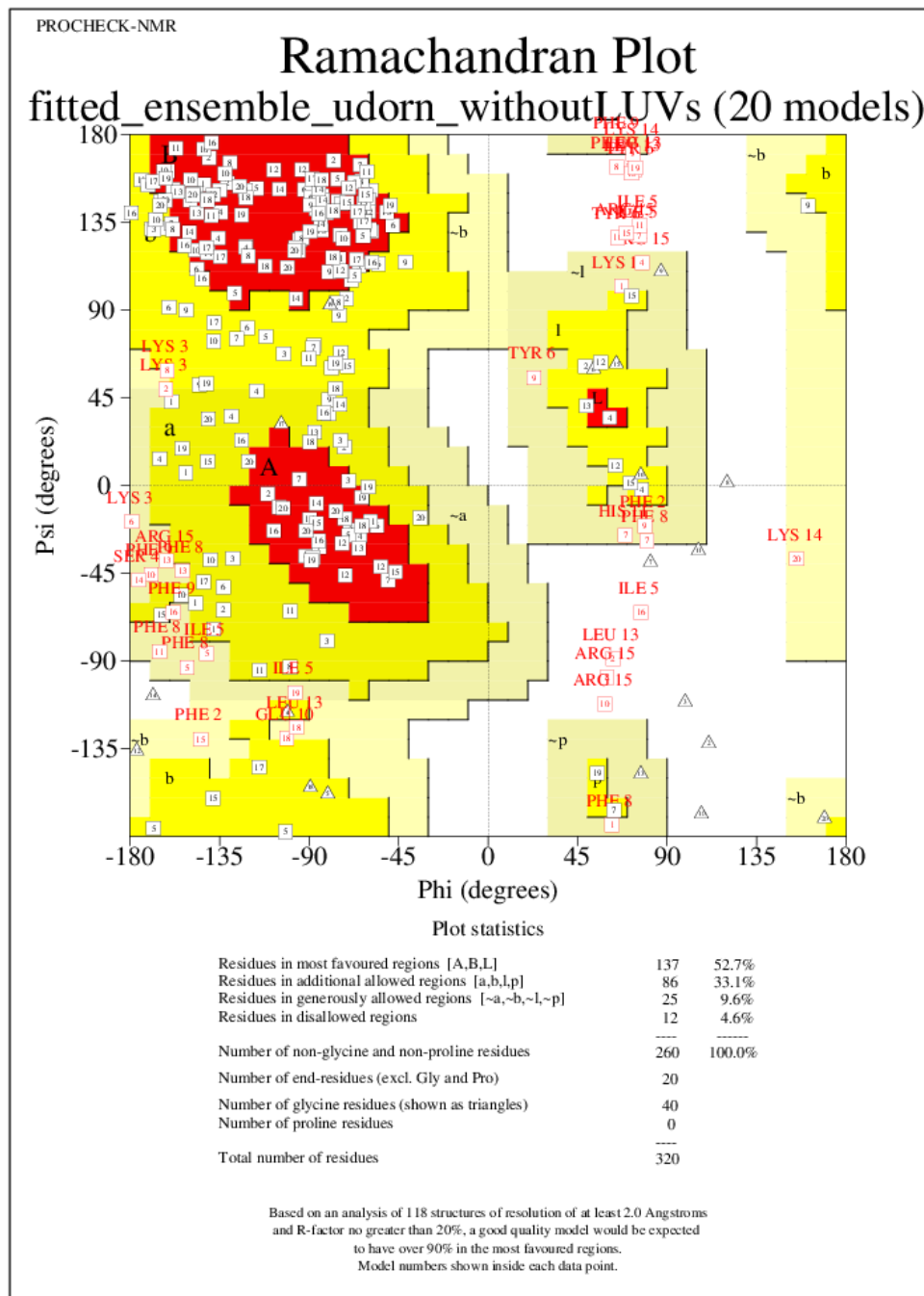
Zhirnov, O. P. and H.-D. Klenk (2009). "Alterations in caspase cleavage motifs of NP and M2 proteins attenuate virulence of a highly pathogenic avian influenza virus." Virology **394**(1): 57-63.

6. APPENDIX

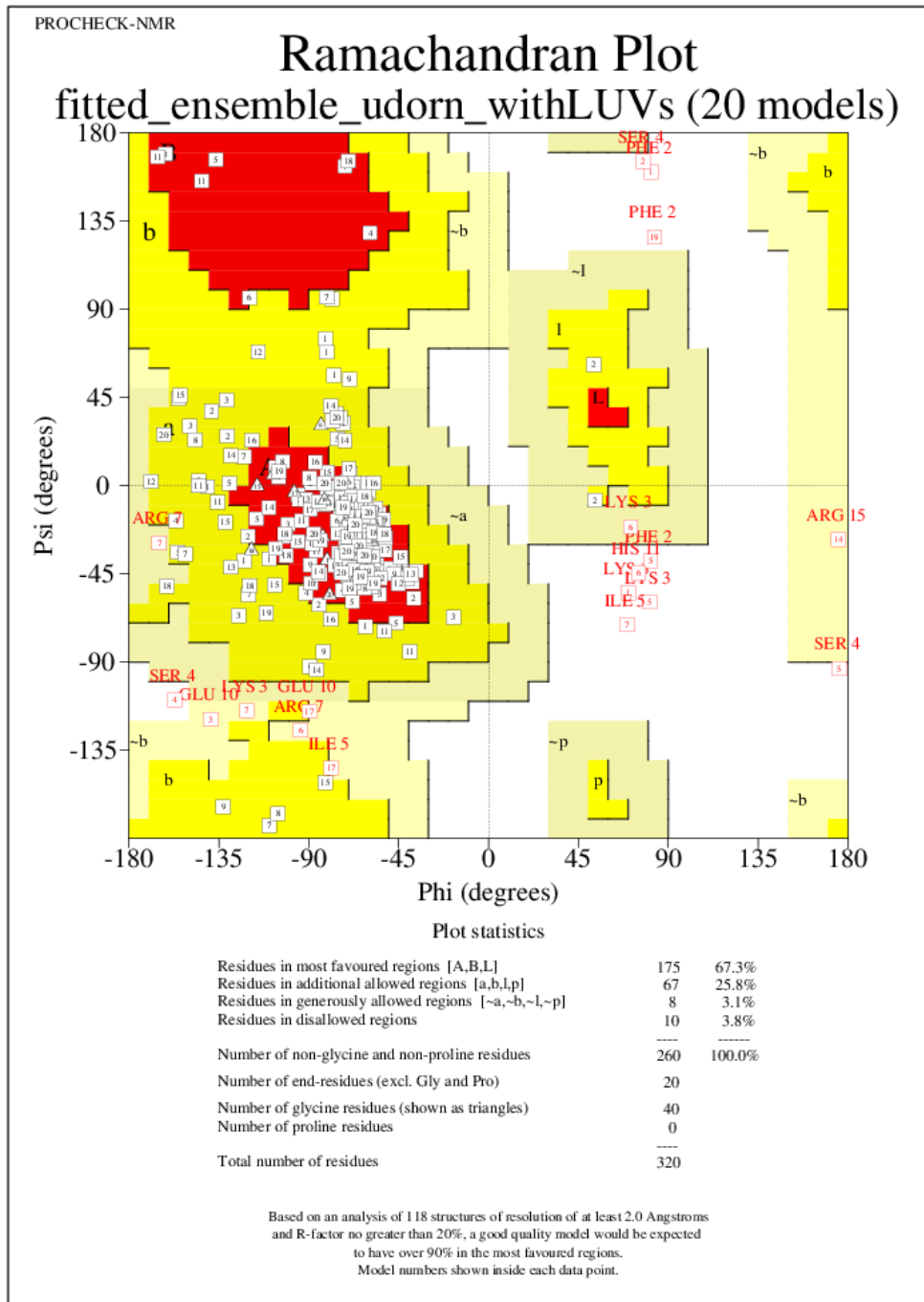
6.1 Restriction map of pCAGGS plasmid encoding M2 protein from A/Udorn/72 strain



6.2 Ramachandran plots



fitted_ensemble_udorn_withoutLUVs_01.ps

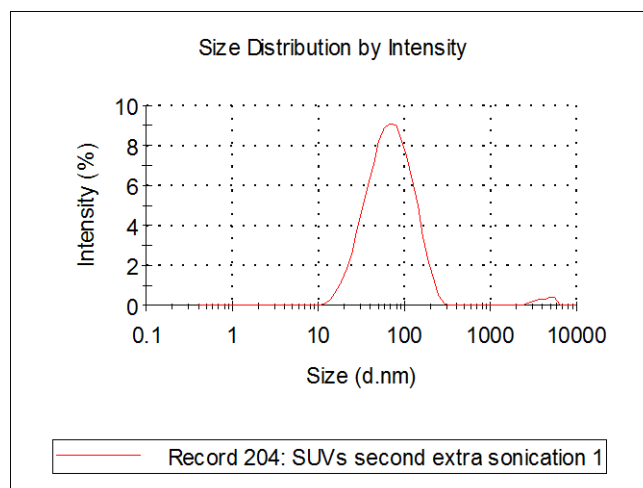


fitted_ensemble_udorn_withLUVs_01.ps

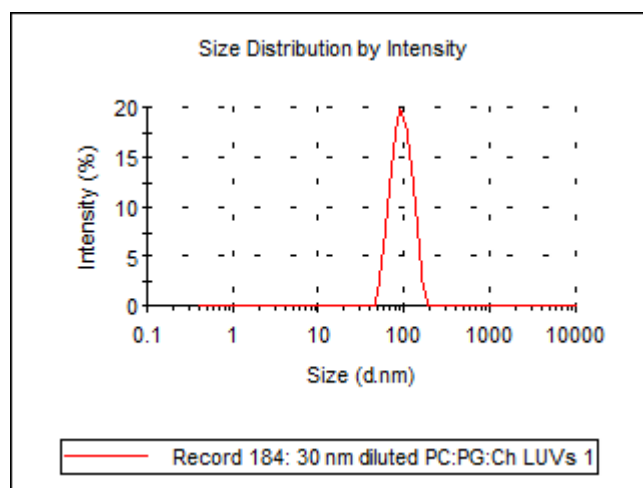
6.3 DLS data

A. Standard vesicles

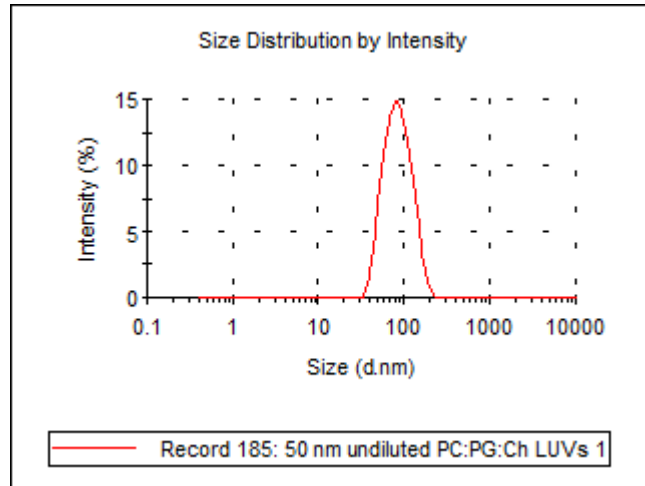
SUVs – 58.88 d. nm



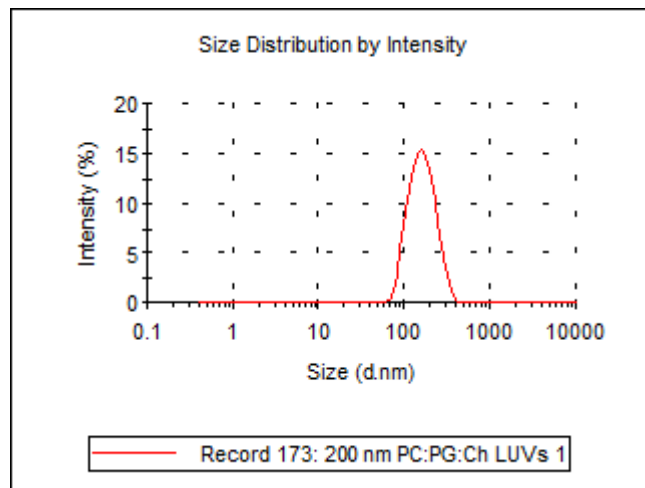
LUVs – 89.19 d. nm



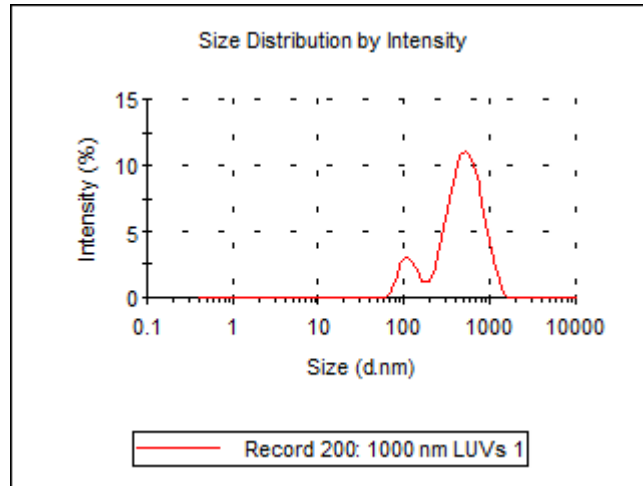
LUVs – 77.7 d. nm



LUVs – 150.4 d. nm

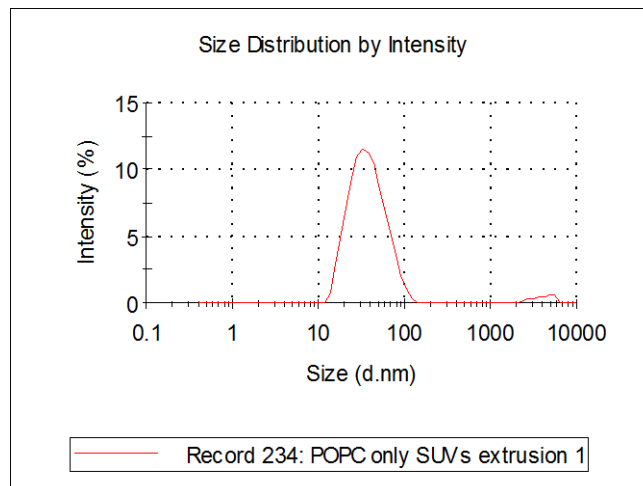


LUVs – 350.4 d. nm

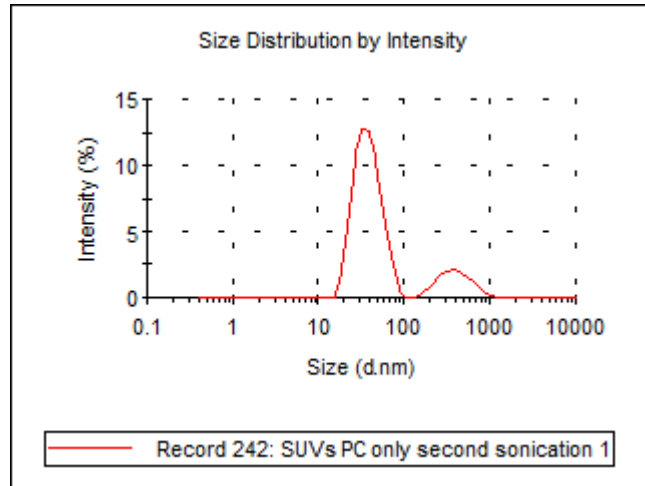


B. Vesicles without anionic lipids

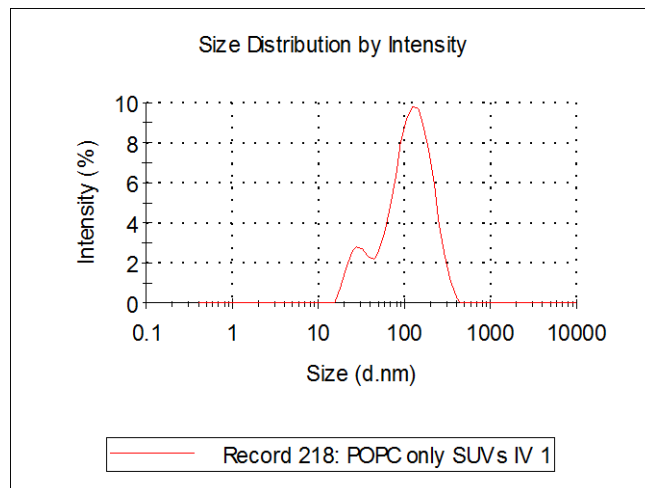
SUVs - 34.52 d. nm



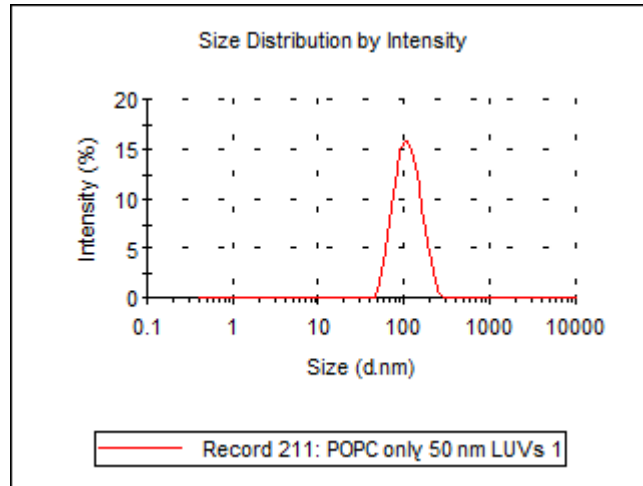
SUVs - 41.69 d. nm



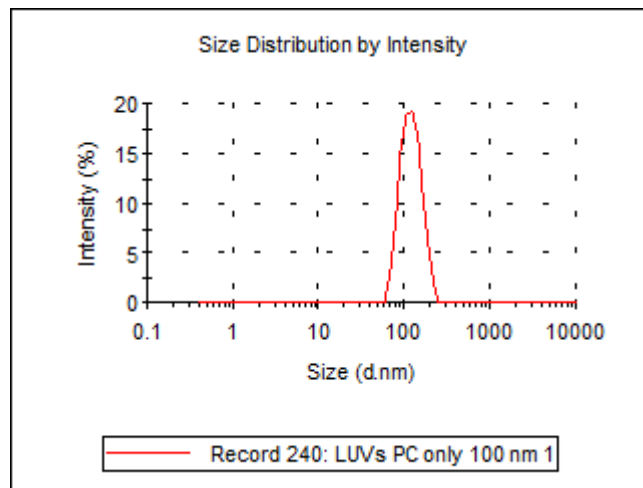
SUVs - 85.56 d. nm



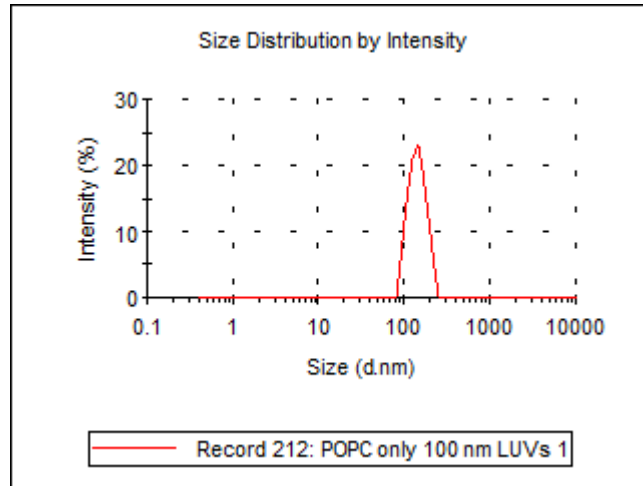
LUVs - 101.9 d. nm



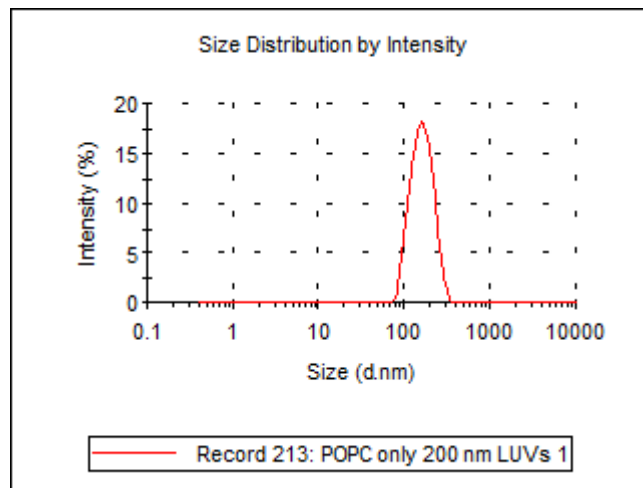
LUVs - 113.7 d. nm



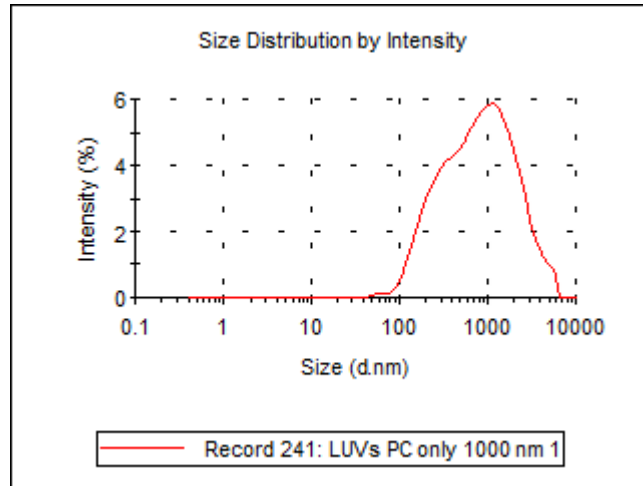
LUVs - 136.5 d. nm



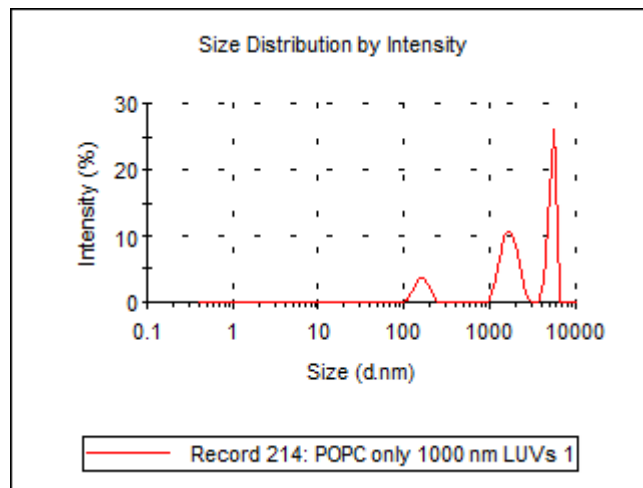
LUVs - 153.6 d. nm



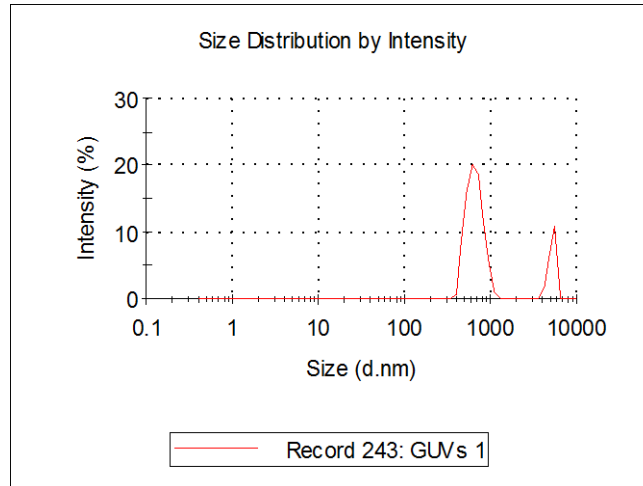
LUVs - 540 d. nm



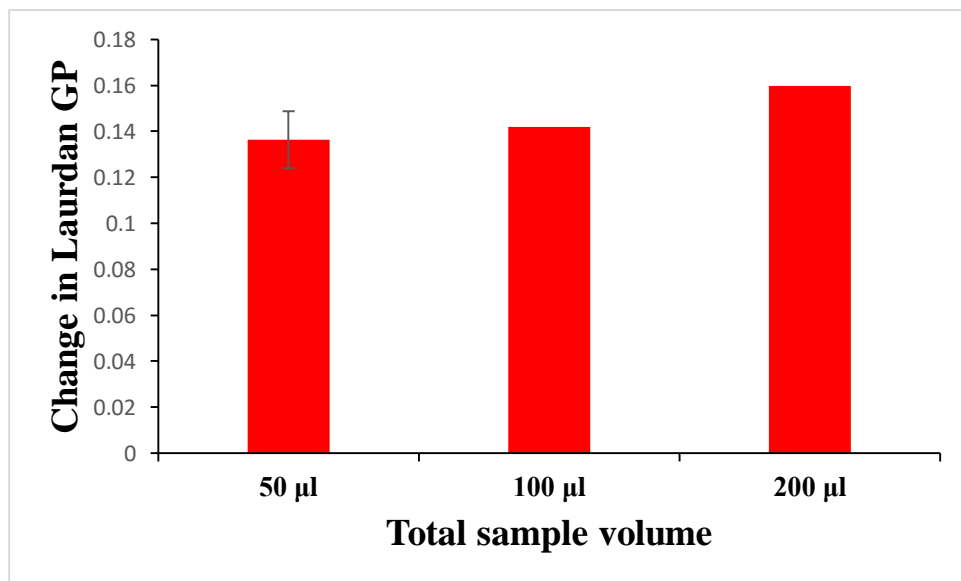
LUVs - 3135 d. nm



GUVs - 1119 d. nm



6.4 Laurdan assay titration



Change in Laurdan GP value with 100 µM of the M2 AH and 2.5 mM of standard LUVs at 1:100 lipid:dye ratio with an increasing total volume of the sample.

6.5 Protein sequences comparison

A. Sequence of the M2 CT with 5 PM:

R	L	A	A	K	C	A	A	R	F	A	E	H	G	L	K	R	G	P	S	T	E	G	V	P	E	S
45	46	47	48	49	50	51	52	53	54	55	56	57	58	59	60	61	62	63	64	65	66	67	68	69	70	71
M	R	E	E	Y	R	K	E	Q	Q	S	A	V	D	A	D	D	S	H	F	V	S	I	E	L	E	*
72	73	74	75	76	77	78	79	80	81	82	83	84	85	86	87	88	89	90	91	92	93	94	95	96	97	

B. Sequence of the M2 CT with 5 PM after 14 passages detected with M_UTR_R primer:

R	L	A	A	K	C	A	A	R	F	A	E	H	G	L	K	R	G	P	S	T	G	G	V	P	E	F
45	46	47	48	49	50	51	52	53	54	55	56	57	58	59	60	61	62	63	64	65	66	67	68	69	70	71
M	R	E	E	Y	R	K	E	Q	Q	S	A	V	D	A	D	D	S	-	-	-	-	-	-	-	-	-
72	73	74	75	76	77	78	79	80	81	82	83	84	85	86	87	88	89	90	91	92	93	94	95	96	97	